E2 Circular beam analytical solution

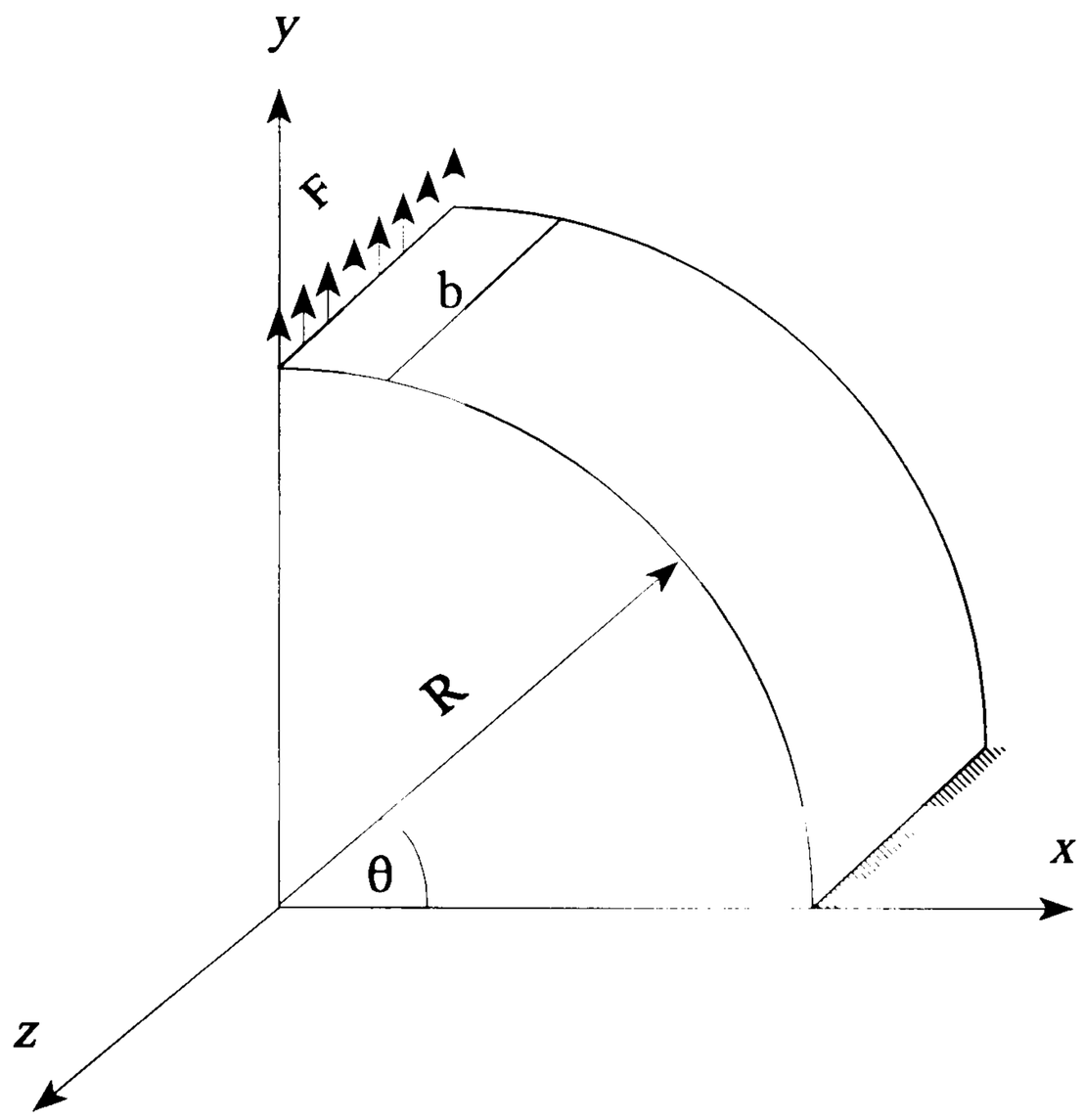

$$u(\theta) = \frac{FR^3}{2EI} \sin^2\theta$$

$$v(\theta) = \frac{FR^4}{4EI} (2\theta - \sin 2\theta)$$

CRANFIELD UNIVERSITY

School of Mechanical Engineering
Department of Turbomachinery
and Engineering Mechanics

Ph.D. Thesis

Academic Year 1995-96

Osama Abdel Moniem Mohamied ATTIA

FINITE ELEMENT STATIC, DYNAMIC, AND FLUTTER ANALYSIS OF ROTATING COMPOSITE LAYERED PLATES AND SHELLS

Supervisor: Dr. A. EL-Zafrany

External Examiner: Professor R. T. Fenner (DSc)

This thesis is submitted in candidature for
the degree of Doctor of Philosophy

February 1996

To the memory of my parents

IHSAN GABALLA RAMADAN

ABD-EL MONIEM MOHAMAD ATTIA

ABSTRACT

This thesis introduces new conforming and non-conforming finite elements for the static and dynamic analysis of rotating composite layered plates and shells. The elements consider parabolic distributions of transverse shear stresses, and based on Lagrangian and Hermitian shape functions. They can deal with variable thickness distributions as well as uniform distributions, and they are fully capable to deal with rotating plate and shell structures, *i.e.* centrifugal stiffening and Coriolis force effects are considered. Natural frequency analysis, forced vibration analysis, and flutter analysis of composite layered plate and shell structures, employing those elements, have been investigated. A computer programming package based on the developed theory was designed, and it is machine independent and user friendly. A modular approach was adopted in the package structure to allow any further development to be considered. Efficient frontal solvers were adopted in the package for different types of analysis. The developed package has been successfully validated on a main frame computer (VAX), Unix workstations, and personal computers. Several case studies were investigated and the results obtained were compared with corresponding published theoretical and/or experimental work. The package has proved to be a very useful tool for the design optimization of composite layered plates and shells by means of using different fibre angles for different layers so as to achieve the required strength and/or stiffness.

ACKNOWLEDGEMENTS

The author owes an enormous debt of gratitude to Dr. A. El-Zafrany, who was a mine of advice and knowledge. His excellent supervision, productive guidance, innovative ideas, and continuous support made completion of this work possible. The author wishes to thank him also for the scientific debate, information, his painstaking attention to detail and accuracy, and his limitless and unconditional hospitality and generosity.

The author wishes to thank Professor R. Elder, Head of the Department of Turbomachinary and Engineering Mechanics, and the members of staff for their support, and encouragement in completing this work.

The author appreciates the support of his friends, Dr. S. A. Fadhil, Mr M. Fawzy, Mr. W. El-Sharawy, and Mr. Mamdouh.

The author is deeply grateful to his sisters Iglal and Afaf, and his brothers Effat, Dr. Attia, Dr. Ahmad, Labieb, and Dr. Nagy for their moral support and inspiration.

Last but by no means least, the author is especially beholden to his wife Shelley for her continuous support, help, and sacrifice which enabled him to finish this work, and he is blessed to have his children Ihsan, Fatimah, and Yumnah for the joy, happiness and love they brought to his life.

LIST OF CONTENTS

LIST OF FIGURES

LIST OF TABLES

LIST OF NOTATIONS

a	Acceleration
$\boldsymbol{B}$	Strain-displacement matrix
$\boldsymbol{C}$	Coriolis pseudo mass matrix
$\boldsymbol{D}$	Material stiffness matrix
E	Young's modulus
$\boldsymbol{F}_o$	Equivalent nodal force vector
h	Plate or shell thickness
$\boldsymbol{J}$	Jacobian matrix
$\boldsymbol{K}$	Stiffness matrix
KE	Kinetic energy
l, m, n	Directional cosines
M_∞	Mach number of free stream flow
$\boldsymbol{M}$	Mass matrix
$\boldsymbol{S}$	Compliance matrix
U	Strain energy
u, v, w	Displacement components in the x, y and z directions, respectively
V_∞	Velocity of free stream flow
x, y, z	Cartesian coordinates
x', y', z'	Material principal axes
γ	Shear strain
$\boldsymbol{\delta}$	Nodal displacement vector
$\boldsymbol{\epsilon}$	Strain vector
θ	Slope angle
μ	Shear modulus
ρ	Density
$\boldsymbol{\sigma}$	Stress vector
υ	Poisson's ratio
Ω	Rotational speed

Some other parameters are defined within the text.

CHAPTER 1

INTRODUCTION

1.1 GENERAL INTRODUCTION

The need for stiffness and strength combined with low density has led designers of military and commercial aircraft, aerospace industry, sports equipment and cars to turn to composite materials. Composites that meet the added requirement of resistance to high temperature are found in jet engine turbine blades and missile nose cones. Wherever advancing technology has created a need for combinations of properties which no single material can provide, composites are becoming the material of choice.

Composites are a strategy for producing advanced materials that take advantage of the enhanced properties of fibres. A bundle of fibres as such, has little structural value. To harness their strength in a practical material, the designer of a composite material embeds them in a matrix of another material. The matrix acts as an adhesive, binding the fibres and lending solidity to the material. It also protects the fibres from environmental stress and physical damage that could initiate cracks.

Composite materials are usually classified within three types; particulate composites which consist of particles of reinforcing material in a matrix such as concrete, fibrous composites which consist of reinforcing fibres in a matrix such as glass or boron fibres in an epoxy matrix, and laminated composites which consist of bonded composite layers.

The type of composite most commonly used in automotive and aircraft structures is the laminated fibrous composites. These involve fibrous composites and the lamination techniques. Layers of fibre reinforced materials are built-up with the fibre direction in each layer oriented in a different direction to give the desired stiffness and strength in the various directions. When the constituent materials in each layer are the same, the laminated layers are called "laminates", but if they are different, the laminates are then said to be "hybrid laminates".

The reinforcing fibres in the fibrous composites should desirably have the following properties:

- high modulus of elasticity to give efficient reinforcement
- high ultimate strength
- low variation of strength between individual fibres
- stability and retention of strength during handling and fabrication
- uniform fibre cross-section.

The matrix is used with the fibres together to form a structural element capable of withstanding loads and is usually required to:

- bind the fibres together
- transfer the loads to the fibres
- stop a crack from propagating straight through a mass of fibres
- be chemically and thermally compatible with the fibres.

The mechanical behaviour of a fibrous composite is also governed, not only by the fibres alone, but by the synergy between the fibres and the matrix. The ultimate tensile strength of a composite is a product of this advantageous combination. For example, when a bundle of fibres, without a surrounding matrix, is stressed, the failure of a single fibre eliminates it as a load carrier. The load carried by that fibre shifts to the remaining intact fibres, moving them closer to failure, but if the fibres are embedded in a matrix, a fibre fracture does not necessarily end the mechanical strength function of the broken fibre. The reason is that matrix materials are usually ductile, and as broken ends of the fibre pull apart, elastic deformation or plastic flow of the matrix exerts shear forces which gradually build stress back into the fragments. The load on the surrounding intact fibres therefore increases less than it would in the absence of the matrix and the load carrying efficiency of the composite is therefore improved.

The basic types of finite elements available in the literature for the analysis of plates and shells are summarized as follows:-

(i) *Kirchhoff-type elements*

These are based upon Kirchhoff's plate-bending theory, in which transverse stresses are ignored, and normals to midplane of the plate before deformation remain normals after deformation. The element interpolation is based upon Hermitian shape functions, where the slope continuity is partially, or fully maintained, and may be called nonconforming or conforming elements according to the fulfilment of that condition. Such elements may be employed for thin plates, but they are not accurate for thick plates.

(ii) *Mindlin-type elements*

These elements are based upon Mindlin's plate-bending theory, in which transverse shear stresses are considered, as average values along the thickness, and normals to the midplane of the plate before deformation are assumed to stay straight lines but they are not necessarily normal to the midplane after deformation. Such elements are based upon Lagrangian shape functions, and suitable for moderately thick plates. Nonetheless, if they are employed for thin plates, they may become over stiff due to the shear locking phenomenon, and an appropriate reduced integration scheme might be invoked.

It is advantageous to have plate-bending finite elements which consider transverse shear stresses based on the parabolic distributions of Reissner (Reissner, 1945), and to make them valid for thin and thick plates, and plates with variable thickness.

1.2 INTEGRITY OF ROTATING TURBOMACHINE BLADES

A vital component in modern gas turbines is turbomachines, which are axial or centrifugal compressors and turbines, and the critical part of a turbomachine is the blades, which are not only subjected to aerodynamic forces, but they are also rotating with very high speeds that generate large inertial forces. Blades are excited, or subjected to forced vibrations, due to fixed wake or stationary flow disturbance excitations, which arise from vanes or spokes (stator blades). As the rotating blades

pass through these wakes the aerodynamic forces are reduced causing the blades to be subjected to pulses, the frequency of which is equal to the number of wakes times the speed of rotation. Wherever this frequency is equal to one of the natural frequencies of the rotating blades, resonance occurs, causing very large amplitudes which may lead to blade failure. Hence, it is essential for the integrity assessment of rotating blades to evaluate their natural frequencies and to be sure that serious resonance will not occur within the operating speed of the blades.

Rotating plate or shell structures usually become stiffer with the increase of the rotational speed, and the inertia forces which act on the rotating structure cause this extra stiffness, which is known as the centrifugal stiffening. The natural frequency is usually increased with the increase of the rotational speed, or with the increase of the centrifugal stiffening. On the other hand, the natural frequency may be decreased with the increase of the generated damping, which is known as the Coriolis effects.

Engineering components such as compressor blades and gas turbine blades are designed nowadays from composite layered materials. It is not easy to find a commercial finite element package with efficient finite elements that can deal with such components.

1.3 FLUTTER PHENOMENON

Aeroelasticity is the study of the effect of aerodynamic forces on elastic bodies, such as aircraft wings or compressor blades. The classical theory of elasticity deals with stress and deformation of an elastic body under prescribed forces or displacements. For such a case, the external loads acting on the elastic body are, in general, independent of the deformation of the body, and it is usually assumed that the deformation is small and has no great effect on the values of the external forces. In the problems associated with bending and buckling of plates and shells, the external loading and the boundary constraints are usually considered as prescribed parameters. However, the situation is quite different when such structures are immersed in high

speed flows, since the generated aerodynamic forces depend fully on the deformed shape of the structure in the flow.

One of the aeroelasticity problems is the stability, or rather the instability, of a structure in a flow. For a given initial shape of an elastic structure, the aerodynamic force increases rapidly with the flow speed, and there may exist a critical flow speed at which the structure becomes unstable. Such instability may cause excessive deformation, and may lead to the destruction of the structure.

The interplay of aerodynamic, elastic, and inertia forces is usually called flutter or dynamic aeroelastic instability. If a structure is excited with an external force in the presence of no flow the structure will oscillate and the oscillation will damp gradually. With the presence of a flow, the rate of damping of the oscillation may increase at low flow speeds, and on increasing the flow speed, a point will be reached at which the damping rapidly decreases, and the oscillation can just maintain itself with a steady amplitude. This speed is known as the critical flutter speed, and at a speed of flow just above that critical speed, a great violent oscillation will be triggered, at any small disturbance to the structure, and the structure is said to flutter.

The full aeroelastic and flutter analysis of a practical aerodynamic engineering component is based on computational fluid dynamics coupled with structural mechanics, and hence it requires enormous computational resources. Simplified analysis may be possible, if the generated aerodynamic forces due to structural deformation can be mathematically modelled, and inserted in a structural analysis procedure.

1.4 OBJECTIVES

The basic objectives of this work are summarized as follows:-

(i) Derivation of new finite elements for static and dynamic analysis of

composite layered plates and shells. The elements will consider parabolic distributions of transverse shear stresses, and based on Lagrangian and Hermitian shape functions so as to be very accurate for a wide range of thickness. Uniform and variable thickness distributions will also be considered.

(ii) The elements will be fully capable to deal with rotating structures, *i.e.* the centrifugal stiffening and Coriolis force effects will be considered.

(iii) The elements will also consider aeroelastic effects for composite layered panels in supersonic flow.

(iv) Static stress analysis, natural frequency analysis, forced vibration analysis, and prediction of resonant frequencies for rotating blades made of composite layered materials, together with flutter analysis aiming at predicting the critical flutter boundary conditions, are to be considered.

(v) A computer programming package, based on the developed theory, will be designed. The package should be machine independent and user friendly. A modular approach should be adopted in the package structure to allow any further development to be considered. Efficient frontal solvers should be included for different types of analysis.

(vi) The developed package should be properly validated and tested on main frame computers (VAX), Unix workstations, and personal computers. Case studies with existing theoretical and/or experimental results, will be employed for package validation.

(vii) Exploring the potential of the package for being a useful tool for the optimum design of plate and shell structures made of composite layered materials.

1.5 SCOPE OF THESIS

Literature review, which covers existing theories on the analysis of plate and shell structures made of composite materials, and flutter analysis of panels in supersonic

flow, is presented in chapter 2, with a summary of the conclusions resulting from the review.

Chapter 3 describes the basic theory for the analysis of composite layered plates and shells, with explanation of the constitutive equations for laminated composite plates and shells.

Chapter 4 gives the details of the original formulations of the finite element equations for the new higher order elements, derived for rotating composite layered plates and shells, and flutter analysis applications.

The finite element analysis techniques are summarized in chapter 5, and the detailed structure of the finite element programming package is given in chapter 6, with coloured illustration of each package module structure.

Chapter 7 is dedicated to the description and discussion of the results of a number of case studies employed for the validation of the package and study of its full potential. The final conclusions and some recommendations for future work are summarized in chapter 8.

CHAPTER 2

LITERATURE REVIEW

2.1 FINITE ELEMENTS OF PLATES AND SHELLS

The stress analysis theories of plate bending problems began as early as the 19th century. Sophie Germain and Lagrange used a mathematical theory in 1811 for the stress analysis of rectangular plates, and some years later many names appeared in this area, such as Navier, Poisson, Cauchy, and Kirchhoff (Todhunter and Pearson, 1986).

Analytical solutions of plate bending problems are limited to cases with simple geometrical shapes, simple loading, and boundary conditions, such as the well-known Navier solution for simply-supported rectangular plates. (Love, 1944 and Timoshenko and Kreiger 1959).

Turner *et al.* (1956) introduced a new method, based upon matrix methods for structural analysis, in which the in-plane plate problems were solved by dividing or discretizing the domain of the plate into sub-domains of triangular shapes. These were known later as the three-node triangular in-plain finite elements, but the first to use finite element terminology was Clough (1960)

Melosh (1963) introduced some basic conditions for the derivation of accurate finite elements, and derived the element stiffness matrix of the 4-node non-conforming rectangular plate bending element. The first conforming rectangular element was developed by Bogner *et al.* (1965). Since then an enormous number of publications dealing with finite element analysis of plates and shells have appeared in the literature.

A large number of finite element text books have been published since the appearance of the finite element method, and many of those contain the details of the basic types of plate bending elements, *i.e.* Kirchhoff and Mindlin elements, such as those by Zienkiewicz (1977), Hinton and Owen (1984), Irons and Ahmed (1980), Cook (1981), El-Zafrany (1994), and many others.

In the field of derivation of different types of shape functions, which are necessary for the finite element technique, El-Zafrany and Cookson (1985) introduced an explicit expression for the one-dimensional Hermitian interpolation problem with arbitrary nodal derivatives, which can be used for the derivation of Hermitian shape functions. Later, El-Zafrany and Cookson (1986b) introduced a general theory for the derivation of quadrilateral finite element shape functions, and the theory can deal with the Lagrangian and Hermitian shape functions for uniform and boundary-described elements. An engineering approach to the derivation of Lagrangian and Hermitian shape functions, was introduced by El-Zafrany and Cookson (1986a), for boundary described triangular elements.

Many publications, which have appeared recently, are dedicated to the derivation of accurate theories and elements for thick plates. A higher-order shear deformation theory of plates was introduced by Reddy (1984a). This theory accounts for the parabolic distribution of the transverse shear strains through the thickness of the plate and predicts deflections, stresses, and frequencies accurately than the first-order theory employed in the derivation of Mindlin elements (Hinton *et al.* 1975).

Basar and Ding (1990) developed a finite-rotation element for the non-linear analysis of thin shell structures via the displacement formulation. This formulation starts from a consistent finite-rotation shell theory, which is transformed by a variational procedure into an incremental formulation. Thus, the geometrical non-linearity can be treated by an incremental-iterative technique. A new plate bending triangular element with discrete constraints has been introduced by Zienkiewicz *et al.* (1990).

A good review of thin shell finite elements and some applications was presented by Yang *et al.* (1990). This was an attempt to review the advances of the formulations for thin shell finite elements in the form of flat plates, axisymmetrical shells and curved shells. The discrete Kirchhoff theory shell elements and the degenerated shell elements were discussed. This survey was further illustrated with some extensions and applications to cases such as static and dynamic responses, static and dynamic

bucklings, laminated composites, random loadings and structural and material properties.

Shi and Voyiadjis (1991) introduced an element which reduced the four-node quadrilateral C^0 plate element to a three-node triangular element automatically. The element formulation is based on the updated Lagrangian formulation, the von Karman assumption and the quasi-conforming element method.

Cofer and Will (1991) introduced a three-dimensional, shell-solid transition element for general nonlinear analysis. This element can connect curved shell elements to isoparametric solid elements, and one of its edges is modelled as a solid face that is compatible with solid elements, while the remaining edges are compatible with eight-node shell elements. Such an element can be used to model complex situations, for example when analysing welded connections.

A higher-order linear theory for isotropic plates was introduced by Blocki (1992). This theory was developed by refining the linear theory of isotropic plates using estimates of the strain field. The accuracy of the strain energy in this theory is of the order $(h/L)^4$ where h is the plate thickness, L is the wave length of the deformation pattern, whereas the plate classical theory has accuracy of the order $(h/L)^2$.

Ramm and Buechter (1992) introduced a comparison study between the shell theory versus degenerated solid approach, and they have shown that both formulations differ only in the kind of discretizations if they are based on the same mechanical assumptions. The other part of their study was concerned with the large rotation formulations for shells, where the formulations were based on purely geometrical considerations.

By using the Ritz method, McGee *et al.* (1992) determined accurate natural frequencies of skewed cantilevered thin plate. The authors of this paper also

presented vibration study for the effects of stress singularities at the reentrant corner of skewed plates.

The approximation between the displacement vector and the finite strain tensor has been analysed by Sacco (1992), and he also proposed a new moderate rotation theory. In his work the non-linear differential equation problem was solved by deriving the governing equations for the beam and the plate problems then an iterative numerical procedure based on the finite element method and the secant stiffness matrix was developed.

Onate *et al.* (1992) re-interpreted the good behaviour of shear constrained Reissner-Mindlin plate elements for thick and thin plate situations and obtained a simple explicit form of the substitute shear strain matrix. This paper just re-formulated some well known quadrilateral plate elements and some triangular plate elements.

Yuqiu and Fei (1992) presented a universal method which can be used to generalize thin plate elements to thick ones without adding any extra degree of freedom. They also constructed a rectangular moderately thick plate element with 12 degrees of freedom.

Zhongnian (1992) introduced a simple triangular finite element for plate bending applications. This element has three nodes with three basic degrees of freedom per node and two internal rotation degrees of freedom.

Gebhardt and Schweizerhof (1993) presented the possible discretization errors when Reissner-Mindlin shell elements with bilinear shape functions are used, and the modifications to prevent such errors. They also discussed the methods to prevent the membrane locking with low order Reissner-Mindlin elements.

A recent paper by Karakostas and Talaslidis (1993) introduced a triangular C bending element. This element avoids coupling of bending and transverse shear and the appearance of excessive shear energy.

2.2 COMPOSITE LAYERED PLATES AND SHELLS

Composite materials have increasingly been accepted as suitable materials in the high-performance but weight-sensitive structures such as space vehicles and automobiles. This is mainly due to the high strength to weight and high stiffness to weight ratios, which is offered by composite materials. Since laminated composites are made of different material layers, material properties are discontinuous through the thickness. The miss-match of the material across the laminate interfaces, bending, stretching and coupling makes the analysis of composite structures very complicated.

There are a number of finite element publications for composite materials reported in the literature, most of which involve the static analysis. Epstein and Huttelmaier (1983) presented a finite element formulation for the analysis of multilayered thick plates, where the transverse shear and normal strains were considered. Widera and Moumene (1984). used an eight-node isoparametric quadrilateral shell element, which included the effect of transverse shear strain, in the analysis of laminated plates and shells.

In the area of dynamic analysis of laminated structures, Has and Wang (1970) presented an analytical approach to the analysis of laminated cylindrical shells. They ignored the Kirchhoff hypothesis of non-deformable normals by including the inertia terms in the equilibrium equations. Witt and Sobczyk (1980), discussed the dynamic response of laminated plates to random loading. Pillasch *et al.*(1983), analysed thick laminated plates with a finite element model based on a three-dimensional element rather than plate theory.

The assumption that displacements are linear functions of z, the coordinate in the thickness direction, has proved to be inadequate for predicting gross laminate

response. Therefore many higher order theories incorporating transverse shear strains have been proposed for better accuracy. Nelson and Lorch (1974), used up to second order terms of z *i.e.* z^2 in their displacement field.

Reddy (1984b, and 1985) introduced a refined nonlinear theory of plates with transverse shear deformation, and a simple higher order theory for laminated composite plates. The deduction of two-dimensional theories from the three-dimensional theories in a transversely isotropic body was presented by Wang (1990). Chomkwah and Avula (1990) presented also a high order theory for laminated composite plates with shear deformation using the Lagrangian multiplier technique. Analytical solutions for displacements and stresses in composite laminates are developed by Barbero *et al.* (1990), using the laminate plate theory of Reddy (1984b).

Chang *et al.* (1990) advanced a Lagrangian formulation for large translation and rotation analysis of deformable rectangular homogeneous plates. They included the coupling effects between bending and stretching, in the finite element analysis of homogeneous plates.

Wung and Reddy (1991) presented a first-order shear/fourth-order transverse deformation theory for laminated composite plates. Kabir (1992) introduced an analytical solution to a moderately thick simply supported rectangular plate, subjected to transverse loads, and his work considered Reissner and Mindlin Theories (Reissner 1945, Mindlin 1951).

A recent theory was introduced by Tessler (1993), who derived a two-dimensional laminated theory for linear elastic analysis of thick composite plates with the equivalent single-layer assumptions for the displacements, transverse shear strain, and transverse normal stress.

Cho and Parmerter (1994) devolved a three-node non-conforming triangular bending element, with five degrees of freedom, for symmetric laminated composites. The derivation of this element is based on a higher order plate theory devolved earlier by the same authors.

With the advances in digital computers, the FEM has become widely used in the analysis of many engineering components. A number of commercial computer packages are widely used nowadays, such as ANSYS, NASTRAN, PAFEC, and ABAQUS. Each of those packages contains several types of elements and performs static, dynamic, and heat transfer analysis for isotropic and composite materials. Some other packages have additional capabilities, *i.e.* preprocessing and postprocessing with graphic tools, such as I-deas. Nevertheless, it was not possible to find any publication or commercial finite element package that can deal with static and dynamic analysis of rotating composite layered plates and shells of variable thickness.

2.3 PANEL FLUTTER

It has been noticed since the second world war that wings and control surfaces of high speed aircraft are most unstable, aeroelastically. Ashley and Zartarian (1956) introduced a method, based upon the piston theory, for calculating the aerodynamic loads on a surface, on which the local pressure generated by the body's motion is related to the local normal component of fluid velocity.

A progress has been made in applying the finite-element techniques to dynamic elastic problems. As early as 1963, Leckie and Lindberg (1963), Archer (1963, 1965), and Argyris (1965) presented a major development in distributing the mass over each element for beam vibration problems. Further applications to plate vibrations have been given by Lindberg (1963), Zienkiewicz and Cheung (1964), Guyan (1965), and Dawe (1965).

Panel flutter is a self-excited oscillation of a plate in supersonic flow. It differs from wing flutter only in that the aerodynamic force resulting from the airflow acts on one side of the panel. The finite element method was first applied to two-dimensional panel flutter by Olson (1967), who showed that only a few elements were required to yield completely satisfactory results. Later the same author (Olson 1970) extended his method to three-dimensional applications using both rectangular and triangular plate bending elements.

Simultaneously but independently, Appa and Somashekar (1969) formulated the aerodynamic matrix for a 12 degrees of freedom rectangular plate element. Appa *et al.* (1970) extended the work to cover skew panels and yawed flow by means of coordinate transformation.

Dowell (1970) reviewed the aeroelastic stability of plates and shells. His work begins with the simplest geometry; flat, unloaded plate, and proceeds to more complicated; the cylindrical shell. In his review an attempt was made to differentiate between what is known beyond a reasonable doubt, what is guessed, and what is unknown, in this subject.

Sander *et al.* (1973) employed a conforming quadrilateral plate finite element for flutter analysis of rectangular panels with yawed flow and in plane stresses. In all of the preceding finite element work the linearized piston theory was employed, and the airflow Mach numbers were above 1.6.

A finite element formulation and a solution procedure were developed by Yang and Sung (1977) for flutter prediction of rectangular panels with one surface exposed to three-dimensional supersonic potential flow. In that work the aerodynamic matrix is based on the numerically computed velocity potentials, and the effect of in-plane forces is included. Rao and Rao (1980) investigated the large-amplitude supersonic flutter of two-dimensional panels with ends elastically restrained against rotation. Dungundji (1986) presented the theoretical considerations of linear panel flutter.

Sarma and Varadan (1988) derived the finite element governing equations for nonlinear panel flutter from energy considerations by using the Lagrangian equation of motion without any approximation. He adopted two solution approaches to solve the nonlinear panel flutter equations. The first approach considers the nonlinear vibration mode as the starting point, whereas the second approach considers the linear panel flutter mode as the starting point.

Recently, Gray *et al.* (1991) extended the finite element method to investigate the limit-cycle oscillations of two-dimensional panels subjected to hypersonic flow described by a third-order piston theory aerodynamics.

A finite element frequency domain method for predicating nonlinear flutter response of panels with temperature effects was presented by Xue and Mei (1993). They formulated the element nonlinear stiffness for a panel under combined thermal and aerodynamic loads from the principle of virtual work, considering von Karman's large deflection plate theory, the first-order piston theory aerodynamics, and the quasisteady thermal stress theory.

Bismarck-Nasr (1993) presented a finite element analysis of the supersonic flutter of cylindrically curved panels based on Reissner's two field variational principle.

As result of their superior strength-to-weight and stiffness-to-weight ratios, as compared with conventional materials, composite materials have been widely used in aeronautical industries. However, to use them efficiently a good understanding of their structural and dynamic behaviour under various loading conditions is needed.

Srinivasan and Babu (1987) investigated the free vibration and flutter of laminated quadrilateral plates with clamped edges. In this paper the differential equation of motion was solved by the use of an integral equation technique.

Shiau and Chang (1991) employed the finite element method to study the flutter characteristics of composite panels on multiple supports.

Lee and Cho (1991) analysed the flutter phenomena for a composite plate in supersonic flow by the finite element method, and their analysis was based on the shear deformable theory. They also obtained the effects of the geometrical shape, the flow direction, and the fibre orientation on the flutter boundaries for trapezoidal composite plates with simply supported and clamped edges.

Namini (1991) developed two elements for finite element modelling; the first element formulation was developed with shape functions identical to those used for a three-dimensional space frame element, and the second element had a lumped formulation, which simply assigns one-half of the overall load to each member end.

Jacquet-Richardet and Henry (1994) presented a general coupling formulation suitable for the flutter analysis of rotating blades. The aeroelastic displacements written as a linear combination of a number of undamped modes leading to a complex eigenvalues eigenvectors problem. In this work the blade dynamic displacements were modelled by using the finite element method.

There are a number of text books useful for the study of the governing equations of aeroelasticity and flutter, such as Fung (1955), Bisplinghoff *et al.* (1955), Bisplinghoff and Ashley (1962), Dowell (1975), Dowell *et al.* (1978), and Dowell and Ilgamov (1988).

2.4 CONCLUDING REMARKS

Important remarks have been ascertained from the literature search, and they are summarised next:-

- There is an enormous amount of publications dealing with linear and non-linear static and dynamic analysis of thin and thick isotropic and composite layered plates and shells. Nevertheless, to the best of the author's knowledge there is no element in the literature, which can deal efficiently with the static and dynamic analysis of rotating plate and shell structures made of composite layered materials, *i.e.* considers the centrifugal stiffening, and Coriolis force effects, and deals accurately with thin and thick structures as such.

- The simplified piston theory is up to now the main source for modelling the governing equations of aeroelastic effects for panels placed in supersonic flow.

- Conforming finite elements are more accurate than non-conforming elements for the analysis of panel flutter.

CHAPTER 3

BASIC THEORY FOR THE ANALYSIS OF COMPOSITE LAYERED PLATES AND SHELLS

3.1 STRESS-STRAIN EQUATIONS FOR COMPOSITE LAYERED PLATES AND SHELLS

A composite layered plate or shell usually consists of a number of layers (N_l) bonded firmly with each other. Each layer is a lamina and it is flat for plates and curved for shells, and it represents an assemblage of reinforcing fibres in a supporting isotropic matrix. From a macroscopic scale, the layer is considered homogeneous and orthotropic. The material properties of the layer are defined with respect to the material principal axes $x^{\backprime}$, $y^{\backprime}$, $z^{\backprime}$ such that :

- The $z^{\backprime}$ axis is normal to the midsurface of the layer.
- The $x^{\backprime}$, $y^{\backprime}$ axes are normal to the $z^{\backprime}$ axis, in another word they are in the midplane of the layer in case of plates and tangential to the midsurface of the layer in case of shells.

The material properties which are required for an elastic analysis are:-

$E_x^{\backprime}$, $E_y^{\backprime}$, $E_z^{\backprime}$	Young's moduli in the $x^{\backprime}$, $y^{\backprime}$, $z^{\backprime}$ directions respectively.
$\nu_{xy}^{\backprime}$, $\nu_{yz}^{\backprime}$, $\nu_{zx}^{\backprime}$	Poisson's ratios, with respect to $x^{\backprime}$, $y^{\backprime}$, $z^{\backprime}$ axes.
$\mu_{xy}^{\backprime}$, $\mu_{yz}^{\backprime}$, $\mu_{zx}^{\backprime}$	Shear moduli, with respect to $x^{\backprime}$, $y^{\backprime}$, $z^{\backprime}$ axes.

The stress and strain states at any point inside a layer may be defined in terms of the following engineering stress and strain vectors:-

$$\boldsymbol{\sigma} = \{\sigma_x \quad \sigma_y \quad \sigma_z \quad \tau_{xy} \quad \tau_{yz} \quad \tau_{zx}\} \tag{3.1}$$

$$\boldsymbol{\epsilon} = \{\epsilon_x \quad \epsilon_y \quad \epsilon_z \quad \gamma_{xy} \quad \gamma_{yz} \quad \gamma_{zx}\} \tag{3.2}$$

and for an orthotropic layer, the elastic stress-strain equations may be expressed in the following matrix form:-

$$\boldsymbol{\epsilon}^{\backprime} = \boldsymbol{C}^{\backprime}\, \boldsymbol{\sigma}^{\backprime} \tag{3.3}$$

and

$$\boldsymbol{\sigma}^{\backprime} = \boldsymbol{D}^{\backprime}\, \boldsymbol{\epsilon}^{\backprime} \tag{3.4}$$

where

$$\boldsymbol{D}^{\backprime} = \boldsymbol{C}^{\backprime -1} \tag{3.5}$$

$$\text{and} \qquad \boldsymbol{C}^{\backprime} = \begin{bmatrix} \frac{1}{E_x^{\backprime}} & -\frac{\nu_{xy}^{\backprime}}{E_y^{\backprime}} & -\frac{\nu_{xz}^{\backprime}}{E_z^{\backprime}} & 0 & 0 & 0 \\ -\frac{\nu_{yx}^{\backprime}}{E_x^{\backprime}} & \frac{1}{E_y^{\backprime}} & -\frac{\nu_{yz}^{\backprime}}{E_z^{\backprime}} & 0 & 0 & 0 \\ -\frac{\nu_{zx}^{\backprime}}{E_x^{\backprime}} & -\frac{\nu_{zy}^{\backprime}}{E_y^{\backprime}} & \frac{1}{E_z^{\backprime}} & 0 & 0 & 0 \\ o & o & o & \frac{1}{\mu_{xy}^{\backprime}} & o & o \\ o & o & o & o & \frac{1}{\mu_{yz}^{\backprime}} & o \\ o & o & o & o & o & \frac{1}{\mu_{zx}^{\backprime}} \end{bmatrix} \tag{3.6}$$

where $(\ )^{\backprime}$ refers to properties measured with respect to $x^{\backprime}$, $y^{\backprime}$, $z^{\backprime}$ axes, and from the symmetry of the $\boldsymbol{C}^{\backprime}$ matrix it can be deduced that:-

$$\frac{\nu_{xy}^{\backprime}}{E_y^{\backprime}} = \frac{\nu_{yx}^{\backprime}}{E_x^{\backprime}}, \qquad \frac{\nu_{xz}^{\backprime}}{E_z^{\backprime}} = \frac{\nu_{zx}^{\backprime}}{E_x^{\backprime}}, \qquad \frac{\nu_{yz}^{\backprime}}{E_z^{\backprime}} = \frac{\nu_{zy}^{\backprime}}{E_y^{\backprime}}$$

Using minors and cofactors the $\boldsymbol{C}^{\backprime}$ matrix can be inverted, resulting in the following $\boldsymbol{D}^{\backprime}$ matrix:-

$$\boldsymbol{D}^{\backprime} = \left[\begin{array}{c|ccc} \boldsymbol{d}^{\backprime}_{3\times 3} & \multicolumn{3}{c}{\mathbf{O}_{3\times 3}} \\ \hline & \mu_{xy}^{\backprime} & 0 & 0 \\ \mathbf{O}_{3\times 3} & 0 & \mu_{yz}^{\backprime} & 0 \\ & 0 & 0 & \mu_{zx}^{\backprime} \end{array}\right] \tag{3.7}$$

where $$\boldsymbol{d}^{\backprime}_{3\times 3} = \frac{1}{Q}\begin{bmatrix} E^{\backprime}_x(1-\nu^{\backprime}_{yz}\nu_{zy}) & E^{\backprime}_x(\nu_{xy}+\nu_{xz}\nu_{zy}) & E^{\backprime}_x(\nu_{xz}+\nu_{xy}\nu_{yz}) \\ E^{\backprime}_y(\nu^{\backprime}_{yx}+\nu^{\backprime}_{yz}\nu^{\backprime}_{zx}) & E_y(1-\nu^{\backprime}_{xz}\nu_{zx}) & E_y(\nu^{\backprime}_{yz}+\nu^{\backprime}_{yx}\nu_{xz}) \\ E^{\backprime}_z(\nu^{\backprime}_{zx}+\nu^{\backprime}_{zy}\nu^{\backprime}_{yx}) & E^{\backprime}_z(\nu^{\backprime}_{zy}+\nu^{\backprime}_{zx}\nu^{\backprime}_{xy}) & E^{\backprime}_z(1-\nu^{\backprime}_{xy}\nu^{\backprime}_{yx}) \end{bmatrix}$$

and $$Q = 1-\nu^{\backprime}_{xy}\nu^{\backprime}_{yx}-\nu^{\backprime}_{yz}\nu^{\backprime}_{zy}-\nu^{\backprime}_{zx}\nu^{\backprime}_{xz}-\nu^{\backprime}_{xy}\nu^{\backprime}_{yz}\nu^{\backprime}_{zx}-\nu^{\backprime}_{xz}\nu^{\backprime}_{zy}\nu^{\backprime}_{yx}$$

Generally the layers of composite plates or shells are made of the same material, but each lamina (layer) has its fibres placed in a different angle, *i.e.* each layer l will have different $x^{\backprime}$, $y^{\backprime}$ axes, rotated by an angle θ_l from the global x, y, z axes as illustrated in Fig. (3.1). For the case of plates, the global z axis is always normal to the midplane of the layer and in the direction of the material $z^{\backprime}$ axis, and it is advantageous to define the material axes with respect to the global axes in terms of the angle θ_l.

Defining $\hat{i}, \hat{j}, \hat{k}$ as unit vectors in the direction of the global axes x, y, z and $\hat{i}^{\backprime}, \hat{j}^{\backprime}, \hat{k}^{\backprime}$ as the unit vectors in the direction of the local $x^{\backprime}$, $y^{\backprime}$, $z^{\backprime}$ axes of layer l, therefore the directional cosines of the material axes with respect to the global (geometrical) axes are presented in the following matrix equation:-

$$\begin{bmatrix} \hat{i}^{\backprime} \\ \hat{j}^{\backprime} \\ \hat{k}^{\backprime} \end{bmatrix} = \boldsymbol{R}_l \begin{bmatrix} \hat{i} \\ \hat{j} \\ \hat{k} \end{bmatrix} \qquad (3.8)$$

where
$$\boldsymbol{R}_l = \begin{bmatrix} m & n & 0 \\ -n & m & 0 \\ 0 & 0 & 1 \end{bmatrix}$$

and
$$m = \cos\theta_l , \quad n = \sin\theta_l$$

By using the stress-rotation equations (El-Zafrany,1995), the stress vector with respect to the local axes can be expressed in terms of the stress vector with respect to the global axes as follows:-

$$\boldsymbol{\sigma}' = \boldsymbol{R}_\sigma \, \boldsymbol{\sigma} \tag{3.9}$$

$$\boldsymbol{R}_\sigma = \begin{bmatrix} m^2 & n^2 & 0 & 2mn & 0 & 0 \\ n^2 & m^2 & 0 & -2mn & 0 & 0 \\ 0 & 0 & 1 & 0 & 0 & 0 \\ -mn & mn & 0 & m^2-n^2 & 0 & 0 \\ 0 & 0 & 0 & 0 & m & -n \\ 0 & 0 & 0 & 0 & n & m \end{bmatrix} \tag{3.10}$$

and it can be deduced that:-

$$\boldsymbol{\sigma} = \boldsymbol{R}_\sigma^{-1} \, \boldsymbol{\sigma}' \tag{3.11}$$

which can be obtained as a special case of equation (3.9) with the axes rotated by $-\theta_l$, *i.e.*:-

$$\boldsymbol{R}_\sigma^{-1} = \begin{bmatrix} m^2 & n^2 & 0 & -2mn & 0 & 0 \\ n^2 & m^2 & 0 & 2mn & 0 & 0 \\ 0 & 0 & 1 & 0 & 0 & 0 \\ mn & -mn & 0 & m^2-n^2 & 0 & 0 \\ 0 & 0 & 0 & 0 & m & n \\ 0 & 0 & 0 & 0 & -n & m \end{bmatrix} \tag{3.12}$$

Similarly the strain vectors can also be derived in the same way, *i.e.*:-

$$\boldsymbol{\epsilon}' = \boldsymbol{R}_\epsilon \, \boldsymbol{\epsilon} \tag{3.13}$$

$$\boldsymbol{\epsilon} = \boldsymbol{R}_\epsilon^{-1} \, \boldsymbol{\epsilon}' \tag{3.14}$$

where $$\boldsymbol{R}_{\epsilon} = \begin{bmatrix} m^2 & n^2 & 0 & mn & 0 & 0 \\ n^2 & m^2 & 0 & -mn & 0 & 0 \\ 0 & 0 & 1 & 0 & 0 & 0 \\ -2mn & 2mn & 0 & m^2 - n^2 & 0 & 0 \\ 0 & 0 & 0 & 0 & m & -n \\ 0 & 0 & 0 & 0 & n & m \end{bmatrix} \qquad (3.15)$$

and $$\boldsymbol{R}_{\epsilon}^{-1} = \begin{bmatrix} m^2 & n^2 & 0 & -mn & 0 & 0 \\ n^2 & m^2 & 0 & mn & 0 & 0 \\ 0 & 0 & 1 & 0 & 0 & 0 \\ 2mn & -2mn & 0 & m^2 - n^2 & 0 & 0 \\ 0 & 0 & 0 & 0 & m & n \\ 0 & 0 & 0 & 0 & -n & m \end{bmatrix} \qquad (3.16)$$

The stress-strain equations with respect to global axes can be expressed as follows:-

$$\boldsymbol{\sigma} = \boldsymbol{D}\ \boldsymbol{\epsilon} \qquad (3.17)$$

Substituting from Equation (3.9) and (3.13) into (3.4) then

$$\boldsymbol{R}_{\sigma}\ \boldsymbol{\sigma} = \boldsymbol{D}`\ \boldsymbol{R}_{\epsilon}\ \boldsymbol{\epsilon}$$

i.e. $$\boldsymbol{\sigma} = \left(\boldsymbol{R}_{\sigma}^{-1}\ \boldsymbol{D}`\ \boldsymbol{R}_{\epsilon}\right)\boldsymbol{\epsilon} \qquad (3.18)$$

Comparing Equation (3.18) with (3.17) it can be deduced that

$$\boldsymbol{D} = \boldsymbol{R}_{\sigma}^{-1}\ \boldsymbol{D}`\ \boldsymbol{R}_{\epsilon} \qquad (3.19)$$

which can be expanded in the following form:-

$$d_{11} = m^4 d_{11}` + n^4 d_{22}` + 2m^2n^2(d_{12}` + 2d_{44}`)$$

$$d_{22} = n^4 d_{11}` + m^4 d_{22}` + 2m^2n^2(d_{12}` + 2d_{44}`)$$

$$d_{12} = m^2n^2(d_{11}` + d_{22}`) + (m^4 + n^4)d_{12}` - 4m^2n^2 d_{44}`$$

$$d_{13} = m^2 d_{13}` + n^2 d_{23}`$$

$$d_{23} = n^2 d_{13}^{\backprime} + m^2 d_{23}^{\backprime}$$

$$d_{14} = -mn\left[n^2 d_{22}^{\backprime} - m^2 d_{11}^{\backprime} + (m^2 - n^2)(d_{12} + 2d_{44})\right]$$

$$d_{24} = -mn\left[m^2 d_{22} - n^2 d_{11}^{\backprime} + (n^2 - m^2)(d_{12} + 2d_{44})\right]$$

$$d_{15} = d_{16} = d_{25} = d_{26} = 0$$

$$d_{33} = d_{33}^{\backprime}$$

$$d_{34} = -mn(d_{23}^{\backprime} - d_{13}^{\backprime})$$

$$d_{44} = m^2 n^2 (d_{11} + d_{22}^{\backprime} - 2d_{12}) + (m^2 - n^2)^2 d_{44}$$

$$d_{35} = d_{36} = d_{45} = d_{46} = 0$$

$$d_{55} = m^2 d_{55}^{\backprime} + n^2 d_{66}^{\backprime}$$

$$d_{66} = n^2 d_{55}^{\backprime} + m^2 d_{66}^{\backprime}$$

$$d_{56} = -mn(d_{55}^{\backprime} - d_{66})$$

and $$d_{ji} = d_{ij}$$

Hence

$$\boldsymbol{D} = \begin{bmatrix} d_{11} & d_{12} & d_{13} & d_{14} & 0 & 0 \\ & d_{22} & d_{23} & d_{24} & 0 & 0 \\ & & d_{33} & d_{34} & 0 & 0 \\ & & & d_{44} & 0 & 0 \\ & symm. & & & d_{55} & d_{56} \\ & & & & & d_{66} \end{bmatrix} \qquad (3.20)$$

The transverse shear stress and strain vectors are defined as follows:-

$$\boldsymbol{\tau} = \{\, \tau_{xz} \quad \tau_{yz} \,\} \qquad (3.21)$$

$$\boldsymbol{\gamma} = \{ \gamma_{xz} \quad \gamma_{yz} \} \tag{3.22}$$

then it is clear from Equation (3.17) that:-

$$\boldsymbol{\tau} = \boldsymbol{\mu}_{2\times 2} \quad \boldsymbol{\gamma} \tag{3.23}$$

where

$$\boldsymbol{\mu}_{2\times 2} = \begin{bmatrix} d_{55} & d_{56} \\ d_{65} & d_{66} \end{bmatrix} \tag{3.24}$$

If σ_z is negligible then:-

$$\sigma_z = d_{31}\,\epsilon_x + d_{32}\,\epsilon_y + d_{34}\,\epsilon_{xy} + d_{33}\,\epsilon_z \approx 0$$

i.e.

$$\epsilon_z = \frac{1}{d_{33}} \left(d_{31}\,\epsilon_x + d'_{32}\,\epsilon_y + d_{34}\,\epsilon_{xy} \right) \tag{3.25}$$

Defining

$$\boldsymbol{\sigma}_{xy} = \{ \sigma_x \quad \sigma_y \quad \tau_{xy} \} \tag{3.26}$$

and

$$\boldsymbol{\epsilon}_{xy} = \{ \epsilon_x \quad \epsilon_y \quad \gamma_{xy} \} \tag{3.27}$$

hence it can be deduced from Equations (3.17), (3.20), (3.25) that:-

$$\boldsymbol{\sigma}_{xy} = \boldsymbol{D}_{xy} \quad \boldsymbol{\epsilon}_{xy} \tag{3.28}$$

where

$$\boldsymbol{D}_{xy} = \begin{bmatrix} d_{11} - \dfrac{d_{13}\,d_{31}}{d_{33}} & d_{12} - \dfrac{d_{13}\,d_{32}}{d_{33}} & d_{14} - \dfrac{d_{13}\,d_{34}}{d_{33}} \\ d_{21} - \dfrac{d_{23}\,d_{31}}{d_{33}} & d_{22} - \dfrac{d_{23}\,d_{32}}{d_{33}} & d_{24} - \dfrac{d_{23}\,d_{34}}{d_{33}} \\ d_{41} - \dfrac{d_{43}\,d_{31}}{d_{33}} & d_{42} - \dfrac{d_{43}\,d_{32}}{d_{33}} & d_{44} - \dfrac{d_{43}\,d_{34}}{d_{33}} \end{bmatrix}$$

3.2 DEFORMATION AND STRAIN

3.2.1 Transverse strain modelling

Consider a composite layered plate, at an instant of time *t* consisting of a number of orthotropic layers N_l , as shown in Fig. (3.1). Let the midplane of the plate be the cartesian *x*-*y* plane, and the total thickness at any point *(x,y)* on the midplane is *h(x,y)*. The upper surface of the plate *(z = h/2)* may be subjected to a shear force per

unit area $q_u(x,y)$ and the lower surface ($z = - h/2$) subjected to a shear force per unit area $q_l(x,y)$. The boundary conditions at the lower and upper surfaces of the plate are

at $z = - h/2$ $\qquad \tau_{xz} = \tau_{yz} = 0, \qquad \sigma_z = - q_l$ (3.29)

at $z = h/2$ $\qquad \tau_{xz} = \tau_{yz} = 0, \qquad \sigma_z = q_u$ (3.30)

and from Equation (3.23) we can prove that:-

at $z = \pm h/2$ $\qquad \gamma_{xz} = \gamma_{yz} = 0$ (3.31)

If the values of $\gamma^{\circ}_{xz}(x, y, t)$ and $\gamma^{\circ}_{yz}(x, y, t)$ represent the transverse shear strains at the midplane, then the following values of transverse shear strains are defined as follows:-

at $z_1 = - h/2$ $\qquad \gamma_{xz} = \gamma_{yz} = 0$

at $z_2 = 0$ $\qquad \gamma_{xz} = \gamma^{\circ}_{xz}$ and $\gamma_{yz} = \gamma^{\circ}_{yz}$

at $z_3 = h/2$ $\qquad \gamma_{xz} = \gamma_{yz} = 0$

The composite layers are considered to be firmly bonded together, hence the distribution of displacement components represent continuous functions with respect to the z-direction. Since the components of ϵ_{xy} do not contain partial derivatives of displacement components with respect to z, then it is clear that ϵ_{xy} should be continuous with respect to z.

Considering infinitesimal transverse shear strains

$$\gamma_{xz} = \frac{\partial u}{\partial z} + \frac{\partial w}{\partial x} \tag{3.32}$$

$$\gamma_{yz} = \frac{\partial v}{\partial z} + \frac{\partial w}{\partial y} \tag{3.33}$$

and for negligible transverse shear strains

$$\frac{\partial u}{\partial z} \approx - \frac{\partial w}{\partial x} \tag{3.34}$$

$$\frac{\partial v}{\partial z} \approx -\frac{\partial w}{\partial y} \tag{3.35}$$

which lead to $\frac{\partial u}{\partial z}$ and $\frac{\partial v}{\partial z}$ being defined in terms of z-continuous functions. Since the magnitude of transverse shear strains are expected to be much lower than the magnitudes of $\frac{\partial w}{\partial x}$ and $\frac{\partial w}{\partial y}$, we shall consider $\frac{\partial u}{\partial z}$ and $\frac{\partial v}{\partial z}$ always continuous with respect to z, *i.e.* the transverse shear strains will be assumed to be continuous functions with respect to z. Hence, the distributions of the transverse shear strains across the plate thickness can be deduced by applying Lagrangian interpolation to the values of transverse shear strains listed above, *i.e.*

$$\left.\begin{aligned} \gamma_{xz}(x,y,z,t) &= \frac{(z-z_1)(z-z_3)}{(z_2-z_1)(z_2-z_3)}\,\gamma^{\circ}_{xz}(x,y,t) \\ &\equiv \gamma^{\circ}_{xz}(x,y,t)\left[1-\left(\frac{z}{h/2}\right)^2\right] \end{aligned}\right\} \tag{3.36}$$

similarly $$\gamma_{yz}(x,y,z,t) = \gamma^{\circ}_{yz}(x,y,t)\left[1-\left(\frac{z}{h/2}\right)^2\right] \tag{3.37}$$

and it is useful to mention that in this work the transverse normal stress σ_z will be considered negligible.

3.2.2 Displacement and velocity components

Substituting from Equation (3.36) and (3.37) into (3.32) and (3.33) then:-

$$\frac{\partial u}{\partial z} = -\frac{\partial w}{\partial x} + \gamma^{\circ}_{xz}(x,y,t)\left[1-\left(\frac{z}{h/2}\right)^2\right] \tag{3.38}$$

$$\frac{\partial v}{\partial z} = -\frac{\partial w}{\partial y} + \gamma^{\circ}_{yz}(x,y,t)\left[1-\left(\frac{z}{h/2}\right)^2\right] \tag{3.39}$$

The lateral deflection w can be obtained in terms of a Taylor expansion with respect to z as follows:-

$$\left.\begin{aligned} w(x,y,z,t) &= w_{\circ}(x,y,t) + z\,w_1(x,y,t) - \frac{z^2}{2!}\,w_2(x,y,t) \\ &\quad + \cdots + \frac{z^n}{n!}\,w_n(x,y,t) \end{aligned}\right\} \quad (3.40)$$

where $w_{\circ}(x,y,t)$ is the value of w at $z = 0$

and $w_i(x,y,t) = \dfrac{\partial^i w}{\partial z^i}$ at $z = 0$

Substituting from Equation (3.40) into (3.38) and (3.39) then

$$\frac{\partial u}{\partial z} = -\sum_{i=0}^{n} \frac{z^i}{i!}\,\frac{\partial w_i}{\partial x} + \gamma^{\circ}_{xz}(x,y,t)\left[1 - \left(\frac{z}{h/2}\right)^2\right] \quad (3.41)$$

$$\frac{\partial v}{\partial z} = -\sum_{i=0}^{n} \frac{z^i}{i!}\,\frac{\partial w_i}{\partial y} + \gamma^{\circ}_{yz}(x,y,t)\left[1 - \left(\frac{z}{h/2}\right)^2\right] \quad (3.42)$$

and by integrating Equations (3.41) and (3.42) with respect to z, we get

$$u(x,y,z,t) = u_{\circ}(x,y,t) - \sum_{i=0}^{n} \frac{z^{i+1}}{(i+1)\,i!}\,\frac{\partial w_i}{\partial x} + \gamma^{\circ}_{xz}(x,y,t)\left[z - \frac{4z^3}{3h^2}\right] \quad (3.43)$$

$$v(x,y,z,t) = v_{\circ}(x,y,t) - \sum_{i=0}^{n} \frac{z^{i+1}}{(i+1)\,i!}\,\frac{\partial w_i}{\partial y} + \gamma^{\circ}_{yz}(x,y,t)\left[z - \frac{4z^3}{3h^2}\right] \quad (3.44)$$

where $u_{\circ}$ and $v_{\circ}$ represent the values of u and v at $z = 0$.

The lateral deflection w will be approximated in this work, such that it will be considered independent of z, *i.e.*

$$w(x,y,z,t) \cong w_{\circ}(x,y,t) \quad (3.45)$$

Hence, Equations (3.43) and (3.44) can be simplified as follows:-

$$u(x,y,z,t) = u_{\circ}(x,y,t) - z\,\frac{\partial w_{\circ}}{\partial x} + \gamma^{\circ}_{xz}(x,y,t)\left[z - \frac{4z^3}{3h^2}\right] \quad (3.46)$$

$$v(x,y,z,t) = v_{\circ}(x,y,t) - z\,\frac{\partial w_{\circ}}{\partial y} + \gamma^{\circ}_{yz}(x,y,t)\left[z - \frac{4z^3}{3h^2}\right] \quad (3.47)$$

The corresponding velocity components can be obtained by differentiating Equations (3.46), (3.47) and (3.45) with respect to time, *i.e.*

$$\dot{u}(x,y,z,t) = \dot{u}_\circ - z\frac{\partial \dot{w}_\circ}{\partial x} + \dot{\gamma}^\circ_{xz}\left(z - \frac{4z^3}{3h^2}\right) \tag{3.48}$$

$$\dot{v}(x,y,z,t) = \dot{v}_\circ - z\frac{\partial \dot{w}_\circ}{\partial y} + \dot{\gamma}^\circ_{yz}\left(z - \frac{4z^3}{3h^2}\right) \tag{3.49}$$

$$\dot{w}(x,y,z,t) = \dot{w}_\circ(x,y,t) \tag{3.50}$$

where $\dot{f} = \dfrac{\partial f}{\partial t}$.

3.2.3 Strain components

The x-y strain components will be considered finite and by using a Lagrangian frame of reference, they can be expressed in terms of displacement components (El-Zafrany,1995) as follows:-

$$\epsilon_x = \frac{\partial u}{\partial x} + \frac{1}{2}\left[\left(\frac{\partial u}{\partial x}\right)^2 + \left(\frac{\partial v}{\partial x}\right)^2 + \left(\frac{\partial w}{\partial x}\right)^2\right] \tag{3.51}$$

$$\epsilon_y = \frac{\partial v}{\partial y} + \frac{1}{2}\left[\left(\frac{\partial u}{\partial y}\right)^2 + \left(\frac{\partial v}{\partial y}\right)^2 + \left(\frac{\partial w}{\partial y}\right)^2\right] \tag{3.52}$$

$$\gamma_{xy} = \frac{\partial u}{\partial y} + \frac{\partial v}{\partial x} + \left(\frac{\partial u}{\partial x}\frac{\partial u}{\partial y} + \frac{\partial v}{\partial x}\frac{\partial v}{\partial y} + \frac{\partial w}{\partial x}\frac{\partial w}{\partial y}\right) \tag{3.53}$$

i.e. $\boldsymbol{\epsilon}_{xy} = \boldsymbol{\epsilon}_{inf} + \boldsymbol{\epsilon}_L$

where $$\boldsymbol{\epsilon}_{inf} = \begin{bmatrix} \dfrac{\partial u}{\partial x} \\ \dfrac{\partial v}{\partial y} \\ \dfrac{\partial u}{\partial y} + \dfrac{\partial v}{\partial x} \end{bmatrix} \tag{3.54}$$

which represents the infinitesimal terms, and

$$\epsilon_L = \begin{bmatrix} \frac{1}{2}\left(\frac{\partial u}{\partial x}\right)^2 + \frac{1}{2}\left(\frac{\partial v}{\partial x}\right)^2 + \frac{1}{2}\left(\frac{\partial w}{\partial x}\right)^2 \\ \frac{1}{2}\left(\frac{\partial u}{\partial y}\right)^2 + \frac{1}{2}\left(\frac{\partial v}{\partial y}\right)^2 + \frac{1}{2}\left(\frac{\partial w}{\partial y}\right)^2 \\ \frac{\partial u}{\partial x}\frac{\partial u}{\partial y} + \frac{\partial v}{\partial x}\frac{\partial v}{\partial y} + \frac{\partial w}{\partial x}\frac{\partial w}{\partial y} \end{bmatrix} \qquad (3.55)$$

So it is clear from Equations (3.46) and (3.47) that

$$\frac{\partial u}{\partial x} = \frac{\partial u_\circ}{\partial x} - z\frac{\partial^2 w_\circ}{\partial x^2} + f_1(z)\frac{\partial \gamma^\circ_{xz}}{\partial x} \qquad (3.56a)$$

$$\frac{\partial u}{\partial y} = \frac{\partial u_\circ}{\partial y} - z\frac{\partial^2 w_\circ}{\partial y\,\partial x} + f_1(z)\frac{\partial \gamma^\circ_{xz}}{\partial y} \qquad (3.56b)$$

$$\frac{\partial v}{\partial x} = \frac{\partial v_\circ}{\partial x} - z\frac{\partial^2 w_\circ}{\partial x\,\partial y} + f_1(z)\frac{\partial \gamma^\circ_{yz}}{\partial x} \qquad (3.56c)$$

$$\frac{\partial v}{\partial y} = \frac{\partial v_\circ}{\partial y} - z\frac{\partial^2 w_\circ}{\partial y^2} + f_1(z)\frac{\partial \gamma^\circ_{yz}}{\partial y} \qquad (3.56d)$$

where
$$f_1(z) = z - \frac{4z^3}{3h^2} \qquad (3.57)$$

Hence, the infinitesimal strain vector can be expressed as follows:-

$$\epsilon_{inf}(x,y,z,t) = \epsilon_m(x,y,t) - z\,\epsilon_b(x,y,t) + f_1(z)\,\epsilon_s(x,y,t) \qquad (3.58)$$

where
$$\epsilon_m(x,y,t) = \begin{bmatrix} \frac{\partial u_\circ}{\partial x} \\ \frac{\partial v_\circ}{\partial y} \\ \frac{\partial u}{\partial y} + \frac{\partial v_\circ}{\partial x} \end{bmatrix} \qquad (3.59)$$

$$\epsilon_b(x,y,t) = \begin{bmatrix} \dfrac{\partial^2 w_\circ}{\partial x^2} \\ \dfrac{\partial^2 w_\circ}{\partial y^2} \\ 2\,\dfrac{\partial^2 w_\circ}{\partial x\,\partial y} \end{bmatrix} \tag{3.60}$$

$$\epsilon_s(x,y,t) = \begin{bmatrix} \dfrac{\partial \gamma^\circ_{xz}}{\partial x} \\ \dfrac{\partial \gamma^\circ_{yz}}{\partial y} \\ \dfrac{\partial \gamma^\circ_{xz}}{\partial y} + \dfrac{\partial \gamma^\circ_{yz}}{\partial x} \end{bmatrix} \tag{3.61}$$

The finite strain contributions are

$$\epsilon_x^L = \frac{1}{2}\left[\left(\frac{\partial u}{\partial x}\right)^2 + \left(\frac{\partial v}{\partial x}\right)^2 + \left(\frac{\partial w}{\partial x}\right)^2\right] \tag{3.62a}$$

$$\epsilon_y^L = \frac{1}{2}\left[\left(\frac{\partial u}{\partial y}\right)^2 + \left(\frac{\partial v}{\partial y}\right)^2 + \left(\frac{\partial w}{\partial y}\right)^2\right] \tag{3.62b}$$

$$\gamma_{xy}^L = \frac{\partial u}{\partial x}\frac{\partial u}{\partial y} + \frac{\partial v}{\partial x}\frac{\partial v}{\partial y} + \frac{\partial w}{\partial x}\frac{\partial w}{\partial y} \tag{3.62c}$$

Substituting from Equations (3.56a), (3.56b), (3.56c) and (3.56d) into (3.62a), (3.62b) and (3.62c) it can be proved that:-

$$\begin{aligned} \epsilon_x^L = \frac{1}{2}\Bigg\{ & \left[\left(\frac{\partial u_\circ}{\partial x}\right)^2 + \left(\frac{\partial v_\circ}{\partial x}\right)^2 + \left(\frac{\partial w_\circ}{\partial x}\right)^2\right] + z^2\left[\left(\frac{\partial^2 w_\circ}{\partial x^2}\right)^2 + \left(\frac{\partial^2 w_\circ}{\partial x\,\partial y}\right)^2\right] \\ & + f_1^2(z)\left[\left(\frac{\partial \gamma^\circ_{xz}}{\partial x}\right)^2 + \left(\frac{\partial \gamma^\circ_{yz}}{\partial x}\right)^2\right] - 2z\left(\frac{\partial u}{\partial x}\frac{\partial^2 w_\circ}{\partial x^2} + \frac{\partial v_\circ}{\partial x}\frac{\partial^2 w_\circ}{\partial x\,\partial y}\right) \qquad \cdots \\ & - 2z f_1(z)\left(\frac{\partial \gamma^\circ_{xz}}{\partial x}\frac{\partial^2 w_\circ}{\partial x^2} + \frac{\partial \gamma^\circ_{yz}}{\partial x}\frac{\partial^2 w_\circ}{\partial x\,\partial y}\right) + 2 f_1(z)\left(\frac{\partial u}{\partial x}\frac{\partial \gamma^\circ_{xz}}{\partial x} + \frac{\partial v}{\partial x}\frac{\partial \gamma^\circ_{yz}}{\partial x}\right)\Bigg\} \end{aligned} \tag{3.63a}$$

$$\epsilon_y^L = \frac{1}{2}\left\{\left[\left(\frac{\partial u_\circ}{\partial y}\right)^2 + \left(\frac{\partial v_\circ}{\partial y}\right)^2 + \left(\frac{\partial w_\circ}{\partial y}\right)^2\right]\right.$$

$$+ z^2\left[\left(\frac{\partial^2 w_\circ}{\partial y \partial x}\right)^2 + \left(\frac{\partial^2 w}{\partial y^2}\right)^2\right] + f_1^2(z)\left[\left(\frac{\partial \gamma_{xz}^\circ}{\partial y}\right)^2 + \left(\frac{\partial \gamma_{yz}^\circ}{\partial y}\right)^2\right]$$

$$- 2z\left(\frac{\partial u_\circ}{\partial y}\frac{\partial^2 w_\circ}{\partial y \partial x} + \frac{\partial v_\circ}{\partial y}\frac{\partial^2 w_\circ}{\partial y^2}\right) \quad \cdots\cdots$$

$$- 2z f_1(z)\left(\frac{\partial \gamma_{xz}^\circ}{\partial y}\frac{\partial^2 w_\circ}{\partial y \partial x} + \frac{\partial \gamma_{yz}^\circ}{\partial y}\frac{\partial^2 w_\circ}{\partial y^2}\right)$$

$$\left.+ 2 f_1(z)\left(\frac{\partial u_\circ}{\partial y}\frac{\partial \gamma_{xz}^\circ}{\partial y} + \frac{\partial v_\circ}{\partial y}\frac{\partial \gamma_{yz}^\circ}{\partial y}\right)\right\} \quad (3.63b)$$

$$\gamma_{xy}^L = \frac{\partial u_\circ}{\partial x}\frac{\partial u_\circ}{\partial y} + \frac{\partial v_\circ}{\partial x}\frac{\partial v_\circ}{\partial y} + \frac{\partial w_\circ}{\partial x}\frac{\partial w_\circ}{\partial y}$$

$$- z\left[\frac{\partial u_\circ}{\partial x}\frac{\partial^2 w_\circ}{\partial y \partial x} + \frac{\partial u_\circ}{\partial y}\frac{\partial^2 w_\circ}{\partial x^2} + \frac{\partial v_\circ}{\partial x}\frac{\partial^2 w_\circ}{\partial y^2} + \frac{\partial v_\circ}{\partial y}\frac{\partial^2 w_\circ}{\partial x \partial y}\right]$$

$$- z f_1(z)\left[\frac{\partial \gamma_{xz}^\circ}{\partial x}\frac{\partial^2 w_\circ}{\partial x \partial y} + \frac{\partial \gamma_{xz}^\circ}{\partial y}\frac{\partial^2 w_\circ}{\partial x^2} + \frac{\partial \gamma_{yz}^\circ}{\partial x}\frac{\partial^2 w_\circ}{\partial y^2} + \frac{\partial \gamma_{yz}^\circ}{\partial y}\frac{\partial^2 w_\circ}{\partial x \partial y}\right]$$

$$+ f_1(z)\left[\frac{\partial u_\circ}{\partial x}\frac{\partial \gamma_{xz}^\circ}{\partial y} + \frac{\partial u_\circ}{\partial y}\frac{\partial \gamma_{xz}^\circ}{\partial x} + \frac{\partial v_\circ}{\partial x}\frac{\partial \gamma_{yz}^\circ}{\partial y} + \frac{\partial v_\circ}{\partial y}\frac{\partial \gamma_{xz}^\circ}{\partial x}\right] \quad (3.63c)$$

$$+ z^2\left[\frac{\partial^2 w_\circ}{\partial x^2}\frac{\partial^2 w_\circ}{\partial x \partial y} + \frac{\partial^2 w_\circ}{\partial x \partial y}\frac{\partial^2 w_\circ}{\partial y^2}\right]$$

$$+ f_1^2(z)\left[\frac{\partial \gamma_{xz}^\circ}{\partial x}\frac{\partial \gamma_{xz}^\circ}{\partial y} + \frac{\partial \gamma_{yz}^\circ}{\partial x}\frac{\partial \gamma_{yz}^\circ}{\partial y}\right]$$

3.3 INERTIAL EFFECTS

Consider an engineering structure, such as a composite layered plate or shell, rotating around a fixed axis of rotation with an angular velocity $\vec{\Omega}$ as shown in Fig. (3.2). The direction of $\vec{\Omega}$ may be defined with respect to a global system of axes by means of two points O and A on the axis of rotation. The directional cosines of the axis of rotation can simply be defined as follows:-

$$l = \frac{x_A - x_O}{\overline{OA}}, \qquad m = \frac{y_A - y_O}{\overline{OA}}, \qquad n = \frac{z_A - z_O}{\overline{OA}} \tag{3.64}$$

and the angular speed vector may also be represented as follows:-

$$\begin{aligned} \vec{\Omega} &= \Omega_x \hat{i} + \Omega_y \hat{j} + \Omega_z \hat{k} \\ &\equiv \Omega \left(l\hat{i} + m\hat{j} + n\hat{k} \right) \end{aligned} \tag{3.65}$$

where

$$\Omega = \sqrt{\Omega_x^2 + \Omega_y^2 + \Omega_z^2} \tag{3.66}$$

The global axes are assumed fixed on the structure, *i.e.* the coordinates (x, y, z) of a point inside an undeformable structure are independent of Ω. For such a system of coordinates, the unit vectors in the directions of x, y, z axes are functions of time, and it can be proved from simple mechanics that:-

$$\frac{d\hat{i}}{dt} = \vec{\Omega} \wedge \hat{i}, \qquad \frac{d\hat{j}}{dt} = \vec{\Omega} \wedge \hat{j}, \qquad \frac{d\hat{k}}{dt} = \vec{\Omega} \wedge \hat{k} \tag{3.67}$$

Considering an infinitesimal mass Δm at a point $P_o (x, y, z)$ before deformation, the position vector from the point O (on the axis of rotation) to point P_o can be defined as follows:-

$$\overrightarrow{OP_\circ} \equiv \overrightarrow{R_\circ} = (x - x_\circ)\,\hat{i} + (y - y_\circ)\,\hat{j} + (z - z_\circ)\,\hat{k} \tag{3.68}$$

After deformation point P_o may move to point P,

where

$$\overrightarrow{P_\circ P} \equiv \vec{q} = u\,\hat{i} + v\,\hat{j} + w\,\hat{k} \tag{3.69}$$

and

$$\overrightarrow{OP_\circ} \equiv \vec{R}(t) = \vec{R} + \vec{q}\,(t) \tag{3.70}$$

Differentiating Equation (3.70) with respect to time, and using Equations (3.67), then the velocity vector of the infinitesimal mass due to its rotation is:-

$$\vec{V} = \frac{d\vec{R}}{dt} = \vec{V}_{\circ} + \vec{\dot{q}} + \vec{\Omega} \wedge \vec{q} \qquad (3.71)$$

where $$\vec{V}_{\circ} = \vec{\Omega} \wedge \vec{R}_{\circ}$$

and $$\vec{\dot{q}} = \dot{u}\,\hat{i} + \dot{v}\,\hat{j} + \dot{w}\,\hat{k}$$

Differentiating again Equation (3.71) with respect to time to get the acceleration vector of the infinitesimal mass due to its rotation then:-

$$\vec{a} = \frac{d\vec{V}}{dt} = \vec{a}_{\circ} + \vec{\ddot{q}} + 2\vec{\Omega} \wedge \vec{\dot{q}} + \vec{\Omega} \wedge (\vec{\Omega} \wedge \vec{q}) + \frac{d\vec{\Omega}}{dt} \wedge \vec{q} \qquad (3.72)$$

where $$\vec{a}_{\circ} = \frac{d\vec{V}_{\circ}}{dt}$$

$$\vec{\ddot{q}} = \ddot{u}\,\hat{i} + \ddot{v}\,\hat{j} + \ddot{w}\,\hat{k}$$

and $\dot{f} \equiv \dfrac{df}{dt}$, $\ddot{f} = \dfrac{d^2 f}{dt^2}$

Consider for simplicity a case with a constant rotational speeds $\left(\vec{\dot{\Omega}} = 0\right)$ then Equation (3.72) may be simplified as follows:-

$$\vec{a} = \vec{a}_{\circ} + \vec{a}_r + \vec{a}_c + \vec{a}_p \qquad (3.73)$$

where $$\vec{a}_{\circ} = \vec{\Omega} \wedge (\vec{\Omega} \wedge \vec{R}_{\circ}) \qquad (3.74)$$

$$\vec{a}_r = \vec{\ddot{q}} \qquad (3.75)$$

$$\vec{a}_c = 2\vec{\Omega} \wedge \vec{\dot{q}} \qquad (3.76)$$

$$\vec{a}_p = \vec{\Omega} \wedge (\vec{\Omega} \wedge \vec{q}) \qquad (3.77)$$

The vectors $\vec{a}_r$, $\vec{a}_c$ and $\vec{a}_p$ are known as the relative, Coriolis, and centripetal accelerations respectively. Using equivalent matrix representation where a cartesian vector

$$\vec{V} = V_x\,\hat{i} + V_y\,\hat{j} + V_z\,\hat{k} \qquad (3.78)$$

is represented by a column matrix $$V = \begin{bmatrix} V_x \\ V_y \\ V_z \end{bmatrix} \qquad (3.79)$$

then the previous components of accelerations can be represented in the following matrix forms:-

$$\boldsymbol{a}_{\circ} = -\Omega^2 \boldsymbol{C}_1 \boldsymbol{R} \tag{3.80}$$

$$\boldsymbol{a}_r = \ddot{\boldsymbol{q}} \tag{3.81}$$

$$\boldsymbol{a}_c = 2\,\Omega\,\boldsymbol{C}_2\,\dot{\boldsymbol{q}} \tag{3.82}$$

$$\boldsymbol{a}_p = -\Omega^2\,\boldsymbol{C}_1\,\boldsymbol{q} \tag{3.83}$$

where

$$\boldsymbol{R}_{\circ} = \begin{bmatrix} x - x_{\circ} \\ y - y_{\circ} \\ z - z_{\circ} \end{bmatrix} \tag{3.84}$$

$$\boldsymbol{q} = \begin{bmatrix} u \\ v \\ w \end{bmatrix} \tag{3.85}$$

$$\dot{\boldsymbol{q}} = \begin{bmatrix} \dot{u} \\ \dot{v} \\ \dot{w} \end{bmatrix} \tag{3.86}$$

$$\ddot{\boldsymbol{q}} = \begin{bmatrix} \ddot{u} \\ \ddot{v} \\ \ddot{w} \end{bmatrix} \tag{3.87}$$

$$\boldsymbol{C}_1 = \begin{bmatrix} 1 - l^2 & -lm & -ln \\ -ml & 1 - m^2 & -mn \\ -nl & -nm & 1 - n^2 \end{bmatrix} \tag{3.88}$$

$$\boldsymbol{C}_2 = \begin{bmatrix} 0 & -n & m \\ n & 0 & -l \\ -m & l & 0 \end{bmatrix} \tag{3.89}$$

3.4 AERODYNAMIC PRESSURE

Consider an aerodynamic structure, which may be a composite layered plate or shell, in a stream of air or fluid flow. The surface of the structure will be subjected to an aerodynamic pressure distribution which can be split into two parts as follows:-

$$p = p_{\circ} + p_a \tag{3.90}$$

The term $p_{\circ}$ represents the *external* aerodynamic pressure, which is independent of the structure deformation, *i.e.* any pressure caused due to turbulent boundary layer fluctuation. It may be obtained experimentally or by employing a separate computational fluid dynamic analysis.

The term p_a represents the aerodynamic pressure due to aeroelastic effects caused by the deformation of the structure. The basic types of modelling of p_a employed in panel flutter are summarized next.

(a) The quasi-steady first-order piston theory

Let a composite plate represent a panel configured in such a way that one side of it is exposed to a uniform air flow parallel to the x axis, and the other side is part of a structural cavity, or no flow going under the panel as shown in Fig. (3.3). For a very high supersonic speed ($M_{\infty} > 2.2$), the first-order quasi-steady aerodynamic piston theory (Ashley and Zartarian, 1956) leads to:-

$$p_a(x, y, t) \cong \frac{\rho_{\infty} V_{\infty}}{M_{\infty}} \left[U_{\infty} \frac{\partial w}{\partial x} + \frac{\partial w}{\partial t} \right] \tag{3.91}$$

where ρ_{∞}, V_{∞}, M_{∞} are the density, velocity and Mach number of the free stream flow, respectively. The above approximation is based upon assuming that the deflection is zero at the panel leading and trailing edges.

(b) Model for $M_{\infty} > 1.6$

Dowell (1975) has derived an aerodynamic theory for the modelling of p_a, leading

to the following approximation for $M_\infty > 1.6$:-

$$p_a(x,y,t) \cong \frac{\rho_\infty V_\infty^2}{\sqrt{M_\infty^2 - 1}} \left[\frac{\partial w}{\partial x} + \left(\frac{M_\infty^2 - 2}{M_\infty^2 - 1} \right) \frac{1}{V_\infty} \frac{\partial w}{\partial t} \right] \tag{3.92}$$

which can be approximated to Equation (3.91) at very high Mach numbers. Equation (3.92) can also be employed for a cylindrical shell with the x-axis being its axis as shown in Fig. (3.4) (Bismarck-Nasr,1993).

(c) Effect of flow angle

For a given panel geometry, consider the case with the flow being yawed in the plane of the panel rather than in the x-direction. Consider x' being the axis in the flow direction and y' normal to it, as shown in Fig. (3.5). Equation (3.92) may be employed with $\frac{\partial w}{\partial x'}$ instead of $\frac{\partial w}{\partial x}$ (Dowel, 1975). Using the chain rule of partial differentiation, it can be deduced that:-

$$\frac{\partial w}{\partial x'} = \frac{\partial w}{\partial x}\frac{\partial x}{\partial x'} + \frac{\partial w}{\partial y}\frac{\partial y}{\partial x'}$$

$$= (\cos\alpha)\frac{\partial w}{\partial x} + (\sin\alpha)\frac{\partial w}{\partial y} \tag{3.93}$$

i.e.

$$p_a(x,y,t) \cong \frac{\rho_\infty V_\infty^2}{\sqrt{M_\infty^2 - 1}} \left[(\cos\alpha)\frac{\partial w}{\partial x} + (\sin\alpha)\frac{\partial w}{\partial y} + \left(\frac{M_\infty^2 - 2}{M_\infty^2 - 1} \right) \frac{1}{V_\infty} \frac{\partial w}{\partial t} \right] \tag{3.94}$$

This equation will be employed for a general linear modelling of flutter pressure.

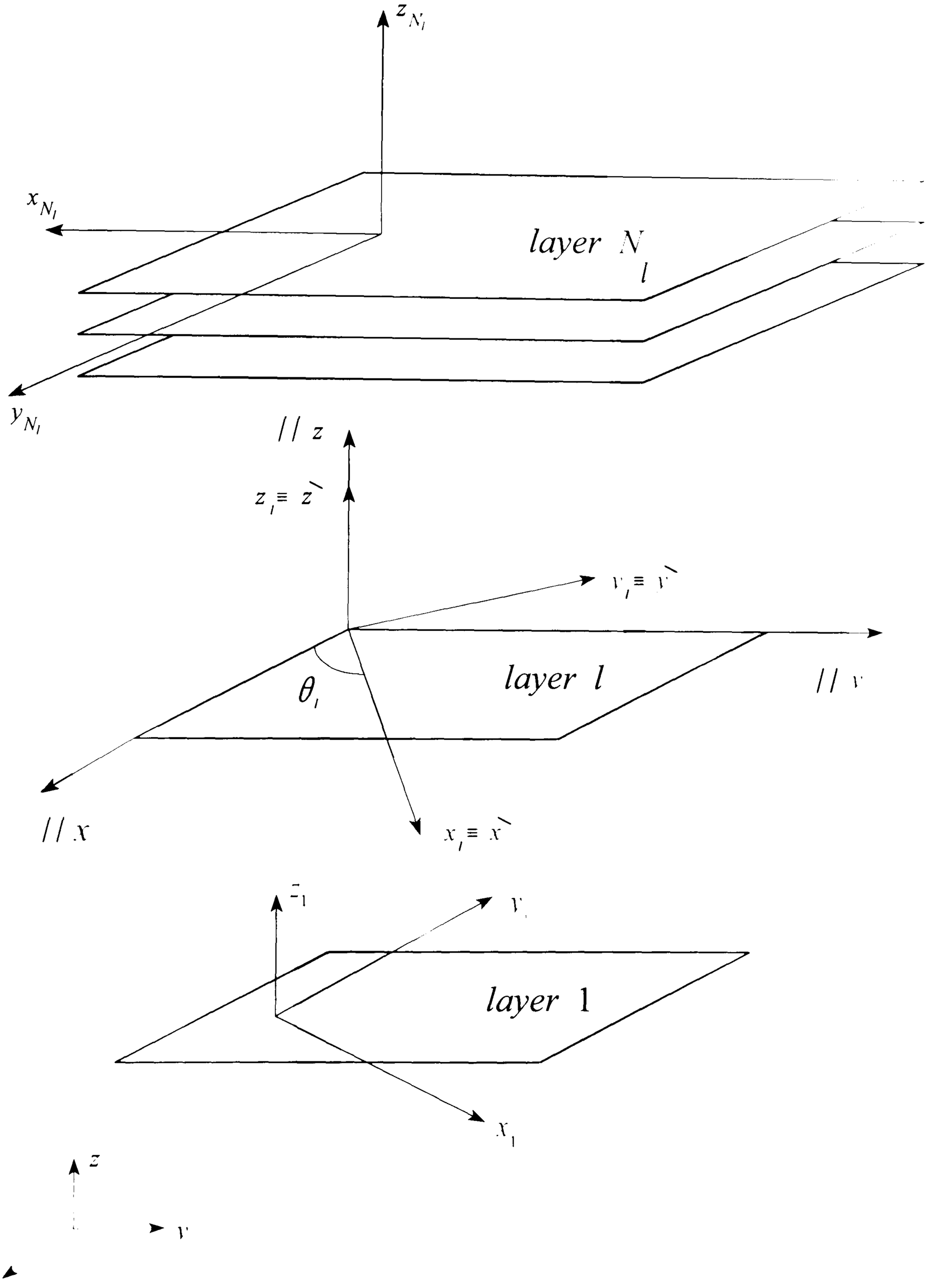

Figure 3.1 Local and global axes of layers.

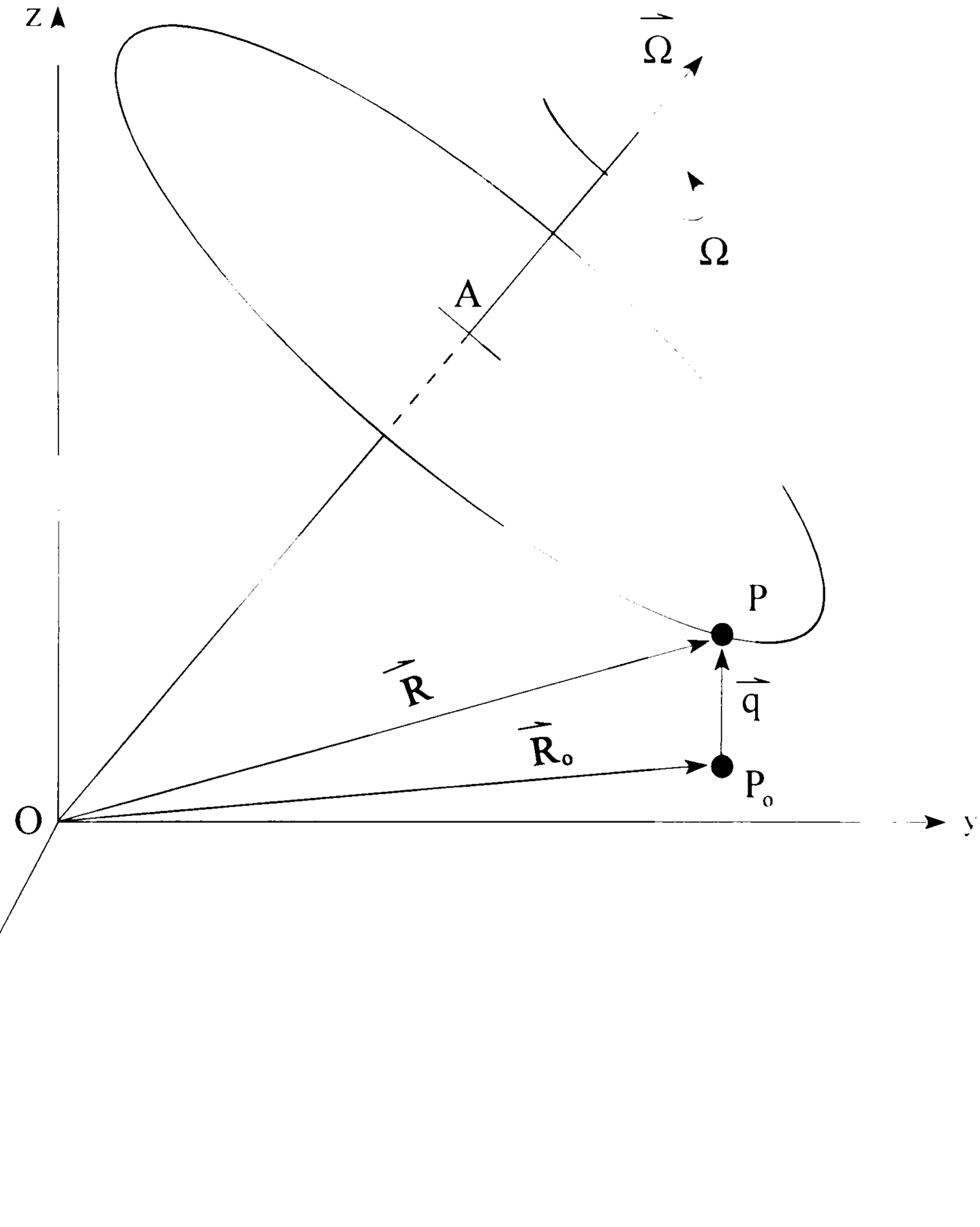

Figure 3.2 Rotating mass in a deformable structure

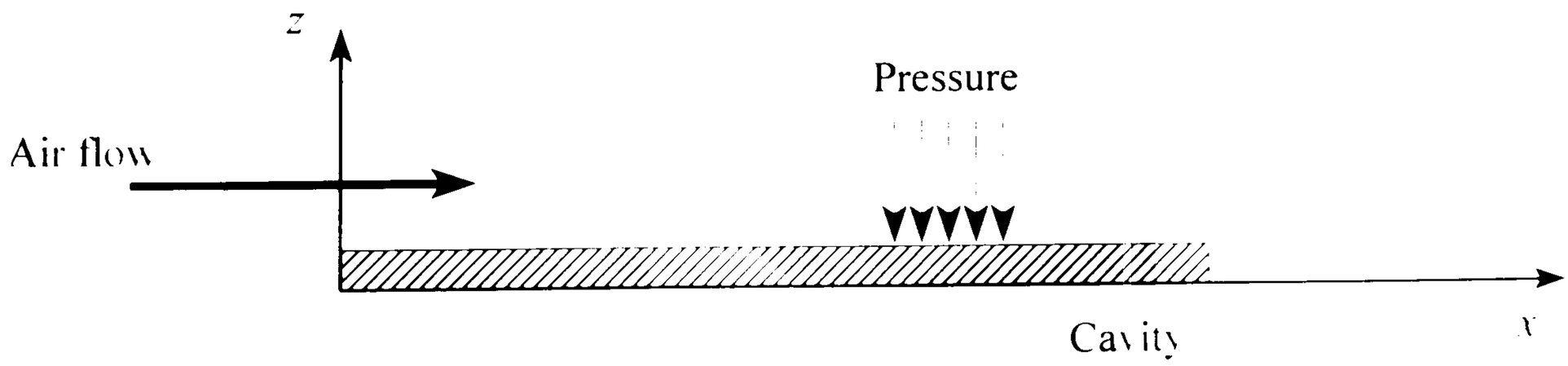

Figure 3.3 Modelling of panel flow

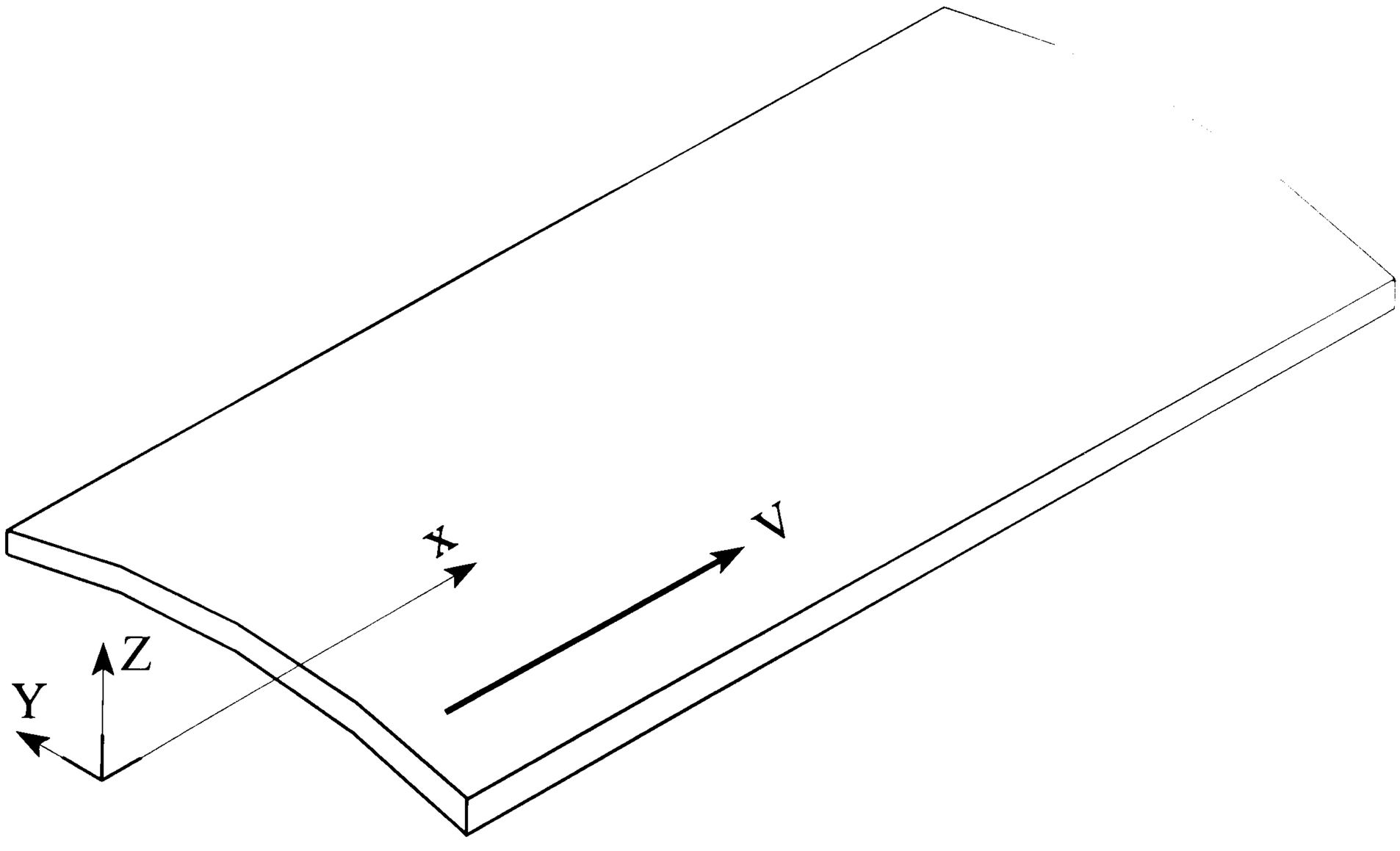

Figure 3.4 Flow over curved panel

Figure 3.5 Yawed flow

CHAPTER 4

FORMULATION OF FINITE ELEMENT EQUATIONS

4.1 DISPLACEMENT AND VELOCITY INTERPOLATION

4.1.1 Introduction

The composite-layered plate element is defined in terms of the midplane ($z = 0$), where also the nodal parameters are defined, which will be explained later. The geometry of the plate midplane is defined in terms of nodal coordinates with respect to a cartesian x-y-z system of coordinates. Most of the derivatives described here are with respect to a local system of axes, where the x-y plane is in the midplane, and the z-axis is normal to that midplane.

Physically, the element is constructed of a number of layers (N_l), as shown in Fig. (4.1). The l^{th} layer's lower surface is described by the following equation:-

$$z = Z_L^{(l)}(x, y) \tag{4.1}$$

and the upper surface by $$z = Z_U^{(l)}(x, y) \tag{4.2}$$

i.e. the thickness distribution is :-

$$h^{(l)}(x, y) = Z_U^{(l)} - Z_L^{(l)} \tag{4.3}$$

The layer has its own material axes, and the stress-strain matrix $D^{(l)}$ is defined with respect to the element local x, y, z axes, as described in section (3.1).

4.1.2 In-plane and transverse-shear parameters

The midplane displacement components in the x and y directions will lead to continuous displacement components, if they are represented by at least C^0 continuous functions. Hence Lagrangian interpolation is suitable for their modelling, and for an n-node finite element:-

$$u_o(x, y, t) = \sum_{i=1}^{n} u_i(t)\, N_i(x, y) \tag{4.4}$$

$$v_o(x, y, t) = \sum_{i=1}^{n} v_i(t)\, N_i(x, y) \tag{4.5}$$

where u_i, v_i are the values of the x-y displacement components, at the midplane node i, and time t, $N_i(x, y)$ represents a Lagrangian shape function.

Isoparametric representation of the element is given as follows:-

$$\left.\begin{aligned} x(\xi, \eta) &= \sum_{i+1}^{n} x_i \; N_i(\xi, \eta) \\ y(\xi, \eta) &= \sum_{i+1}^{n} y_i \; N_i(\xi, \eta) \\ z(\xi, \eta) &= \sum_{i+1}^{n} z_i \; N_i(\xi, \eta) \end{aligned}\right\} \tag{4.6}$$

and the shape functions are expressed in terms of the intrinsic coordinates (ξ, η). Lists of the element Lagrangian shape functions employed in this work are in Appendix A.

Similarly, the transverse shear components, at the midplane can be interpolated in terms of Lagrangian shape functions as follows:-

$$\left.\begin{aligned} \gamma^{\circ}_{xz}(x, y, t) &= \sum_{i=1}^{n} \phi_i(t) \; N_i(x, y) \\ \gamma^{\circ}_{yz}(x, y, t) &= \sum_{i=1}^{n} \psi_i(t) \; N_i(x, y) \end{aligned}\right\} \tag{4.7}$$

where

$$\left.\begin{aligned} \phi_i(t) &\equiv \gamma^{\circ}_{xz}(x_i, y_i, t) \\ \psi_i(t) &\equiv \gamma^{\circ}_{yz}(x_i, y_i, t) \end{aligned}\right\} \tag{4.8}$$

4.1.3 Interpolation of lateral deflection

Due to the presence of first order partial derivatives of w in the equation of displacement components, as can be seen in Equations (3.46) and (3.47), the lateral deflection w must be C^1 continuous over the plate, in other words it should be interpolated by means of a Hermitian interpolation. Two types of interpolation, based upon El-Zafrany and Cookson (1986a, 1986b), are suggested:-

(a) Type 1 (Non-conforming)

The lateral deflection is interpolated in terms of its values, and the first order partial derivatives, *i.e.*

$$w_{\circ}(x,y,t) = \sum_{i=1}^{n} \left\{ w_i(t) f_i(x,y) + w_{i,x}(t) g_i(x,y) + w_{i,y}(t) h_i(x,y) \right\} \quad (4.9)$$

where w_i , $w_{i,x}$ and $w_{i,y}$ represent the values of $w_{\circ}$, $\frac{\partial w_{\circ}}{\partial x}$ and $\frac{\partial w_{\circ}}{\partial y}$ at node i and time t ; f_i, g_i and h_i are the *type 1* Hermitian interpolation functions as listed in Appendix B.

(b) Type 2 (conforming)

The previous type of elements do not satisfy fully the curvature continuity condition, as explained by Zienkiewicz (1977), but it can be fully satisfied if the nodal values of $\partial^2 w / \partial x \partial y$ are included in the interpolation expression, leading to the so-called conforming elements, with the following Hermitian interpolation expression:

$$\left.\begin{aligned} w_{\circ}(x,y,t) = \sum_{i=1}^{n} \Big\{ & w_i(t) F_i(x,y) + w_{i,x}(t) G_i(x,y) \\ & + w_{i,y}(t) H_i(x,y) + w_{i,xy}(t) Q_i(x,y) \Big\} \end{aligned}\right\} \quad (4.10)$$

where $w_{i,xy}$ represents the value of $\partial^2 w_{\circ} / \partial x \partial y$ at node i and time t, and F_i , G_i , H_i and Q_i are *type 2* Hermitian interpolation functions as listed in Appendix C. Notice also that for the remaining parts of this chapter, Equation (4.10) is always assumed, and *type 1* Hermitian interpolation is obtained by using:-

$$\left.\begin{aligned} F_i(x,y) &\equiv f_i(x,y) \qquad G_i(x,y) \equiv g_i(x,y) \\ H_i(x,y) &\equiv h_i(x,y) \qquad Q_i(x,y) \equiv 0 \end{aligned}\right\} \quad (4.11)$$

4.1.4 Nodal displacement vector

From the previous analysis it is clear that the displacement parameters required at each node i are:-

u_i, v_i, ϕ_i, ψ_i, w_i, $w_{i,x}$, $w_{i,y}$, $w_{i,xy}$ where $w_{i,xy}$ is only required for the second type

of Hermitian interpolation. To simplify the derivation, the nodal displacement vector for an n-node element will be defined at time t as follows:-

$$\boldsymbol{\delta}(t) = \{ \boldsymbol{\delta}_m(t) \quad \boldsymbol{\delta}_b(t) \quad \boldsymbol{\delta}_s(t) \} \tag{4.12}$$

where

$$\boldsymbol{\delta}_m(t) \equiv \{ u_1(t) \; v_1(t) \quad u_2(t) \; v_2(t) \; . \; . \; . \; u_n(t) \; v_n(t) \} \tag{4.13}$$

$$\boldsymbol{\delta}_b(t) \equiv \{ w_1(t) \; w_{1,x}(t) \; w_{1,y}(t) \; w_{1,xy}(t) \; . \; . \; .$$
$$w_n(t) \; w_{n,x}(t) \; w_{n,y}(t) \; w_{n,xy}(t) \} \tag{4.14}$$

$$\boldsymbol{\delta}_s(t) \equiv \{ \phi_1(t) \; \psi_1(t) \; . \; . \; . \; \phi_n(t) \; \psi_n(t) \} \tag{4.15}$$

4.1.5 Velocity components

The velocity components at any point (x, y, z) inside the plate at time t are as defined by Equations (3.48), (3.49) and (3.50). They can be represented vectorially as follows:-

$$\dot{\boldsymbol{q}}(x,y,z,t) \equiv \begin{bmatrix} \dot{\boldsymbol{q}}_{xy}(x,y,z,t) \\ \dot{\boldsymbol{q}}_z(x,y,z,t) \end{bmatrix} \tag{4.16}$$

where

$$\dot{\boldsymbol{q}}_{xy}(x,y,z,t) \equiv \begin{bmatrix} \dot{u}(x,y,z,t) \\ \dot{v}(x,y,z,t) \end{bmatrix} \tag{4.17}$$

$$\dot{\boldsymbol{q}}_z(x,y,z,t) \approx [\, \dot{w}_\circ(x,y,t) \,] \tag{4.18}$$

Substituting from Equations (4.4), (4.5), (4.7) and (4.10) into (3.48), (3.49) and (3.50) it can be proved that:-

$$\dot{\boldsymbol{q}}_{xy}(x,y,z,t) = \boldsymbol{N}_L(xy)\dot{\boldsymbol{\delta}}_m(t) - z\,\boldsymbol{N}_b(xy)\dot{\boldsymbol{\delta}}_b(t)$$
$$+ f_1(z)\,\boldsymbol{N}_L(xy)\dot{\boldsymbol{\delta}}_s(t) \tag{4.19}$$

$$\dot{\boldsymbol{q}}_z(x,y,z,t) = \boldsymbol{N}_H(xy)\dot{\boldsymbol{\delta}}_b(t) \tag{4.20}$$

where

$$\boldsymbol{N}_L(x,y) = \begin{bmatrix} N_1 & 0 & N_2 & 0 & . \; . \; . & N_n & 0 \\ 0 & N_1 & 0 & N_2 & . \; . \; . & 0 & N_n \end{bmatrix} \tag{4.21}$$

$$N_b(x,y) = \begin{bmatrix} \cdots & \dfrac{\partial F_i}{\partial x} & \dfrac{\partial G_i}{\partial x} & \dfrac{\partial H_i}{\partial x} & \dfrac{\partial Q_i}{\partial x} & \cdots \\ \cdots & \dfrac{\partial F_i}{\partial y} & \dfrac{\partial G_i}{\partial y} & \dfrac{\partial H_i}{\partial y} & \dfrac{\partial Q_i}{\partial y} & \cdots \end{bmatrix} \tag{4.22}$$

$$N_H(x,y) = \begin{bmatrix} \cdots & F_i & G_i & H_i & Q_i & \cdots \end{bmatrix} \tag{4.23}$$

4.2 STRAIN COMPONENTS

4.2.1 Infinitesimal strain modelling

Substituting from Equations (4.4) and (4.5) into (3.59), it can be deduced that:-

$$\boldsymbol{\epsilon}_m(x,y,t) = \begin{bmatrix} \dfrac{\partial u_\circ}{\partial x} \\ \dfrac{\partial v_\circ}{\partial y} \\ \dfrac{\partial u_\circ}{\partial y} + \dfrac{\partial v_\circ}{\partial x} \end{bmatrix} = \boldsymbol{B}_m(x,y)\boldsymbol{\delta}_m(t) \tag{4.24}$$

where

$$\boldsymbol{B}_m(x,y) = \begin{bmatrix} \cdots & \dfrac{\partial N_i}{\partial x} & 0 & \cdots \\ \cdots & 0 & \dfrac{\partial N_i}{\partial y} & \cdots \\ \cdots & \dfrac{\partial N_i}{\partial y} & \dfrac{\partial N_i}{\partial x} & \cdots \end{bmatrix} \tag{4.25}$$

Similarly it can be proved that:-

$$\boldsymbol{\epsilon}_s(x,y,t) = \boldsymbol{B}_m(x,y)\ \boldsymbol{\delta}_s(t) \tag{4.26}$$

Substituting from Equations (4.10) into (3.60), it can be shown that:-

$$\boldsymbol{\epsilon}_b(x,y,t) = \boldsymbol{B}_b(x,y)\ \boldsymbol{\delta}_b(t) \tag{4.27}$$

where

$$\boldsymbol{B}_b(x,y) = \begin{bmatrix} \cdots & \dfrac{\partial^2 F_i}{\partial x^2} & \dfrac{\partial^2 G_i}{\partial x^2} & \dfrac{\partial^2 H_i}{\partial x^2} & \dfrac{\partial^2 Q_i}{\partial x^2} & \cdots \\ \cdots & \dfrac{\partial^2 F_i}{\partial y^2} & \dfrac{\partial^2 G_i}{\partial y^2} & \dfrac{\partial^2 H_i}{\partial y^2} & \dfrac{\partial^2 Q_i}{\partial y^2} & \cdots \\ \cdots & 2\dfrac{\partial^2 F_i}{\partial x\,\partial y} & 2\dfrac{\partial^2 G_i}{\partial x\,\partial y} & 2\dfrac{\partial^2 H_i}{\partial x\,\partial y} & 2\dfrac{\partial^2 Q_i}{\partial x\,\partial y} & \cdots \end{bmatrix} \tag{4.28}$$

Hence,
$$(\boldsymbol{\epsilon}_{xy})_{inf}(x,y,z,t) = \boldsymbol{B}_m(x,y)\,\boldsymbol{\delta}_m(t) - z\,\boldsymbol{B}_b(x,y)\,\boldsymbol{\delta}_b(t)$$

$$+ f_1(z)\,\boldsymbol{B}_m(x,y)\,\boldsymbol{\delta}_s(t) \tag{4.29}$$

Notice also that the transverse shear strain components, as defined by Equation (3.36) and (3.37) can be represented vectorially as follows:-

$$\boldsymbol{\gamma}(x,y,z,t) \equiv \begin{bmatrix} \gamma_{xz} \\ \gamma_{yz} \end{bmatrix} = f_2(z) \begin{bmatrix} \overset{\circ}{\gamma}_{xz}(x,y,t) \\ \overset{\circ}{\gamma}_{yz}(x,y,t) \end{bmatrix} \tag{4.30}$$

where
$$f_2(z) = \left[1 - \frac{4z^2}{h^2}\right] \tag{4.31}$$

Substituting from Equations (4.7) and (4.8) into (4.30), it can be shown that

$$\boldsymbol{\gamma}(x,y,z,t) = f_2(z)\,\boldsymbol{B}_s(x,y)\,\boldsymbol{\delta}_s(t) \tag{4.32}$$

where
$$\boldsymbol{B}_s(x,y) = \boldsymbol{N}_L(x,y) \tag{4.33}$$

4.2.2 Modelling of finite strain contributions

Defining the following *rotation* vectors:-

$$\boldsymbol{\theta}_m = \left\{ \begin{array}{cccc} \dfrac{\partial u_\circ}{\partial x} & \dfrac{\partial v_\circ}{\partial x} & \dfrac{\partial u_\circ}{\partial y} & \dfrac{\partial u_\circ}{\partial y} \end{array} \right\} \tag{4.34}$$

$$\boldsymbol{\theta}_s = \left\{ \begin{array}{cccc} \dfrac{\partial \phi}{\partial x} & \dfrac{\partial \psi}{\partial x} & \dfrac{\partial \phi}{\partial y} & \dfrac{\partial \psi}{\partial y} \end{array} \right\} \tag{4.35}$$

$$\boldsymbol{\theta}_b = \left\{ \begin{array}{cccc} \dfrac{\partial^2 w_\circ}{\partial x^2} & \dfrac{\partial^2 w_\circ}{\partial x\,\partial y} & \dfrac{\partial^2 w_\circ}{\partial y\,\partial x} & \dfrac{\partial^2 w_\circ}{\partial y^2} \end{array} \right\} \tag{4.36}$$

$$\boldsymbol{\theta}_w = \left\{ \begin{array}{cc} \dfrac{\partial w_\circ}{\partial x} & \dfrac{\partial w_\circ}{\partial y} \end{array} \right\} \tag{4.37}$$

where $\phi \equiv \gamma^{\circ}_{xz}$ and $\psi \equiv \gamma^{\circ}_{yz}$

then Equations (3.63a), (3.63b) and (3.63c) can be represented in the following matrix form:-

$$\left.\begin{aligned} \boldsymbol{\epsilon}_L &= \begin{bmatrix} \epsilon^L_x \\ \epsilon^L_y \\ \gamma^L_{xy} \end{bmatrix} \\ &= \frac{1}{2}\Big\{ \boldsymbol{A}_m \boldsymbol{\theta}_m + \boldsymbol{A}_w \boldsymbol{\theta}_w + z^2 \boldsymbol{A}_b \boldsymbol{\theta}_b + f_1^2(z) \boldsymbol{A}_s \boldsymbol{\theta}_s \\ &- z f_1(z)\big[\boldsymbol{A}_b \boldsymbol{\theta}_s + \boldsymbol{A}_s \boldsymbol{\theta}_b\big] \quad z\big[\boldsymbol{A}_b \boldsymbol{\theta}_m + \boldsymbol{A}_m \boldsymbol{\theta}_b\big] \\ &+ f_1(z)\big[\boldsymbol{A}_m \boldsymbol{\theta}_s + \boldsymbol{A}_s \boldsymbol{\theta}_m\big]\Big\} \end{aligned}\right\} \tag{4.38}$$

where

$$\boldsymbol{A}_m = \begin{bmatrix} \dfrac{\partial u_\circ}{\partial x} & \dfrac{\partial v_\circ}{\partial x} & 0 & 0 \\ 0 & 0 & \dfrac{\partial u_\circ}{\partial y} & \dfrac{\partial v_\circ}{\partial y} \\ \dfrac{\partial u_\circ}{\partial y} & \dfrac{\partial v_\circ}{\partial y} & \dfrac{\partial u_\circ}{\partial x} & \dfrac{\partial v_\circ}{\partial x} \end{bmatrix} \tag{4.39}$$

$$\boldsymbol{A}_s = \begin{bmatrix} \dfrac{\partial \phi}{\partial x} & \dfrac{\partial \psi}{\partial x} & 0 & 0 \\ 0 & 0 & \dfrac{\partial \phi}{\partial y} & \dfrac{\partial \psi}{\partial y} \\ \dfrac{\partial \phi}{\partial y} & \dfrac{\partial \psi}{\partial y} & \dfrac{\partial \phi}{\partial x} & \dfrac{\partial \psi}{\partial x} \end{bmatrix} \tag{4.40}$$

$$\boldsymbol{A}_b = \begin{bmatrix} \dfrac{\partial^2 w_\circ}{\partial x^2} & \dfrac{\partial^2 w_\circ}{\partial x\,\partial y} & 0 & 0 \\ 0 & 0 & \dfrac{\partial^2 w_\circ}{\partial y\,\partial x} & \dfrac{\partial^2 w_\circ}{\partial y^2} \\ \dfrac{\partial^2 w_\circ}{\partial y\,\partial x} & \dfrac{\partial^2 w_\circ}{\partial y^2} & \dfrac{\partial^2 w_\circ}{\partial x^2} & \dfrac{\partial^2 w_\circ}{\partial x\,\partial y} \end{bmatrix} \tag{4.41}$$

$$\boldsymbol{A}_w = \begin{bmatrix} \dfrac{\partial w_\circ}{\partial x} & 0 \\ 0 & \dfrac{\partial w_\circ}{\partial y} \\ \dfrac{\partial w_\circ}{\partial y} & \dfrac{\partial w_\circ}{\partial x} \end{bmatrix} \tag{4.42}$$

Due to the non-linearity of terms in $\boldsymbol{\epsilon}_L$ equation, it will be represented in the derivations as an integration of its differential values, *i.e.*

$$\boldsymbol{\epsilon}_L = \int d\,\boldsymbol{\epsilon}_L \tag{4.43}$$

and it can be proved that:-

$$\left.\begin{aligned} d\,\boldsymbol{\epsilon}_L = {} & \boldsymbol{A}_m d\boldsymbol{\theta}_m + \boldsymbol{A}_w d\boldsymbol{\theta}_w + f_1^2(z)\,\boldsymbol{A}_s d\boldsymbol{\theta}_s + z^2 \boldsymbol{A}_b d\boldsymbol{\theta}_b \\ & - z f_1(z)\left[\boldsymbol{A}_b d\boldsymbol{\theta}_s + \boldsymbol{A}_s d\boldsymbol{\theta}_b\right] - z\left[\boldsymbol{A}_b d\boldsymbol{\theta}_m + \boldsymbol{A}_m d\boldsymbol{\theta}_b\right] \\ & + f_1(z)\left[\boldsymbol{A}_m d\boldsymbol{\theta}_s + \boldsymbol{A}_s d\boldsymbol{\theta}_m\right] \end{aligned}\right\} \tag{4.44}$$

Using the interpolation equations for displacement components, it can be shown that:-

$$d\,\boldsymbol{\theta}_m = \boldsymbol{G}_m\, d\,\boldsymbol{\delta}_m \tag{4.45}$$

$$d\,\boldsymbol{\theta}_s = \boldsymbol{G}_m\, d\,\boldsymbol{\delta}_s \tag{4.46}$$

$$d\,\boldsymbol{\theta}_b = \boldsymbol{G}_b\, d\,\boldsymbol{\delta}_b \tag{4.47}$$

$$d\,\boldsymbol{\theta}_w = \boldsymbol{G}_w\, d\,\boldsymbol{\delta}_b \tag{4.48}$$

where

$$\boldsymbol{G}_m = \begin{bmatrix} \cdots & \dfrac{\partial N_i}{\partial x} & 0 & \cdots \\ \cdots & 0 & \dfrac{\partial N_i}{\partial x} & \cdots \\ \cdots & \dfrac{\partial N_i}{\partial y} & 0 & \cdots \\ \cdots & 0 & \dfrac{\partial N_i}{\partial y} & \cdots \end{bmatrix} \tag{4.49}$$

$$\boldsymbol{G}_w = \begin{bmatrix} \cdots & \dfrac{\partial F_i}{\partial x} & \dfrac{\partial G_i}{\partial x} & \dfrac{\partial H_i}{\partial x} & \dfrac{\partial Q_i}{\partial x} & \cdots \\ \cdots & \dfrac{\partial F_i}{\partial y} & \dfrac{\partial G_i}{\partial y} & \dfrac{\partial H_i}{\partial y} & \dfrac{\partial Q_i}{\partial y} & \cdots \end{bmatrix} \tag{4.50}$$

$$\equiv \boldsymbol{N}_b$$

$$\boldsymbol{G}_b = \begin{bmatrix} \cdots & \dfrac{\partial^2 F_i}{\partial x^2} & \dfrac{\partial^2 G_i}{\partial x^2} & \dfrac{\partial^2 H_i}{\partial x^2} & \dfrac{\partial^2 Q_i}{\partial x^2} & \cdots \\ \cdots & \dfrac{\partial^2 F_i}{\partial x \partial y} & \dfrac{\partial^2 G_i}{\partial x \partial y} & \dfrac{\partial^2 H_i}{\partial x \partial y} & \dfrac{\partial^2 Q_i}{\partial x \partial y} & \cdots \\ \cdots & \dfrac{\partial^2 F_i}{\partial y \partial x} & \dfrac{\partial^2 G_i}{\partial y \partial x} & \dfrac{\partial^2 H_i}{\partial y \partial x} & \dfrac{\partial^2 Q_i}{\partial y \partial x} & \cdots \\ \cdots & \dfrac{\partial^2 F_i}{\partial y^2} & \dfrac{\partial^2 G_i}{\partial y^2} & \dfrac{\partial^2 H_i}{\partial y^2} & \dfrac{\partial^2 Q_i}{\partial y^2} & \cdots \end{bmatrix} \tag{4.51}$$

Hence Equation (4.44) can be rewritten in terms of nodal values, as follows:-

$$\left.\begin{aligned} d\boldsymbol{\epsilon}_L = {} & \boldsymbol{A}_m \boldsymbol{G}_m d\boldsymbol{\delta}_m + \boldsymbol{A}_w \boldsymbol{G}_w d\boldsymbol{\delta}_w + f_1^2(z) \boldsymbol{A}_s \boldsymbol{G}_m d\boldsymbol{\delta}_s + z^2 \boldsymbol{A}_b \boldsymbol{G}_b d\boldsymbol{\delta}_b \\ & - z f_1(z) \left[\boldsymbol{A}_b \boldsymbol{G}_m d\boldsymbol{\delta}_s + \boldsymbol{A}_s \boldsymbol{G}_b d\boldsymbol{\delta}_b \right] - z \left[\boldsymbol{A}_b \boldsymbol{G}_m d\boldsymbol{\delta}_m + \boldsymbol{A}_m \boldsymbol{G}_b d\boldsymbol{\delta}_b \right] \\ & + f_1(z) \left[\boldsymbol{A}_m \boldsymbol{G}_m d\boldsymbol{\delta}_s + \boldsymbol{A}_s \boldsymbol{G}_m d\boldsymbol{\delta}_m \right] \end{aligned}\right\} \tag{4.52}$$

4.3 ELEMENT STIFFNESS MATRIX FOR INFINITESIMAL STRAINS

The stresses at any point inside the l^{th} layer, can be related to strains by means of Equations (3.28) and (3.23), *i.e.*

$$\boldsymbol{\sigma}_{xy}^{(l)} = \boldsymbol{D}_{xy}^{(l)} \boldsymbol{\epsilon}_{xy} \tag{4.53}$$

$$\boldsymbol{\tau}^{(l)} = \boldsymbol{\mu}_{2\times 2}^{(l)} \boldsymbol{\gamma} \tag{4.54}$$

where

$$\boldsymbol{\sigma}_{xy} = \{ \sigma_x \quad \sigma_y \quad \tau_{xy} \}$$

$$\boldsymbol{\tau} = \{ \tau_{xz} \quad \tau_{yz} \}$$

and $\boldsymbol{D}_{xy}^{(l)}$, $\boldsymbol{\mu}^{(l)}$ are stress-strain matrices defined with respect to element local axes. Their derivation from the corresponding matrices defined with respect to material axes has been explained in section (3.1).

For the case of infinitesimal strains, it can be deduced from Equations (4.29), (4.32), (4.53) and (4.54) that:-

$$\boldsymbol{\sigma}_{xy}^{(l)} = \boldsymbol{D}_{xy}^{(l)} \left[\boldsymbol{B}_m \boldsymbol{\delta}_m - z \boldsymbol{B}_b \boldsymbol{\delta}_b + f_1(z) \boldsymbol{B}_m \boldsymbol{\delta}_s \right] \tag{4.55}$$

$$\boldsymbol{\tau}^{(l)} = \boldsymbol{\mu}^{(l)} \left[f_2(z) \boldsymbol{B}_s \boldsymbol{\delta}_s \right] \tag{4.56}$$

The strain energy density or the strain energy per unit volume at any point inside the element can be expressed as follows:-

$$\overline{U}(x, y, z, t) = \frac{1}{2} \boldsymbol{\sigma}^t \boldsymbol{\epsilon} \equiv \frac{1}{2} \boldsymbol{\epsilon}^t \boldsymbol{\sigma}$$

$$= \frac{1}{2} \boldsymbol{\epsilon}_{xy}^t \boldsymbol{\sigma}_{xy} + \frac{1}{2} \boldsymbol{\gamma}^t \boldsymbol{\tau} \tag{4.57}$$

Hence, for the case of infinitesimal strains, the strain energy density at a point inside the l^{th} layer will be:-

$$\overline{U}^{(l)} = \frac{1}{2}\left[\boldsymbol{\delta}_m^t \boldsymbol{B}_m^t - z\,\boldsymbol{\delta}_b^t \boldsymbol{B}_b^t + f_1(z)\,\boldsymbol{\delta}_s^t \boldsymbol{B}_m^t \right]$$

$$\boldsymbol{D}_{xy}^{(l)} \left[\boldsymbol{B}_m \boldsymbol{\delta}_m - z\,\boldsymbol{B}_b \boldsymbol{\delta}_b + f_1(z)\,\boldsymbol{B}_m \boldsymbol{\delta}_s \right]$$

$$+ \frac{1}{2}\left[\boldsymbol{\delta}_s^t \boldsymbol{B}_s^t f_2^2(z)\ \boldsymbol{\mu}^{(l)}\ \boldsymbol{B}_s\ \boldsymbol{\delta}_s \right] \Big]$$

Hence

$$\overline{U}^{(l)} = \frac{1}{2}\ \boldsymbol{\delta}_m^t \boldsymbol{B}_m^t\ \ \boldsymbol{D}_{xy}^{(l)}\ \ \boldsymbol{B}_m \boldsymbol{\delta}_m$$

$$+ \frac{1}{2}\ \boldsymbol{\delta}_b^t \boldsymbol{B}_b^t\ \ z^2\, \boldsymbol{D}_{xy}^{(l)}\ \ \boldsymbol{B}_b \boldsymbol{\delta}_b$$

$$+ \frac{1}{2}\ \boldsymbol{\delta}_s^t \boldsymbol{B}_m^t\ \ f_1^2(z)\, \boldsymbol{D}_{xy}^{(l)}\ \ \boldsymbol{B}_m \boldsymbol{\delta}_s$$

$$+ \frac{1}{2}\ \boldsymbol{\delta}_s^t \boldsymbol{B}_s^t\ \ f_2^2(z)\, \boldsymbol{\mu}^{(l)}\ \ \boldsymbol{B}_s \boldsymbol{\delta}_s$$

$$- \frac{1}{2}\left\{ \boldsymbol{\delta}_b^t \boldsymbol{B}_b^t\ \ z\, \boldsymbol{D}_{xy}^{(l)}\ \ \boldsymbol{B}_m \boldsymbol{\delta}_m \right.$$

$$\left. + \boldsymbol{\delta}_m^t \boldsymbol{B}_m^t\ \ z\, \boldsymbol{D}_{xy}^{(l)}\ \ \boldsymbol{B}_b \boldsymbol{\delta}_b \right\}$$

$$+ \frac{1}{2}\left\{ \boldsymbol{\delta}_s^t \boldsymbol{B}_m^t\ \ f_1(z)\, \boldsymbol{D}_{xy}^{(l)}\ \ \boldsymbol{B}_m \boldsymbol{\delta}_m \right.$$

$$\left. + \boldsymbol{\delta}_m^t \boldsymbol{B}_m^t\ \ f_1(z)\, \boldsymbol{D}_{xy}^{(l)}\ \ \boldsymbol{B}_m \boldsymbol{\delta}_s \right\}$$

$$- \frac{1}{2}\left\{ \boldsymbol{\delta}_b^t \boldsymbol{B}_b^t\ \ z\ f_1(z)\ \ \boldsymbol{B}_m \boldsymbol{\delta}_s \right.$$

$$\left. + \boldsymbol{\delta}_s^t \boldsymbol{B}_m^t\ \ z\ f_1(z)\ \ \boldsymbol{B}_b \boldsymbol{\delta}_b \right\} \qquad (4.58)$$

The strain energy per unit area is defined as follows:-

$$U`(x,y,t) = \int_{-h/2}^{h/2} \overline{U}\ \ dz \qquad (4.59)$$

and the strain energy of the element at time t is

$$U(t) = \iint_{element} U`(x,y,t)\ \ dx\,dy \qquad (4.60)$$

Notice that all the $\boldsymbol{B}$ matrices are functions of (x, y), that means that all functions of z and the $\boldsymbol{D}$ matrices, which may be different for different layers, need to be integrated over the thickness. Writing the integration of a function $f(z)$ over the total thickness in terms of integrations over different layers, *i.e.*

$$\int_{-h/2}^{h/2} f(z)\ dz = \sum_{l=1}^{N_l} \int_{Z_L^{(L)}}^{Z_U^{(L)}} f(z)\ dz \tag{4.61}$$

then the following expressions of modified $\boldsymbol{D}$ matrices, at any point (x, y) on the midplane, can be deduced from the integration of Equation (4.58) with respect to z:-

$$\boldsymbol{D}_{mm}(x,y) = \int_{-h/2}^{h/2} \boldsymbol{D}_{xy}^{(l)}\ dz = \sum_{l=1}^{N_l} \left[Z_U^{(l)} - Z_L^{(l)} \right]\ \boldsymbol{D}_{xy}^{(l)} \tag{4.62}$$

$$\boldsymbol{D}_{bb}(x,y) = \int_{-h/2}^{h/2} z^2\, \boldsymbol{D}_{xy}^{(l)}\ dz = \sum_{l=1}^{N_l} \left[\frac{(Z_U^{(l)})^3 - (Z_L^{(l)})^3}{3} \right] \boldsymbol{D}_{xy}^{(l)} \tag{4.63}$$

$$\left.\begin{aligned} \boldsymbol{D}_{ss}(x,y) &= \int_{-h/2}^{h/2} f_1^2(z)\, \boldsymbol{D}_{(x,y)}^{(l)}\ dz \\ &= \sum_{l=1}^{N_l} \left\{ \left[\frac{(Z_U^{(l)})^3 - (Z_L^{(l)})^3}{3} \right] \right. \\ &\quad - \frac{8}{15\,h^2} \left[(Z_U^{(l)})^5 - (Z_L^{(l)})^5 \right] \\ &\quad \left. + \frac{16}{63\,h^4} \left[(Z_U^{(l)})^7 - (Z_L^{(l)})^7 \right] \right\} \boldsymbol{D}_{xy}^{(l)} \end{aligned}\right\} \tag{4.64}$$

$$\boldsymbol{\mu}_{ss}(x,y) = \int_{-h/2}^{h/2} f_1^2(z)\, \boldsymbol{\mu}^{(l)}\, dz$$

$$= \sum_{l=1}^{N_l} \left\{ \left[(Z_U^{(l)}) - (Z_L^{(l)}) \right] - \frac{8}{3h^2} \left[(Z_U^{(l)})^3 - (Z_L^{(l)})^3 \right] + \frac{16}{5h^4} \left[(Z_U^{(l)})^5 - (Z_L^{(l)})^5 \right] \right\} \boldsymbol{\mu}^{(l)} \qquad (4.65)$$

$$\boldsymbol{D}_{mb}(x,y) = \boldsymbol{D}_{bm}(x,y) = \int_{-h/2}^{h/2} z\, \boldsymbol{D}_{(x,y)}^{(l)}\, dz$$

$$= \sum_{l=1}^{N_l} \left[\frac{(Z_U^{(l)})^2 - (Z_L^{(l)})^2}{2} \right] \boldsymbol{D}_{xy}^{(l)} \qquad (4.66)$$

$$\boldsymbol{D}_{ms}(x,y) = \boldsymbol{D}_{sm}(x,y) = \int_{-h/2}^{h/2} f_1(z)\, \boldsymbol{D}_{xy}^{(l)}\, dz$$

$$= \sum_{l=1}^{N_l} \left\{ \left[\frac{(Z_U^{(l)})^2 - (Z_L^{(l)})^2}{2} \right] - \frac{1}{3h^2} \left[(Z_U^{(l)})^4 - (Z_L^{(l)})^4 \right] \right\} \boldsymbol{D}_{xy}^{(l)} \qquad (4.67)$$

$$\boldsymbol{D}_{bs}(x,y) = \boldsymbol{D}_{sb}(x,y) = \int_{-h/2}^{h/2} z\, f_1(z)\, \boldsymbol{D}_{xy}^{(l)}\, dz$$

$$= \sum_{l=1}^{N_l} \left\{ \left[\frac{(Z_U^{(l)})^3 - (Z_L^{(l)})^3}{3} \right] - \frac{4}{15h^2} \left[(Z_U^{(l)})^5 - (Z_L^{(l)})^5 \right] \right\} \boldsymbol{D}_{xy}^{(l)} \qquad (4.68)$$

where $Z_U^{(l)}$, $Z_L^{(l)}$ are measured at (x, y).

Hence, the strain energy per unit area can be expressed as follows:-

$$\left.\begin{aligned} U`(x,y,t) \;=\; & \frac{1}{2}\,\boldsymbol{\delta}_m^t\,\boldsymbol{B}_m^t\,\boldsymbol{D}_{mm}\,\boldsymbol{B}_m\,\boldsymbol{\delta}_m \;+\; \frac{1}{2}\,\boldsymbol{\delta}_b^t\,\boldsymbol{B}_b^t\,\boldsymbol{D}_{bb}\,\boldsymbol{B}_b\,\boldsymbol{\delta}_b \\ & +\; \frac{1}{2}\,\boldsymbol{\delta}_s^t\,\boldsymbol{B}_m^t\,\boldsymbol{D}_{ss}\,\boldsymbol{B}_m\,\boldsymbol{\delta}_s \;+\; \frac{1}{2}\,\boldsymbol{\delta}_s^t\,\boldsymbol{B}_s^t\,\boldsymbol{\mu}_{ss}\,\boldsymbol{B}_s\,\boldsymbol{\delta}_s \\ & -\; \frac{1}{2}\left\{\boldsymbol{\delta}_b^t\,\boldsymbol{B}_b^t\,\boldsymbol{D}_{bm}\,\boldsymbol{B}_m\,\boldsymbol{\delta}_m \;+\; \boldsymbol{\delta}_m^t\,\boldsymbol{B}_m^t\,\boldsymbol{D}_{mb}\,\boldsymbol{B}_b\,\boldsymbol{\delta}_b\right\} \\ & +\; \frac{1}{2}\left\{\boldsymbol{\delta}_s^t\,\boldsymbol{B}_m^t\,\boldsymbol{D}_{sm}\,\boldsymbol{B}_m\,\boldsymbol{\delta}_m \;+\; \boldsymbol{\delta}_m^t\,\boldsymbol{B}_m^t\,\boldsymbol{D}_{ms}\,\boldsymbol{B}_m\,\boldsymbol{\delta}_s\right\} \\ & -\; \frac{1}{2}\left\{\boldsymbol{\delta}_b^t\,\boldsymbol{B}_b^t\,\boldsymbol{D}_{bs}\,\boldsymbol{B}_m\,\boldsymbol{\delta}_s \;+\; \boldsymbol{\delta}_s^t\,\boldsymbol{B}_m^t\,\boldsymbol{D}_{sb}\,\boldsymbol{B}_b\,\boldsymbol{\delta}_b\right\} \end{aligned}\right\} \qquad (4.69)$$

Integrating Equation (4.69) with respect to the area of the element, then the strain energy of the element can be expressed at any time t as follows:-

$$\begin{aligned} U(t) \;=\; & \frac{1}{2}\left\{\boldsymbol{\delta}_m^t\,\boldsymbol{K}_{mm}\,\boldsymbol{\delta}_m \;+\; \boldsymbol{\delta}_b^t\,\boldsymbol{K}_{bb}\,\boldsymbol{\delta}_b \;-\; \boldsymbol{\delta}_m^t\,\boldsymbol{K}_{mb}\,\boldsymbol{\delta}_b\right. \\ & +\; \boldsymbol{\delta}_s^t\left[\boldsymbol{K}_{ss}^{(x,y)} \;+\; \boldsymbol{K}_{ss}^{(\mu)}\right]\boldsymbol{\delta}_s \;-\; \boldsymbol{\delta}_b^t\,\boldsymbol{K}_{mb}^t\,\boldsymbol{\delta}_m \;+\; \boldsymbol{\delta}_m^t\,\boldsymbol{K}_{ms}\,\boldsymbol{\delta}_s \\ & \left.+\; \boldsymbol{\delta}_s^t\,\boldsymbol{K}_{ms}^t\,\boldsymbol{\delta}_m \;-\; \boldsymbol{\delta}_b^t\,\boldsymbol{K}_{bs}\,\boldsymbol{\delta}_s \;-\; \boldsymbol{\delta}_s^t\,\boldsymbol{K}_{bs}^t\,\boldsymbol{\delta}_b\right\} \end{aligned} \qquad (4.70)$$

where

$$\boldsymbol{K}_{mm} \;=\; \iint_{element} \boldsymbol{B}_m^t\,\boldsymbol{D}_{mm}\,\boldsymbol{B}_m \;\; dx\,dy \qquad (4.71)$$

$$\boldsymbol{K}_{bb} \;=\; \iint_{element} \boldsymbol{B}_b^t\,\boldsymbol{D}_{bb}\,\boldsymbol{B}_b \;\; dx\,dy \qquad (4.72)$$

$$\boldsymbol{K}_{ss}^{(x,y)} \;=\; \iint_{element} \boldsymbol{B}_m^t\,\boldsymbol{D}_{ss}\,\boldsymbol{B}_m \;\; dx\,dy \qquad (4.73)$$

$$\boldsymbol{K}_{ss}^{(\mu)} \;=\; \iint_{element} \boldsymbol{B}_s^t\,\boldsymbol{\mu}_{ss}\,\boldsymbol{B}_s \;\; dx\,dy \qquad (4.74)$$

$$\boldsymbol{K}_{mb} \;=\; \iint_{element} \boldsymbol{B}_m^t\,\boldsymbol{D}_{mb}\,\boldsymbol{B}_b \;\; dx\,dy \qquad (4.75)$$

$$\boldsymbol{K}_{ms} = \iint_{element} \boldsymbol{B}_m^t \, \boldsymbol{D}_{ms} \, \boldsymbol{B}_m \; dx\, dy \tag{4.76}$$

$$\boldsymbol{K}_{bs} = \iint_{element} \boldsymbol{B}_b^t \, \boldsymbol{D}_{bs} \, \boldsymbol{B}_m \; dx\, dy \tag{4.77}$$

Equation (4.70) may be rewritten as follows:-

$$U(t) = \frac{1}{2} \, \boldsymbol{\delta}^t(t) \, \boldsymbol{K} \, \boldsymbol{\delta}(t) \tag{4.78}$$

where $\boldsymbol{\delta}(t)$ is the nodal displacement vector of the element at time t, as defined by Equation (4.12), and $\boldsymbol{K}$ is the element stiffness matrix for the case of infinitesimal strains and can be constructed as follows:-

$$\boldsymbol{K} = \begin{bmatrix} \boldsymbol{K}_{mm} & -\boldsymbol{K}_{mb} & \boldsymbol{K}_{ms} \\ -\boldsymbol{K}_{mb}^t & \boldsymbol{K}_{bb} & -\boldsymbol{K}_{bs} \\ \boldsymbol{K}_{ms}^t & -\boldsymbol{K}_{bs}^t & \boldsymbol{K}_{ss}^{(x,y)} + \boldsymbol{K}_{ss}^{(\mu)} \end{bmatrix} \tag{4.79}$$

4.4 ELEMENT MASS MATRIX

The kinetic energy per unit volume, at any point inside the element is:-

$$\overline{KE} = \frac{1}{2} \rho \left[\dot{u}^2 + \dot{v}^2 + \dot{w}^2 \right] \tag{4.80}$$

Using the velocity vector defined by Equations (4.16), then the previous equation can be rewritten in the following matrix form:-

$$\overline{KE} = \frac{1}{2} \rho \left[\dot{\boldsymbol{q}}_{xy}^t \dot{\boldsymbol{q}}_{xy} + \dot{\boldsymbol{q}}_z^t \dot{\boldsymbol{q}}_z \right] \tag{4.81}$$

Substituting from Equation (4.19) and (4.20) into (4.81), it can be shown that:-

$$\overline{KE} = \frac{1}{2}\rho\left\{\left[\dot{\boldsymbol{\delta}}_m^t N_L^t - z\,\dot{\boldsymbol{\delta}}_b^t N_b^t + f_1(z)\,\dot{\boldsymbol{\delta}}_s^t N_L^t\right]\right.$$

$$\left[N_L\,\dot{\boldsymbol{\delta}}_m - z\,N_b\,\dot{\boldsymbol{\delta}}_b + f_1(z)\,N_L\,\dot{\boldsymbol{\delta}}_s\right]$$

$$\left. + \dot{\boldsymbol{\delta}}_b^t N_H^t N_H\,\dot{\boldsymbol{\delta}}_b\right\}$$

Hence

$$\left.\begin{aligned}\overline{KE} = \frac{1}{2}\rho\Big\{ & \dot{\boldsymbol{\delta}}_m^t N_L^t N_L\,\dot{\boldsymbol{\delta}}_m + z^2\,\dot{\boldsymbol{\delta}}_b^t N_b^t N_b\,\dot{\boldsymbol{\delta}}_b \\ & + f_1^2(z)\,\dot{\boldsymbol{\delta}}_s^t N_L^t N_L\,\dot{\boldsymbol{\delta}}_s + \dot{\boldsymbol{\delta}}_b^t N_H^t N_H\,\dot{\boldsymbol{\delta}}_b \\ & - z\,\dot{\boldsymbol{\delta}}_m^t N_L^t N_b\,\dot{\boldsymbol{\delta}}_b - z\,\dot{\boldsymbol{\delta}}_b^t N_b^t N_L\,\dot{\boldsymbol{\delta}}_m \\ & + f_1(z)\,\dot{\boldsymbol{\delta}}_m^t N_L^t N_L\,\dot{\boldsymbol{\delta}}_s + f_1(z)\,\dot{\boldsymbol{\delta}}_s^t N_L^t N_L\,\dot{\boldsymbol{\delta}}_m \\ & - zf_1(z)\,\dot{\boldsymbol{\delta}}_b^t N_b^t N_L\,\dot{\boldsymbol{\delta}}_s - zf_1(z)\,\dot{\boldsymbol{\delta}}_s^t N_L^t N_b\,\dot{\boldsymbol{\delta}}_b\Big\}\end{aligned}\right\} \quad (4.82)$$

The kinetic energy per unit area of the element can be defined as follows:-

$$KE^{\backslash} = \int_{-h/2}^{h/2} \overline{KE}\,dz = \sum_{l=1}^{N_l} \int_{Z_L^{(l)}}^{Z_U^{(l)}} \overline{KE}^{(l)}\,dz \quad (4.83)$$

The N matrices, in Equation (4.82), are independent of z, and the following density functions can be defined at any point (x, y) on the element midplane:-

$$\left.\begin{aligned}\rho_{mm}(x,y) &= \int_{-h/2}^{h/2} \rho\ \ dz \\ &= \sum_{l=1}^{N_l} \left[Z_U^{(l)}(x,y) - Z_L^{(l)}(x,y)\right]\ \ \rho^{(l)}\end{aligned}\right\} \quad (4.84)$$

$$\left.\begin{aligned}\rho_{bb}(x,y) &= \int_{-h/2}^{h/2} z^2(x,y)\,\rho\ dz \\ &= \sum_{l=1}^{N_l} \left[\frac{\left(Z_U^{(l)}(x,y)\right)^3 - \left(Z_L^{(l)}(x,y)\right)^3}{3}\right]\ \ \rho^{(l)}\end{aligned}\right\} \quad (4.85)$$

$$\rho_{HH}(x,y) = \int_{-h/2}^{h/2} \rho \quad dz \qquad = \qquad \rho_{mm}(x,y) \tag{4.86}$$

$$\left.\begin{aligned}
\rho_{ss}(x,y) &= \int_{-h/2}^{h/2} \left(z - \frac{4z^3}{3h^2} \right)^2 \rho \quad dz \\
&= \sum_{l=1}^{N_l} \left\{ \left[\frac{\left(Z_U^{(l)}(x,y)\right)^3 - \left(Z_L^{(l)}(x,y)\right)^3}{3} \right] \right. \\
&\quad - \frac{8}{15h^2} \left[\left(Z_U^{(l)}(x,y)\right)^5 - \left(Z_L^{(l)}(x,y)\right)^5 \right] \\
&\quad \left. + \frac{16}{63h^2} \left[\left(Z_U^{(l)}(x,y)\right)^7 - \left(Z_L^{(l)}(x,y)\right)^7 \right] \right\} \rho^{(l)}
\end{aligned}\right\} \tag{4.87}$$

$$\left.\begin{aligned}
\rho_{mb}(x,y) &= \int_{-h/2}^{h/2} z(x,y)\, \rho \; dz \\
&= \sum_{l=1}^{N_l} \left[\frac{\left(Z_U^{(l)}(x,y)\right)^2 - \left(Z_L^{(l)}(x,y)\right)^2}{2} \right] \rho^{(l)}
\end{aligned}\right\} \tag{4.88}$$

$$\left.\begin{aligned}
\rho_{ms}(x,y) &= \rho_{sm}(x,y) = \int_{-h/2}^{h/2} \left(z - \frac{4z^3}{3h^2} \right) \rho \quad dz \\
&= \sum_{l=1}^{N_l} \left\{ \left[\frac{\left(Z_U^{(l)}(x,y)\right)^2 - \left(Z_L^{(l)}(x,y)\right)^2}{2} \right] \right. \\
&\quad \left. - \frac{1}{3h^2} \left[\left(Z_U^{(l)}(x,y)\right)^4 - \left(Z_L^{(l)}(x,y)\right)^4 \right] \right\} \rho^{(l)}
\end{aligned}\right\} \tag{4.89}$$

$$\rho_{bs}(x,y) = \rho_{sb}(x,y) = \int_{-h/2}^{h/2} z\left(z - \frac{4z^3}{3h^2}\right)\rho \quad dz$$

$$= \sum_{l=1}^{N_l} \left\{ \left[\frac{\left(Z_U^{(l)}(x,y)\right)^3 - \left(Z_L^{(l)}(x,y)\right)^3}{3} \right. \right.$$

$$\left. \left. - \frac{4}{15h^2}\left[\left(Z_U^{(l)}(x,y)\right)^5 - \left(Z_L^{(l)}(x,y)\right)^5\right] \right\} \rho^{(l)} \right\} \qquad (4.90)$$

Hence the kinetic energy per unit area can be expressed as follows:-

$$KE' = \frac{1}{2}\left\{ \rho_{mm}\,\dot{\boldsymbol{\delta}}_m^t\,\boldsymbol{N}_L^t\,\boldsymbol{N}_L\,\dot{\boldsymbol{\delta}}_m + \rho_{bb}\,\dot{\boldsymbol{\delta}}_b^t\,\boldsymbol{N}_b^t\,\boldsymbol{N}_b\,\dot{\boldsymbol{\delta}}_b \right.$$

$$+ \rho_{HH}\,\dot{\boldsymbol{\delta}}_b^t\,\boldsymbol{N}_H^t\,\boldsymbol{N}_H\,\dot{\boldsymbol{\delta}}_b + \rho_{ss}\,\dot{\boldsymbol{\delta}}_s^t\,\boldsymbol{N}_L^t\,\boldsymbol{N}_L\,\dot{\boldsymbol{\delta}}_s$$

$$- \rho_{bm}\,\dot{\boldsymbol{\delta}}_b^t\,\boldsymbol{N}_b^t\,\boldsymbol{N}_L\,\dot{\boldsymbol{\delta}}_m - \rho_{mb}\,\dot{\boldsymbol{\delta}}_m^t\,\boldsymbol{N}_L^t\,\boldsymbol{N}_b\,\dot{\boldsymbol{\delta}}_b$$

$$+ \rho_{ms}\,\dot{\boldsymbol{\delta}}_m^t\,\boldsymbol{N}_L^t\,\boldsymbol{N}_L\,\dot{\boldsymbol{\delta}}_s + \rho_{sm}\,\dot{\boldsymbol{\delta}}_s^t\,\boldsymbol{N}_L^t\,\boldsymbol{N}_L\,\dot{\boldsymbol{\delta}}_m$$

$$\left. - \rho_{bs}\,\dot{\boldsymbol{\delta}}_b^t\,\boldsymbol{N}_b^t\,\boldsymbol{N}_L\,\dot{\boldsymbol{\delta}}_s - \rho_{sb}\,\dot{\boldsymbol{\delta}}_s^t\,\boldsymbol{N}_L^t\,\boldsymbol{N}_b\,\dot{\boldsymbol{\delta}}_b \right\} \qquad (4.91)$$

Integrating the previous equation over the area of the element, then the kinetic energy of the element at a time t can be expressed as follows:-

$$KE(t) = \frac{1}{2}\left\{ \dot{\boldsymbol{\delta}}_m^t\,\boldsymbol{M}_{mm}\,\dot{\boldsymbol{\delta}}_m + \dot{\boldsymbol{\delta}}_b^t\left(\boldsymbol{M}_{bb} + \boldsymbol{M}_{HH}\right)\dot{\boldsymbol{\delta}}_b \right.$$

$$+ \dot{\boldsymbol{\delta}}_s^t\,\boldsymbol{M}_{ss}\,\dot{\boldsymbol{\delta}}_s - \dot{\boldsymbol{\delta}}_m^t\,\boldsymbol{M}_{mb}\,\dot{\boldsymbol{\delta}}_b$$

$$- \dot{\boldsymbol{\delta}}_b^t\,\boldsymbol{M}_{mb}^t\,\dot{\boldsymbol{\delta}}_m + \dot{\boldsymbol{\delta}}_m^t\,\boldsymbol{M}_{ms}\,\dot{\boldsymbol{\delta}}_s$$

$$\left. + \dot{\boldsymbol{\delta}}_s^t\,\boldsymbol{M}_{ms}^t\,\dot{\boldsymbol{\delta}}_m - \dot{\boldsymbol{\delta}}_b^t\,\boldsymbol{M}_{bs}\,\dot{\boldsymbol{\delta}}_s - \dot{\boldsymbol{\delta}}_s^t\,\boldsymbol{M}_{bs}^t\,\dot{\boldsymbol{\delta}}_b \right\} \qquad (4.92)$$

where
$$\boldsymbol{M}_{mm} = \int\int_{element} \rho_{mm}\,\boldsymbol{N}_L^t\,\boldsymbol{N}_L \quad dx\,dy \qquad (4.93)$$

$$\boldsymbol{M}_{bb} = \int\int_{element} \rho_{bb}\, \boldsymbol{N}_b^t\, \boldsymbol{N}_b \; dx\, dy \tag{4.94}$$

$$\boldsymbol{M}_{HH} = \int\int_{element} \rho_{HH}\, \boldsymbol{N}_H^t\, \boldsymbol{N}_H \; dx\, dy \tag{4.95}$$

$$\boldsymbol{M}_{ss} = \int\int_{element} \rho_{ss}\, \boldsymbol{N}_L^t\, \boldsymbol{N}_L \; dx\, dy \tag{4.96}$$

$$\boldsymbol{M}_{mb} = \int\int_{element} \rho_{mb}\, \boldsymbol{N}_L^t\, \boldsymbol{N}_b \; dx\, dy \tag{4.97}$$

$$\boldsymbol{M}_{ms} = \int\int_{element} \rho_{ms}\, \boldsymbol{N}_L^t\, \boldsymbol{N}_L \; dx\, dy \tag{4.98}$$

$$\boldsymbol{M}_{bs} = \int\int_{element} \rho_{bs}\, \boldsymbol{N}_b^t\, \boldsymbol{N}_L \; dx\, dy \tag{4.99}$$

Equation (4.92) can also be simplified as follows:-

$$KE(t) = \frac{1}{2}\, \dot{\boldsymbol{\delta}}^t(t) \quad \boldsymbol{M} \quad \dot{\boldsymbol{\delta}}(t) \tag{4.100}$$

where

$$\dot{\boldsymbol{\delta}}(t) = \left\{ \dot{\boldsymbol{\delta}}_m(t) \quad \dot{\boldsymbol{\delta}}_b(t) \quad \dot{\boldsymbol{\delta}}_s(t) \right\} \tag{4.101}$$

and $\boldsymbol{M}$ is the mass matrix of the element which is constructed as follows:-

$$\boldsymbol{M} = \begin{bmatrix} \boldsymbol{M}_{mm} & -\boldsymbol{M}_{mb} & \boldsymbol{M}_{ms} \\ -\boldsymbol{M}_{mb}^t & \boldsymbol{M}_{bb} + \boldsymbol{M}_{HH} & -\boldsymbol{M}_{bs} \\ \boldsymbol{M}_{ms}^t & -\boldsymbol{M}_{bs}^t & \boldsymbol{M}_{ss} \end{bmatrix} \tag{4.102}$$

4.5 ELEMENT STIFFNESS MATRIX FOR FINITE STRAIN CONTRIBUTIONS AND CENTRIFUGAL STIFFENING

The virtual or differential value of the finite strain contributions, due to a virtual or differential displacement field is

$$d\boldsymbol{\epsilon}_L(x, y, z, t) = \left\{ \; d\boldsymbol{\epsilon}_x^L \quad d\boldsymbol{\epsilon}_y^L \quad d\boldsymbol{\gamma}_{xy}^L \; \right\} \tag{4.103}$$

assuming negligible finite strain contributions for the transverse shear strains. The vector $d\boldsymbol{\epsilon}_L$ is expressed in terms of nodal displacements and shape functions by means of Equation (4.52). The corresponding increment of strain energy density at any point *(x,y,z)* in layer *l* is

$$d\overline{U}_L^{(l)}(x,y,z,t) = d\boldsymbol{\epsilon}_L^t \; \boldsymbol{\sigma}_{xy}^{(l)} \tag{4.104}$$

Substituting from Equation (4.52) into Equation (4.104) then :-

$$\left.\begin{aligned} d\overline{U}_L^{(l)}(x,y,z,t) = \Big\{ & d\boldsymbol{\delta}_m^t \, \boldsymbol{G}_m^t \, \boldsymbol{A}_m^t + d\boldsymbol{\delta}_b^t \, \boldsymbol{G}_w^t \, \boldsymbol{A}_w^t \\ & + z^2 \, d\boldsymbol{\delta}_b^t \, \boldsymbol{G}_b^t \, \boldsymbol{A}_b^t + f_1^2(z) \, d\boldsymbol{\delta}_s^t \, \boldsymbol{G}_m^t \, \boldsymbol{A}_s^t \\ & - z\left[d\boldsymbol{\delta}_m^t \, \boldsymbol{G}_m^t \, \boldsymbol{A}_b^t + d\boldsymbol{\delta}_b^t \, \boldsymbol{G}_b^t \, \boldsymbol{A}_m^t \right] \\ & + f_1(z)\left[d\boldsymbol{\delta}_m^t \, \boldsymbol{G}_m^t \, \boldsymbol{A}_s^t + d\boldsymbol{\delta}_s^t \, \boldsymbol{G}_m^t \, \boldsymbol{A}_m^t \right] \\ & - z f_1(z)\left[d\boldsymbol{\delta}_b^t \, \boldsymbol{G}_b^t \, \boldsymbol{A}_s^t + d\boldsymbol{\delta}_s^t \, \boldsymbol{G}_b^t \, \boldsymbol{A}_b^t \right] \Big\} \, \boldsymbol{\sigma}_{xy}^{(l)} \end{aligned}\right\} \tag{4.105}$$

By direct multiplication of matrices, the following equations can be proved:-

$$\boldsymbol{A}_m^t \, \boldsymbol{\sigma}_{xy} \equiv \boldsymbol{S} \, \boldsymbol{\theta}_m = \boldsymbol{S} \, \boldsymbol{G}_m \, \boldsymbol{\delta}_m \tag{4.106}$$

$$\boldsymbol{A}_s^t \, \boldsymbol{\sigma}_{xy} \equiv \boldsymbol{S} \, \boldsymbol{\theta}_s = \boldsymbol{S} \, \boldsymbol{G}_m \, \boldsymbol{\delta}_s \tag{4.107}$$

$$\boldsymbol{A}_b^t \, \boldsymbol{\sigma}_{xy} \equiv \boldsymbol{S} \, \boldsymbol{\theta}_b = \boldsymbol{S} \, \boldsymbol{G}_b \, \boldsymbol{\delta}_b \tag{4.108}$$

$$\boldsymbol{A}_w^t \, \boldsymbol{\sigma}_{xy} \equiv \boldsymbol{S}_w \, \boldsymbol{\theta}_w = \boldsymbol{S}_w \, \boldsymbol{G}_w \, \boldsymbol{\delta}_b \tag{4.109}$$

where

$$\boldsymbol{S} = \begin{bmatrix} \sigma_x & 0 & \tau_{xy} & 0 \\ 0 & \sigma_x & 0 & \tau_{xy} \\ \tau_{xy} & 0 & \sigma_y & 0 \\ 0 & \tau_{xy} & 0 & \sigma_y \end{bmatrix} \tag{4.110}$$

and

$$\boldsymbol{S}_w = \begin{bmatrix} \sigma_x & \tau_{xy} \\ \tau_{xy} & \sigma_y \end{bmatrix} \tag{4.111}$$

Hence, Equation (4.105) can be rewritten as follows:-

$$\left.\begin{aligned} d\overline{U}_L^{(l)} = \; & d\boldsymbol{\delta}_m^t \, \boldsymbol{G}_m^t \, \boldsymbol{S}^{(l)} \, \boldsymbol{G}_m \, \boldsymbol{\delta}_m + d\boldsymbol{\delta}_b^t \, \boldsymbol{G}_w^t \, \boldsymbol{S}_w^{(l)} \, \boldsymbol{G}_w \, \boldsymbol{\delta}_b \\ & + z^2 \, d\boldsymbol{\delta}_b^t \, \boldsymbol{G}_b^t \, \boldsymbol{S}^{(l)} \, \boldsymbol{G}_b \, \boldsymbol{\delta}_b + f_1^2(z) \, d\boldsymbol{\delta}_s^t \, \boldsymbol{G}_m^t \, \boldsymbol{S}^{(l)} \, \boldsymbol{G}_m \, \boldsymbol{\delta}_s \\ & - z\left[d\boldsymbol{\delta}_m^t \, \boldsymbol{G}_m^t \, \boldsymbol{S}^{(l)} \, \boldsymbol{G}_b \, \boldsymbol{\delta}_b + d\boldsymbol{\delta}_b^t \, \boldsymbol{G}_b^t \, \boldsymbol{S}^{(l)} \, \boldsymbol{G}_m \, \boldsymbol{\delta}_m \right] \\ & + f_1(z)\left[d\boldsymbol{\delta}_m^t \, \boldsymbol{G}_m^t \, \boldsymbol{S}^{(l)} \, \boldsymbol{G}_m \, \boldsymbol{\delta}_s + d\boldsymbol{\delta}_s^t \, \boldsymbol{G}_m^t \, \boldsymbol{S}^{(l)} \, \boldsymbol{G}_m \, \boldsymbol{\delta}_m \right] \\ & - z f_1(z)\left[d\boldsymbol{\delta}_b^t \, \boldsymbol{G}_b^t \, \boldsymbol{S}^{(l)} \, \boldsymbol{G}_m \, \boldsymbol{\delta}_s + d\boldsymbol{\delta}_s^t \, \boldsymbol{G}_m^t \, \boldsymbol{S}^{(l)} \, \boldsymbol{G}_b \, \boldsymbol{\delta}_b \right] \end{aligned}\right\} \quad (4.112)$$

Notice that the $\boldsymbol{G}$ matrices are independent of z, but $\boldsymbol{S}$ and $\boldsymbol{S}_w$ may vary with z even within the same layer. To simplify the derivations, the average value of the stress vector inside the layer will be employed as a constant parameter within the thickness of the layer, *i.e.*

$$\boldsymbol{S}^{(l)} \approx \frac{1}{2}\left[\boldsymbol{S}\left(Z_L^{(l)}\right) + \boldsymbol{S}\left(Z_U^{(l)}\right) \right] \quad (4.113)$$

$$\boldsymbol{S}_w^{(l)} \approx \frac{1}{2}\left[\boldsymbol{S}_w\left(Z_L^{(l)}\right) + \boldsymbol{S}_w\left(Z_U^{(l)}\right) \right] \quad (4.114)$$

The following integrated z functions can also be defined as:-

$$\boldsymbol{S}_{mm} = \int_{-h/2}^{h/2} \boldsymbol{S} \, dz = \sum_{l=1}^{N_l} \left[Z_U^{(l)} - Z_L^{(l)} \right] \boldsymbol{S}^{(l)} \quad (4.115)$$

$$\boldsymbol{S}_{ww} = \int_{-h/2}^{h/2} \boldsymbol{S}_w \, dz = \sum_{l=1}^{N_l} \left[Z_U^{(l)} - Z_L^{(l)} \right] \boldsymbol{S}_w^{(l)} \quad (4.116)$$

$$\left.\begin{aligned} \boldsymbol{S}_{bb} = & \int_{-h/2}^{h/2} z^2 \, \boldsymbol{S} \, dz \\ = & \sum_{l=1}^{N_l} \left[\frac{\left(Z_U^{(l)}\right)^3 - \left(Z_L^{(l)}\right)^3}{3} \right] \boldsymbol{S}^{(l)} \end{aligned}\right\} \quad (4.117)$$

$$
\begin{aligned}
S_{ss} &= \int_{-h/2}^{h/2} \left(z - \frac{4z^3}{3h^2} \right)^2 S \quad dz \\
&= \sum_{l=1}^{N_l} \left\{ \left[\frac{\left(Z_U^{(l)}\right)^3 - \left(Z_L^{(l)}\right)^3}{3} \right] \right. \\
&\quad - \frac{8}{15h^2} \left[\left(Z_U^{(l)}\right)^5 - \left(Z_L^{(l)}\right)^5 \right] \\
&\quad \left. + \frac{16}{63h^4} \left[\left(Z_U^{(l)}\right)^7 - \left(Z_L^{(l)}\right)^7 \right] \right\} \quad S^{(l)}
\end{aligned}
\tag{4.118}
$$

$$
\begin{aligned}
S_{mb} &= S_{bm} = \int_{-h/2}^{h/2} z \; S \; dz \\
&= \sum_{l=1}^{N_l} \left[\frac{\left(Z_U^{(l)}\right)^2 - \left(Z_L^{(l)}\right)^2}{2} \right] \quad S^{(l)}
\end{aligned}
\tag{4.119}
$$

$$
\begin{aligned}
S_{ms} &= S_{sm}(x,y) = \int_{-h/2}^{h/2} \left(z - \frac{4z^3}{3h^2} \right) S \; dz \\
&= \sum_{l=1}^{N_l} \left\{ \left[\frac{\left(Z_U^{(l)}\right)^2 - \left(Z_L^{(l)}\right)^2}{2} \right] \right. \\
&\quad \left. - \frac{1}{3h^2} \left[\left(Z_U^{(l)}\right)^4 - \left(Z_L^{(l)}\right)^4 \right] \right\} \quad S^{(l)}
\end{aligned}
\tag{4.120}
$$

$$S_{bs}(x,y) = S_{sb} = \int_{-h/2}^{h/2} z\left(z - \frac{4z^3}{3h^2}\right) S\, dz$$

$$= \sum_{l=1}^{N_l} \left\{ \left[\frac{\left(Z_U^{(l)}\right)^3 - \left(Z_L^{(l)}\right)^3}{3} \right] - \frac{4}{15h^2}\left[\left(Z_U^{(l)}\right)^5 - \left(Z_L^{(l)}\right)^5\right] \right\} S^{(l)} \qquad (4.121)$$

The increment of the strain energy per unit area, due to finite strain contributions, at point *(x, y)* on the midplane of the element and time *t* can be expressed as follows:-

$$dU_L^{\backprime}(x,y,t) = \int_{-h/2}^{h/2} d\overline{U}_L^{(l)}\, dz$$

$$\begin{aligned}
&= d\boldsymbol{\delta}_m^t\, \boldsymbol{G}_m^t\, \boldsymbol{S}_{mm}\, \boldsymbol{G}_m\, \boldsymbol{\delta}_m + d\boldsymbol{\delta}_b^t\, \boldsymbol{G}_w^t\, \boldsymbol{S}_{ww}\, \boldsymbol{G}_w\, \boldsymbol{\delta}_b \\
&+ d\boldsymbol{\delta}_b^t\, \boldsymbol{G}_b^t\, \boldsymbol{S}_{bb}\, \boldsymbol{G}_b\, \boldsymbol{\delta}_b + d\boldsymbol{\delta}_s^t\, \boldsymbol{G}_m^t\, \boldsymbol{S}_{ss}\, \boldsymbol{G}_m\, \boldsymbol{\delta}_s \\
&- d\boldsymbol{\delta}_m^t\, \boldsymbol{G}_m^t\, \boldsymbol{S}_{mb}\, \boldsymbol{G}_b\, \boldsymbol{\delta}_b - d\boldsymbol{\delta}_b^t\, \boldsymbol{G}_b^t\, \boldsymbol{S}_{bm}\, \boldsymbol{G}_m\, \boldsymbol{\delta}_m \\
&+ d\boldsymbol{\delta}_m^t\, \boldsymbol{G}_m^t\, \boldsymbol{S}_{ms}\, \boldsymbol{G}_m\, \boldsymbol{\delta}_s + d\boldsymbol{\delta}_s^t\, \boldsymbol{G}_m^t\, \boldsymbol{S}_{sm}\, \boldsymbol{G}_m\, \boldsymbol{\delta}_m \\
&- d\boldsymbol{\delta}_b^t\, \boldsymbol{G}_b^t\, \boldsymbol{S}_{bs}\, \boldsymbol{G}_m\, \boldsymbol{\delta}_s - d\boldsymbol{\delta}_s^t\, \boldsymbol{G}_m^t\, \boldsymbol{S}_{sb}\, \boldsymbol{G}_b\, \boldsymbol{\delta}_b
\end{aligned} \qquad (4.122)$$

Integrating over the area of the element, the increment of the strain energy due to finite-strain contributions and centrifugal stiffening is expressed as follows:-

$$
\begin{aligned}
dU_L(t) &= \iint_{element} dU_L \, dx\, dy \\
&= d\boldsymbol{\delta}_m^t \, \boldsymbol{K}_{mm}^{\sigma} \, \boldsymbol{\delta}_m + d\boldsymbol{\delta}_b^t \left((\boldsymbol{K}_{bb}^{\sigma} + (\boldsymbol{K}_{ww}^{\sigma} \right) \boldsymbol{\delta}_b \\
&+ d\boldsymbol{\delta}_s^t \, \boldsymbol{K}_{ss}^{\sigma} \, \boldsymbol{\delta}_s - d\boldsymbol{\delta}_m^t \, \boldsymbol{K}_{mb}^{\sigma} \, \boldsymbol{\delta}_m - d\boldsymbol{\delta}_b^t \left(\boldsymbol{K}_{mb}^{\sigma} \right)^t \boldsymbol{\delta}_m \\
&+ d\boldsymbol{\delta}_m^t \, \boldsymbol{K}_{ms}^{\sigma} \, \boldsymbol{\delta}_s + d\boldsymbol{\delta}_s^t \left(\boldsymbol{K}_{ms}^{\sigma} \right)^t \boldsymbol{\delta}_m \\
&- d\boldsymbol{\delta}_b^t \, \boldsymbol{K}_{bs}^{\sigma} \, \boldsymbol{\delta}_s - d\boldsymbol{\delta}_s^t \left(\boldsymbol{K}_{bs}^{\sigma} \right)^t \boldsymbol{\delta}_b
\end{aligned}
\qquad (4.123)
$$

where

$$\boldsymbol{K}_{mm}^{\sigma} = \iint_{element} \boldsymbol{G}_m^t \, \boldsymbol{S}_{mm} \, \boldsymbol{G}_m \; dx\, dy \qquad (4.124)$$

$$\boldsymbol{K}_{bb}^{\sigma} = \iint_{element} \boldsymbol{G}_b^t \, \boldsymbol{S}_{bb} \, \boldsymbol{G}_b \; dx\, dy \qquad (4.125)$$

$$\boldsymbol{K}_{ww}^{\sigma} = \iint_{element} \boldsymbol{G}_w^t \, \boldsymbol{S}_{ww} \, \boldsymbol{G}_w \; dx\, dy \qquad (4.126)$$

$$\boldsymbol{K}_{ss}^{\sigma} = \iint_{element} \boldsymbol{G}_m^t \, \boldsymbol{S}_{ss} \, \boldsymbol{G}_m \; dx\, dy \qquad (4.127)$$

$$\boldsymbol{K}_{mb}^{\sigma} = \iint_{element} \boldsymbol{G}_m^t \, \boldsymbol{S}_{mb} \, \boldsymbol{G}_b \; dx\, dy \qquad (4.128)$$

$$\boldsymbol{K}_{ms}^{\sigma} = \iint_{element} \boldsymbol{G}_m^t \, \boldsymbol{S}_{ms} \, \boldsymbol{G}_m \; dx\, dy \qquad (4.129)$$

$$\boldsymbol{K}_{bs}^{\sigma} = \iint_{element} \boldsymbol{G}_b^t \, \boldsymbol{S}_{bs} \, \boldsymbol{G}_m \; dx\, dy \qquad (4.130)$$

Equation (4.123) can also be rewritten as follows:-

$$dU_L(t) = d\boldsymbol{\delta}^t(t) \, \boldsymbol{K}^{\sigma} \, \boldsymbol{\delta}(t) \qquad (4.131)$$

where

$$\boldsymbol{K}^{\sigma} = \begin{bmatrix} \boldsymbol{K}^{\sigma}_{mm} & -\boldsymbol{K}^{\sigma}_{mb} & \boldsymbol{K}^{\sigma}_{ms} \\ -\left(\boldsymbol{K}^{\sigma}_{mb}\right)^{t} & \boldsymbol{K}^{\sigma}_{bb} + \boldsymbol{K}^{\sigma}_{ww} & -\boldsymbol{K}^{\sigma}_{bs} \\ \left(\boldsymbol{K}^{\sigma}_{ms}\right)^{t} & -\left(\boldsymbol{K}^{\sigma}_{bs}\right)^{t} & \boldsymbol{K}^{\sigma}_{ss} \end{bmatrix} \tag{4.132}$$

and the total increment of the strain energy will be

$$dU(t) = d\boldsymbol{\delta}^{t}(t) \left[\boldsymbol{K} + \boldsymbol{K}^{\sigma} \right] \boldsymbol{\delta}(t) \tag{4.133}$$

where $\boldsymbol{K}$ has been previously defined by Equation (4.79).

4.6 DERIVATION OF STATIC EQUATIONS FOR A ROTATING ELEMENT

4.6.1 Equivalent nodal loading to inertial effects

If a rotating composite layered plate or shell has a steady-state case of deformation, where the vector of deformation $\vec{q}$ at any point inside it is independent of time, then the acceleration at that point due to rotation is

$$\boldsymbol{a} = \boldsymbol{a}_{\circ} \equiv -\Omega^{2} \boldsymbol{C}_{1} \boldsymbol{R}_{\circ} \tag{4.134}$$

and $\boldsymbol{C}_1$, $\boldsymbol{R}_{\circ}$ are as defined in section (3.3).

So far the equations derived for the element are described with respect to local axes of the element, where the z axis is always normal to the element midplane. If the local x, y and z axes have directional cosines (l_1, m_1, n_1), (l_2, m_2, n_2) and (l_3, m_3, n_3) with respect to the structural global axes respectively, then:-

$$\begin{bmatrix} \hat{i} \\ \hat{j} \\ \hat{k} \end{bmatrix}_{local} = \boldsymbol{R}_{3\times 3} \begin{bmatrix} \hat{i} \\ \hat{j} \\ \hat{k} \end{bmatrix}_{global} \tag{4.135}$$

where

$$\boldsymbol{R}_{3\times 3} = \begin{bmatrix} l_1 & m_1 & n_1 \\ l_2 & m_2 & n_2 \\ l_3 & m_3 & n_3 \end{bmatrix} \tag{4.136}$$

If the matrix $\boldsymbol{C}_1$ is defined in terms of directional cosines (l, m, n) with respect to the global system of axes, then $\boldsymbol{a}$ given by Equation (4.134) contains components with respect to global axes. Using Equation (4.135), it can be shown that:-

$$\boldsymbol{a}_{local} = \boldsymbol{R}_{3\times 3}\, \boldsymbol{a}_{global} \tag{4.137}$$

For simplicity, the $\boldsymbol{R}_o$ vector will represent the position vector of a point on the midplane of the element, *i.e.* with a constant value of z, and the acceleration vector will be partitioned as follows:-

$$\boldsymbol{a}_{local} = \begin{bmatrix} a_x \\ a_y \\ a_z \end{bmatrix} = \begin{bmatrix} \boldsymbol{a}_{xy} \\ \boldsymbol{a}_z \end{bmatrix} \tag{4.138}$$

where $\boldsymbol{a}_{xy} = \begin{bmatrix} a_x \\ a_y \end{bmatrix}$, $\boldsymbol{a}_z = \begin{bmatrix} a_z \end{bmatrix}$

D'Alembert's force due to acceleration for an infinitesimal mass Δm in the l^{th} layer is

$$\Delta \boldsymbol{F}^{(l)} = -\Delta m\, \boldsymbol{a}_{local} = -\rho^{(l)} \begin{bmatrix} \boldsymbol{a}_{xy} \\ \boldsymbol{a}_z \end{bmatrix} \Delta x\, \Delta y\, \Delta z \tag{4.139}$$

The work done due to a virtual displacement field $d\boldsymbol{q}$ (x, y, z) will be

$$\left.\begin{aligned} d\left(\Delta W^{(l)}\right) &= d\boldsymbol{q}^t\, \Delta \boldsymbol{F}^{(l)} \\ &= -\rho^{(l)} \left\{ d\boldsymbol{q}_{xy}^t\, \boldsymbol{a}_{xy} + d\boldsymbol{q}_z^t\, \boldsymbol{a}_z \right\} \Delta x\, \Delta y\, \Delta z \end{aligned}\right\} \tag{4.140}$$

From the analysis given in section (4.1), the displacement components, can be expressed in terms of nodal parameters, and shape functions as follows:-

$$d\,\boldsymbol{q}_{xy} \equiv \begin{bmatrix} du \\ dv \end{bmatrix} = \boldsymbol{N}_L\, d\boldsymbol{\delta}_m - z\,\boldsymbol{N}_b\, d\boldsymbol{\delta}_b + f_1(z)\,\boldsymbol{N}_L\, d\boldsymbol{\delta}_s \tag{4.141}$$

$$d\,\boldsymbol{q}_z \equiv [dw] = \boldsymbol{N}_H\, d\boldsymbol{\delta}_b \tag{4.142}$$

Hence

$$\left.\begin{aligned} d\left(\Delta \boldsymbol{W}^{(l)}\right) = -\rho^{(l)} \Big\{ \Big[& d\boldsymbol{\delta}_m^t \boldsymbol{N}_L^t - z\, d\boldsymbol{\delta}_b^t \boldsymbol{N}_b^t \\ & + f_1(z)\, d\boldsymbol{\delta}_s^t \boldsymbol{N}_L^t \Big] \boldsymbol{a}_{xy} + d\boldsymbol{\delta}_b^t \boldsymbol{N}_H^t \boldsymbol{a}_z \Big\} \Delta x\, \Delta y\, \Delta z \end{aligned}\right\} \tag{4.143}$$

Integrating over the volume of the element, it can be shown that the work done on the element during the virtual displacement is

$$dW = d\boldsymbol{\delta}_m^t \boldsymbol{F}_m + d\boldsymbol{\delta}_b^t \boldsymbol{F}_b + d\boldsymbol{\delta}_s^t \boldsymbol{F}_s + d\boldsymbol{\delta}_b^t \boldsymbol{F}_w \tag{4.144}$$

where

$$\boldsymbol{F}_m = -\iint_{element} \rho_m\, \boldsymbol{N}_L^t\, \boldsymbol{a}_{xy}\; dx\, dy \tag{4.145}$$

$$\boldsymbol{F}_b = -\iint_{element} \rho_b\, \boldsymbol{N}_b^t\, \boldsymbol{a}_{xy}\; dx\, dy \tag{4.146}$$

$$\boldsymbol{F}_s = -\iint_{element} \rho_s\, \boldsymbol{N}_L^t\, \boldsymbol{a}_{xy}\; dx\, dy \tag{4.147}$$

$$\boldsymbol{F}_w = -\iint_{element} \rho_w\, \boldsymbol{N}_H^t\, \boldsymbol{a}_z\; dx\, dy \tag{4.148}$$

and

$$\left.\begin{aligned} \rho_m &= \int_{-h/2}^{h/2} \rho^{(l)}\; dz \\ &= \sum_{l=1}^{N_l} \left[Z_U^{(l)} - Z_L^{(l)} \right] \rho^{(l)} \end{aligned}\right\} \tag{4.149}$$

$$\left.\begin{aligned}\rho_b &= -\int_{-h/2}^{h/2} z\,\rho^{(l)}\,dz \\ &= -\sum_{l=1}^{N_l}\left[\frac{\left(Z_U^{(l)}\right)^2-\left(Z_L^{(l)}\right)^2}{2}\right]\rho^{(l)}\end{aligned}\right\} \tag{4.150}$$

$$\left.\begin{aligned}\rho_s &= \int_{-h/2}^{h/2}\left(z-\frac{4z^3}{3h^2}\right)\rho^{(l)}\,dz \\ &= \sum_{l=1}^{N_l}\left\{\left[\frac{\left(Z_U^{(l)}\right)^2-\left(Z_L^{(l)}\right)^2}{2}\right]\right. \\ &\quad \left.-\frac{1}{3h^2}\left[\left(Z_U^{(l)}\right)^4-\left(Z_L^{(l)}\right)^4\right]\right\}\rho^{(l)}\end{aligned}\right\} \tag{4.151}$$

$$\rho_w = \rho_m = \int_{-h/2}^{h/2}\rho^{(l)}\,dz \tag{4.152}$$

Equation (4.144) can also be expressed as follows:-

$$dW = d\boldsymbol{\delta}^t\,\boldsymbol{F} \tag{4.153}$$

where

$$\boldsymbol{F} = \begin{bmatrix}\boldsymbol{F}_m \\ \boldsymbol{F}_b + \boldsymbol{F}_w \\ \boldsymbol{F}_s\end{bmatrix} \tag{4.154}$$

4.6.2 Element static equations

Applying the principle of virtual work, the change of the total potential energy of the element due to a virtual displacement field is zero, or

$$dU - dW = 0$$

Using matrix equations developed in sections (4.3), (4.5) and (4.6.1) for a case with steady-state deformation, then:-

$$d\boldsymbol{\delta}^t(\boldsymbol{K} + \boldsymbol{K}^\sigma) - d\boldsymbol{\delta}^t\boldsymbol{F} = 0$$

or
$$d\boldsymbol{\delta}\left[(\boldsymbol{K} + \boldsymbol{K}^\sigma)\boldsymbol{\delta} - \boldsymbol{F}\right] = 0$$

i.e.
$$(\boldsymbol{K} + \boldsymbol{K}^\sigma)\boldsymbol{\delta} = \boldsymbol{F} \qquad (4.155)$$

The finite element equations of the whole composite layered plate or shell are assembled from element equations in the usual way, provided that element stiffness matrices and nodal vectors are represented with respect to the same global system of axes, as will be explained in section (4.9).

4.7 DERIVATION OF DYNAMIC EQUATIONS FOR A ROTATING ELEMENT

4.7.1 Rotational speed in terms of local axes

If the angular velocity vector $\vec{\Omega}$, as described in section (3.3), is represented in terms of global components, then:-

$$\vec{\Omega} = \Omega\left(l_G\hat{i}_G + m_G\hat{j}_G + n_G\hat{k}_G\right) \qquad (4.156)$$

where (l_G, m_G, n_G) are the directional cosines of $\vec{\Omega}$ with respect to the global axes, and $\left(\hat{i}_G, \hat{j}_G, \hat{k}_G\right)$ are unit vectors in the directions of the global axes.

Using Equation (4.135), it can be shown that:-

$$\boldsymbol{\Omega}_{local} = \boldsymbol{R}_{3\times3}\ \boldsymbol{\Omega}_{global} \qquad (4.157)$$

i.e.
$$\Omega\begin{bmatrix} l \\ m \\ n \end{bmatrix} = \boldsymbol{R}_{3\times3}\ \boldsymbol{\Omega}_{global} \qquad (4.158)$$

where (l, m, n) are the directional cosines of $\vec{\Omega}$ with respect to element local axes.

Hence, it can be deduced that:-

$$\left.\begin{aligned} l &= l_G l_1 + m_G m_1 + n_G n_1 \\ m &= l_G l_2 + m_G m_2 + n_G n_2 \\ n &= l_G l_3 + m_G m_3 + n_G n_3 \end{aligned}\right\} \qquad (4.159)$$

and the Equations derived in section (3.3) can be employed with the vectors and matrices given by Equations (3.84)-(3.89) being defined with respect to element local axes.

4.7.2 Effect of relative acceleration

The relative acceleration at an instant of time t, as defined by Equation (3.81) can be expressed as follows:-

$$\boldsymbol{a}_r(x,y,z,t) = \ddot{\boldsymbol{q}} = \begin{bmatrix} \ddot{\boldsymbol{q}}_{xy} \\ \ddot{\boldsymbol{q}}_z \end{bmatrix} \qquad (4.160)$$

where $\ddot{\boldsymbol{q}}_{xy} = \begin{bmatrix} \ddot{u} \\ \ddot{v} \end{bmatrix}$, and $\ddot{\boldsymbol{q}}_z = [\ddot{w}]$

For an infinitesimal mass in layer l, D'Alembert's force due to relative acceleration can be expressed as follows:

$$\Delta \boldsymbol{F}_r^{(l)} = -\rho^{(l)} \begin{bmatrix} \ddot{\boldsymbol{q}}_{xy} \\ \ddot{\boldsymbol{q}}_z \end{bmatrix} \Delta x \, \Delta y \, \Delta z \qquad (4.161)$$

and the work done due to a virtual displacement field $d\boldsymbol{q}(x,y,z,t)$ will be:-

$$\left.\begin{aligned} d\left(\Delta W_r^{(l)}\right) &= d\boldsymbol{q}^t \, \Delta \, d\boldsymbol{F}_r^{(l)} \\ &= -\rho^{(l)} \left[d\boldsymbol{q}_{xy}^t \, \ddot{\boldsymbol{q}}_{xy} + d\boldsymbol{q}_z^t \, \ddot{\boldsymbol{q}}_z \right] \Delta x \, \Delta y \, \Delta z \end{aligned}\right\} \qquad (4.162)$$

Expressing $d\boldsymbol{q}$ and $\ddot{\boldsymbol{q}}$ in terms of nodal parameters and shape function, and integrating over the element, it can be proved that the work done due to D'Alembert's force of the relative acceleration during the virtual displacement is:-

$$dW_r = -d\boldsymbol{\delta}^t \, \boldsymbol{M} \, \ddot{\boldsymbol{\delta}} \qquad (4.163)$$

where $\boldsymbol{M}$ is the mass matrix of the element, which is identical to that derived in section (4.4) from the kinetic energy approach.

4.7.3 Effect of centripetal acceleration

D'Alembert's force acting on any infinitesimal mass at layer l, due to the centripetal acceleration is:-

$$\Delta \boldsymbol{F}_p^{(l)} = \boldsymbol{a}_p \, \Delta m = -\rho^{(l)} \, \boldsymbol{a}_p \, \Delta x \, \Delta y \, \Delta z$$

i.e.

$$\Delta \boldsymbol{F}_p^{(l)} = \left(\rho^{(l)} \, \Omega^2 \, \boldsymbol{C}_1 \, \boldsymbol{q} \right) \Delta x \, \Delta y \, \Delta z \qquad (4.164)$$

where

$$\boldsymbol{C}_1 = \begin{bmatrix} 1 - l^2 & -lm & -ln \\ -ml & 1 - m^2 & -mn \\ -nl & -nm & 1 - n^2 \end{bmatrix}$$

The work done by $\Delta \boldsymbol{F}_p$ due to the virtual displacement $d\boldsymbol{q}$ is

$$\left.\begin{aligned} d\left(\Delta \boldsymbol{W}_p^{(l)}\right) &= d\boldsymbol{q}^t \, \Delta \boldsymbol{F}_p^{(l)} \\ &= \rho^{(l)} \, \Omega^2 \left(d\boldsymbol{q}^t \, \boldsymbol{C}_1 \, \boldsymbol{q} \right) \Delta x \, \Delta y \, \Delta z \end{aligned}\right\} \qquad (4.165)$$

Defining the following sub-matrices of $\boldsymbol{C}_1$:-

$$\boldsymbol{a}_{22} = \begin{bmatrix} 1 - l^2 & -lm \\ -ml & 1 - m^2 \end{bmatrix} \qquad (4.166)$$

$$\boldsymbol{a}_{12} = \begin{bmatrix} -ln & -nm \end{bmatrix} \qquad (4.167)$$

$$\boldsymbol{a}_{21} = \begin{bmatrix} -ln \\ -mn \end{bmatrix} \equiv \boldsymbol{a}_{12}^t \qquad (4.168)$$

$$\boldsymbol{a}_{33} = \begin{bmatrix} 1 - n^2 \end{bmatrix} \qquad (4.169)$$

then it can be shown that:-

$$\left.\begin{aligned} d\boldsymbol{q}^t \, \boldsymbol{C}_1 \, \boldsymbol{q} = {} & d\boldsymbol{q}_{xy}^t \, \boldsymbol{a}_{22} \, \boldsymbol{q}_{xy} + d\boldsymbol{q}_{xy}^t \, \boldsymbol{a}_{21} \, \boldsymbol{q}_z \\ & + d\boldsymbol{q}_z^t \, \boldsymbol{a}_{12} \, \boldsymbol{q}_{xy} + d\boldsymbol{q}_z^t \, \boldsymbol{a}_{33} \, \boldsymbol{q}_z \end{aligned}\right\} \qquad (4.170)$$

Substituting from Equation (4.141) and (4.142) into (4.170) then it can be deduced that:-

$$
\begin{aligned}
d\mathbf{q}^t\,\mathbf{C}_1\,\mathbf{q} \;=\; & d\boldsymbol{\delta}_m^t\,\mathbf{N}_L^t\,\mathbf{a}_{22}\,\mathbf{N}_L\,\boldsymbol{\delta}_m \;+\; z^2\,d\boldsymbol{\delta}_b^t\,\mathbf{N}_b^t\,\mathbf{a}_{22}\,\mathbf{N}_b\,\boldsymbol{\delta}_b \\
& + f_1^2(z)\,d\boldsymbol{\delta}_s^t\,\mathbf{N}_L^t\,\mathbf{a}_{22}\,\mathbf{N}_L\,\boldsymbol{\delta}_S \;+\; d\boldsymbol{\delta}_b^t\,\mathbf{N}_H^t\,\mathbf{a}_{33}\,\mathbf{N}_H\,\boldsymbol{\delta}_b \\
& - z\,d\boldsymbol{\delta}_b^t\,\mathbf{N}_b^t\,\mathbf{a}_{21}\,\mathbf{N}_H\,\boldsymbol{\delta}_b \;-\; z\,d\boldsymbol{\delta}_b^t\,\mathbf{N}_H^t\,\mathbf{a}_{12}\,\mathbf{N}_b\,\boldsymbol{\delta}_b \\
& - z\,d\boldsymbol{\delta}_m^t\,\mathbf{N}_L^t\,\mathbf{a}_{22}\,\mathbf{N}_b\,\boldsymbol{\delta}_b \;-\; z\,d\boldsymbol{\delta}_b^t\,\mathbf{N}_b^t\,\mathbf{a}_{22}\,\mathbf{N}_L\,\boldsymbol{\delta}_m \\
& + d\boldsymbol{\delta}_m^t\,\mathbf{N}_L^t\,\mathbf{a}_{21}\,\mathbf{N}_H\,\boldsymbol{\delta}_b \;+\; d\boldsymbol{\delta}_b^t\,\mathbf{N}_H^t\,\mathbf{a}_{12}\,\mathbf{N}_L\,\boldsymbol{\delta}_m \\
& + f_1(z)\,d\boldsymbol{\delta}_m^t\,\mathbf{N}_L^t\,\mathbf{a}_{22}\,\mathbf{N}_L\,\boldsymbol{\delta}_S \;+\; f_1(z)\,d\boldsymbol{\delta}_s^t\,\mathbf{N}_L^t\,\mathbf{a}_{22}\,\mathbf{N}_L\,\boldsymbol{\delta}_m \\
& - zf_1(z)\,d\boldsymbol{\delta}_b^t\,\mathbf{N}_b^t\,\mathbf{a}_{22}\,\mathbf{N}_L\,\boldsymbol{\delta}_S \;-\; zf_1(z)\,d\boldsymbol{\delta}_s^t\,\mathbf{N}_L^t\,\mathbf{a}_{22}\,\mathbf{N}_b\,\boldsymbol{\delta}_b \\
& + f_1(z)\,d\boldsymbol{\delta}_b^t\,\mathbf{N}_H^t\,\mathbf{a}_{12}\,\mathbf{N}_L\,\boldsymbol{\delta}_S \;+\; f_1(z)\,d\boldsymbol{\delta}_s^t\,\mathbf{N}_L^t\,\mathbf{a}_{21}\,\mathbf{N}_H\,\boldsymbol{\delta}_b
\end{aligned}
\qquad (4.171)
$$

Defining

$$\rho_{mm} \;=\; \int_{-h/2}^{h/2} \rho\; dz \;=\; \rho_{HH} \;=\; \rho_{mH} \;=\; \rho_{Hm} \qquad (4.172)$$

$$\rho_{mb} \;=\; \int_{-h/2}^{h/2} z\,\rho\; dz \;=\; \rho_{bm} \;=\; \rho_{bH} \;=\; \rho_{Hb} \qquad (4.173)$$

$$\rho_{ms} \;=\; \int_{-h/2}^{h/2} f_1(z)\,\rho\; dz \;=\; \rho_{sm} \;=\; \rho_{sH} \;=\; \rho_{Hs} \qquad (4.174)$$

$$\rho_{bb} \;=\; \int_{-h/2}^{h/2} z^2\,\rho\; dz \qquad (4.175)$$

$$\rho_{ss} \;=\; \int_{-h/2}^{h/2} f_1^2(z)\,\rho\; dz \qquad (4.176)$$

$$\rho_{ms} \;=\; \int_{-h/2}^{h/2} z\,f_1(z)\,\rho\; dz \qquad (4.177)$$

which have explicit expressions similar to those given by Equations (4.84)-(4.90). then the work done on the element by D'Alembert's force due to the centripetal acceleration, during the virtual displacement $d\boldsymbol{q}$, can be expressed as follows:-

$$
\begin{aligned}
dW_p = \Omega^2 \Big\{ & d\,\boldsymbol{\delta}_m^t\, \overline{\boldsymbol{M}}_{mm}\, \boldsymbol{\delta}_m + d\,\boldsymbol{\delta}_b^t\, \overline{\boldsymbol{M}}_{bb}\, \boldsymbol{\delta}_b \\
& + d\,\boldsymbol{\delta}_b^t\, \overline{\boldsymbol{M}}_{HH}\, \boldsymbol{\delta}_b + d\,\boldsymbol{\delta}_s^t\, \overline{\boldsymbol{M}}_{ss}\, \boldsymbol{\delta}_s \\
& - d\,\boldsymbol{\delta}_b^t\, \overline{\boldsymbol{M}}_{bH}\, \boldsymbol{\delta}_b - d\,\boldsymbol{\delta}_b^t \left(\overline{\boldsymbol{M}}_{bH}\right)^t \boldsymbol{\delta} t_b \\
& - d\,\boldsymbol{\delta}_m^t\, \overline{\boldsymbol{M}}_{mb}\, \boldsymbol{\delta}_b - d\,\boldsymbol{\delta}_b^t \left(\boldsymbol{M}_{mb}\right)^t \dot{\boldsymbol{\delta}}_m \\
& + d\,\boldsymbol{\delta}_m^t\, \overline{\boldsymbol{M}}_{mH}\, \boldsymbol{\delta}_b + d\,\boldsymbol{\delta}_b^t \left(\overline{\boldsymbol{M}}_{Hm}\right)^t \boldsymbol{\delta}_m \\
& + d\,\boldsymbol{\delta}_m^t\, \overline{\boldsymbol{M}}_{ms}\, \boldsymbol{\delta}_s + d\,\boldsymbol{\delta}_s^t \left(\overline{\boldsymbol{M}}_{ms}\right)^t \boldsymbol{\delta}_m \\
& - d\,\boldsymbol{\delta}_b^t\, \overline{\boldsymbol{M}}_{bs}\, \boldsymbol{\delta}_s - d\,\boldsymbol{\delta}_s^t \left(\overline{\boldsymbol{M}}_{bs}\right)^t \boldsymbol{\delta}_b \\
& + d\,\boldsymbol{\delta}_b^t\, \overline{\boldsymbol{M}}_{Hs}\, \boldsymbol{\delta}_s + d\,\boldsymbol{\delta}_s^t \left(\overline{\boldsymbol{M}}_{Hs}\right)^t \boldsymbol{\delta}_b \Big\}
\end{aligned}
\tag{4.178}
$$

where

$$
\overline{\boldsymbol{M}}_{mm} = \iint_{element} \rho_{mm}\ \boldsymbol{N}_L^t\, \boldsymbol{a}_{22}\, \boldsymbol{N}_L\ dx\,dy \tag{4.179}
$$

$$
\overline{\boldsymbol{M}}_{bb} = \iint_{element} \rho_{bb}\ \boldsymbol{N}_b^t\, \boldsymbol{a}_{22}\, \boldsymbol{N}_b\ dx\,dy \tag{4.180}
$$

$$
\overline{\boldsymbol{M}}_{HH} = \iint_{element} \rho_{HH}\ \boldsymbol{N}_H^t\, \boldsymbol{a}_{33}\, \boldsymbol{N}_H\ dx\,dy \tag{4.181}
$$

$$
\overline{\boldsymbol{M}}_{ss} = \iint_{element} \rho_{ss}\ \boldsymbol{N}_L^t\, \boldsymbol{a}_{22}\, \boldsymbol{N}_L\ dx\,dy \tag{4.182}
$$

$$
\overline{\boldsymbol{M}}_{bH} = \iint_{element} \rho_{bH}\ \boldsymbol{N}_b^t\, \boldsymbol{a}_{21}\, \boldsymbol{N}_H\ dx\,dy \tag{4.183}
$$

$$
\overline{\boldsymbol{M}}_{mb} = \iint_{element} \rho_{mb}\ \boldsymbol{N}_L^t\, \boldsymbol{a}_{22}\, \boldsymbol{N}_b\ dx\,dy \tag{4.184}
$$

$$
\overline{\boldsymbol{M}}_{mH} = \iint_{element} \rho_{mH}\ \boldsymbol{N}_L^t\, \boldsymbol{a}_{21}\, \boldsymbol{N}_H\ dx\,dy \tag{4.185}
$$

$$\overline{\boldsymbol{M}}_{ms} = \iint_{element} \rho_{ms} \; \boldsymbol{N}_L^t \, \boldsymbol{a}_{22} \, \boldsymbol{N}_L \; dx\, dy \tag{4.186}$$

$$\overline{\boldsymbol{M}}_{bs} = \iint_{element} \rho_{bs} \; \boldsymbol{N}_b^t \, \boldsymbol{a}_{22} \, \boldsymbol{N}_L \; dx\, dy \tag{4.187}$$

$$\overline{\boldsymbol{M}}_{Hs} = \iint_{element} \rho_{Hs} \; \boldsymbol{N}_H^t \, \boldsymbol{a}_{12} \, \boldsymbol{N}_L \; dx\, dy \tag{4.188}$$

Equation (4.178) can also be rewritten as follows:-

$$dW_p = \Omega^2 \, d\boldsymbol{\delta}^t \, \overline{\boldsymbol{M}} \, \boldsymbol{\delta} \tag{4.189}$$

where

$$\overline{\boldsymbol{M}} = \begin{bmatrix} \overline{\boldsymbol{M}}_{mm} & \left(-\overline{\boldsymbol{M}}_{mb} + \overline{\boldsymbol{M}}_{mH}\right) & \overline{\boldsymbol{M}}_{ms} \\ \left(-\overline{\boldsymbol{M}}_{mb} + \overline{\boldsymbol{M}}_{mH}\right)^t & \begin{pmatrix} \overline{\boldsymbol{M}}_{bb} & + \overline{\boldsymbol{M}}_{HH} \\ -\overline{\boldsymbol{M}}_{bH} & -\overline{\boldsymbol{M}}_{bH}^t \end{pmatrix} & \left(-\overline{\boldsymbol{M}}_{bs} + \overline{\boldsymbol{M}}_{Hs}\right) \\ \left(\overline{\boldsymbol{M}}_{ms}\right)^t & \left(-\overline{\boldsymbol{M}}_{bs} + \overline{\boldsymbol{M}}_{Hs}\right)^t & \overline{\boldsymbol{M}}_{ss} \end{bmatrix} \tag{4.190}$$

4.7.4 Effect of Coriolis acceleration

D'Alembert's force acting on an infinitesimal mass at layer l, due to Coriolis acceleration is:-

$$\begin{aligned} \Delta \boldsymbol{F}_c^{(l)} &= -\rho^{(l)} \, \boldsymbol{a}_c \; \Delta x \, \Delta y \, \Delta z \\ &= -2\,\rho^{(l)} \, \Omega \, \boldsymbol{C}_2 \, \dot{\boldsymbol{q}} \; \Delta x \, \Delta y \, \Delta z \end{aligned} \tag{4.191}$$

where $$\boldsymbol{C}_2 = \begin{bmatrix} 0 & -n & m \\ n & 0 & -l \\ -m & l & 0 \end{bmatrix}$$

The work done by $\Delta \boldsymbol{F}_c$ due to a virtual displacement $d\boldsymbol{q}$ is:-

$$\left.\begin{aligned} d\left(\Delta\, W_c^{(l)}\right) &= d\,\boldsymbol{q}^t\ \Delta\, \boldsymbol{F}_c^{(l)} \\ &= -\,\rho^{(l)}\, 2\,\Omega\left(d\boldsymbol{q}^t\, C_2\,\dot{\boldsymbol{q}}\right)\ \Delta x\,\Delta y\,\Delta z \end{aligned}\right\} \quad (4.192)$$

defining the following sub-matrices of C_2:-

$$\boldsymbol{b}_{22} = \begin{bmatrix} 0 & -n \\ n & 0 \end{bmatrix} \quad (4.193)$$

$$\boldsymbol{b}_{12} = [\,-m \qquad l\,] \quad (4.194)$$

$$\boldsymbol{b}_{21} = \begin{bmatrix} m \\ -l \end{bmatrix} \equiv -\,\boldsymbol{b}_{12}^t \quad (4.195)$$

then it can be shown that:-

$$\left.\begin{aligned} d\boldsymbol{q}^t\, \boldsymbol{C}_2\ \dot{\boldsymbol{q}} &= d\boldsymbol{q}_{xy}^t\ \boldsymbol{b}_{22}\ \dot{\boldsymbol{q}}_{xy} + d\boldsymbol{q}_{xy}^t\ \boldsymbol{b}_{21}\ \dot{\boldsymbol{q}}_z \\ &\quad + d\boldsymbol{q}_z^t\ \boldsymbol{b}_{12}\ \dot{\boldsymbol{q}}_{xy} \end{aligned}\right\} \quad (4.1.96)$$

By substituting from Equations (4.141) and (4.142) into (4.196) it can be shown that:-

$$\left.\begin{aligned} d\boldsymbol{q}^t\, \boldsymbol{C}_2\ \dot{\boldsymbol{q}} &= d\boldsymbol{\delta}_m^t\, \boldsymbol{N}_L^t\, \boldsymbol{b}_{22}\, \boldsymbol{N}_L\, \dot{\boldsymbol{\delta}}_m + z^2\, d\boldsymbol{\delta}_b^t\, \boldsymbol{N}_b^t\, \boldsymbol{b}_{22}\, \boldsymbol{N}_b\, \dot{\boldsymbol{\delta}}_b \\ &\quad + f_1^2(z)\, d\boldsymbol{\delta}_s^t\, \boldsymbol{N}_L^t\, \boldsymbol{b}_{22}\, \boldsymbol{N}_L\, \dot{\boldsymbol{\delta}}_S \\ &\quad - z\, d\boldsymbol{\delta}_b^t\, \boldsymbol{N}_b^t\, \boldsymbol{b}_{21}\, \boldsymbol{N}_H\, \dot{\boldsymbol{\delta}}_b - z\, d\boldsymbol{\delta}_b^t\, \boldsymbol{N}_H^t\, \boldsymbol{b}_{12}\, \boldsymbol{N}_b\, \dot{\boldsymbol{\delta}}_b \\ &\quad - z\, d\boldsymbol{\delta}_m^t\, \boldsymbol{N}_L^t\, \boldsymbol{b}_{22}\, \boldsymbol{N}_b\, \dot{\boldsymbol{\delta}}_b - z\, d\boldsymbol{\delta}_b^t\, \boldsymbol{N}_b^t\, \boldsymbol{b}_{22}\, \boldsymbol{N}_L\, \dot{\boldsymbol{\delta}}_m \\ &\quad + d\boldsymbol{\delta}_m^t\, \boldsymbol{N}_L^t\, \boldsymbol{b}_{21}\, \boldsymbol{N}_H\, \dot{\boldsymbol{\delta}}_b + d\boldsymbol{\delta}_b^t\, \boldsymbol{N}_H^t\, \boldsymbol{b}_{12}\, \boldsymbol{N}_L\, \dot{\boldsymbol{\delta}}_m \\ &\quad + f_1(z)\, d\boldsymbol{\delta}_m^t\, \boldsymbol{N}_L^t\, \boldsymbol{b}_{22}\, \boldsymbol{N}_L\, \dot{\boldsymbol{\delta}}_S + f_1(z)\, d\boldsymbol{\delta}_s^t\, \boldsymbol{N}_L^t\, \boldsymbol{b}_{22}\, \boldsymbol{N}_L\, \dot{\boldsymbol{\delta}}_m \\ &\quad - zf_1(z)\, d\boldsymbol{\delta}_b^t\, \boldsymbol{N}_b^t\, \boldsymbol{b}_{22}\, \boldsymbol{N}_L\, \dot{\boldsymbol{\delta}}_S - zf_1(z)\, d\boldsymbol{\delta}_s^t\, \boldsymbol{N}_L^t\, \boldsymbol{b}_{22}\, \boldsymbol{N}_b\, \dot{\boldsymbol{\delta}}_b \\ &\quad + f_1(z)\, d\boldsymbol{\delta}_b^t\, \boldsymbol{N}_H^t\, \boldsymbol{b}_{12}\, \boldsymbol{N}_L\, \dot{\boldsymbol{\delta}}_S + f_1(z)\, d\boldsymbol{\delta}_s^t\, \boldsymbol{N}_L^t\, \boldsymbol{b}_{21}\, \boldsymbol{N}_H\, \dot{\boldsymbol{\delta}}_b \end{aligned}\right\} \quad (4.197)$$

Integrating over the volume of the element, then the work done on the element by D'Alembert's force due to Coriolis acceleration during the virtual displacement dq

can be expressed as follows:-

$$
\begin{aligned}
dW_c = -2\Omega \Big\{ & d\boldsymbol{\delta}_m^t \boldsymbol{C}_{mm} \dot{\boldsymbol{\delta}}_m + d\boldsymbol{\delta}_b^t \boldsymbol{C}_{bb} \dot{\boldsymbol{\delta}}_b + d\boldsymbol{\delta}_s^t \boldsymbol{C}_{ss} \dot{\boldsymbol{\delta}}_s \\
& - d\boldsymbol{\delta}_b^t \boldsymbol{C}_{bH} \dot{\boldsymbol{\delta}}_b + d\boldsymbol{\delta}_b^t (\boldsymbol{C}_{bH})^t \dot{\boldsymbol{\delta}}_b \\
& - d\boldsymbol{\delta}_m^t \boldsymbol{C}_{mb} \dot{\boldsymbol{\delta}}_b - d\boldsymbol{\delta}_b^t (\boldsymbol{C}_{mb})^t \dot{\boldsymbol{\delta}}_m \\
& + d\boldsymbol{\delta}_m^t \boldsymbol{C}_{mH} \dot{\boldsymbol{\delta}}_b - d\boldsymbol{\delta}_b^t (\boldsymbol{C}_{mH})^t \dot{\boldsymbol{\delta}}_m \\
& + d\boldsymbol{\delta}_m^t \boldsymbol{C}_{ms} \dot{\boldsymbol{\delta}}_s + d\boldsymbol{\delta}_s^t (\boldsymbol{C}_{ms})^t \dot{\boldsymbol{\delta}}_m \\
& - d\boldsymbol{\delta}_b^t \boldsymbol{C}_{bs} \dot{\boldsymbol{\delta}}_s - d\boldsymbol{\delta}_s^t (\boldsymbol{C}_{bs})^t \dot{\boldsymbol{\delta}}_m \\
& - d\boldsymbol{\delta}_b^t \boldsymbol{C}_{Hs} \dot{\boldsymbol{\delta}}_s - d\boldsymbol{\delta}_s^t (\boldsymbol{C}_{Hs})^t \dot{\boldsymbol{\delta}}_b \Big\}
\end{aligned}
\tag{4.198}
$$

where

$$\boldsymbol{C}_{mm} = \iint_{element} \rho_{mm} \; \boldsymbol{N}_L^t \, \boldsymbol{b}_{22} \, \boldsymbol{N}_L \; dx\, dy \tag{4.199}$$

$$\boldsymbol{C}_{bb} = \iint_{element} \rho_{bb} \; \boldsymbol{N}_b^t \, \boldsymbol{b}_{22} \, \boldsymbol{N}_b \; dx\, dy \tag{4.200}$$

$$\boldsymbol{C}_{ss} = \iint_{element} \rho_{ss} \; \boldsymbol{N}_L^t \, \boldsymbol{b}_{22} \, \boldsymbol{N}_L \; dx\, dy \tag{4.201}$$

$$\boldsymbol{C}_{bH} = \iint_{element} \rho_{bH} \; \boldsymbol{N}_b^t \, \boldsymbol{b}_{21} \, \boldsymbol{N}_H \; dx\, dy \tag{4.202}$$

$$\boldsymbol{C}_{mb} = \iint_{element} \rho_{mb} \; \boldsymbol{N}_L^t \, \boldsymbol{b}_{22} \, \boldsymbol{N}_b \; dx\, dy \tag{4.203}$$

$$\boldsymbol{C}_{mH} = \iint_{element} \rho_{mH} \; \boldsymbol{N}_L^t \, \boldsymbol{b}_{21} \, \boldsymbol{N}_H \; dx\, dy \tag{4.204}$$

$$\boldsymbol{C}_{ms} = \iint_{element} \rho_{ms} \; \boldsymbol{N}_L^t \, \boldsymbol{b}_{22} \, \boldsymbol{N}_L \; dx\, dy \tag{4.205}$$

$$\boldsymbol{C}_{bs} = \int\int_{element} \rho_{bs} \quad \boldsymbol{N}_b^t \, \boldsymbol{b}_{22} \, \boldsymbol{N}_L \quad dx\, dy \tag{4.206}$$

$$\boldsymbol{C}_{Hs} = \int\int_{element} \rho_{Hs} \quad \boldsymbol{N}_H^t \, \boldsymbol{b}_{12} \, \boldsymbol{N}_L \quad dx\, dy \tag{4.207}$$

Equation (4.198) can be rewritten as follows:-

$$d\boldsymbol{W}_c = -2\,\Omega \; d\boldsymbol{\delta}^t \; \boldsymbol{C} \; \dot{\boldsymbol{\delta}} \tag{4.208}$$

where

$$\boldsymbol{C} = \begin{bmatrix} \boldsymbol{C}_{mm} & \left(-\boldsymbol{C}_{mb} + \boldsymbol{C}_{mH}\right) & \boldsymbol{C}_{ms} \\ -\left(\boldsymbol{C}_{mb} + \boldsymbol{C}_{mH}\right)^t & \begin{pmatrix} \boldsymbol{C}_{bb} & \\ -\boldsymbol{C}_{bH} & +\boldsymbol{C}_{bH}^t \end{pmatrix} & \left(-\boldsymbol{C}_{bs} + \boldsymbol{C}_{Hs}\right) \\ \left(\boldsymbol{C}_{ms}\right)^t & \left(-\boldsymbol{C}_{bs} - \boldsymbol{C}_{Hs}\right)^t & \boldsymbol{C}_{ss} \end{bmatrix} \tag{4.209}$$

Notice that although the $\boldsymbol{K}$, $\boldsymbol{K}^{\sigma}$, $\boldsymbol{M}$ and $\overline{\boldsymbol{M}}$ matrices defined earlier are symmetric matrices, the matrix $\boldsymbol{C}$ *is not* symmetric.

4.7.5 Element dynamic equations

Consider a composite layered plate or shell under dynamic force, the structure, or every element of it, can be considered in a state of dynamic equilibrium under applied and D'Alembert's forces, and the principle of virtual work can be applied. Assuming that the element is subjected to a virtual displacement field $d\boldsymbol{q}\,(x, y, z, t)$, then:-

(a) The change of the strain energy of the element is expressed in Equation (4.133) as follows:-

$$dU(t) = d\boldsymbol{\delta}^t(t) \left[\boldsymbol{K} + \boldsymbol{K}^{\sigma}\right] \boldsymbol{\delta}(t)$$

(b) The work done by applied forces, at an instant of time t, due to $d\boldsymbol{q}$ can be expressed as follows:-

$$d\boldsymbol{W}_F(t) = d\boldsymbol{\delta}^t(t) \quad \boldsymbol{F}(t)$$

where $\boldsymbol{F}\ (t)$ represents a nodal loading system equivalent to the actual applied force, (El-Zafrany, 1994).

(c) The work done by D'Alembert's force due to relative acceleration is expressed in Equation (4.163) as follows:-

$$dW_r(t) = -d\boldsymbol{\delta}^t(t)\ \boldsymbol{M}\ \ddot{\boldsymbol{\delta}}(t)$$

(d) The work done by D'Alembert's force due to centripetal acceleration is defined by Equation (4.189) as follows:-

$$dW_p(t) = \Omega^2\ d\boldsymbol{\delta}^t(t)\ \overline{\boldsymbol{M}}\ \boldsymbol{\delta}(t)$$

(e) The work done by D'Alembert's force due to Coriolis acceleration is given by Equation (4.208) as follows:-

$$dW_c(t) = -2\,\Omega\ d\boldsymbol{\delta}^t(t)\ \boldsymbol{C}\ \dot{\boldsymbol{\delta}}(t)$$

Applying the principle of virtual work at an instant of time *t*, then:-

$$dU(t) - \left[dW_F(t) + dW_r(t) + dW_p(t) + dW_c(t)\right] = 0$$

or

$$\left.\begin{aligned} d\boldsymbol{\delta}^t(t)\ \Big\{&\left[\boldsymbol{K} + \boldsymbol{K}^{\sigma}\right]\boldsymbol{\delta}(t) - \boldsymbol{F}(t) + \boldsymbol{M}\ \ddot{\boldsymbol{\delta}}(t) \\ &- \Omega^2\ \overline{\boldsymbol{M}}\ \boldsymbol{\delta}(t) + 2\,\Omega\ \boldsymbol{C}\ \dot{\boldsymbol{\delta}}(t)\Big\} = 0 \end{aligned}\right\} \qquad (4.210)$$

Since $d\boldsymbol{\delta}$ is due to the virtual displacement field, then its coefficient in the previous equation should vanish for arbitrary values of $d\boldsymbol{q}$, *i.e.*

$$\left.\begin{aligned} &\boldsymbol{M}\ \ddot{\boldsymbol{\delta}}(t) + 2\,\Omega\ \boldsymbol{C}\ \dot{\boldsymbol{\delta}}(t) \\ &\left[\boldsymbol{K} + \boldsymbol{K}^{\sigma} - \Omega^2\ \overline{\boldsymbol{M}}\right]\boldsymbol{\delta}(t) = \boldsymbol{F}(t) \end{aligned}\right\} \qquad (4.211)$$

which represents the dynamic matrix equation of the element. The dynamic equations for the whole structure are assembled from the element equations using the usual assembly procedure.

4.8 ELEMENT MATRICES FOR AEROELASTIC EFFECT

4.8.1 Nodal loading equivalent to external aerodynamic pressure

Consider a composite layered plate or shell subjected to an external aerodynamic

pressure p_o (x, y, t) at its upper surface. Taking one finite element, described with respect to a local system of axes, where the z axis is normal to the surface of the element, then the force in the z direction, acting on an infinitesimal area $\Delta x \Delta y$ due to p_o will be as shown in Fig. (4.2), *i.e.*

$$\Delta F_\circ = - p_\circ(x, y, t) \Delta x \Delta y \tag{4.212}$$

Applying an infinitesimal displacement field $d\boldsymbol{q}$ (x, y, z, t) then the work done will be :

$$d(\Delta W_\circ) = - dw(x, y, t)\ p_\circ(x, y, t) \Delta x \Delta y \tag{4.213}$$

Using Equation (4.142) then

$$dw = \boldsymbol{N}_H\ d\boldsymbol{\delta}_b$$

and the total work done on the element can be expressed as follows:-

$$dW_\circ = - d\boldsymbol{\delta}_b^t \iint_{element} p_\circ(x, y, t)\, \boldsymbol{N}_H^t \ \ dx\, dy \tag{4.214}$$

$$\equiv - d\boldsymbol{\delta}_b^t\ \boldsymbol{F}_\circ(t)$$

where $$\boldsymbol{F}_\circ(t) = \iint_{element} p_\circ(x, y, t)\, \boldsymbol{N}_H^t \ \ dx\, dy \tag{4.215}$$

which represents the equivalent nodal force vector.

If $dW_\circ$ is represented as follows:-

$$dW_\circ = - d\boldsymbol{\delta}^t\ \boldsymbol{F}^T(t)$$

then $$\boldsymbol{F}_\circ^T(t) = \left\{ \mathbf{O} \quad \boldsymbol{F}_\circ \quad \mathbf{O} \right\} \tag{4.216}$$

where $\mathbf{O}$ is a null vector, and the two null vectors correspond to $d\boldsymbol{\delta}_m$, $d\boldsymbol{\delta}_s$.

If the pressure distribution p_o (x, y, t) is defined numerically, with given nodal values at every time instant t, then at that instant one can use a Lagrangian interpolation such that:-

$$p(x, y, t) = \sum_{i=1}^{n} \left(p_\circ(t)\right)_i\ N_i(x, y) \tag{4.217}$$

4.8.2 Element flutter matrices

Using the previous notations, the force acting on an infinitesimal element of area $\Delta x \, \Delta y$ due to the aeroelastic pressure p_a will be:-

$$\Delta F_a = - p_a(x,y,t) \, \Delta x \, \Delta y$$

$$\equiv - \left[a \frac{\partial w}{\partial x} + b \frac{\partial w}{\partial y} + c \frac{\partial w}{\partial t} \right] \Delta x \, \Delta y \qquad (4.218)$$

where

$$a = \frac{\rho_\infty V_\infty^2}{\sqrt{M_\infty^2 - 1}} \cos \alpha$$

$$b = \frac{\rho_\infty V_\infty^2}{\sqrt{M_\infty^2 - 1}} \sin \alpha$$

$$c = \frac{\left(M_\infty^2 - 2 \right)}{\left(M_\infty^2 - 1 \right)^{\frac{3}{2}}} \rho V_\infty$$

as can be deduced from Equation (3.94)

The work done by ΔF_a due to a virtual displacement field $dq\,(x,y,z,t)$ will be:-

$$d\left(\Delta W_a\right) = - dw(x,y,t) \left[a \frac{\partial w}{\partial x} + b \frac{\partial w}{\partial y} + c \frac{\partial w}{\partial t} \right] \Delta x \, \Delta y \qquad (4.219)$$

Using Equation (4.142), it can be deduced that:-

$$\frac{\partial w}{\partial x} = \boldsymbol{N}_{H,x} \, \boldsymbol{\delta}_b \qquad (4.220)$$

$$\frac{\partial w}{\partial y} = \boldsymbol{N}_{H,y} \, \boldsymbol{\delta}_b \qquad (4.221)$$

$$\frac{\partial w}{\partial t} = \boldsymbol{N}_H \, \dot{\boldsymbol{\delta}}_b \qquad (4.222)$$

where

$$\boldsymbol{N}_H = \left[\cdots \quad F_i \quad G_i \quad H_i \quad Q_i \quad \cdots \right]$$

$$\boldsymbol{N}_{H,x} = \left[\cdots \quad \frac{\partial F_i}{\partial x} \quad \frac{\partial G_i}{\partial x} \quad \frac{\partial H_i}{\partial x} \quad \frac{\partial Q_i}{\partial x} \quad \cdots \right]$$

$$N_{H,y} = \left[\cdots \quad \frac{\partial F_i}{\partial y} \quad \frac{\partial G_i}{\partial y} \quad \frac{\partial H_i}{\partial y} \quad \frac{\partial Q_i}{\partial y} \quad \cdots \right]$$

Substituting from Equations (4.220)-(4.222) into (4.219) and integrating over the area of the element, then the work done by p_a over the element can be written as follows:-

$$dW_a = -d\boldsymbol{\delta}_b^t \left[\boldsymbol{K}_a \boldsymbol{\delta}_b + \boldsymbol{C}_a \dot{\boldsymbol{\delta}}_b \right] \tag{4.223}$$

where

$$\boldsymbol{K}_a = \iint_{element} \boldsymbol{N}_H^t \left(a \boldsymbol{N}_{H,x} + b \boldsymbol{N}_{H,y} \right) dx\, dy \tag{4.224}$$

$$\boldsymbol{C}_a = \iint_{element} c\, \boldsymbol{N}_H^t\, \boldsymbol{N}_H\, dx\, dy \tag{4.225}$$

Adding the work terms represented by Equations (4.214) and (4.223) into Equation (4.210), then the generalized dynamic matrix equation of the element in case of rotation and aeroelastic effects is:-

$$\left.\begin{aligned} &\boldsymbol{M}\, \ddot{\boldsymbol{\delta}}(t) + \left(2\Omega\, \boldsymbol{C} + \boldsymbol{C}_a^T \right) \dot{\boldsymbol{\delta}}(t) + \\ &\left(\boldsymbol{K} + \boldsymbol{K}^{\sigma} - \Omega^2 \overline{\boldsymbol{M}} + \boldsymbol{K}_a^T \right) \boldsymbol{\delta}(t) \\ &= \boldsymbol{F}(t) + \boldsymbol{F}_{\circ}^T(t) \end{aligned}\right\} \tag{4.226}$$

where

$$\boldsymbol{C}_a^T = \begin{bmatrix} \mathbf{O} & \mathbf{O} & \mathbf{O} \\ \mathbf{O} & \boldsymbol{C}_a & \mathbf{O} \\ \mathbf{O} & \mathbf{O} & \mathbf{O} \end{bmatrix}$$

$$\boldsymbol{K}_a^T = \begin{bmatrix} \mathbf{O} & \mathbf{O} & \mathbf{O} \\ \mathbf{O} & \boldsymbol{K}_a & \mathbf{O} \\ \mathbf{O} & \mathbf{O} & \mathbf{O} \end{bmatrix}$$

according to the similar partitions shown in Equations (4.79), (4.102), . . . , etc.

4.8.3 Simplified theory for flutter matrices of thin panels with uniform layer thickness

The simplification is based upon:

(i) Ignoring in-plane coupling, *i.e.* assuming isotropic material or symmetric composites, hence neglecting the in-plane terms in element matrices because they have no effect on flutter.

(ii) Assuming thin panels, which will lead to ignoring transverse shear terms.

Simplified element strain energy

Considering only the bending degrees of freedom, then:-

$$\boldsymbol{\delta}(t) \cong \boldsymbol{\delta}_b(t)$$

and the element strain energy can be reduced to:-

$$U(t) \cong U_b(t) = \frac{1}{2}\,\boldsymbol{\delta}_b^t(t)\,\boldsymbol{K}_{bb}\,\boldsymbol{\delta}_b(t)$$

where

$$\boldsymbol{K}_{bb} = \iint_{element} \boldsymbol{B}_b^t\,\boldsymbol{D}_{bb}\,\boldsymbol{B}_b\;dx\,dy$$

Simplified element kinetic energy

Similarly, the element kinetic energy per unit volume becomes:-

$$\overline{KE} \simeq \frac{1}{2}\,\rho\,\dot{w}^2 = \frac{1}{2}\,\rho\,\dot{\boldsymbol{\delta}}_b^t\,\boldsymbol{N}_H^t\,\boldsymbol{N}_H\,\dot{\boldsymbol{\delta}}_b$$

Hence

$$KE = \frac{1}{2}\,\dot{\boldsymbol{\delta}}_b^t\,\rho_{mm}\left(\iint_{elmnent} \boldsymbol{N}_H^t\,\boldsymbol{N}_H\;dx\,dy\right)\dot{\boldsymbol{\delta}}_b$$

where

$$\rho_{mm} = \int_{-\frac{h}{2}}^{\frac{h}{2}} \rho\;dz = \sum_{l=1}^{N_l} h^{(l)}\,\rho^{(l)}$$

and $h^{(l)}$ is the total thickness of the element, which is assumed to be independent of (x, y) for the simplified case.

Work done due to aerodynamic pressure

This can be expressed as follows:-

$$dW_a = -d\,\boldsymbol{\delta}_b^t(t)\left[\boldsymbol{K}_a\,\boldsymbol{\delta}_b(t) + \boldsymbol{C}_a\,\boldsymbol{\delta}_b\right]$$

where

$$\boldsymbol{K}_a = -\iint_{element} \boldsymbol{N}_H^t\left(a\,\boldsymbol{N}_{H,x} + b\,\boldsymbol{N}_{H,y}\right)\,dx\,dy$$

$$\boldsymbol{C}_a = c\iint_{element} \boldsymbol{N}_H^t\,\boldsymbol{N}_H\,dx\,dy$$

Defining

$$\boldsymbol{M}_H = \iint_{element} \boldsymbol{N}_H^t\,\boldsymbol{N}_H\,dx\,dy$$

then virtual energy changes can be expressed as follows:-

$$d\,U(t) = d\boldsymbol{\delta}_b^t\,\boldsymbol{K}_{bb}\,\boldsymbol{\delta}_b(t)$$

$$d\,KE(t) = d\boldsymbol{\delta}_b^t\,\rho_{mm}\,\boldsymbol{M}_H\,\ddot{\boldsymbol{\delta}}_b(t)$$

$$dW_a = -d\,\boldsymbol{\delta}_b^t(t)\left[\boldsymbol{K}_a\,\boldsymbol{\delta}_b(t) + c\,\boldsymbol{M}_H\,\dot{\boldsymbol{\delta}}_b(t)\right]$$

Applying the energy principle that the total potential energy is stationary, then:-

$$d\chi = 0 = dU + d\,KE - dW_a$$

i.e.

$$d\boldsymbol{\delta}_b^t\left[\rho_{mm}\,\boldsymbol{M}_H\,\ddot{\boldsymbol{\delta}}_b(t) + c\,\boldsymbol{M}_H\,\dot{\boldsymbol{\delta}}_b(t) + \left(\boldsymbol{K}_{bb} + \boldsymbol{K}_a\right)\boldsymbol{\delta}_b(t)\right] = 0$$

Hence the simplified dynamic equation can be expressed as follows:-

$$\rho_{mm}\,\boldsymbol{M}_H\,\ddot{\boldsymbol{\delta}}_b(t) + c\,\boldsymbol{M}_H\,\dot{\boldsymbol{\delta}}_b(t) + \left(\boldsymbol{K}_{bb} + \boldsymbol{K}_a\right)\boldsymbol{\delta}_b(t) = 0$$

4.9 ELEMENT AXES AND ROTATED MATRICES

4.9.1 Local and global axes

The element matrices derived in the previous sections are defined with respect to element local axes, which have the local z axis normal to the midplane of the element. The x axis of the material (the fibre axis) is defined in terms of an angle θ

with the local x axis of the element. The orientation of fluid velocity, for flutter cases are defined with respect to the local x axis of the element. Hence, the definition of the local axes should be dealt with carefully to avoid any unnecessary confusion. For the analysis of plates, the local axes are the same as the global axes, however for facetted shells, the local axes are defined as explained next.

(a) Definition of the local z axis ($z^{\backslash}$ axis)

Let i, j, k be three non-collinear nodes in the midplane of the element, as shown in Fig. 4.3. Two position vectors can therefore, be defined in the midplane, as follows:-

$$\left.\begin{aligned} \overrightarrow{V}_{ij} &= (x_j - x_i)\,\hat{i} + (y_j - y_i)\,\hat{j} + (z_j - z_i)\,\hat{k} \\ \overrightarrow{V}_{ik} &= (x_k - x_i)\,\hat{i} + (y_k - y_i)\,\hat{j} + (z_k - z_i)\,\hat{k} \end{aligned}\right\} \qquad (4.227)$$

Hence, a vector normal to the midplane can be defined as the vectorial product of the previous vectors, *i.e.*

$$V_{z^{\backslash}} = V_{ij} \wedge V_{ik} \qquad (4.228)$$

or

$$\overrightarrow{V}_{z^{\backslash}} = \begin{vmatrix} \hat{i} & \hat{j} & \hat{k} \\ x_j - x_i & y_j - y_i & z_j - z_i \\ x_k - x_i & y_k - y_i & z_k - z_i \end{vmatrix}$$

$$\equiv A_3\,\hat{i} + B_3\,\hat{j} + C_3\,\hat{k} \qquad (4.229)$$

where

$$A_3 = (y_j - y_i)(z_k - z_i) - (y_k - y_i)(z_j - z_i)$$

$$B_3 = (z_j - z_i)(x_k - x_i) - (z_k - z_i)(x_j - x_i)$$

$$C_3 = (x_j - x_i)(y_k - y_i) - (x_k - x_i)(y_j - y_i)$$

Hence, the direction cosines of the local z axis can be defined as the components of a unit vector in $\overrightarrow{V}_{z^{\backslash}}$ direction, *i.e.*

$$\hat{k}` = \frac{\overrightarrow{V_{z}`}}{V_{z}`} \equiv l_3\,\hat{i} + m_3\,\hat{j} + n_3\,\hat{k} \qquad (4.230)$$

where $l_3 = \dfrac{A_3}{V_z`}, \qquad m_3 = \dfrac{B_3}{V_z`}, \qquad n_3 = \dfrac{C_3}{V_z`}$

and $V_{z`} = \sqrt{A_3^2 + B_3^2 + C_3^2}$

(b) Definition of the local x axis (x` axis)

For flutter problems, the local x axis should be parallel to the global x axis to facilitate the definition of fluid flow direction, *i.e.*

$$\hat{i}` \equiv \hat{i} = l_1\,\hat{i} + m_1\,\hat{j} + n_1\,\hat{k} \qquad (4.231)$$

where $l_1 = 1, \qquad m_1 = n_1 = 0$

However, the second type of Hermitian functions *(conforming)* are based upon rectangular elements, where local and intrinsic axes are as shown in Fig. (4.4). This requires that the local x axis should be in the direction of $\overrightarrow{V_{12}}$, *i.e.*

$$l_1 = \frac{x_2 - x_1}{A}, \qquad m_1 = \frac{y_2 - y_1}{A}, \qquad n_1 = \frac{z_2 - z_1}{A}$$

where $A = \sqrt{(x_2 - x_1)^2 + (y_2 - y_1)^2 + (z_2 - z_1)^2}$

and (x_1, y_1, z_1), (x_2, y_2, z_2) are the global coordinates of the element first and second nodes. If this type of element is employed in flutter analysis, then the local x axis should be parallel to the global x axis.

A generalized definition is employed in the first type of Hermitian elements (*non-conforming*), which includes triangular and quadrilateral elements , that is to assume that the local x axis is normal to the local z axis and the global y axis, (provided that these two axes are not themselves parallel to each other). Hence , if $z`$ axis is parallel to $y$ axis, take $x`$ axis in the direction of x axis, otherwise use:-

$$\hat{i}` = \frac{\hat{j} \wedge \hat{k}`}{|\hat{j} \wedge \hat{k}`|} \qquad (4.232)$$

i.e. $l_1 = \dfrac{n_3}{\sqrt{l_3^2 + n_3^2}}$, $m_1 = 0$ and $n_1 = \dfrac{l_3}{\sqrt{l_3^2 + n_3^2}}$

(c) Definition of the local y axis (y` axis)

By default, this is defined normal to the local z and x axes, *i.e.*

$$\hat{j}` = \hat{k}` \wedge \hat{i}` \qquad (4.233)$$

Hence
$$l_2 = m_3 n_1 - m_1 n_3$$

$$m_2 = n_3 l_1 - n_1 l_3$$

$$n_2 = l_3 m_1 - l_1 m_3$$

4.9.2 Element rotation matrix

For an n-node element, an expanded local nodal displacement vector will be defined as follows:-

$$\boldsymbol{\delta}_{local} = \left\{ \ldots \; u_i \; v_i \; w_i \quad w_{i,x} \; w_{i,y} \; (\theta_z)_i \quad (\gamma_{xz})_i \; (\gamma_{yz})_i \; (\phi_z)_i \; \ldots \right\} \qquad (4.234)$$

and the derived element matrices can be redefined accordingly by partitioning them for each node. Notice also in Equation (4.234) that:-

(i) u_i, v_i, w_i — are the displacement components in the local x, y and z directions respectively.

(ii) $w_{i,x} = (\theta_y)_i$ — represents a rotation in the local y direction.

$w_{i,y} \equiv -(\theta_x)_i$ — represents a rotation in the opposite local x direction

$(\theta_z)_i = 0$ — for non-conforming elements.

$\equiv w_{i,xy}$ — represents a *rotation* in the local z direction for conforming elements.

(iii) $(\gamma_{xz})_i \equiv -(\phi_y)_i$ — transverse shear strain causing a change of angle measured vectorially in the local y direction.

$(\gamma_{yz})_i \equiv (\phi_x)_i$ transverse shear strain causing a change of angle measured vectorially in the local x direction.

$(\phi_z)_i = 0$

The corresponding global vector for shell applications and folded plates will generally be defined as follows:-

$$\boldsymbol{\delta}_{global} = \left\{ \ldots \; u_i \; v_i \; w_i \quad (\theta_x)_i \, (\theta_y)_i \, (\theta_z)_i \quad (\phi_x)_i \, (\phi_z)_i \, (\phi_y)_i \ldots \right\} \tag{4.235}$$

and the element rotation matrix is defined such that:-

$$\boldsymbol{\delta}_{local} = \boldsymbol{R}_{element} \; \boldsymbol{\delta}_{global} \tag{4.236}$$

which is not required for plate analysis, *i.e.* $\boldsymbol{\delta}_{local} = \boldsymbol{\delta}_{global}$ for plates.

The rotation matrix is defined in terms of 3×3 sub-rotation matrices as follows:-

$$\boldsymbol{R}_{element} = \left[\ldots \quad \boldsymbol{R}_i \quad \boldsymbol{S}_i \quad \boldsymbol{T}_i \quad \ldots \right] \tag{4.237}$$

with the following definitions:-

(a) $\boldsymbol{R}_i$ is the rotation matrix of the axes, *i.e.*

$$\boldsymbol{R}_i = \boldsymbol{R}_{3\times 3} = \begin{bmatrix} l_1 & m_1 & n_1 \\ l_2 & m_2 & n_2 \\ l_3 & m_3 & n_3 \end{bmatrix} \tag{4.238}$$

(b) $\boldsymbol{S}_i$ has two definitions, *i.e.*

(i) For conforming elements, since there are contributions in element matrices corresponding to θ_z then

$$\boldsymbol{S}_i \equiv \boldsymbol{R}^{*}_{3\times 3} \tag{4.239}$$

(ii) For non-conforming elements there are two possibilities:-

\# If node i is on the intersection of two planes as shown in position number 1 in Fig. (4.5) or on a curved surface then:-

$\boldsymbol{S}_i \equiv \boldsymbol{R}^{*}_{3\times 3}$

\# If node i is on a plane away from the intersection line as shown in position number 2 in Fig. (4.5) then:- $\boldsymbol{S}_i \equiv I_{3\times 3}$

$$\text{where } \boldsymbol{R}^{*}_{3\times 3} = \begin{bmatrix} l_2 & m_2 & n_2 \\ -l_1 & -m_1 & -n_1 \\ l_3 & m_3 & n_3 \end{bmatrix} \qquad (4.240)$$

(c) $\boldsymbol{T}_i$ for all elements :

If node i is on the intersection of two planes or on a curved surface then:-

$$\boldsymbol{T}_i \equiv \boldsymbol{R}^{*}_{3\times 3} \qquad (4.241)$$

If node i is on a plane away from the line of intersection then:-

$$\boldsymbol{T}_i \equiv \boldsymbol{I}_{3\times 3} \qquad (4.242)$$

i.e. the global $(\phi_x)_i$ and $(\phi_y)_i$ will be replaced by the local $(\gamma_{xz})_i$ and $(\gamma_{yz})_i$

(d) Effect on the boundary conditions:

To avoid having singular element matrices, zero rows or columns will be deleted by putting additional boundary conditions as follows:-

(i) For conforming element cases with $\boldsymbol{T}_i = \boldsymbol{I}_{3\times 3}$ we assume also the boundary condition: $(\phi_z)_i = 0$ (4.243)

(ii) For non-conforming elements cases with $\boldsymbol{S}_i = \boldsymbol{T}_i = \boldsymbol{I}_{3\times 3}$ we assume the boundary condition: $(\theta_z)_i = (\phi_z)_i = 0$ (4.244)

4.9.3 Rotated element matrices

The strain energy of the element can be expressed as follows:-

$$U = \frac{1}{2}\,\boldsymbol{\delta}^{t}_{local}\,\boldsymbol{K}_{local}\boldsymbol{\delta}_{local}$$

using

$$\boldsymbol{\delta}_{local} = \boldsymbol{R}_{element}\,\boldsymbol{\delta}_{global}$$

$$\boldsymbol{\delta}^{t}_{local} = \boldsymbol{\delta}^{t}_{global}\,\boldsymbol{R}_{element} \qquad (4.245)$$

then

$$U = \frac{1}{2}\,\boldsymbol{\delta}^{t}_{global}\,\boldsymbol{R}^{t}_{element}\,\boldsymbol{K}_{local}\,\boldsymbol{R}_{element}\,\boldsymbol{\delta}_{global}$$

i.e.
$$U \equiv \frac{1}{2} \boldsymbol{\delta}^{t}_{global} \boldsymbol{K}_{global} \boldsymbol{\delta}_{global} \tag{4.246}$$

Hence, it can be deduced that:-

$$\boldsymbol{K}_{global} = \boldsymbol{R}^{t}_{element} \boldsymbol{K}_{local} \boldsymbol{R}_{element} \tag{4.247}$$

Similarly it can be proved that

$$\boldsymbol{M}_{global} = \boldsymbol{R}^{t}_{element} \boldsymbol{M}_{local} \boldsymbol{R}_{element} \tag{4.248}$$

The work done by D'Alembert's force equivalent to Coriolis acceleration during virtual displacement is defined by Equation (4.208) as:-

$$dW_c = -2\,\Omega\; d\boldsymbol{\delta}^{t}_{local} (\boldsymbol{C})_{local} \dot{\boldsymbol{\delta}}_{local}$$

$$= -2\,\Omega\; d\boldsymbol{\delta}^{t}_{global} \boldsymbol{R}^{t}_{element} (\boldsymbol{C})_{local} \boldsymbol{R}_{element} \dot{\boldsymbol{\delta}}_{global}$$

$$= -2\,\Omega\; d\boldsymbol{\delta}^{t}_{global} (\boldsymbol{C})_{global} \boldsymbol{\delta}_{global}$$

i.e.
$$(\boldsymbol{C})_{global} = \boldsymbol{R}^{t}_{element} (\boldsymbol{C})_{local} \boldsymbol{R}_{element} \tag{4.249}$$

Similarly it can be proved that:-

$$(\overline{\boldsymbol{M}})_{global} = \boldsymbol{R}^{t}_{element} (\overline{\boldsymbol{M}})_{local} \boldsymbol{R}_{element} \tag{4.250}$$

The work done by a nodal force vector during a virtual displacement is:-

$$dW = d\boldsymbol{\delta}^{t}_{local} \boldsymbol{F}_{local}$$

$$\equiv d\boldsymbol{\delta}^{t}_{global} \boldsymbol{R}^{t}_{element} \boldsymbol{F}_{local}$$

$$\equiv d\boldsymbol{\delta}^{t}_{global} \boldsymbol{F}_{global}$$

i.e.
$$(\boldsymbol{F})_{global} = \boldsymbol{R}^{t}_{element} (\boldsymbol{F})_{local} \tag{4.251}$$

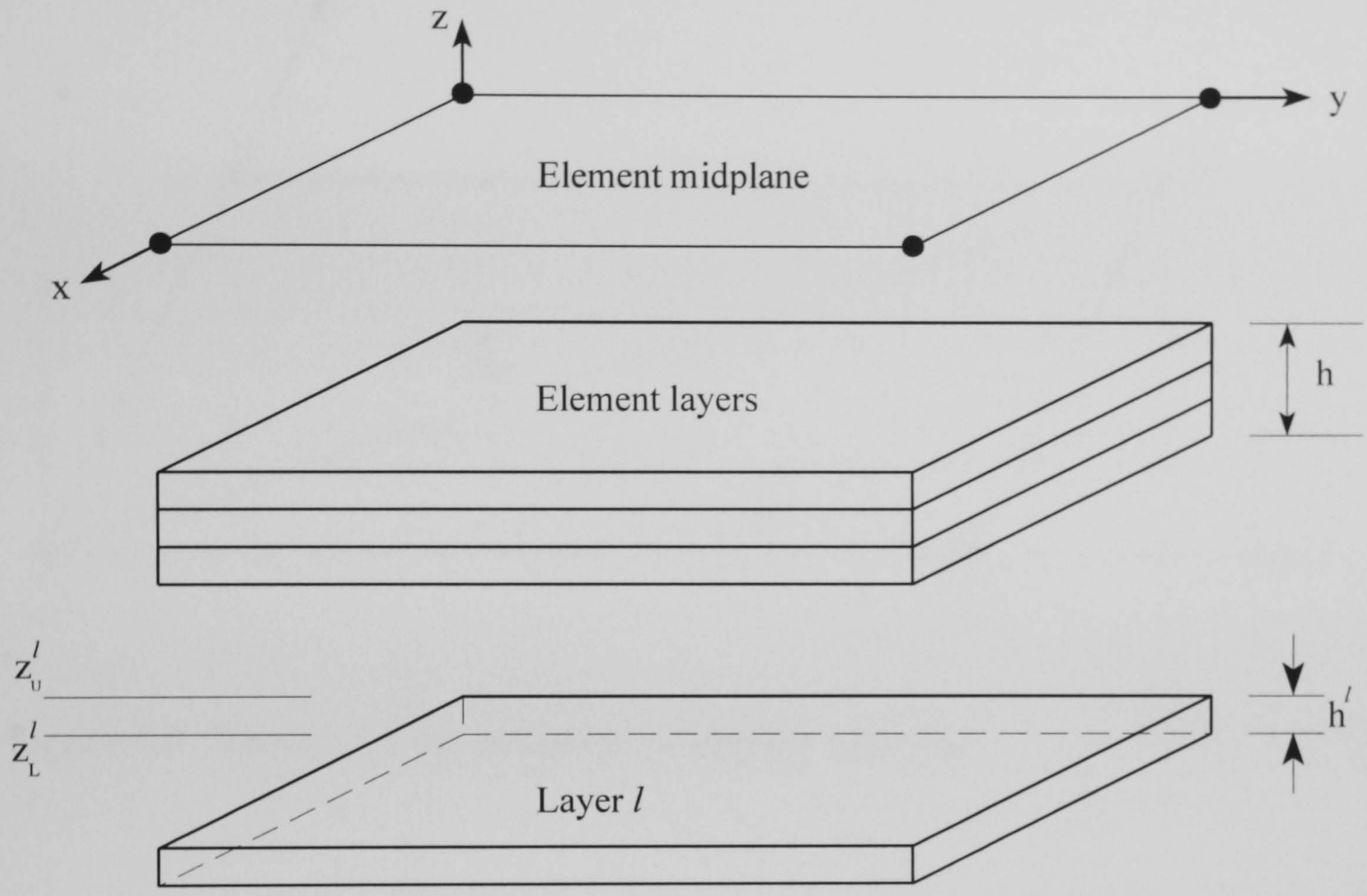

Figure 4.1 Typical composite layered element

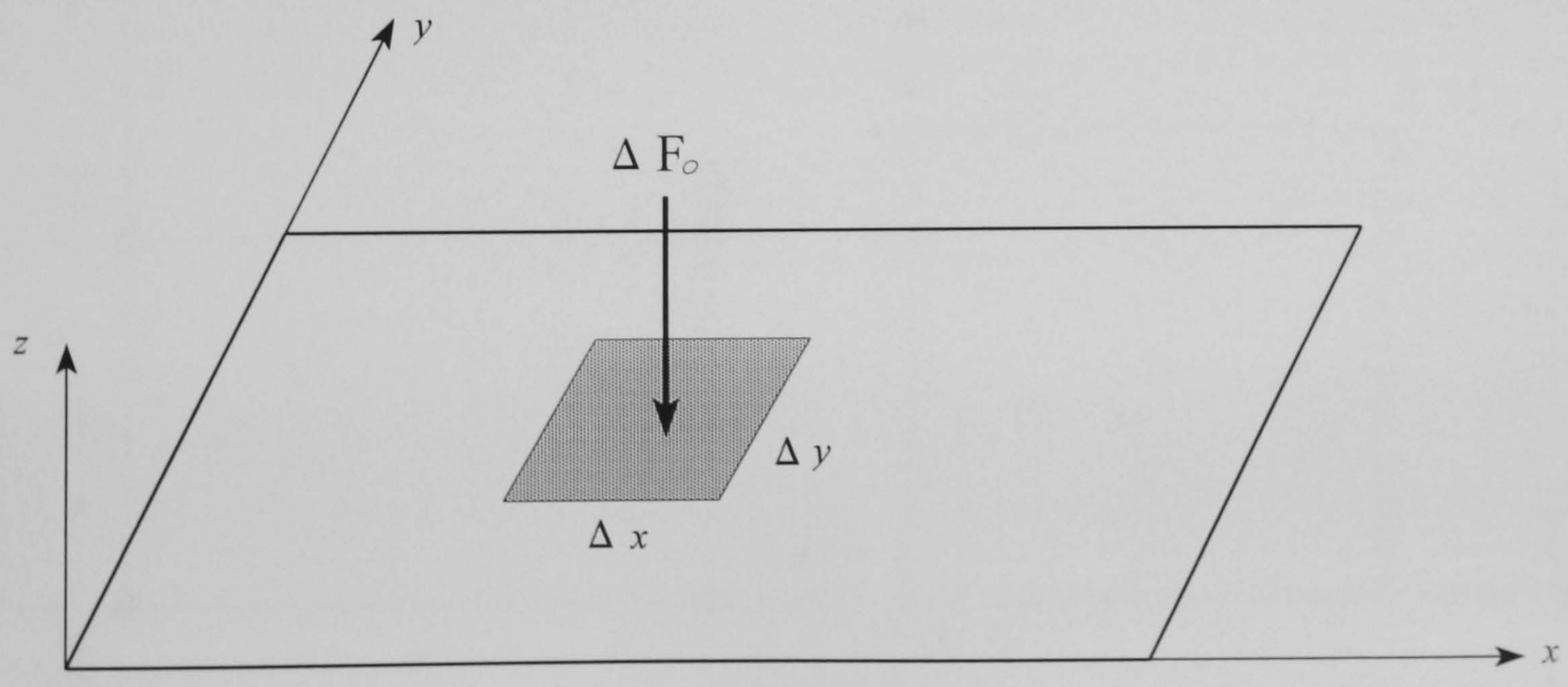

Figure 4.2 Force on an infinitesimal area

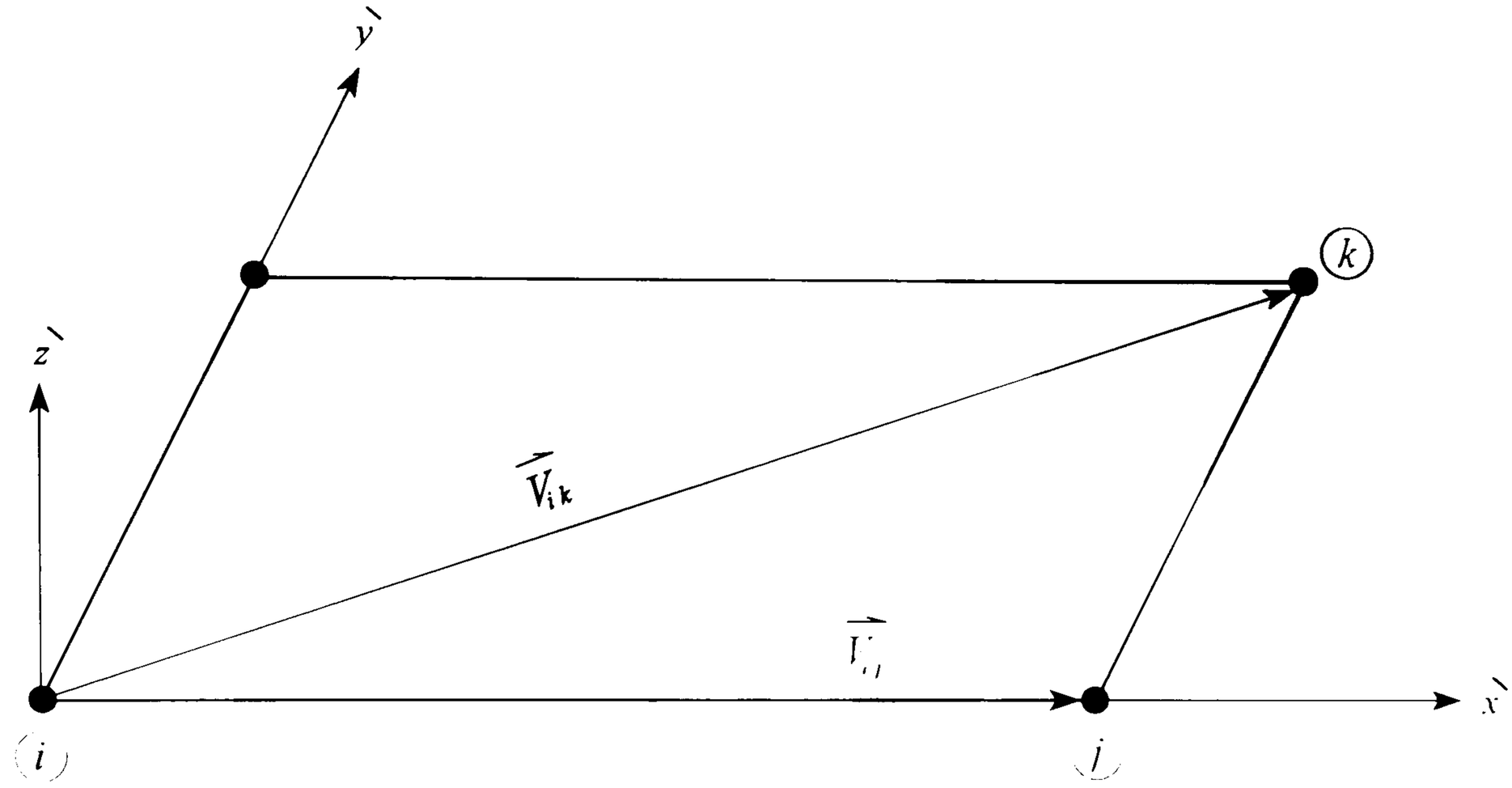

Figure 4.3 Vectors for the definition of element local axes

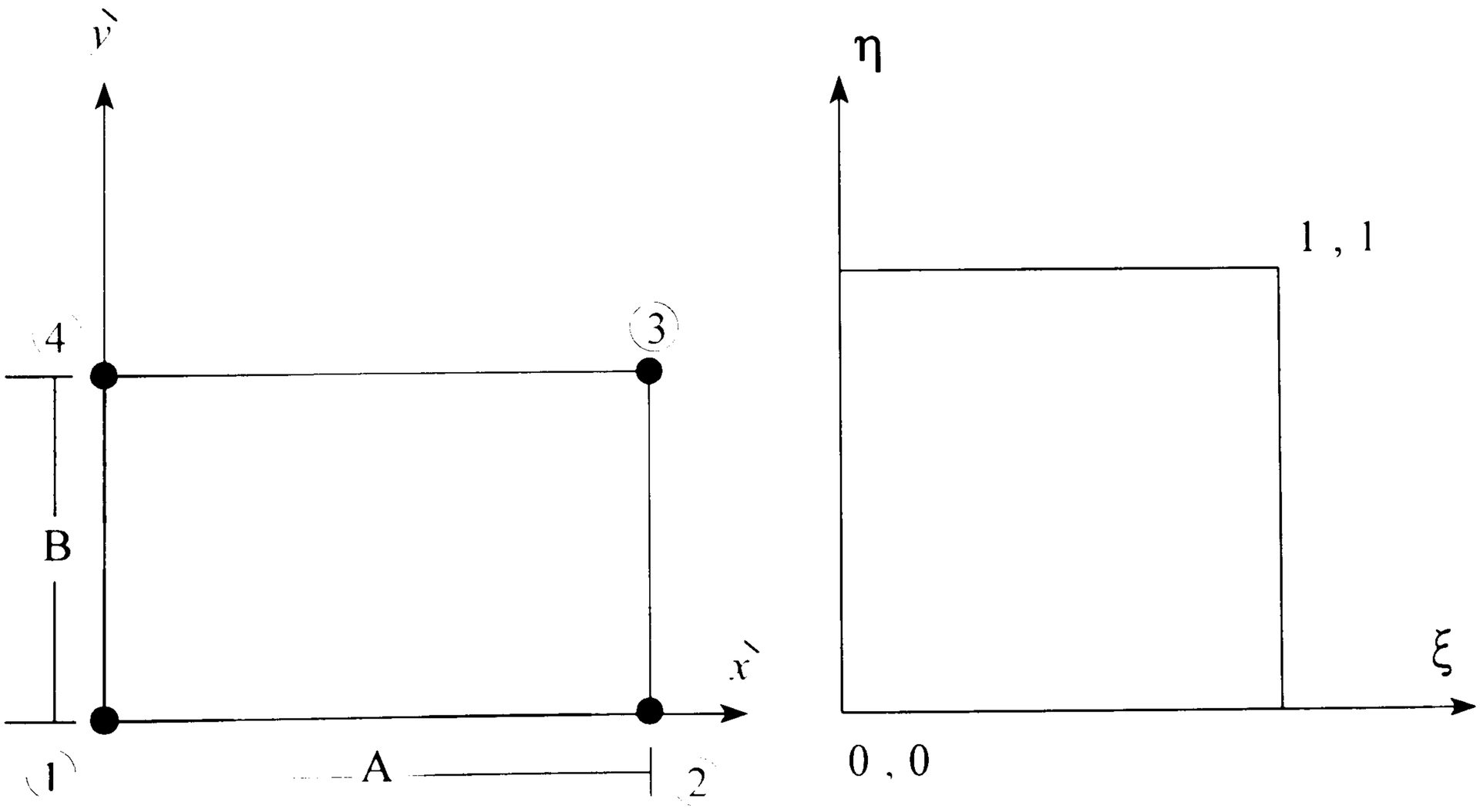

Figure 4.4 Local and intrinsic axes for conforming Hermitian element

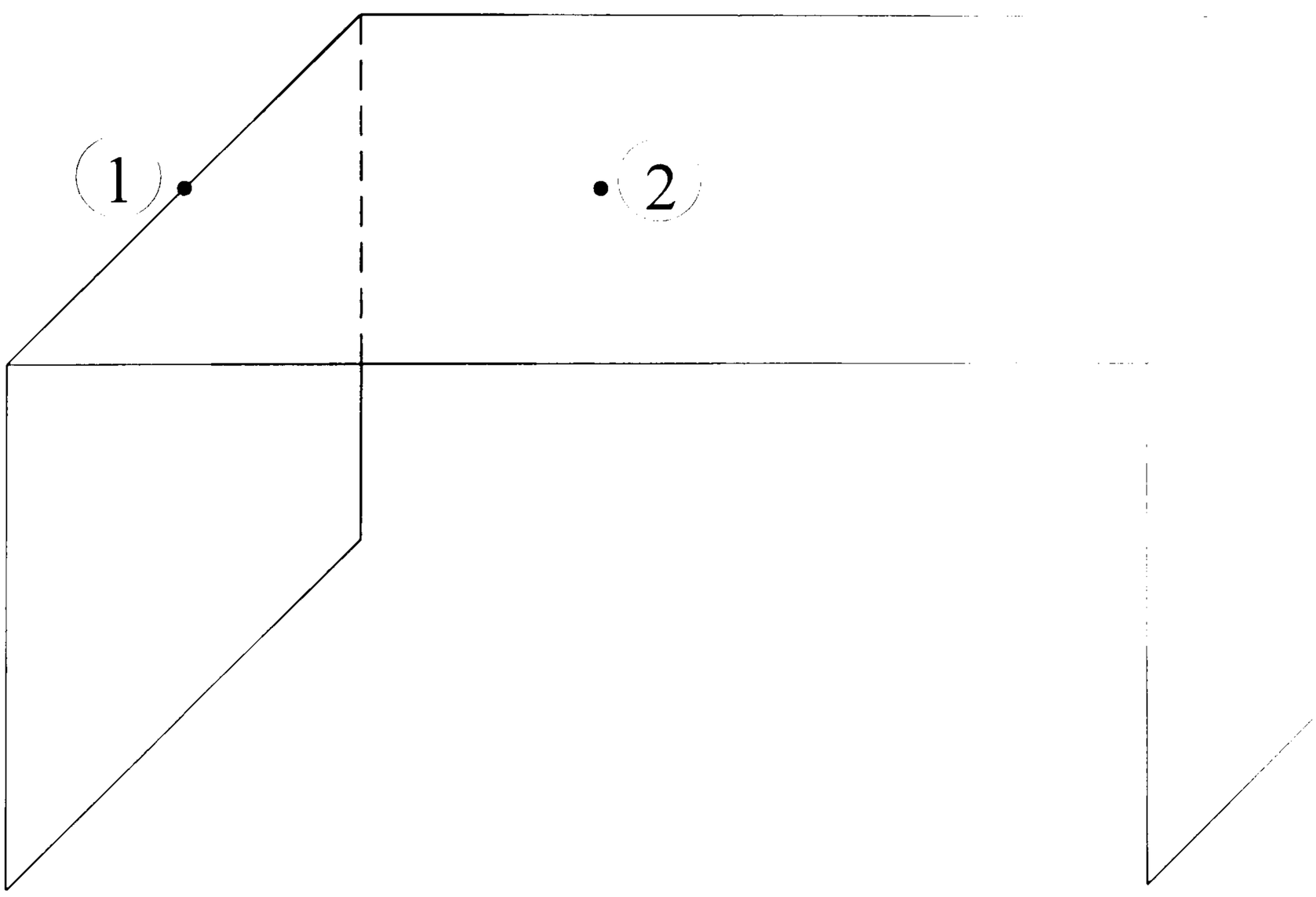

Figure 4.5 Points with different numbers of degrees of freedom

CHAPTER 5

FINITE ELEMENT ANALYSIS

5.1 INTRODUCTION

New conforming and non-conforming finite elements with parabolic transverse shear stress distributions for rotating plate and shell structures, made of composite layered materials, have been developed. The basic procedures of different types of finite element analysis employed in this work are summarized in this chapter, and the corresponding programming modules are reviewed in the next chapter.

Although the main area of research in this thesis is the natural frequency and flutter analysis, it is essential to carry out static analysis prior to dynamic analysis of rotating structures in order to estimate stresses due to rotation, which are required for the derivation of centrifugal stiffness matrix. Hence, dynamic analysis modules have the static analysis as an option prior to dynamic analysis. Due to the versatility of the FEM, most of the finite element procedures described in this chapter are not completely original, and we only summarize here their basic aspects for the completion of work description.

5.2 STATIC ANALYSIS

The finite element package developed in this work was designed to run on PC's with reasonable resources. Hence, it was essential to employ an efficient equation solver, and the most efficient one in terms of RAM requirements and CPU time is the frontal solver. The frontal technique was originated by Irons (1970), and it assembles equations and eliminate variables at the same time. When the coefficients of an equation are completely assembled, from the contributions of all relevant elements, the corresponding variables are eliminated, keeping only a small proportion of the matrix of coefficients in the computer random access memory . Hence, reducing the RAM requirements, and also by avoiding the arithmetic operations on zero terms, the computer CPU time is reduced.

A frontal solver with a dynamic front width, developed originally by Cranfield Computational Mechanics Group, and shown to be very efficient when used with

virtual-memory computers such as VAX and Workstations, has been modified to deal with asymmetric matrices, and employed in this work. Asymmetric matrices arise in flutter analysis, and in the presence of dampers with nonsymmetric coefficients.

Nodal loading vectors equivalent to centrifugal loading have been derived in section 4.6.1, and the stresses and strains at different layers can be obtained from equations similar to those given in sections 4.2 and 4.3.

5.3 NATURAL FREQUENCY ANALYSIS

5.3.1 General theory

The dynamic matrix equation for a rotating element is given in section 4.7.5, and it can be assembled and rewritten for the whole domain of the problem as follows:-

$$\boldsymbol{M}^T \ddot{\boldsymbol{\delta}}(t) + 2\Omega \boldsymbol{C}^T \dot{\boldsymbol{\delta}}(t) + \boldsymbol{K}^T \boldsymbol{\delta}(t) = \boldsymbol{F}(t) \tag{5.1}$$

where

$$\boldsymbol{M}^T = \sum_{elments} \boldsymbol{M}_{elment}$$

$$\boldsymbol{C}^T = \sum_{elments} \boldsymbol{C}_{elment}$$

$$\boldsymbol{K}^T = \sum_{elments} \left(\boldsymbol{K} + \boldsymbol{K}^{\sigma} - \Omega^2 \overline{\boldsymbol{M}} \right)$$

If Coriolis forces effects on the natural frequency is negligible, then the previous equation can be reduced to:-

$$\boldsymbol{M}^T \ddot{\boldsymbol{\delta}}(t) + \boldsymbol{K}^T \boldsymbol{\delta}(t) = \boldsymbol{F}(t) \tag{5.2}$$

When there are no external forces, and with the initial conditions been properly imposed, it is possible to induce vibration in any one of several natural modes which are characteristic of the structure. In a natural mode, each point of the structure executes harmonic motion about the position of static equilibrium at the same frequency. Hence, it can be assumed that, at a natural mode of vibration

$$\boldsymbol{\delta}(t) = \tilde{\boldsymbol{\delta}} \cos \omega t$$

where $\tilde{\boldsymbol{\delta}}$ represents the vector of nodal amplitudes. The previous expression of $\boldsymbol{\delta}(t)$ will result in the following matrix equation:-

$$\left(\boldsymbol{K}^T - \omega^2 \boldsymbol{M}^T\right) \tilde{\boldsymbol{\delta}} = \mathbf{O} \tag{5.3}$$

This matrix equation represents a system of homogeneous simultaneous equations which have a non-trivial solution, if the value of λ satisfies the following condition.

$$\left| \boldsymbol{K}^T - \lambda \boldsymbol{M}^T \right| = \mathbf{O} \tag{5.4}$$

where $\lambda = \omega^2$

The previous determinant is a polynomial in λ which is known as the characteristic equation. Its roots $\lambda_1, \lambda_2, \ldots$ are called the eigenvalues. For each root λ_i there exists a vector $\tilde{\boldsymbol{\delta}}_i$, such that:-

$$(\boldsymbol{K}^T - \lambda_i \boldsymbol{M}^T)\, \tilde{\boldsymbol{\delta}}_i = \mathbf{O} \tag{5.5}$$

and $\tilde{\boldsymbol{\delta}}_i$, which is known as the eigenvector, or the mode shape vector, can be obtained in terms of the ratios to one of its components.

5.3.2 Subspace iteration

If the finite element matrix equation of natural vibration:

$$\boldsymbol{K}^T \tilde{\boldsymbol{\delta}} = \lambda \boldsymbol{M}^T \tilde{\boldsymbol{\delta}}$$

has $\boldsymbol{K}^T$ and $\boldsymbol{M}^T$ with a very large order and only relatively few eigenvalues are required, the technique of subspace iteration provides a very economical solution. The method is based upon reducing $\boldsymbol{K}^T$ and $\boldsymbol{M}^T$ whilst retaining the lowest eigenvalues. The subspace iteration algorithm can be summarized as follows (El-Zafrany, 1994):-

(i) Assume a set of load vectors,

$$\boldsymbol{Y}_{m \times p} = \begin{bmatrix} \boldsymbol{y}_1 & \boldsymbol{y}_2 & \cdots & \boldsymbol{y}_p \end{bmatrix}$$

where $\boldsymbol{y}_r$ is a vector of order m, $r = 1, 2, \ldots, p$,

m is total number of unknown degrees of freedom,

p is the number of the required lowest eigenvalues.

A reasonable guess is to take $Y(r, s) = \delta_{rs}$ (the Kronecker delta).

(ii) Solve the following p sets of equations

$$\boldsymbol{K}_{m \times m}\ \tilde{\boldsymbol{\delta}}_r = \boldsymbol{y}_r$$

where $r = 1, 2, \ldots, p$

(iii) Form the following rectangular matrix of eigenvectors:

$$\boldsymbol{X}_{m \times p} = \left[\boldsymbol{\delta}_1 \quad \boldsymbol{\delta}_2 \quad \ldots \quad \boldsymbol{\delta}_p \right]$$

(iv) Obtain the reduced or subspace stiffness and mass matrices as follows:

$$\boldsymbol{K}^*_{p \times p} = \boldsymbol{X}^t_{(p \times m)}\ \boldsymbol{K}^T_{(m \times m)}\ \boldsymbol{X}_{(m \times p)}$$

$$\boldsymbol{M}^*_{p \times p} = \boldsymbol{X}^t_{(p \times m)}\ \boldsymbol{M}^T_{(m \times m)}\ \boldsymbol{X}_{(m \times p)}$$

(v) Solve the subspace eigenvalue problem:

$$\boldsymbol{K}^*_{p \times p}\ \tilde{\boldsymbol{\delta}}^*_{p \times 1} = \lambda\ \boldsymbol{M}^*_{p \times p}\ \tilde{\boldsymbol{\delta}}^*_{p \times 1} \tag{5.6}$$

(vi) Form the following square matrix of the reduced eigenvectors:

$$\boldsymbol{X}^*_{p \times p} = \left[\tilde{\boldsymbol{\delta}}^*_1 \quad \tilde{\boldsymbol{\delta}}^*_2 \quad \ldots \quad \tilde{\boldsymbol{\delta}}^*_p \right]$$

(vii) Transform back to the original space, using:

$$\boldsymbol{X}_{\text{new}_{(m \times p)}} = \boldsymbol{X}_{\text{old}_{(m \times p)}} \cdot \quad \boldsymbol{X}^*_{(p \times p)}$$

(viii) Calculate the new load vector

$$\boldsymbol{Y}_{\text{new}_{(m \times p)}} = \boldsymbol{M}^T_{m \times m}\ \boldsymbol{X}_{\text{new}_{(m \times p)}}$$

(ix) Decision

- Calculate the maximum error

$$e_{\max} = \text{Max}\ \left(\left| \lambda_{i_{\text{new}}} - \lambda_{i_{\text{old}}} \right|, \quad i = 1, 2, \ldots, p \right)$$

- If the maximum error is greater than a given permissible error then go to step (ii).

5.3.3 Simple iteration algorithm

The matrix equation (5.6) of the reduced eigenvalue problem can be written as follows:-

$$\boldsymbol{M}^* \, \tilde{\boldsymbol{\delta}}^* = \frac{1}{\lambda} \boldsymbol{K}^* \, \tilde{\boldsymbol{\delta}}^* \tag{5.7}$$

Multiplying both sides by $\boldsymbol{K}^{*\,-1}$, the problem can be expressed as the following standard eigenvalue problem:-

$$\boldsymbol{Q} \, \tilde{\boldsymbol{\delta}}^* = \frac{1}{\lambda} \boldsymbol{I} \, \tilde{\boldsymbol{\delta}}^* \tag{5.8}$$

where $\boldsymbol{Q} = \boldsymbol{K}^{*\,-1} \boldsymbol{M}^*$, and $\boldsymbol{I}$ is a unit matrix of the same order.

There are many algorithms for the solution of the standard eigenvalue problem (Wilkinson 1965) and (Bathe and Wilson 1973), the simplest of which is the simple iteration algorithm summarized next:-

(a) Iteration for the lowest λ

The following steps can be employed for determining a value of λ which converges to its minimum value.

(i) Assume an initial value for $\tilde{\boldsymbol{\delta}}^*$

(ii) Calculate the vector $\boldsymbol{y} = \boldsymbol{Q} \, \tilde{\boldsymbol{\delta}}^*$

(iii) The smallest eigenvalue is obtained from the ratio of two scalar products, *i.e.* $\lambda = (\boldsymbol{y}^t \boldsymbol{y}) / (\boldsymbol{y}^t \boldsymbol{Q} \boldsymbol{y})$

(iv) The nodal amplitude vector is calculated from:-

$$\tilde{\boldsymbol{\delta}}^* = \boldsymbol{y} / \sqrt{\boldsymbol{y}^t \boldsymbol{M}^* \boldsymbol{y}}$$

(v) If $| \lambda_{new} - \lambda_{old} | >$ a permissible error, then go to step (ii).

(b) Sweeping of λ_1

Defining $\boldsymbol{Q}_1 = \boldsymbol{K}^{*\,-1} \boldsymbol{M}^*$, then from the orthogonality of eigenvectors, it can be proved that the simple iteration algorithm applied to:

$$\boldsymbol{Q}_{j+1}\,\tilde{\boldsymbol{\delta}} = \frac{1}{\lambda}\,\boldsymbol{I}\,\tilde{\boldsymbol{\delta}} \qquad \text{will converge to } \lambda_{-1}$$

where $$\boldsymbol{Q}_{j+1} = \boldsymbol{Q}_j - \frac{1}{\lambda_j}\,\tilde{\boldsymbol{\delta}}_j\,\tilde{\boldsymbol{\delta}}_j^t\,\boldsymbol{M}^*, \quad j = 1, 2, \ldots$$

and $$\lambda_1 \le \lambda_2 \le \lambda_3 \ \ldots$$

5.4 FORCED VIBRATION

Consider the assembled finite element dynamic matrix equation (Eq. 5.1) for a case of a periodic excitation, or

$$\boldsymbol{F}(t) = \boldsymbol{A}\cos(ft) + \boldsymbol{B}\sin(ft) \tag{5.9}$$

where f is the frequency of excitation (*rad/sec*). The corresponding steady-state nodal displacement vector will be

$$\boldsymbol{\delta}(t) = \boldsymbol{\alpha}\cos(ft) + \boldsymbol{\beta}\sin(ft) \tag{5.10}$$

Hence

$$\dot{\boldsymbol{\delta}}(t) = -f\,[\,\boldsymbol{\alpha}\sin(ft) - \boldsymbol{\beta}\cos(ft)\,] \tag{5.11}$$

and

$$\ddot{\boldsymbol{\delta}}(t) = -f^2\,[\,\boldsymbol{\alpha}\cos(ft) + \boldsymbol{\beta}\sin(ft)\,]$$

$$\equiv -f^2\,\boldsymbol{\delta}(t) \tag{5.12}$$

It can also be deduced from complex variables, that:-

$$a\cos\theta + b\sin\theta = \Re\left[(a + ib)\,e^{-i\theta}\right] \tag{5.13}$$

where $i = \sqrt{-1}$, $\Re \equiv$ real part of, and it can therefore be proved that:-

$$\boldsymbol{F}(t) = \Re\left\{(\boldsymbol{A} + i\boldsymbol{B})\,e^{-ift}\right\} \tag{5.14}$$

$$\equiv \Re\left\{\hat{\boldsymbol{F}}\,e^{-ift}\right\}$$

where

$$\hat{\boldsymbol{F}} = \boldsymbol{A} + i\,\boldsymbol{B} \tag{5.15}$$

Similarly, it can be shown that:-

$$\boldsymbol{\delta}(t) = \Re\left\{\hat{\boldsymbol{\delta}}\, e^{-ift}\right\} \tag{5.16}$$

$$\dot{\boldsymbol{\delta}}(t) = \Re\left\{-if\,\hat{\boldsymbol{\delta}}\, e^{-ift}\right\} \tag{5.17}$$

$$\ddot{\boldsymbol{\delta}}(t) = \Re\left\{-f^2\,\hat{\boldsymbol{\delta}}\, e^{-ift}\right\} \tag{5.18}$$

where

$$\hat{\boldsymbol{\delta}} = \boldsymbol{\alpha} + i\,\boldsymbol{\beta} \tag{5.19}$$

Substituting from Equations (5.14), (5.16)-(5.18) into (5.1) then:-

$$\Re\left\{\left[-f^2\boldsymbol{M}^T - (2\Omega f)\,i\boldsymbol{C}^T + \boldsymbol{K}^T\right]\hat{\boldsymbol{\delta}}\, e^{-ift}\right\} \equiv \Re\left\{\hat{\boldsymbol{F}}\, e^{-ift}\right\} \tag{5.20}$$

and the solution of the above matrix equation is equivalent to the solution of the following simplified equation:-

$$\left[-f^2\boldsymbol{M}^T - (2\Omega f)\,i\boldsymbol{C}^T + \boldsymbol{K}^T\right]\hat{\boldsymbol{\delta}} \equiv \hat{\boldsymbol{F}} \tag{5.21}$$

which represents a system of simultaneous algebraic complex equations. Structural or hysteretic damping may be represented in terms of the material property μ, known as the hysteretic damping factor, and $\boldsymbol{K}^T$ is modified as follows:-

$$\boldsymbol{K}^T = \sum_{elements}\left[(1 + i\mu)\boldsymbol{K} + \boldsymbol{K}^{\sigma} - \Omega^2\overline{\boldsymbol{M}}\right]_{element} \tag{5.22}$$

An excitation frequency which causes resonance, the resonant frequency, is the one which leads to very high values of vibration amplitudes $\hat{\boldsymbol{\delta}}$, *i.e.* it is the one which satisfies the following condition:-

$$\Re\left\{\left|\boldsymbol{K}^T - (2\Omega f)\,i\boldsymbol{C}^T - f^2\boldsymbol{M}^T\right|\right\} = 0 \tag{5.23}$$

several values of f can be assumed, and the nodal amplitudes can be plotted versus f, so as to detect the resonant frequencies.

5.5 FLUTTER ANALYSIS

The assembled dynamic matrix equation can contain aeroelastic effects, and resonant frequencies may be detected by using a forced vibration approach similar to that mentioned in section 5.4.

Consider the simplified theory described in section 4.8.3, the assembled equations of a composite layered panel in a supersonic flow, ignoring excitation forces, is:-

$$\rho_{mm} \boldsymbol{M}_H^T \ddot{\boldsymbol{\delta}}_b(t) + c \boldsymbol{M}_H^T \dot{\boldsymbol{\delta}}_b(t) + \boldsymbol{K}_f^T \boldsymbol{\delta}_b(t) = \mathbf{O} \qquad (5.24)$$

where
$$\boldsymbol{K}_f^T = \sum_{elements} \left(\boldsymbol{K}_{bb} + \boldsymbol{K}_a \right)_{element}$$

$$\boldsymbol{M}_H^T = \sum_{elements} \left(\boldsymbol{M}_H \right)_{element}$$

In order to find the corresponding eigenvalues, it is assumed that:-

$$\boldsymbol{\delta}_b(t) = \tilde{\boldsymbol{\delta}}_b \, e^{\alpha t} \qquad (5.25)$$

where $\tilde{\boldsymbol{\delta}}_b$ represents the displacement amplitude vector,

$\alpha = \beta + i\omega$ which is a complex eigenvalue, with β and ω being real values,

then $\dot{\boldsymbol{\delta}}_b(t) = \alpha \, \tilde{\boldsymbol{\delta}}_b \, e^{\alpha t}$

$$\ddot{\boldsymbol{\delta}}_b(t) = \alpha^2 \, \tilde{\boldsymbol{\delta}}_b \, e^{\alpha t}$$

and Equation (5.24) becomes:-

$$\left[\boldsymbol{K}_f^T + \left(\alpha\, c + \alpha^2\, \rho_{mm} \right) \boldsymbol{M}_H^T \right] \tilde{\boldsymbol{\delta}}_b\, e^{\alpha t} = \mathbf{O} \tag{5.26}$$

which leads to the following simple eigenvalue problem:-

$$\boldsymbol{K}_f^T\, \tilde{\boldsymbol{\delta}}_b = \lambda\, \boldsymbol{M}_H^T\, \tilde{\boldsymbol{\delta}}_b \tag{5.27}$$

where $$\lambda = -\left(\alpha\, c + \alpha^2\, \rho_{mm} \right)$$

which generally represents a complex eigenvalue.

The following results can be predicted from the physical concepts of the problem:-

(a) When $V_\infty = 0$, *i.e.* no aerodynamic effect takes place, λ will have a set of real values $\lambda_1, \lambda_2, \ldots,$ representing the bending eigenvalues of the panel, with $\lambda_1 < \lambda_2 < \ldots$

(b) When $V_\infty > 0$, and increases monotonically from zero, the smallest eigenvalues λ_1 and λ_2 approach each other and coalesce to λ_{cr} at $V_\infty = (V_\infty)_{cr}$, and become complex conjugate pairs for $V_\infty > (V_\infty)_{cr}$. The same phenomenon is true for each succeeding pair of eigenvalues, but the smallest critical one will cause failure, *i.e.* the higher critical values of λ will never practically occur.

Using the subspace iteration algorithm, Equation (5.27) can be reduced as follows:-

$$\boldsymbol{K}^*_{2\times 2}\ \boldsymbol{\delta}^*_{2\times 1} = \lambda\ \boldsymbol{M}^*_{2\times 2}\ \boldsymbol{\delta}^*_{2\times 1} \tag{5.28}$$

i.e.

$$\begin{bmatrix} K^*_{11} - \lambda M^*_{11} & K^*_{12} - \lambda M^*_{12} \\ K^*_{21} - \lambda M^*_{21} & K^*_{22} - \lambda M^*_{22} \end{bmatrix} \begin{bmatrix} \delta^*_1 \\ \delta^*_2 \end{bmatrix} = \mathbf{O} \tag{5.29}$$

For non-trivial solution:-

$$\begin{vmatrix} K^*_{11} - \lambda M^*_{11} & K^*_{12} - \lambda M^*_{12} \\ K^*_{21} - \lambda M^*_{21} & K^*_{22} - \lambda M^*_{22} \end{vmatrix} = 0$$

i.e.

$$\left(K_{11}^{*} - \lambda M_{11}^{*}\right)\left(K_{22}^{*} - \lambda M_{22}^{*}\right)$$

$$- \left(K_{12}^{*} - \lambda M_{12}^{*}\right)\left(K_{21}^{*} - \lambda M_{21}^{*}\right) = 0$$

which can be expanded to the following second degree equation:-

$$\alpha_{\circ}\lambda^{2} - \alpha_{1}\lambda + \alpha_{2} = 0$$

where

$$\alpha_{\circ} = M_{11}^{*} M_{22}^{*} - M_{12}^{*} M_{21}^{*} \equiv |\boldsymbol{M}^{*}|$$

$$\alpha_{2} = K_{11}^{*} K_{22}^{*} - K_{12}^{*} K_{21}^{*} \equiv |\boldsymbol{K}^{*}|$$

$$\alpha_{1} = K_{11}^{*} M_{22}^{*} + M_{11}^{*} K_{22}^{*} - K_{12}^{*} M_{21}^{*} - K_{21}^{*} M_{12}^{*}$$

Hence

$$\begin{matrix}\lambda_{1} \\ \lambda_{2}\end{matrix} = \frac{\alpha_{1} \pm \sqrt{\alpha_{1}^{2} - 4\,\alpha_{\circ}\alpha_{2}}}{2\,\alpha_{\circ}}$$

The values of λ_1 and λ_2 can easily be detected, however our present subspace is not suitable for λ_1 and λ_2 when they have complex roots. Since this situation only occurs after the critical flutter boundary (*i.e.* when $\lambda_1 = \lambda_2$), an automatic search for coalescence conditions has been designed, as follows:-

(i) Starting with $V_\infty = 0$ (or $a = 0$), then calculate the expected real values of λ_1 and λ_2

(ii) Update $(V_\infty)_{new} = (V_\infty)_{old} + \Delta V_\infty$ or $(a)_{new} = (a)_{old} + \Delta a$ where ΔV_∞ and Δa are given increments, and calculate the corresponding λ_1 and λ_2.

(iii) Proceed until the subspace iteration solver diverges at certain V_∞ or a, which means that flutter boundary has been exceeded. Then

$(V_\infty)_{old}$ = last V_∞ - ΔV_∞

a_{old} = last a - Δa

decrease the increments, say:

$$(\Delta V_\infty)_{new} = (\Delta V_\infty)_{old} / 5$$

$$(\Delta a)_{new} = (\Delta a)_{old} / 5$$

and repeat from step (ii) with the smaller increments.

(iv) Proceed until $|\lambda_1 - \lambda_2|$ is less than a permissible error.

Since the subspace iteration solver requires initially assumed values for mode shape vectors, the previous search procedure was improved and the number of subspace iterations was drastically reduced when for every new a or V_∞, we use the last calculated values of mode shape vectors as our initially assumed values.

CHAPTER 6

FINITE ELEMENT PROGRAMMING PACKAGE

6.1 INTRODUCTION

Based upon the theory described in previous chapters, a modular finite element computer programming package was designed. The package was coded in FORTRAN 77, and tested on VAX (VMS) main frame computers, Unix workstations, and DOS operating PC's. The package consists of several modules, where each module is a file containing a group of subroutines. For any specific analysis a program can be easily constructed from relevant modules by linking their compiled files, as it will be explained in this chapter.

The package can be employed for finite element analysis of plates and shells made of isotropic or composite layered materials, and the package is capable of static stress analysis, natural frequency analysis, forced vibration analysis, and flutter analysis.

It is not possible within a limited thesis volume to present a detailed description of the different subroutines available in the package. Nevertheless, an attempt is made in this chapter, aiming at introducing the structure of the basic modules, and how different program options can be constructed.

The package modules are illustrated by coloured figures, where the element module is illustrated in blue, the material module is in green, the common module is in red, the Coriolis and centripetal matrices module is in pink, the flutter module is in orange, the solver modules are in brown, and the program structures are in violet.

6.2 ELEMENT MODULE

This module contains the essential subroutines for the derivation of element stiffness and mass matrices. Since some of the data parameters, and stress calculations depend on the type of element, the data and stress subroutines are also included to facilitate future development. For each type of analysis, the module has two versions:-

(a) Plate version, where the analysis of plates is assumed, and the local axes of elements are therefore, considered in the directions of the global axes of the

plate. No rotation of element matrices is required, and relevant plate degrees of freedom are automatically assumed.

(b) Shell version, for the analysis of folded plates and curved shells, and elements will be considered as facetted shell elements, with local axes which may be different from the global axes of the structure.

The different element module files in the package are:-

(i) PLATE-NF.FOR — plate version for static and natural frequency analysis.

(ii) SHELL-NF.FOR — shell version for static and natural frequency analysis.

(iii) PLATE-FV.FOR — plate version for forced vibration analysis. This file is similar to the one for plate natural frequency analysis except it contains complex loading and complex stress routines.

(iv) SHELL-FV.FOR — shell version for forced vibration analysis and it is the same as the plate forced vibration version regarding load and stress.

(v) PLATE-FL.FOR — plate version for flutter analysis

(vi) SHELL-FL.FOR — shell version for flutter analysis.

The last two files are similar to the corresponding ones for the natural frequency analysis, except they contain a subroutine for reading additional flutter data.

All programs were based on *double precision* arithmetic in order to avoid any ill conditioning in thin plate matrices due to the difference of order of magnitude between in-plane and out-of-plane terms in element matrices. However, the version described in this chapter is the PC version, where *double complex* was not possible with the PC compilers used, and hence all files for forced vibration analysis contain single precision parameters.

Each module file consists of a number of sub-modules, each of which is either a subroutine or a group of subroutines, performing a specific task within the finite element procedure, as will be explained in the following sections.

6.2.1 Input subroutine (DATA)

The input data subroutine is called DATA, and it reads an input file which contains all the parameters required to define the geometry of the structure, its loading and boundary conditions, material properties, and Gauss quadrature data, and it transmits sufficient information to other subroutines via a number of COMMON blocks. The input file consists of simple data modules, each with a self explained-title. The DATA subroutine is also based on a number of subroutines, each of which is responsible for reading a specific data module from the input file, and performs basic error diagnosis.

The first three characters of each data record are extracted then transformed to upper case characters and compared with eight three-letter control words. If no match is found, the record is considered a comment line, otherwise an appropriate subroutine is called to read next lines, and perform basic error-diagnosis. Data structure is given in a separate user manual, and the DATA subroutine is using the following subroutines, as illustrated in Fig. (6.1).

(a) *Subroutine UCASE*

This subroutine ignores any leading spaces before extracting the first three characters of a data line, and puts their upper case characters in a key word, to be compared with the built in control words, as explained above.

(b) *Subroutine NODE*

It reads the number of nodes, for a user-defined finite element mesh, and it reads the nodal coordinates with respect to a unique set of global axes.

(c) *Subroutine ELEMENT*

It reads the element type, whether conforming quadrilateral, non-conforming quadrilateral, or non-conforming triangle, and it also reads the topology arrays of the elements in the finite element mesh.

(d) *Subroutine LAYER*

This subroutine identifies whether the material is isotropic, composite with uniform layer thickness, or composite with variable layers thickness, and it reads the corresponding material properties, and thickness distribution. It also calls the DMATRIX subroutine which is explained in section 6.3.

(e) *Subroutine BOUNDARY*

It reads boundary conditions in terms of switches, and it identifies whether the nodes are on a plate or on a curved surface.

(f) *Subroutine LOAD*

There are different versions of this subroutine depending on the type of analysis. REAL loads are considered for static analysis, and COMPLEX loads are assumed for forced vibration analysis. It also contains flutter data for flutter analysis.

(g) *Subroutine DYNAMIC*

This subroutine reads rotating speed data in terms of its value, and the coordinates of two points on the axis of rotation. It also reads data for natural frequency analysis.

(h) *Subroutine GAUSSDATA*

It reads the order of the Gauss quadrature scheme required for the numerical integration of every part of element matrices, thus allowing the use of a reduced integration approach, if required. Gauss data parameters themselves are read by calling subroutine GETGAUSS, which will read the parameters corresponding to a given quadrature order from an existing file.

(i) *Subroutine INFORM*

After all data modules are read and interpreted successfully, this subroutine is called to list all data parameters in the output file, thus allowing a double check on the data parameters provided for the analysis.

6.2.2 Element stiffness matrix generator (ESMG)

This subroutine performs all the operations for the derivation of every element stiffness matrix, and its structure is shown in Fig. (6.2). It calls first subroutine LOCAL, which defines the local axes of the element, and the corresponding local coordinates of element nodes, and calculates the element rotation matrix. It calls next a number of different subroutines, each calculates a part of the element stiffness matrix, as derived in Equation (4.79), then it assembles the total element stiffness matrix. It also rotates the matrix with respect to the global axes in shell versions. The subroutines for the stiffness matrix parts are summarized as follows:-

(a) *Subroutine ESMGMM*

This subroutine calculates $\boldsymbol{K}_{mm}$ defined by Equation (4.71), using the following subroutines:-

(i) DMATRIXMM which calculates $\boldsymbol{D}_{mm}$ defined by Equation (4.62), and PZ, described in section 6.3, may be called for cases with variable thickness.

(ii) BMATRIXM which calculates the matrix $\boldsymbol{B}_m$ defined by Equation (4.25), and it requires the calling of subroutines CARTD, JACOB, INTRD, which are described in section 6.4.

(iii) Matrix manipulation subroutines: MATI, MATM, MATS, which are also described in section 6.4.

(b) *Subroutine ESMGBB*

It calculates the matrix $\boldsymbol{K}_{bb}$ defined by Equation (4.72), using the following subroutines:-

(i) DMATRIXBB which calculates $\boldsymbol{D}_{bb}$ defined by Equation (4.63), and PZ, may be called for cases with variable thickness.

(ii) BMATRIXB which calculates the matrix $\boldsymbol{B}_b$ defined by Equation (4.28). It calls subroutines HCARTD2, HINTRD2,.... as shown in Fig. (6.2)

(iii) Matrix manipulation subroutines which are also shown in Fig. (6.2).

(c) *Subroutine ESMGSS*

It calculates the matrix $\boldsymbol{K}_{ss}^{(x,y)}$ defined by Equation (4.73), and it calls subroutine DMATRIXSS described in section 6.3, and subroutine BMATRIXB described above, and the matrix manipulation subroutines.

(d) *Subroutine ESMGTT*

It calculates the matrix $\boldsymbol{K}_{\gamma\gamma}^{(\mu)}$ defined by Equation (4.74), and it calls subroutine DMATRIXTT described in section 6.3, and subroutine BMATRIXT which calculates $\boldsymbol{B}_s$ defined by Equation (4.33).

(e) *Subroutine ESMGMB*

It calculates the matrix $\boldsymbol{K}_{mb}$ defined by Equation (4.75), with a detailed structure shown in Fig. (6.2).

PAGE

MISSING

IN

ORIGINAL

6.2.4 Element centrifugal stiffness matrix generator (CSMG)

This generator is similar to the previous one, and its structure is shown in Fig. (6.4). The subroutines defined in the element module for the calculation of different matrices required for the element centrifugal stiffness matrix are listed in the following table:-

Subroutine name	Matrix or vector calculated	Defining equation No.
CSMGMM	$\boldsymbol{K}^{\sigma}_{mm}$	4.124
CSMGBB	$\boldsymbol{K}^{\sigma}_{bb}$	4.125
CSMGWW	$\boldsymbol{K}^{\sigma}_{ww}$	4.126
CSMGSS	$\boldsymbol{K}^{\sigma}_{ss}$	4.127
CSMGMB	$\boldsymbol{K}^{\sigma}_{mb}$	4.128
CSMGMS	$\boldsymbol{K}^{\sigma}_{ms}$	4.129
CSMGBS	$\boldsymbol{K}^{\sigma}_{bs}$	4.130
GMATM	$\boldsymbol{G}_{m}$	4.49
GMATW	$\boldsymbol{G}_{w}$	4.50
GMATB	$\boldsymbol{G}_{b}$	4.51
SMATM	$\boldsymbol{S}_{mn}$	4.115
SMATW	$\boldsymbol{S}_{ww}$	4.116
SMATBB	$\boldsymbol{S}_{bb}$	4.117
SMATS	$\boldsymbol{S}_{ss}$	4.118
SMATMB	$\boldsymbol{S}_{mb}$	4.119
SMATMS	$\boldsymbol{S}_{ms}$	4.120
SMATBS	$\boldsymbol{S}_{bs}$	4.121

6.2.5 Element equivalent nodal force generator (NFVG)

This segment is responsible for the derivation of the nodal forces equivalent to inertial loading, and its structure is shown in Fig. (6.5). This subroutine calls a number of different subroutines for the calculation of the different parts of the nodal forces, and shown in the following table:-

Subroutine name	Matrix calculated	Defining equation No.
EQFM	$\boldsymbol{F}_m$	4.145
EQFB	$\boldsymbol{F}_b$	4.146
EQFS	$\boldsymbol{F}_s$	4.147
EQFW	$\boldsymbol{F}_W$	4.148

Each of those subroutine calls an integrated ρ subroutine, as described in section 6.3, in addition to some matrix manipulation subroutines, and it also calls subroutine LACC to calculate the acceleration due to rotation, and subroutine RVECTOR to calculate the axes rotation matrix. The $\boldsymbol{N}$ matrix subroutines, described in section 6.2.3, are also called by the equivalent loading subroutines.

6.3 MATERIAL MODULE

This module contains a number of subroutines designed to calculate any required material dependent data such as integrated stress-strain matrices, integrated density parameters, and integrated thickness parameters. There are only two versions of the material module available in the following files:-

(a) MAT-DP.FOR this is the version which is employed for the double precision analysis.

(b) MAT-SP.FOR this is the corresponding single precision version.

The module consists of four parts, as illustrated in Fig. (6.6)

6.3.1 Stress-strain matrices subroutines

The basic parts of those subroutines are as shown in the following table:-

Subroutine name	Matrix calculated	Defining equation No.
DMATRIXMM	$\boldsymbol{D}_{mm}$	4.62
DMATRIXBB	$\boldsymbol{D}_{bb}$	4.63
DMATRIXSS	$\boldsymbol{\mu}_{ss}$	4.65
DMATRIXTT	$\boldsymbol{D}_{ss}$	4.64
DMATRIXMB	$\boldsymbol{D}_{mb}$	4.66
DMATRIXMS	$\boldsymbol{D}_{ms}$	4.67
DMATRIXBS	$\boldsymbol{D}_{bs}$	4.68

6.3.2 D matrices for layer

For the calculation of stresses, the actual stress-strain matrix is required. For isotropic materials, this is only one unique matrix, but for composite layers, there is one matrix required for every layer. The subroutines summary is explained next:-

(a) *DMATRIX* It calculates the $\boldsymbol{D}$ matrix for isotropic materials, and performs the basic calculation of $\boldsymbol{D}$ matrices for each layer, rotated with respect to structural axes.

(b) LAYERED It extracts the $\boldsymbol{D}$ matrix for a specified layer.

(c) LAYERDM It extracts the $\boldsymbol{D}$ matrix for the x-y stress-strain equations, for a specified layer.

6.3.3 Integrated density parameters

The basic subroutines for the calculation of the integrated density parameters are as shown in the next table:-

Subroutine name	Matrix calculated	Defining equation No.
ROWMM	ρ_{mm}, ρ_{HH}	4.84, 4.86
ROWBB	ρ_{bb}	4.85
ROWSS	ρ_{ss}	4.87
ROWMB	ρ_{mb}	4.88
ROWMS	ρ_{ms}	4.89
ROWBS	ρ_{bs}	4.90

6.3.4 Integrated thickness parameter subroutines

This group contains subroutine PZ which calculates the thickness of the layers, at any given quadrature point for cases with variable thickness distribution. It also contains the subroutines necessary for the calculation of the integration of $f(z)$ functions over the full thickness, as listed in the following table:-

Subroutine name	$f(z)$	Relevant equation No.
HVECTORM	1	4.115, 4.116
HVECTORB	z^2	4.117
HVECTORS	$\left(z - \frac{4z^3}{3h^2}\right)^2$	4.118
HVECTORMB	z	4.119
HVECTORMS	$z - \frac{4z^3}{3h^2}$	4.120
HVECTORBS	$z^2 - \frac{4z^4}{3h^2}$	4.121

6.4 COMMON MODULE

This module consists of all common subroutines employed in the derivation of different element matrices, and it has also a double precision version COM-D.FOR and a single precision version COM-SP.FOR. The module can be divided into the following four groups of subroutines, as shown in Fig. (6.7).

6.4.1 Matrix manipulation subroutines

These are common subroutines for different matrix operations as follows:-

(a) *Subroutine MATI* for initiation of square matrices.

(b) *Subroutine MATM* for multiplication of two matching rectangular matrices.

(c) *Subroutine MATV* for multiplication of a matrix by a vector.

(d) *Subroutine MATT* for transposing a matrix.

(e) *Subroutine MATS* for adding two square matrices.

(f) *Subroutine MATSR* for adding two rectangular matrices.

(g) *Subroutine MATSV* for adding two vectors.

6.4.2 Nodal intrinsic coordinates

This is only one subroutine; INTRCO, which defines the intrinsic nodal coordinates for a given element.

6.4.3 Lagrangian shape function subroutines

These are the subroutines which calculate the values of Lagrangian shape functions, their intrinsic and cartesian derivatives, and the Jacobian determinant at any given quadrature point, and they are as follows:-

(a) *Subroutine SHAPE* calculates the values of Lagrangian shape functions.

(b) *Subroutine INTRD* calculates the values of the intrinsic derivatives of Lagrangian shape functions $\frac{\partial N_i}{\partial \eta}$ and $\frac{\partial N_i}{\partial \xi}$.

(c) *Subroutine JACOB* calculates the Jacobian matrix, its determinant, and its inverse matrix.

(d) *Subroutine CARTD* calculates the cartesian derivatives of Lagrangian shape functions $\frac{\partial N_i}{\partial x}$ and $\frac{\partial N_i}{\partial y}$ using the information generated by subroutine JACOB.

6.4.4 Hermitian shape function subroutines

This group consists of the subroutines which calculate the values of Hermitian shape functions for conforming and non-conforming elements, and their first and second order intrinsic and cartesian derivatives at any given quadrature point, and they are listed as follows:-

(a) *HSHAPE* It calculates the values of Hermitian shape functions for conforming elements via subroutine HSHAPEN, and for non-conforming elements via subroutine HSHAPEO.

(b) *HITRD1* It calculates the values of the first order intrinsic derivatives for Hermitian shape functions by calling subroutine HITRD1N for conforming elements, and subroutine HITRD1O for non-conforming elements.

(c) *HINTRD2* This subroutine calculates the second order intrinsic derivatives $\frac{\partial^2}{\partial \eta^2}$, $\frac{\partial^2}{\partial \xi^2}$ and $\frac{\partial^2}{\partial \eta \, \partial \xi}$ for Hermitian shape functions by calling subroutine HINTRD2N for conforming elements, and subroutine HINTRD2O for non-conforming elements.

(d) *JACOB22* This subroutine calculates the second order Jacobian matrix, as defined in APPENDIX D, and its inverse matrix.

(e) *HCARTD1* It calculates the first order cartesian derivatives; $\frac{\partial}{\partial x}$ and $\frac{\partial}{\partial y}$ of Hermitian shape functions, using the information provided by subroutines JACOB and HITRD1.

(f) *HCARTD2* It calculates the second order cartesian derivatives, $\frac{\partial^2}{\partial x^2}$, $\frac{\partial^2}{\partial y^2}$ and $\frac{\partial^2}{\partial x \, \partial y}$ of Hermitian shape functions using information generated by subroutines JACOB22 and HINTRD2.

6.5 CORIOLIS AND CENTRIPETAL MATRICES MODULE

This module contains the subroutines which generates element Coriolis and centripetal matrices required for the analysis of rotating structures. It has also two versions: CRLS-PL.FOR for plates, and CRLS-SH.FOR for shells, which are similar except the shell version rotates the generated matrices from local axes directions to global axes directions. The module consists of two main subroutines as summarized next.

6.5.1 Coriolis matrix generator (EMCMG)

This subroutine carries out the derivation of the element Coriolis matrix through a number of other subroutines as shown in Fig. (6.8). It calls subroutine LOCAL first to generate local nodal coordinates, and element rotation matrix. Then it calls subroutine BBMATRIX to calculate $\boldsymbol{b}_{22}$, $\boldsymbol{b}_{12}$, and $\boldsymbol{b}_{21}$ defined by Equations (4.193)-(4.195). After that it calls a number of subroutines, each of which calculates a part of the $\boldsymbol{C}$ matrix, as defined by Equation (4.209). Then it assembles the element $\boldsymbol{C}$ matrix, and for shell versions this matrix is rotated to the structure global axes. The subroutines which calculate the different parts of the $\boldsymbol{C}$ matrix are shown in the following table:-

Subroutine name	Matrix calculated	Defining equation No.
EMCGMM	C_{mm}	4.199
EMCGBB	$C_{bb} - C_{bH} + C_{bH}^{t}$	4.200, 4.202
EMCGSS	C_{ss}	4.201
EMCGMB	$- C_{mb} + C_{mH}$	4.203, 4.204
EMCGBM	$- C_{mb}^{t} - C_{mH}^{t}$	4.203, 4.204
EMCGMS	C_{ms}	4.205
EMCGBS	$- C_{bs} + C_{Hs}$	4.206, 4.207
EMCGSB	$- C_{bs}^{t} - C_{Hs}^{t}$	4.206, 4.207

6.5.2 Centripetal matrix generator (EMBMG)

This is similar to the Coriolis matrix generator subroutine (EMCMG), but it uses the AAMATRIX to calculate a_{22}, a_{12}, a_{22}, and a_{33} defined bey equations (4.166)-(4.196), which are employed in the derivations of different parts of element centripetal matrix $\overline{M}$, as defined by Equation (4.190), and with a structure shown in Fig. (6.9). This subroutines calls also other different subroutines to calculate the parts of $\overline{M}$ matrix, as in the following table:-

Subroutine name	Matrix calculated	Defining equation No.
EMBGMM	$\overline{M}_{mm}$	4.179
EMBGBB	$\overline{M}_{bb} + \overline{M}_{HH} - \overline{M}_{bH} - \overline{M}_{bH}^{t}$	4.180, 4.181, 4.183
EMBGSS	$\overline{M}_{ss}$	4.182
EMBGMB	$- \overline{M}_{mb} + \overline{M}_{mH}$	4.184, 4.185
EMBGBM	$- \overline{M}_{mb}^{t} + \overline{M}_{mH}^{t}$	4.184, 4.185
EMBGMS	$\overline{M}_{ms}$	4.186
EMBGBS	$- \overline{M}_{bs} + \overline{M}_{Hs}$	4.187, 4.188
EMBGSB	$- \overline{M}_{bs}^{t} + \overline{M}_{Hs}^{t}$	4.187, 4.188

6.6 FLUTTER MATRICES MODULE

This module consists of the subroutines which generate aeroelastic stiffness and mass matrices, as defined in section 4.8, required for flutter analysis. It also has a plate version FL-PLATE.FOR and shell version FL-SHELL.FOR, which are similar in structure except the plate version does not rotate the element matrices. The structure of the module is as shown in Fig. (6.10), and it consists of the following parts.

6.6.1 Aeroelastic stiffness matrix generator

The matrix $\boldsymbol{K}_a$ as defined by Equation (4.224) is generated by means of subroutine EFKG, and the total element matrix is assembled by subroutine EKFL, and is rotated to global axes in the shell version.

6.6.2 Aeroelastic mass matrix generator

The matrix $\boldsymbol{C}_a$ defined by Equation (4.225) is derived by subroutine EFMG, and assembled by subroutine EMFL. This matrix, with $c = 1$, is employed as a mass matrix with the simplified flutter analysis.

6.7 SOLVER MODULES

These are the files containing the master program and solver subroutines for every type of analysis, and they are as follows:-

6.7.1 Static analysis solver module

This module is listed in a file called STAT.FOR, and represents a master program called STATIC, which controls the operations for static analysis, as shown in Fig. (6.11). The subroutines called by the master program are as follows:-

(a) *Subroutine SET FILE*

This subroutine is employed for interactive definition of the case file name, and the corresponding names of input and output files. It was necessary in that subroutine to overcome a difficulty encountered with the Unix operating system, when dealing with character variables of different sizes.

(b) *Subroutine DATA*

This subroutine reads the input data as described in section 6.2.1.

(c) *Subroutine INITIATION*

This subroutine is required to estimate the front width, so that the right size of records and dynamic dimensions can be used in frontal subroutines. It also initiates some arrays based on boundary conditions, to facilitate equations

reduction and expansion in frontal subroutines.

(d) *Subroutine FRONT*

This is the basic frontal subroutine, which assembles the equations element by element, apply boundary conditions, and Gauss elimination, and only keeps in the computer RAM a small portion of the matrix of equation coefficients, as explained in chapter 5.

(e) *Subroutine SOLVER*

In this subroutine, the backward substitution process takes place, and the reduced nodal displacement vector is obtained.

(f) *Subroutine DISP*

In this subroutine, the full nodal displacement vector is defined from the reduced vector and prescribed values, and the displacement components are listed in the output file at every node.

(g) *Subroutine STRESS*

This subroutine calculates the stress and strain components at every node, by averaging the values obtained from different elements sharing the same node. For composite layered structures, distributions over the thickness are obtained, and values of stress and strains are calculated at lower and upper surfaces of each layer, and all the results are listed in the output file. Stress and strain components for shell structures, are calculated with respect to element local axes.

6.7.2 Natural frequency solver module

This module has a plate version DYNPL-NF.FOR and shell version DYNSH.FOR, which are similar except the plate version, if used, will only calculate the out-of-plane natural frequencies. If the in-plane natural frequencies are required for a plate, the shell version can simply be used, since all modules are fully compatible. The module has the master program NATURAL FREQUENCY, which controls the natural frequency operations. The basic operations, and corresponding subroutines are as shown in Fig. (6.12), and will be summarized next.

(a) *Input data*

Subroutine SET FILE is called to define the input/output files, as explained in the previous section, followed by calling subroutine DATA.

(b) *Frontal matrices*

Frontal operations are carried out by subroutines INITIATION and FRONT, which are similar to those described in section 6.7.1, but subroutine FRONT is designed with a call to a dummy element matrix generator subroutine, and is called first with a corresponding argument STIFF, which is the name of a subroutine which calls the element stiffness matrix generator (ESMG), and equivalent nodal loading subroutine (NFVG). After operating the static analysis, FRONT will be called again to define the mass matrix by using subroutine MASS, and STIFF will also call subroutine CSMG which calculates the centrifugal stiffening matrix. For plate version, the frontal matrices are redefined for plate bending only, after the static analysis is carried out.

(c) *Static analysis*

This is an option provided for rotating structures, which enables stress analysis due to centrifugal loading to be carried out. Subroutines SSOLVER, DISP and STRESS are similar to SOLVER, DISP and STRESS discussed in section 6.7.1, except subroutine STRESS here calculates also stress components at Gaussian points and stores them in direct access files to be used by subroutine CSMG for calculating the centrifugal stiffening matrix.

(d) *Subspace iteration*

This is the basic solver for natural frequency analysis, and it consists of the following subroutines:-

(i) SUBSI which assumes initial values for the selected eigenvectors.

(ii) XMAT which calculates the $\boldsymbol{X}$ matrix, as described in section 5.3.

(iii) TPRODUCT: it performs triple product of matrices to define the reduced stiffness and mass matrices $\boldsymbol{K}^*$, $\boldsymbol{M}^*$.

(iv) EIGENV which is a simple iteration eigenvalue solver as will be described in part (e) of this section.

(v) TRANSF which calculates the updated values of the selected eigenvectors.

(e) *Eigenvalue solver*

The reduced eigenvalue problem is analysed with the simple iteration algorithm discussed in section 5.3. The main subroutine is EIGENV which calls the following subroutines:-

(i) SHIFTI which defines initial shift parameters, if zero or negative eigenvalues are encountered.

(ii) DCOMP which calculates the matrix $\boldsymbol{Q}$, where $\boldsymbol{Q} = \boldsymbol{K}^{*-1}\,\boldsymbol{M}^{*}$, by solving successive equations calling CHOLES subroutine, which is based upon Choleski factorization method.

(iii) EITR calculates the lowest eigenvalue using the simple iteration algorithm.

(iv) SWEEP redefines the matrix $\boldsymbol{Q}$ such that the eigenvalue just calculated will be cancelled or swept, and EITR will then converge to the next eigenvalue.

(f) OUTPUT is just one subroutine, which lists the natural frequency results in the output file.

6.7.3 Forced vibration module

This module controls the operations for forced vibration analysis and has a plate version DYNPL-FV.FOR and shell version SHELL-FV.FOR. The structure of the module is shown in Fig. (6.13), and the operations are controlled by a master program (FORCED VIBRATION), the parts of which are summarized as follows:-

(a) *Input data*

As described in section 6.7.2.

(b) *Stress analysis due to centrifugal loading*

This is a simple static analysis using REAL variables, and the operations are

similar to those described in section 6.7.1. Subroutine names were preceded with letter R to indicate REAL variables, so that the subroutines can be identified from similar ones with *complex* variables having names preceding with letter C. The static analysis is required if there is a rotational speed, and stresses at Gaussian quadrature points are calculated and stored in order to be used for centrifugal stiffening calculations.

(c) *Complex frontal matrices*

A subroutine called CFRONT is used here, which is similar to RFRONT but it deals with the complex dynamic matrix as described in section 5.4. It calls subroutine CSTIFF which defines the elemental complex matrix in terms of:-

(i) Element stiffness matrix $\boldsymbol{K}$ calculated by subroutine ESMG.

(ii) Element mass matrix $\boldsymbol{M}$ calculated by subroutine EMMG.

(iii) Element centripetal matrix $\overline{\boldsymbol{M}}$ calculated by subroutine EMBMG.

(iv) Element Coriolis matrix $\boldsymbol{C}$ calculated by subroutine EMCMG.

(v) Element centrifugal stiffening matrix $\boldsymbol{K}^{\sigma}$ calculated by subroutine CSMG.

(d) *Complex solver*

The analysis is completed with the following subroutines:-

(i) CSOLVER which performs backward substitution for the reduced complex equation.

(ii) CDISP which defines the full complex nodal displacement vector, and lists it in the output file.

(iii) CSTRESS which calculates the corresponding complex stress and strain vectors averaged at nodes, and estimated at the upper and lower surfaces of every layer.

6.7.4 Flutter solver module

This module contains the master program FLUTTER which controls the operation of flutter analysis, together with frontal and subspace iteration subroutines, and it has a plate version DYNPL-FL.FOR and shell version DYNSH-FL.FOR. The plate

version is based upon the simplified algorithm described in section 5.5, and is illustrated in Fig. (6.14). The basic operations are summarized as follows:-

(a) *Input data*

It is similar to those described in previous solver modules.

(b) *Frontal matrices part*

It contains subroutines similar to the natural frequency module, but the aeroelastic stiffness and mass matrices are now assembled. No static analysis is required, since flutter analysis in this package is only possible for non-rotating plates.

(c) *Subspace iteration*

This contains subroutines similar to those described in section 6.7.2.

(d) *Eigenvalue solver*

There are two major changes in the subroutines here compared with those in section 6.7.2, as follows:-

(i) The $\boldsymbol{Q}$ matrix is calculated directly by inverting the matrix $\boldsymbol{K}$, via subroutine INV, and multiplying the results by matrix $\boldsymbol{M}$ via subroutine MATM.

(ii) There is an analytical eigenvalue solver, subroutine EIGENANA, which is automatically invoked if no more than the two smallest eigenvalues are required. This is useful for flutter analysis, and is associated with an automatic search for coalescence eigenvalues, as described in section 5.5.

(e) *Output results*

Output results are stored in the output file, as described early.

6.8 PROGRAMS STRUCTURE

All modules of this package are coded in FORTRAN files, which are compiled in OBJECT files by the FORTRAN compilers used. The EXECUTABLE file required to carry out a particular analysis is obtained by linking together the OBJECT files of the relevant modules as shown in Figs (6.15)-(6.18). All the names shown in those figures are file names.

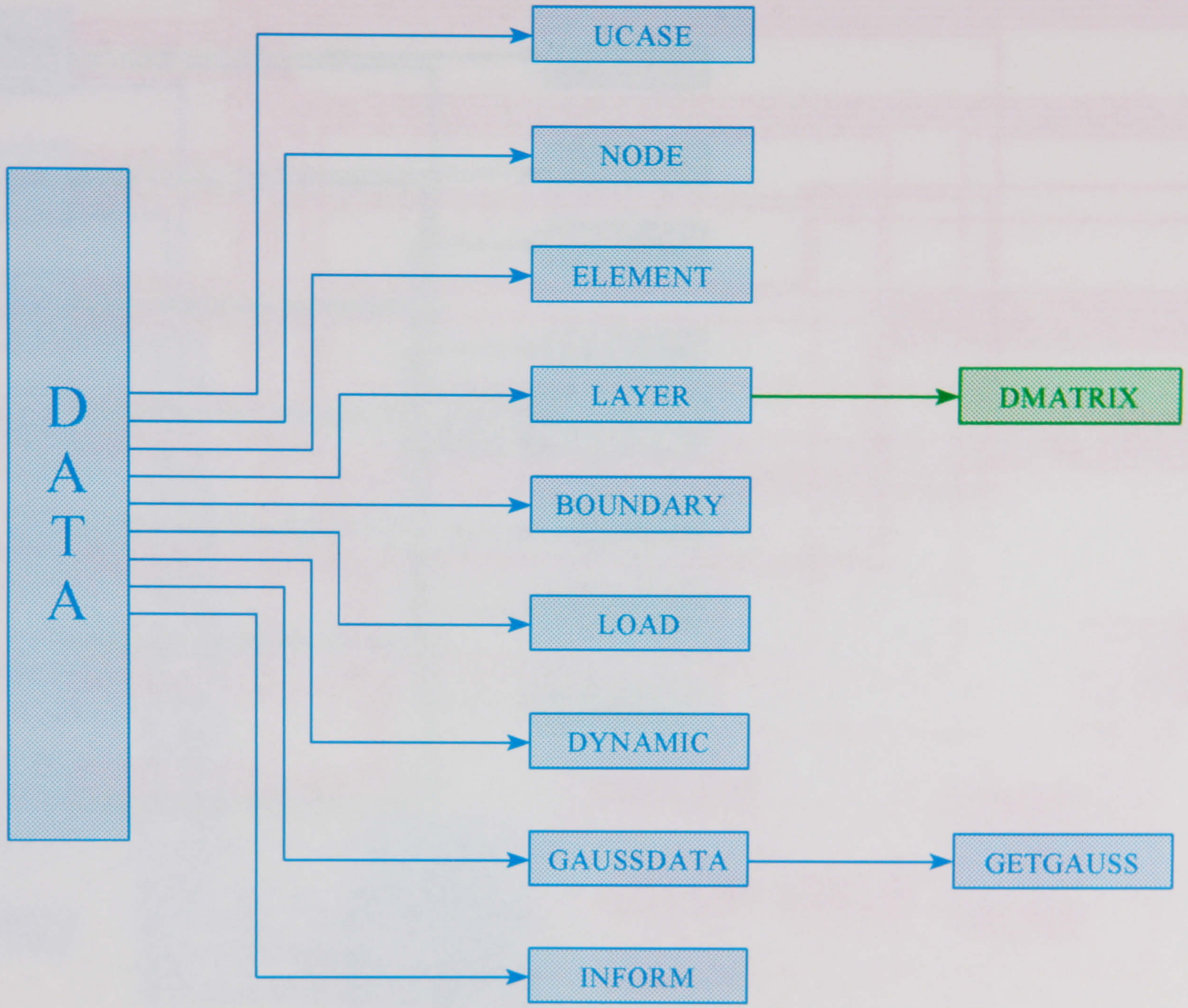

Figure 6.1 DATA subroutine structure

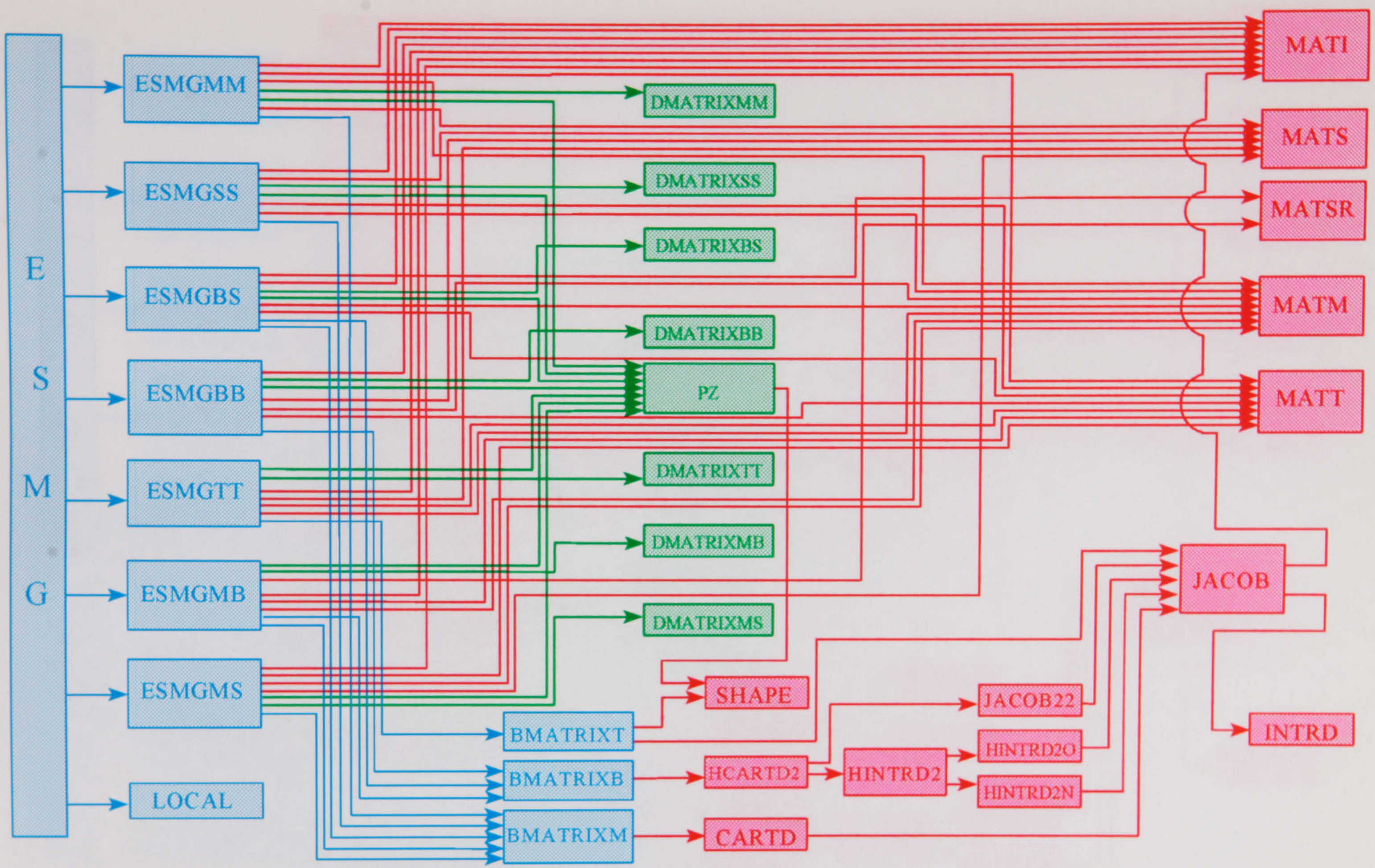

Figure 6.2 Structure of element stiffness matrix subroutine

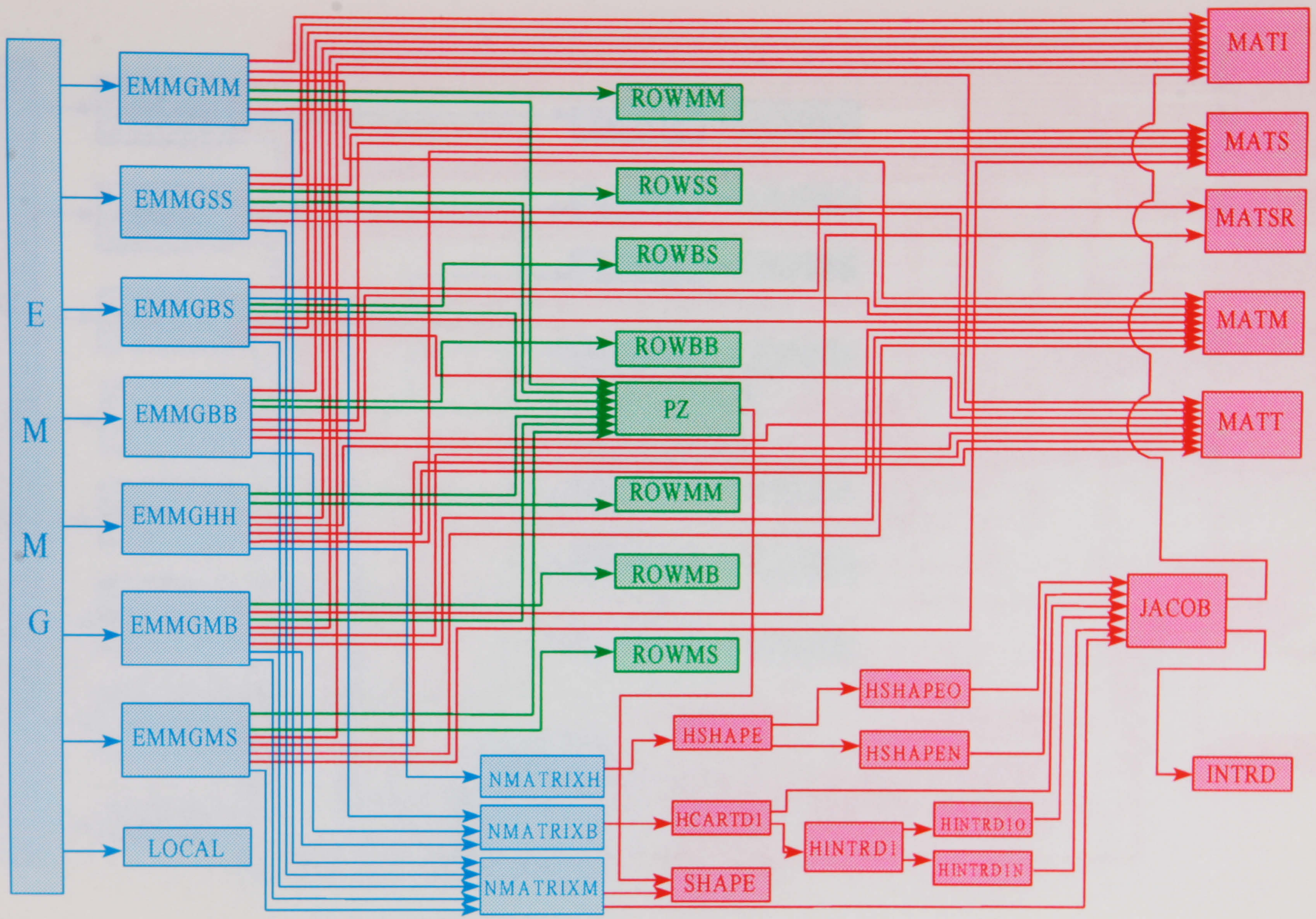

Figure 6.3 Structure of element mass matrix subroutine

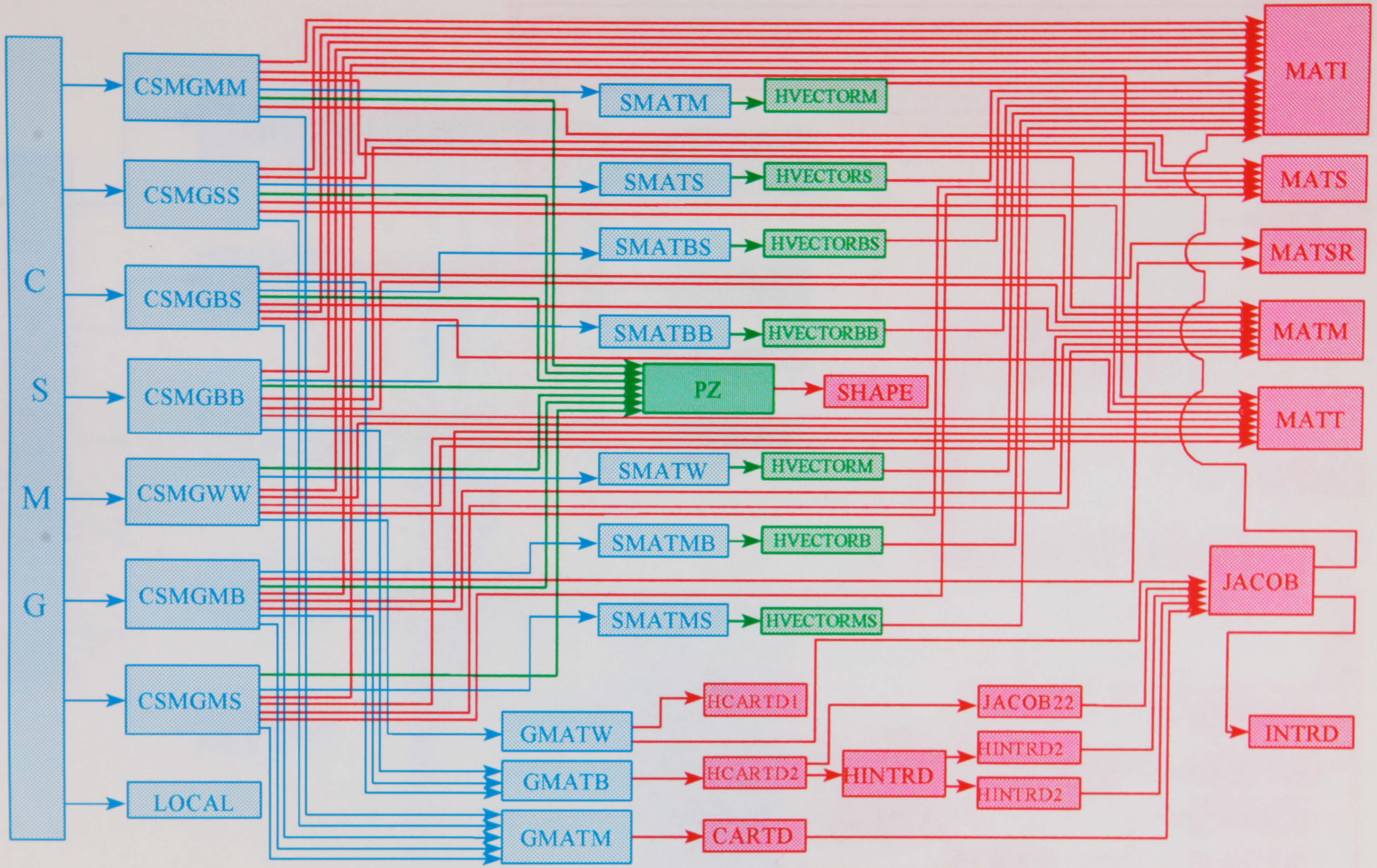

Figure 6.4 Structure of element centrifugal stiffening matrix subroutine

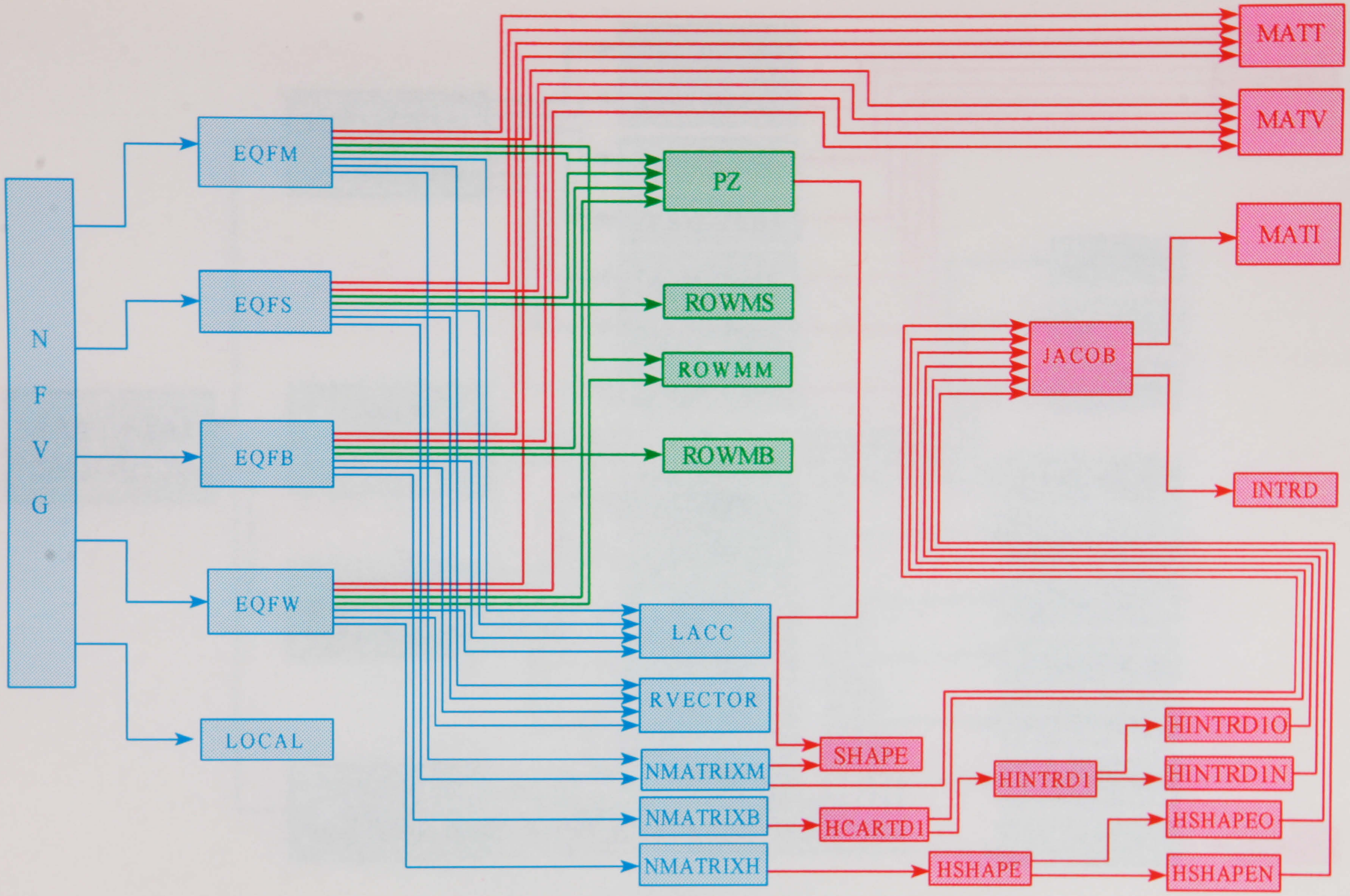

Figure 6.5 Equivalent nodal force subroutine

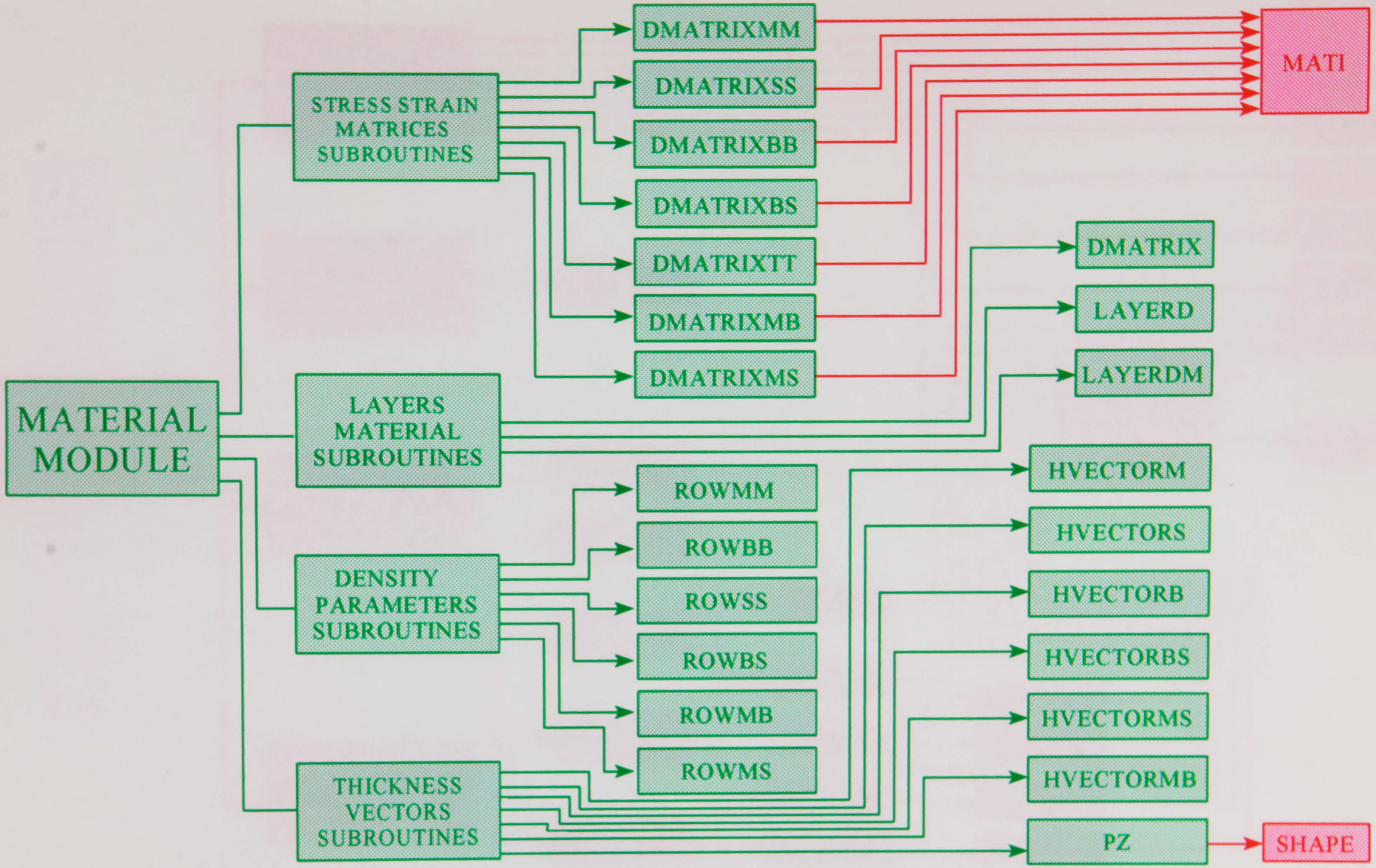

Figure 6.6 Material module structure

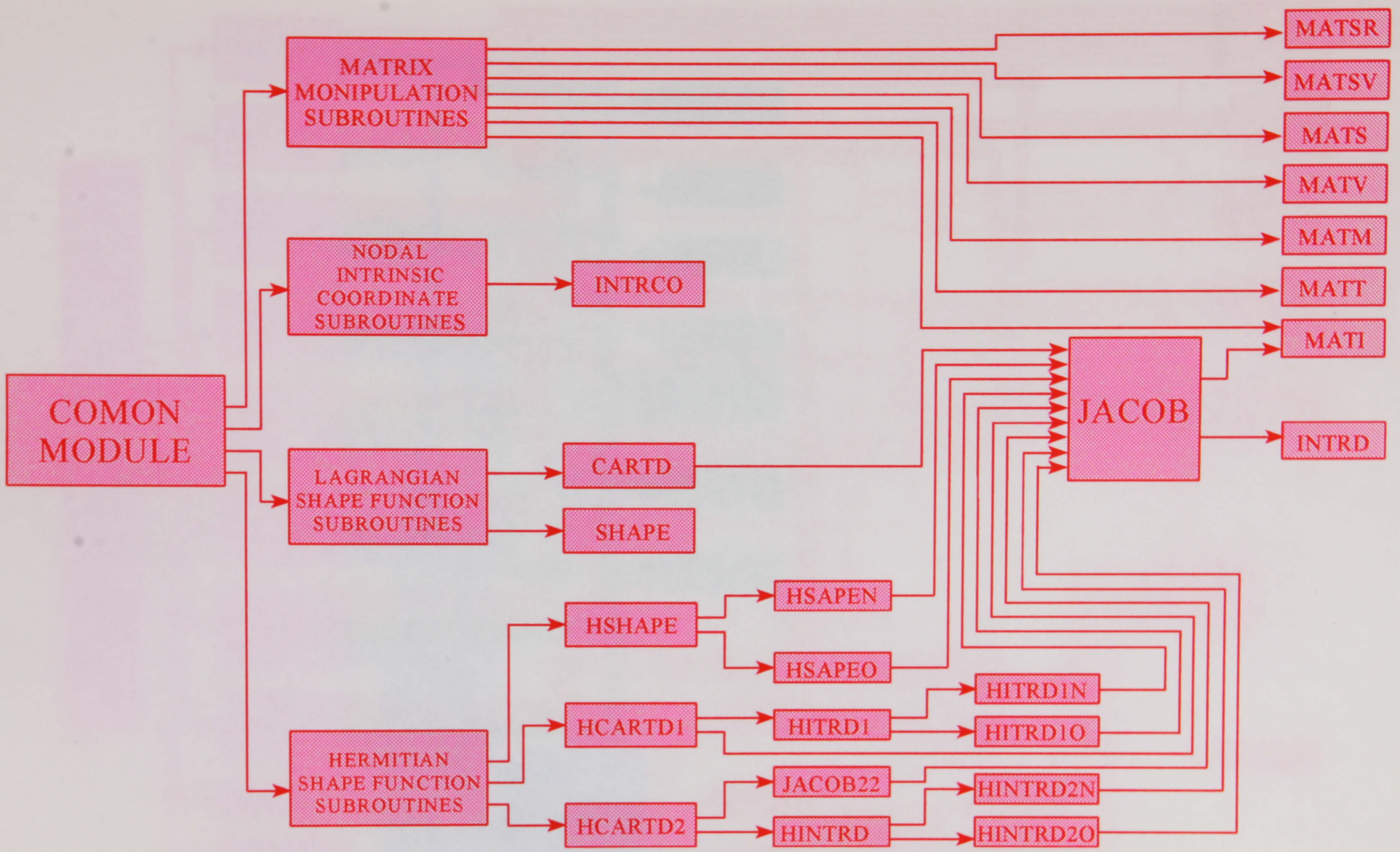

Figure 6.7 Common module structure

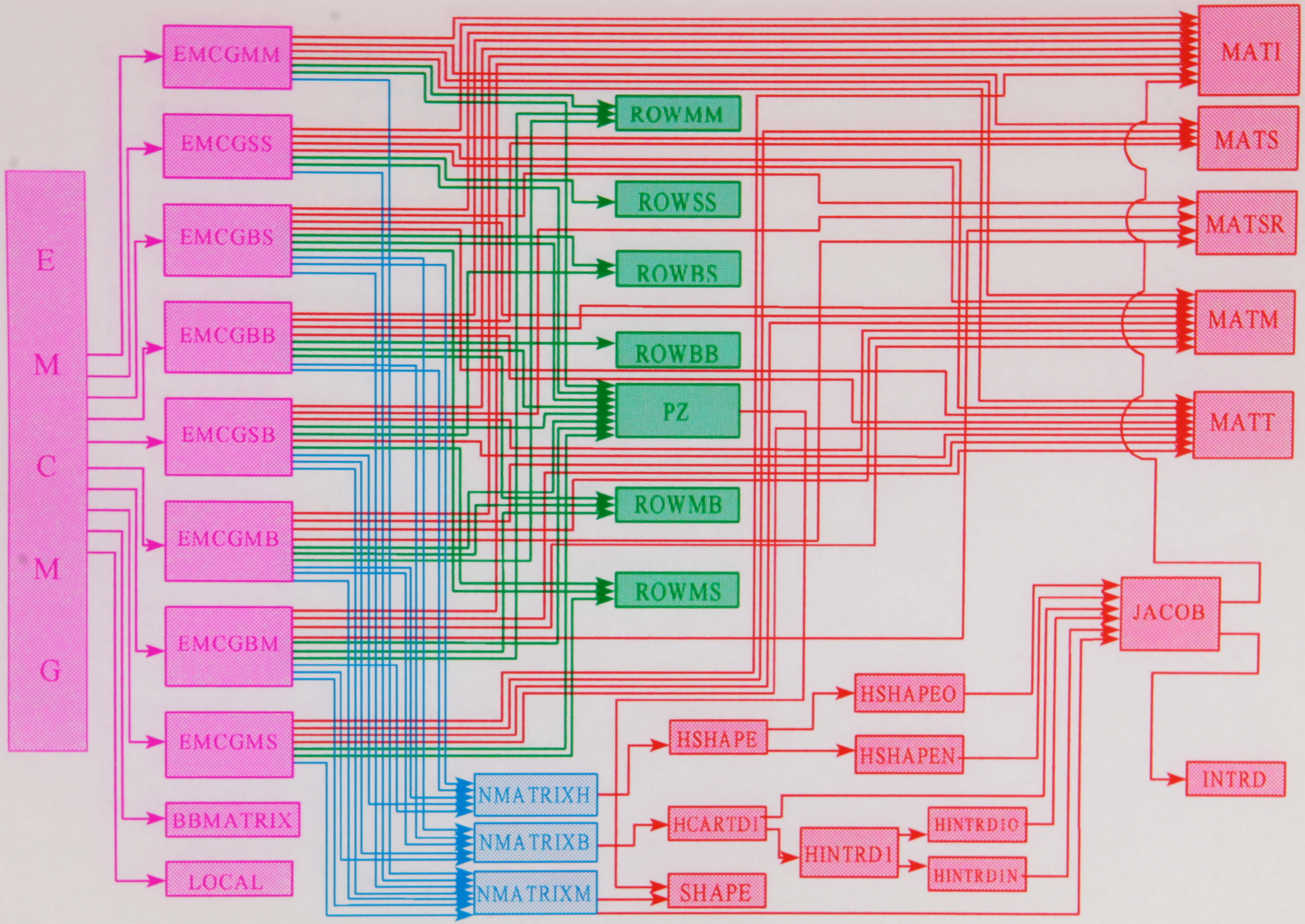

Figure 6.8 Element Coriolis matrix generator subroutine

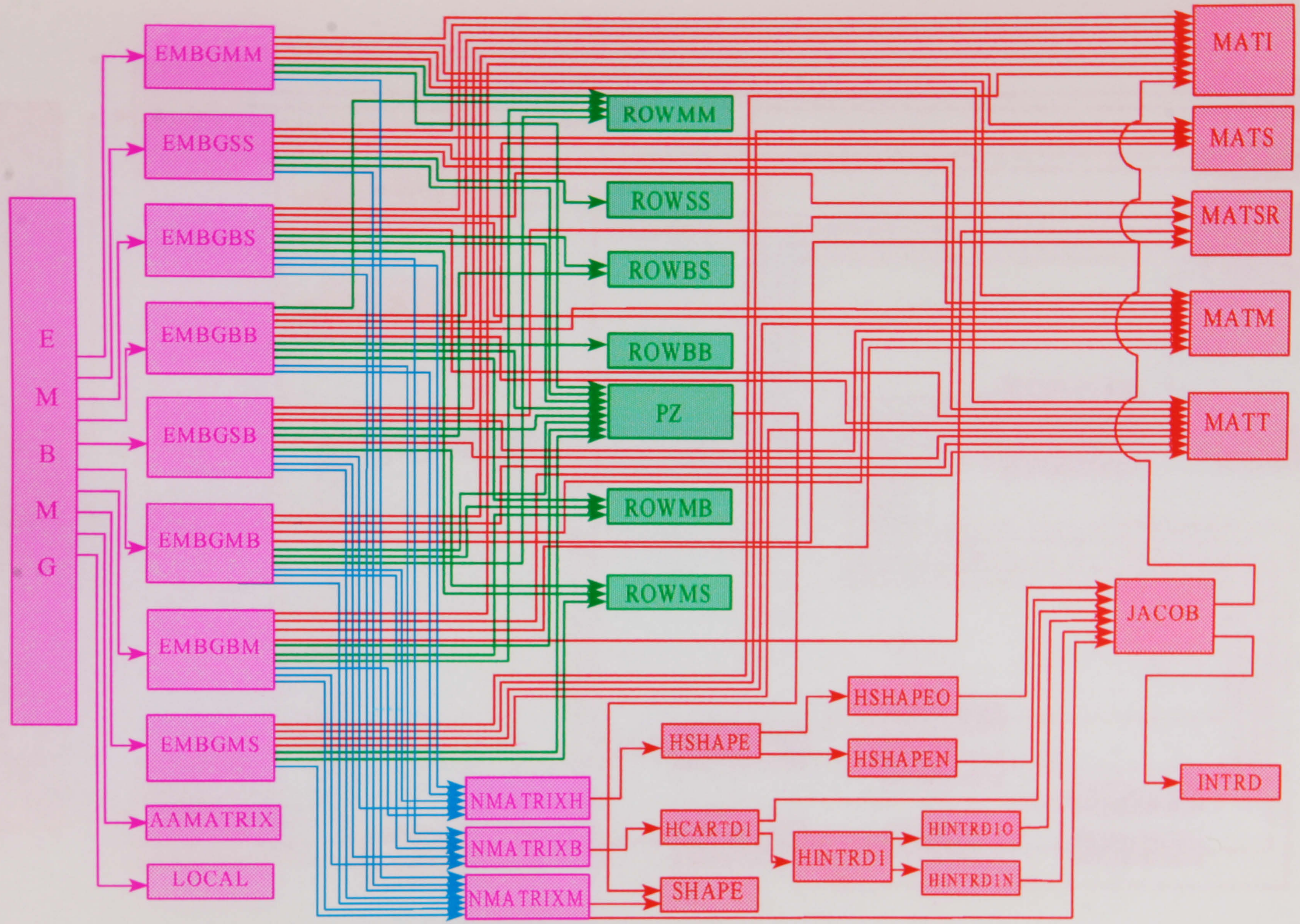

Figure 6.9 Structure of centripetal matrix subroutine

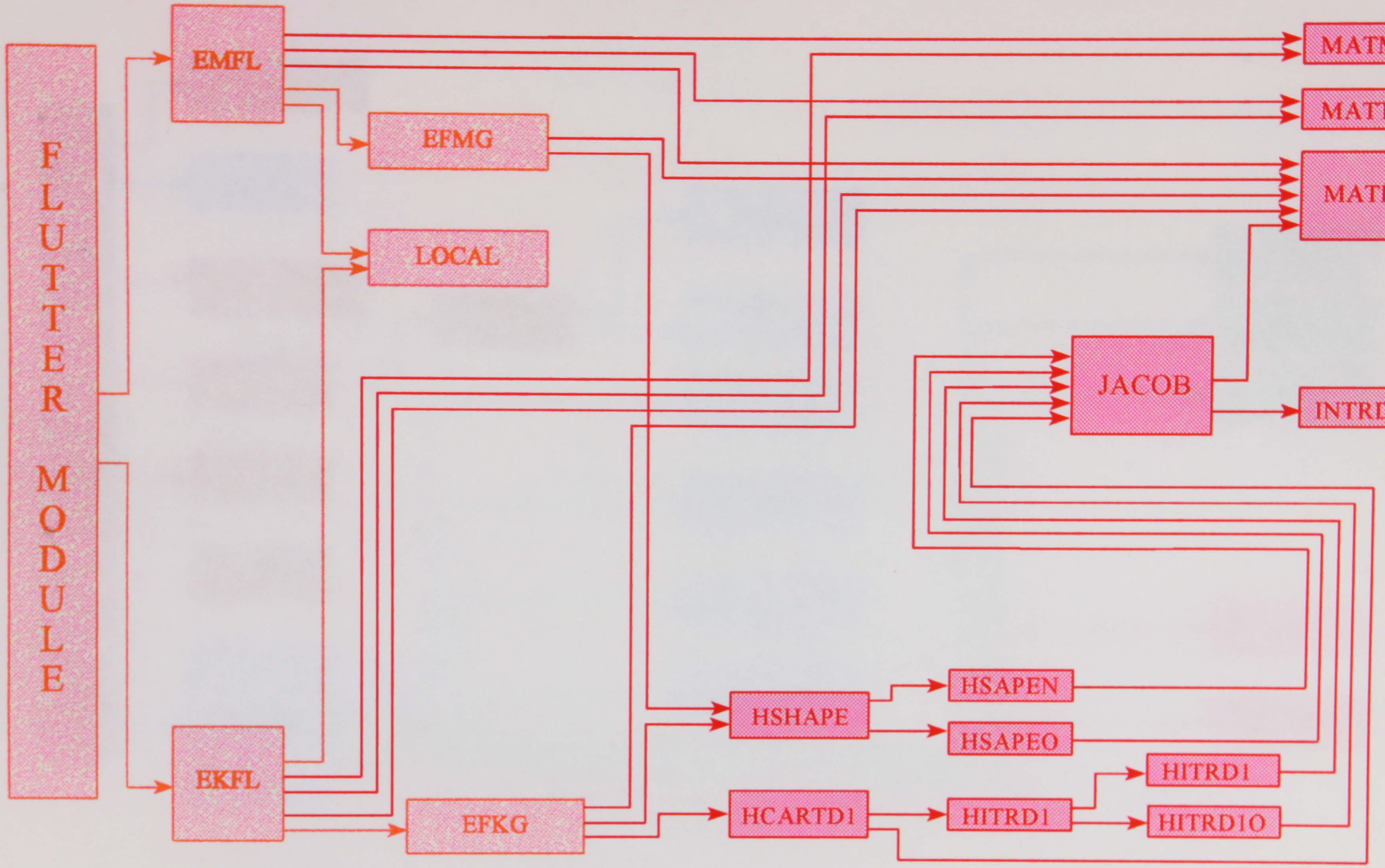

Figure 6.10 Flutter matrices module

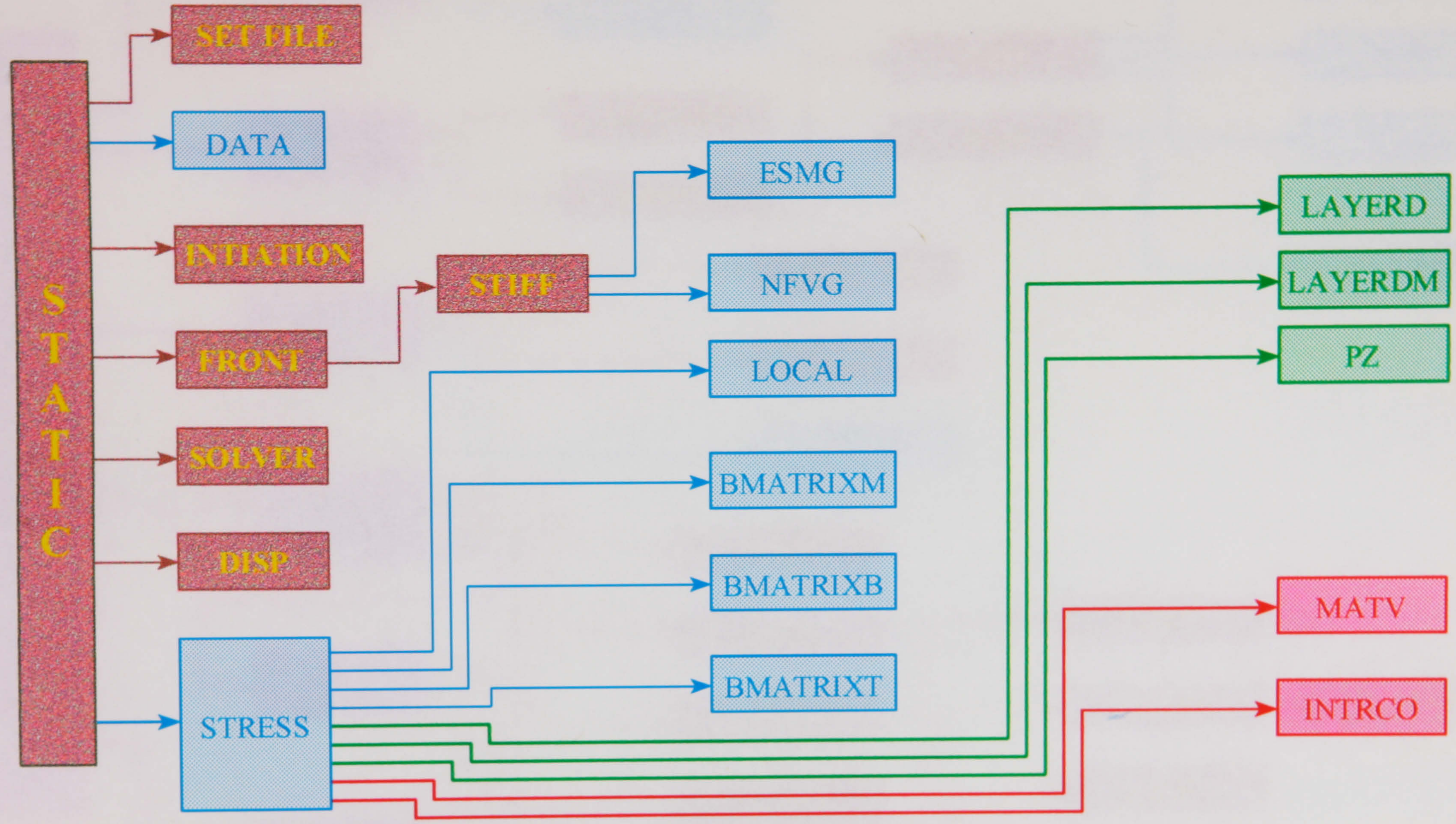

Figure 6.11 Structure of static analysis solver module

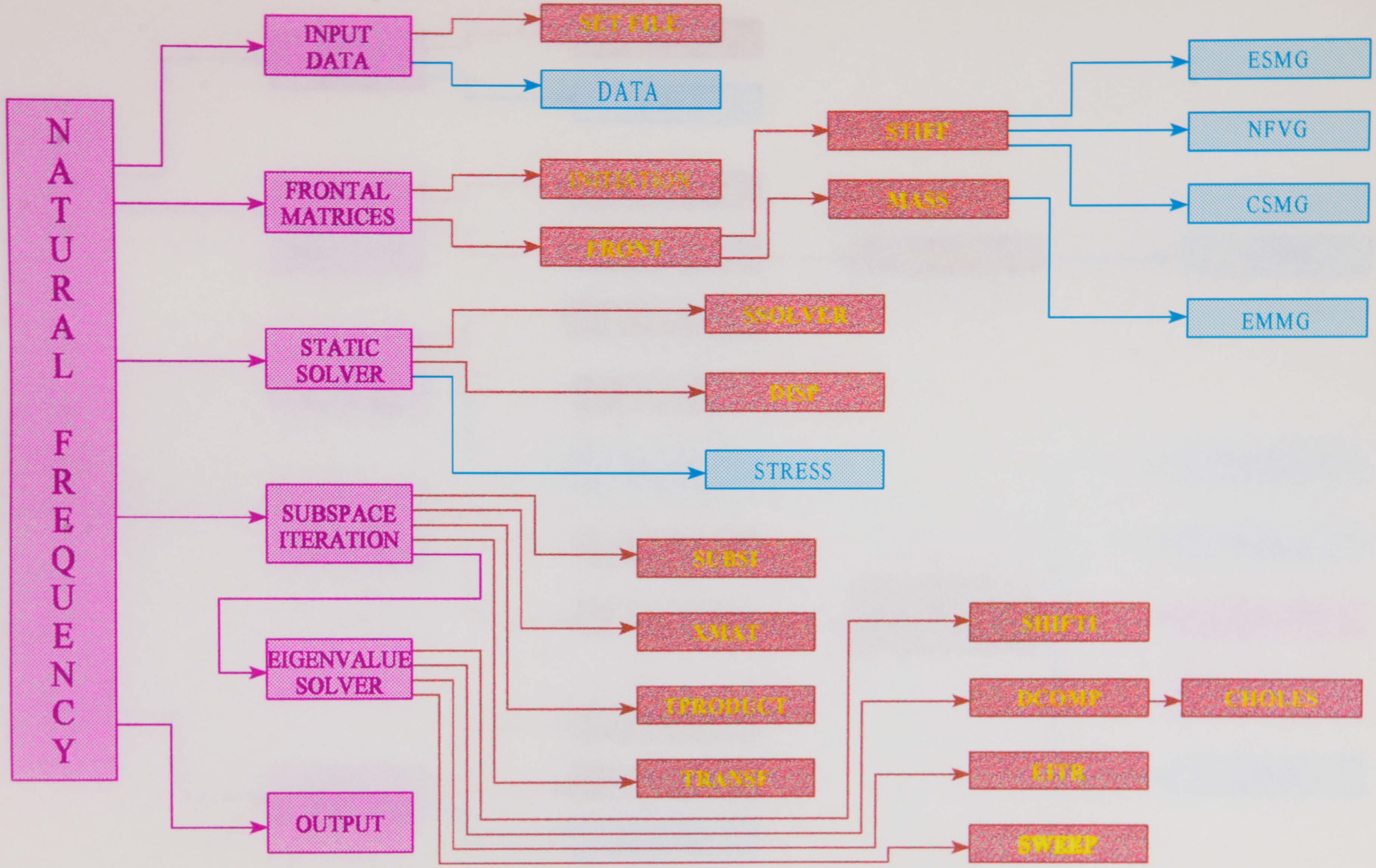

Figure 6.12 Structure of natural frequency module

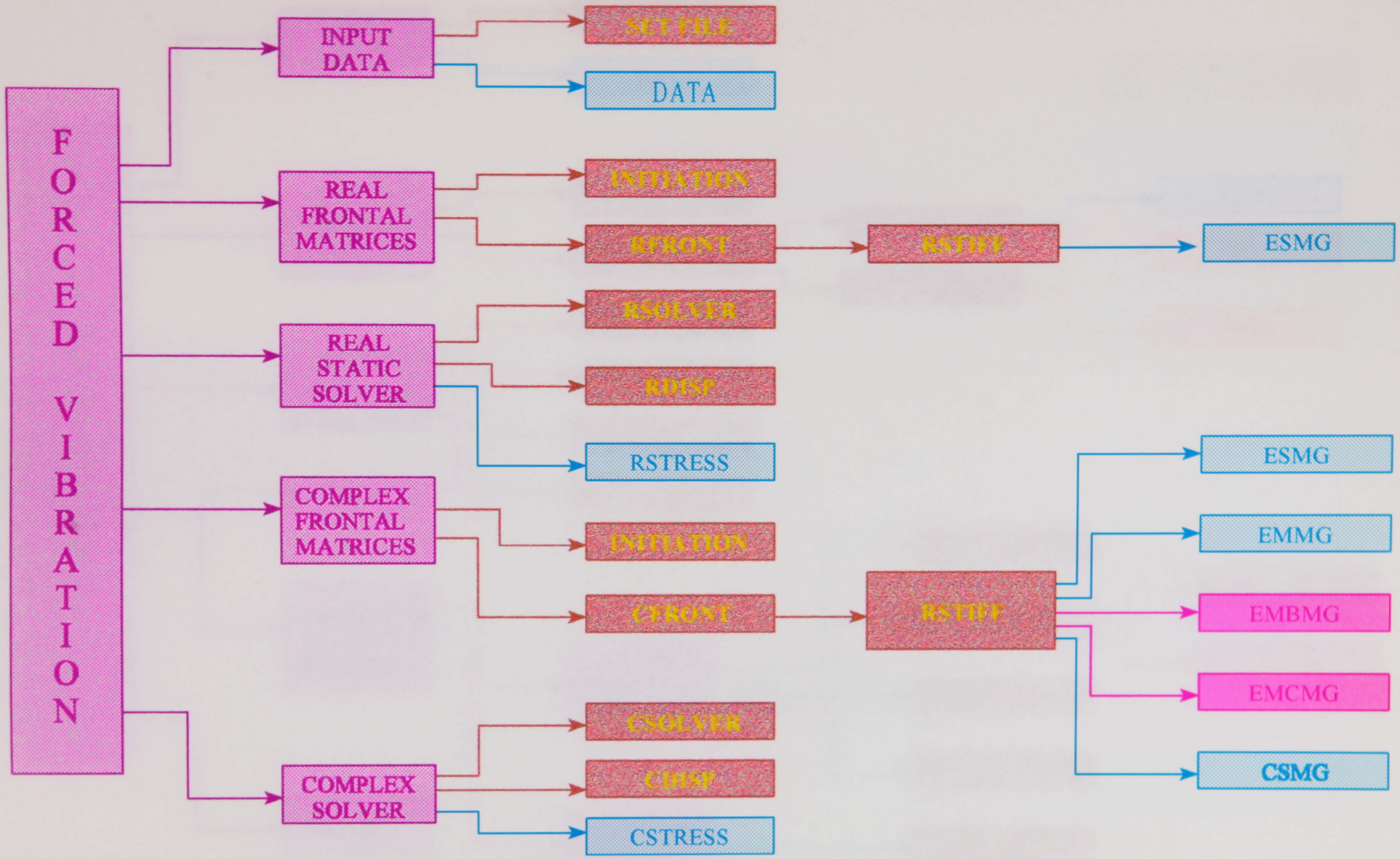

Figure 6.13 Structure of forced vibration module

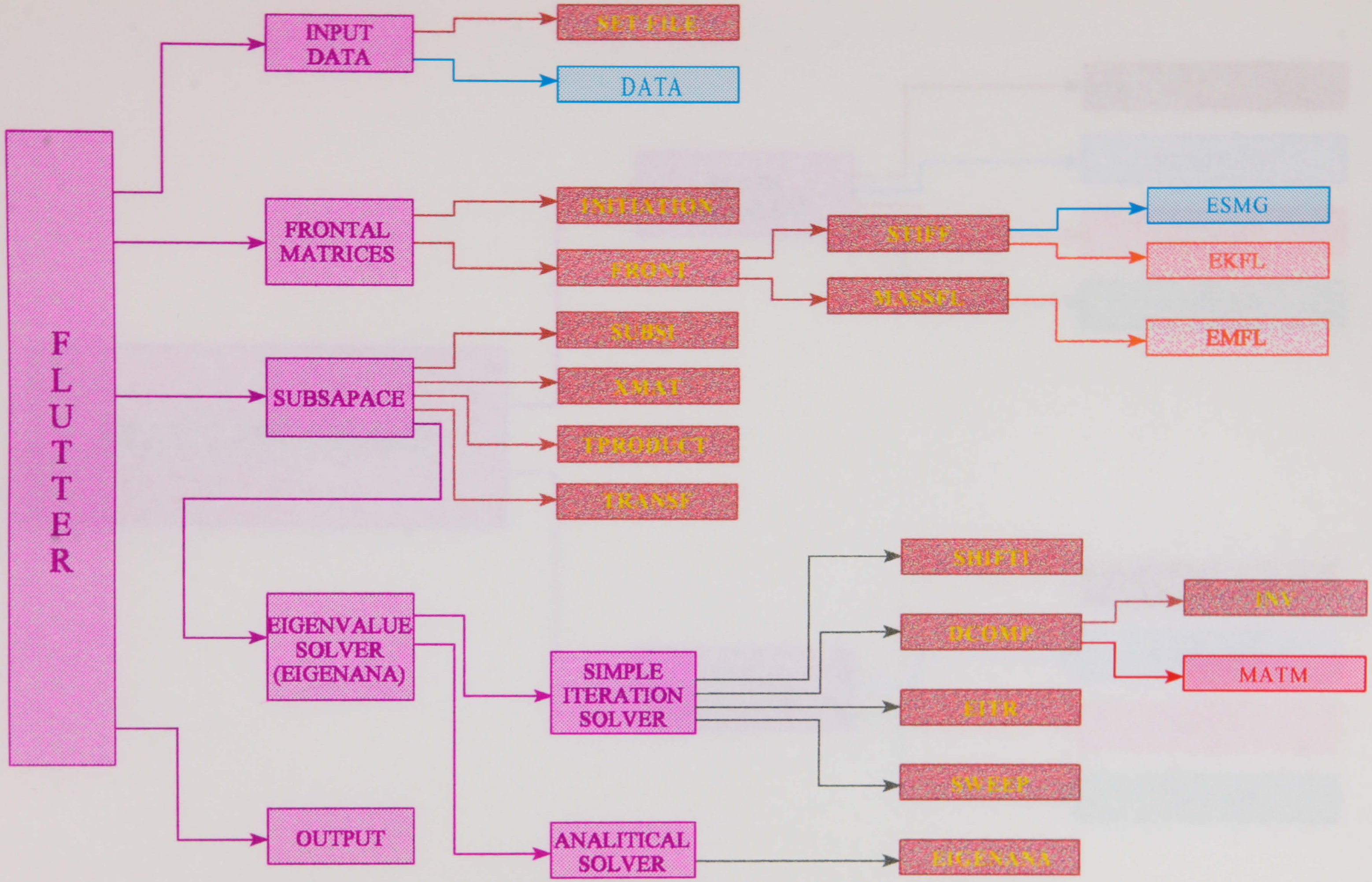

Figure 6.14 Structure of flutter solver module

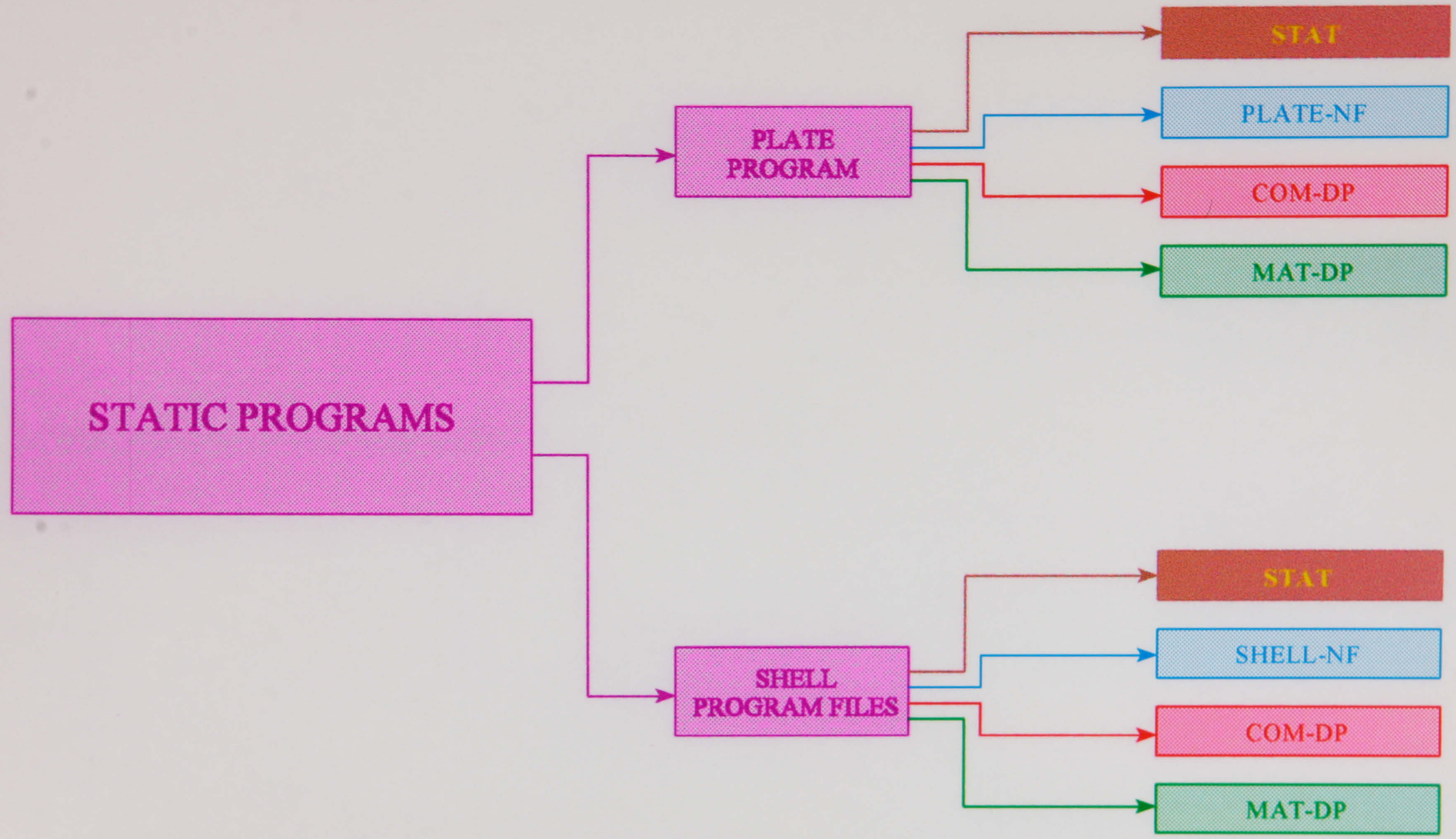

Figure 6.15 Static analysis programs modules

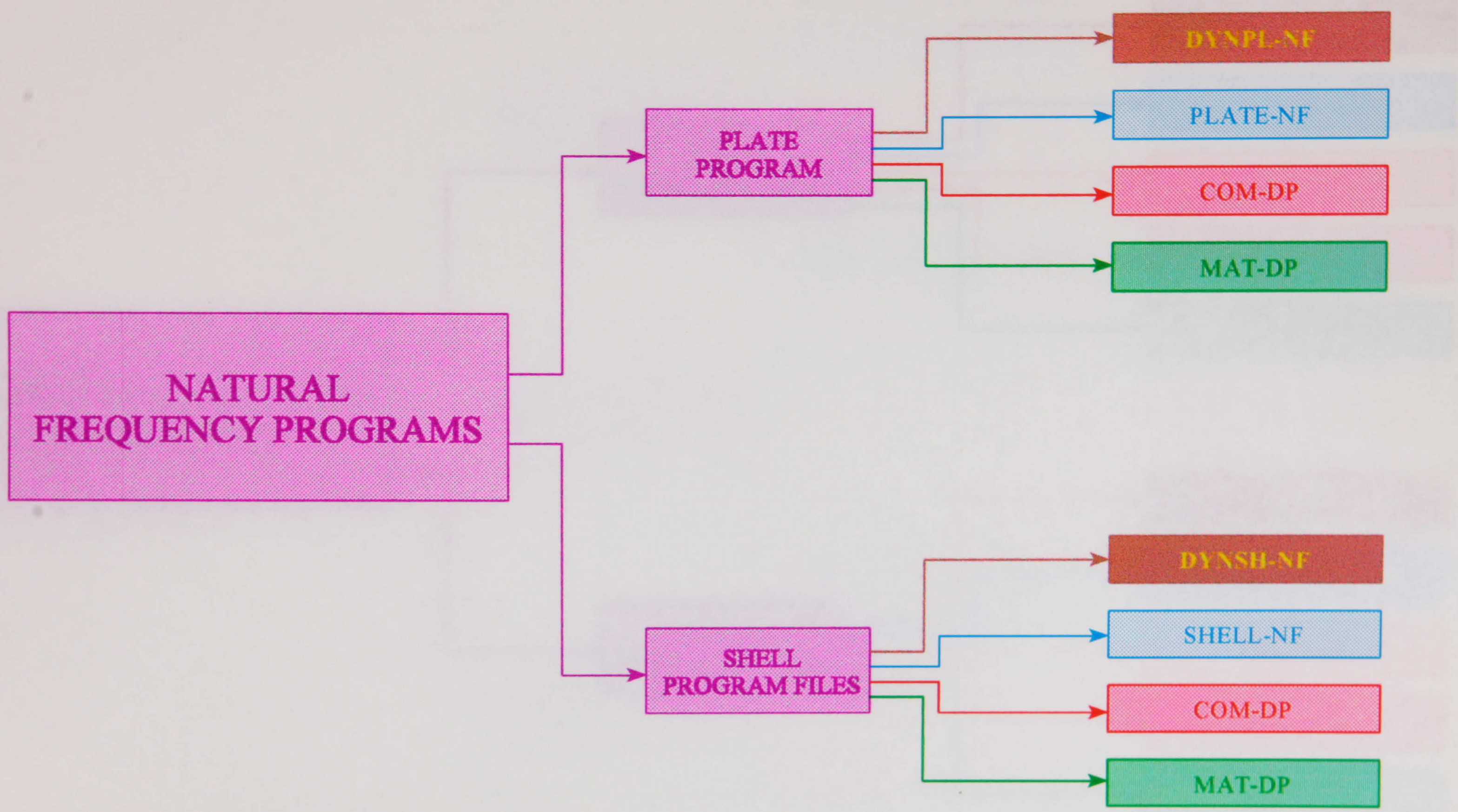

Figure 6.16 Natural frequency programs modules

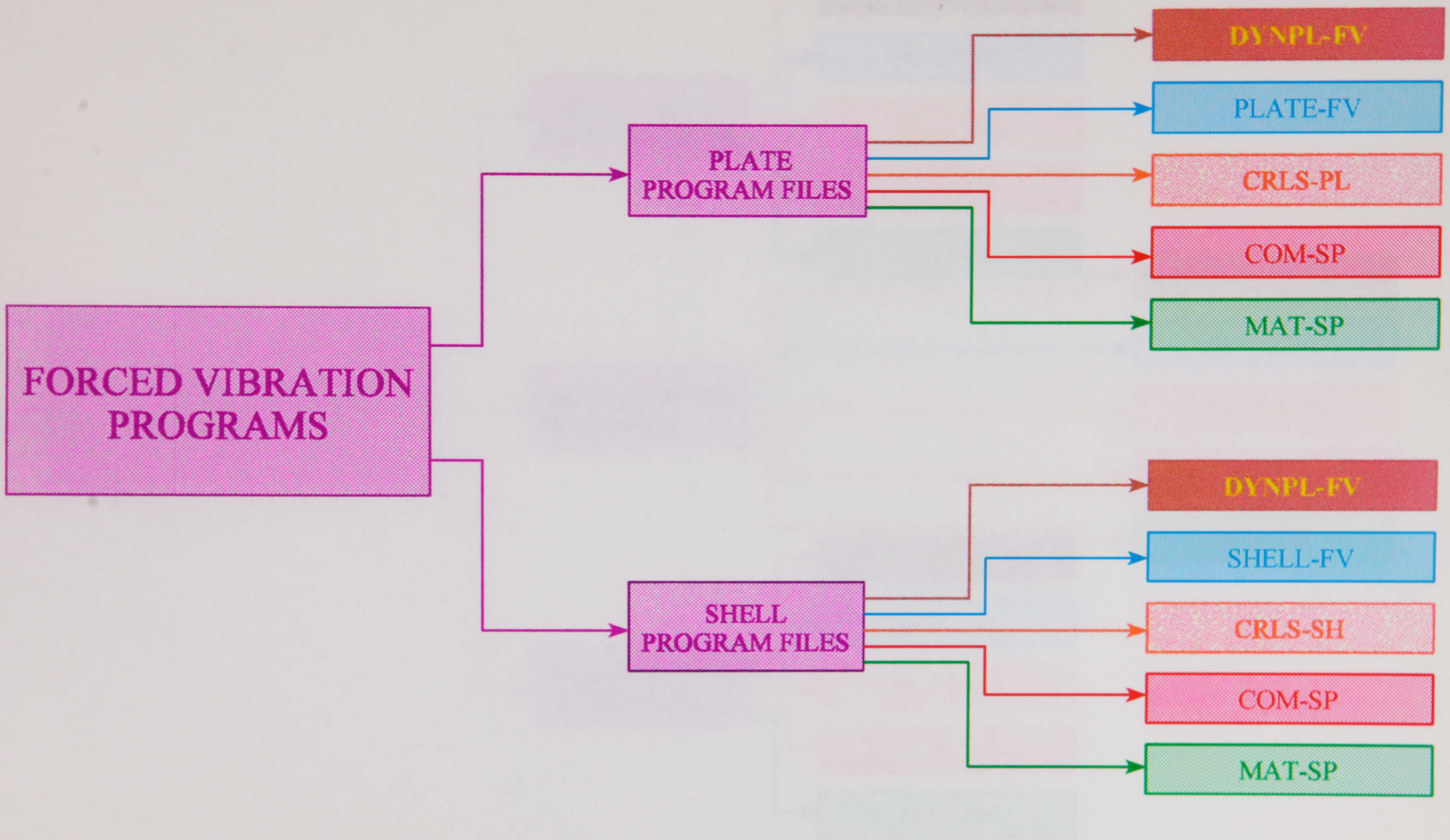

Figure 6.17 Forced vibration programs modules

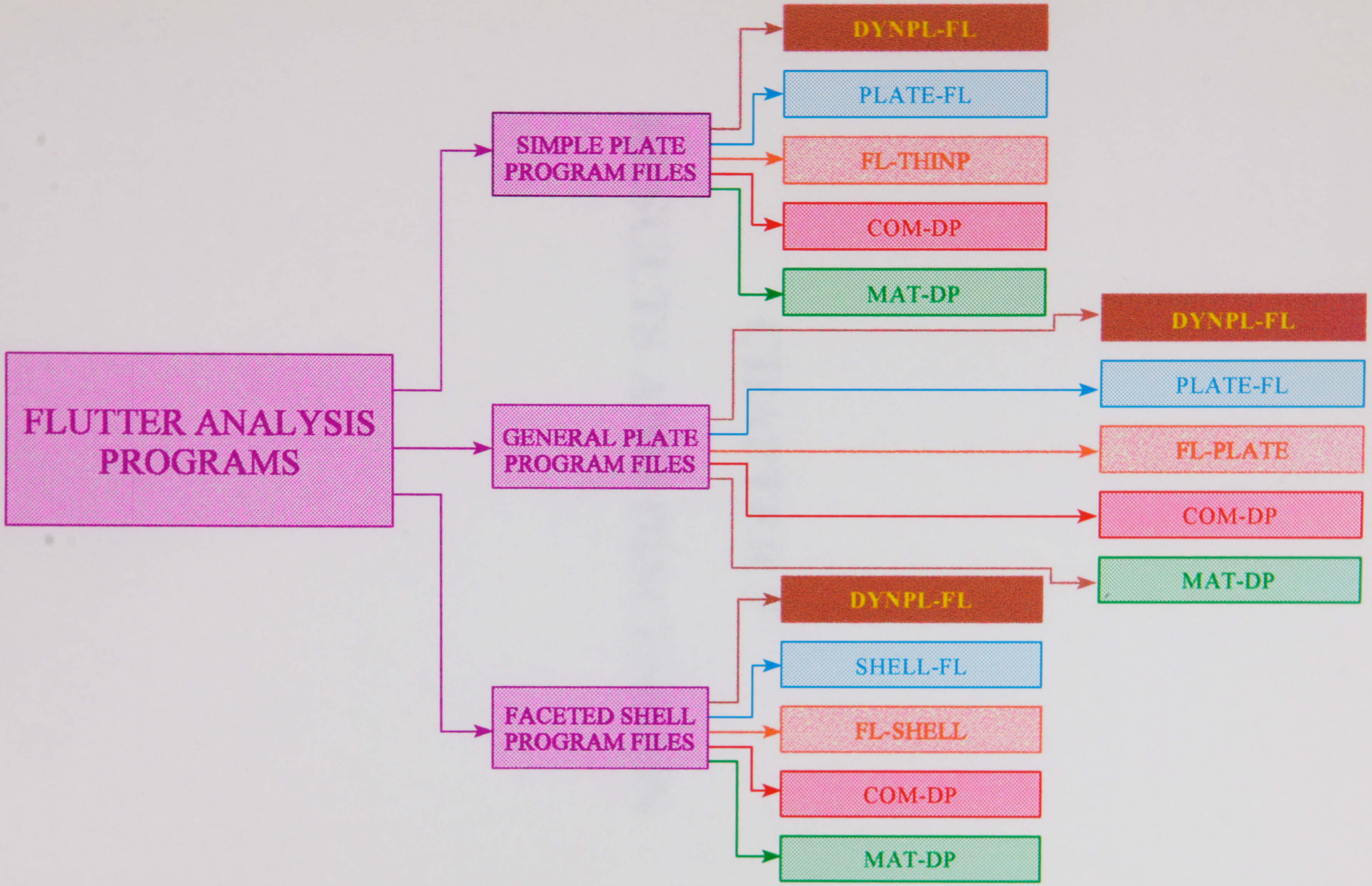

Figure 6.18 Flutter programs modules

CHAPTER 7

RESULTS AND DISCUSSION

7.1 INTRODUCTION

A versatile finite element programming package in Fortran language has been developed for the static and dynamic analysis of non-rotating and rotating composite layered plates and shells, based upon the research carried out in this work. A description of the package is given in chapter 6. This package contains a number of elements, and unique facilities for rotating plate and shell analysis. Consequently, an important step to be taken before the present programming package is used for the analysis of practical engineering components, is to validate the reliability of the different aspects of the package and assess the accuracy of the analysis carried out by means of it against published experimental and/or analytical results. Naturally, during the course of the package development, a large number of individual verifications have been carried out, at the various stages of its development. It is also advantageous to employ the package for the study of the effects of some important parameters, in order to demonstrate how the package can be used for optimum design of composite layered turbomachine blades, or similar engineering components.

Case studies were selected and compared with analytical solutions, and also compared with published experimental results whenever possible, so that the following tasks can be achieved:-

(i) Validation of the developed static solvers and stiffness matrices of the developed elements.

(ii) Validation of developed natural frequency solvers and the mass matrices of the developed elements.

(iii) To demonstrate that the developed elements can provide reliable answers over a wide range of thickness, and to evaluate the effect of transverse shear with the increase of plate thickness.

(iv) To demonstrate the effects of centrifugal stiffening and Coriolis forces on the natural frequencies of rotating plates and shells.

(v) To study the effect of fibre angles on the natural frequencies, and to demonstrate the potential of the use of layers with different fibre directions, which may lead to an optimum design.

(vi) To demonstrate the capability of the developed package for accurate analysis of panel flutter with the prediction of critical flow speeds.

(vii) To assess the advantages of the developed package for the analysis of stationary and rotating composite layered plates and shells.

Most of the selected case studies have been compared with published analytical or experimental results. However due to the lack of publications on the effect of Coriolis forces, and centrifugal stiffening, it was decided to validate them by checking their numerical values, that is because Coriolis, and centripetal matrices have subroutines, similar or based upon element mass matrix subroutines, and it was possible to validate the Coriolis, and centripetal matrices, by comparing their numerical values with corresponding values of mass matrices, which have been properly validated.

7.2 STATIC VALIDATION AND MESH SELECTION

The first part of package validation is to test different solvers and to validate the element stiffness matrix subroutines. Two simple case studies were selected, the first is a composite flat plate and the other is a composite curved shell, both with known analytical solutions. The cases will also be employed for further dynamic analysis, as described in sections 7.4 and 7.5. Hence it was decided to use static analysis for testing the convergence of different meshes, so as to select optimum meshes for dynamic analysis.

7.2.1 Rectangular cantilever plate case

A rectangular plate with length of 0.8 m, width of 0.2 m, and thickness of 0.02 m, was used for the static analysis. The plate is clamped at one end, and subjected to a uniform distributed line load of $F = 5.88\times10^{3}\ N$ at the free end, and the material properties were isotropic properties expressed as orthotropic material properties with $E = 7.5\times10^{10}\ Pa$, $\nu = 0.33$, $\rho = 3000\ \ Kg/m^{3}$, and two layers of fibre angles θ_1 and θ_2 being 45° and -45° respectively. The boundary conditions, loads together with the

geometry of the plate, and a mesh of 16 quadrilateral elements are illustrated in Fig. (7.1). The finite element package results were compared with the Euler-Bernoulli beam solution given in Appendix E.

7.2.1.1 Conforming quadrilateral element results

Three different meshes were attempted; a coarse mesh with 4 elements, a fine mesh with 16 elements, and a very fine mesh with 64 elements, and the element type used in these meshes is the 4-node quadrilateral conforming element, as shown in Figs. (7.2) a, b, and c, respectively. The lateral displacement in the z-direction is plotted against the length in the x-direction, as shown in Fig. (7.3). It is clear from the figure, that all the meshes gave answers close to the analytical solution, with the results of the two fine meshes being very close to each other and closer to the analytical solution than those of the coarse mesh. Hence it was decided to use the 16-element mesh for further analysis, as described in section 7.4.

7.2.1.2 Non-conforming quadrilateral element results

To validate this type of element and select the right mesh for this analysis and further analysis, the same philosophy as in the previous case was adopted. The three meshes shown in Fig. (7.2) have been employed with the change of the type of elements to the 4-node non-conforming quadrilateral element. The displacement distribution is shown in Fig. (7.4), and a similar trend as in Fig. (7.3) was observed. Therefore, the 16-element mesh was also selected for the same reason explained above, and it will be used in further analysis as described in section 7.4.

7.2.1.3 Non-conforming triangular element results

Several meshes with the 3-node non-conforming triangular element were attempted, some of which are shown in Fig. (7.5). The corresponding lateral displacement of the plate in the z-direction is shown in Fig. (7.6). It was observed that the results obtained from meshes (a) and (c) have shown slight differences between corresponding nodes on the two long edges. Therefore it was decided to try a symmetric mesh, such as mesh (b) shown in the same figure, which has led to

symmetric and more accurate answers. Hence mesh (b) of Fig. (7.5) has been chosen for further analysis, which will be explained in section 7.4.

7.2.2 Curved shell case

This case represents a circular shell rigidly fixed at one end, and the other end is free and subjected to a uniformly distributed line load of total value $F = 2.0\times10^5$ N in the y-direction, as shown in Fig. (7.7). The radius of curvature of the shell midsurface is $R = 0.1$ m, its width in the z-direction is $a = 0.04$ m, and the thickness is $h = 0.02$ m. The material of the shell, and the layers configurations are similar to those described for the previous case in section 7.2.1. Different static analysis with different types of elements have been carried out, as summarized next. Finite element results were compared with the corresponding circular beam analytical solution given in Appendix E.

7.2.2.1 Conforming quadrilateral element results

The meshes used in this case are shown in Fig. (7.8) and the element chosen for the analysis is the conforming 4-node quadrilateral element. The displacements in the y-direction are plotted against the angle of curvature of the shell midsurface as shown in Fig. (7.9). It is clear that the results obtained from the two fine meshes are very close to the analytical solution, and the 16-element mesh was therefore selected for the dynamic analysis described in section 7.5.

7.2.2.2 Non-conforming quadrilateral element results

Finite element meshes were as employed for the previous case except the element type was the non-conforming 4-node quadrilateral element. The displacement results obtained from those meshes were plotted in Fig. (7.10), which shows tendencies similar to those observed in Fig. (7.9), therefore the 16-element mesh was also selected for further analysis as given in section 7.5.

7.2.2.3 Non-conforming triangular element results

Three meshes based upon the 3-node non-conforming triangular element, as shown

in Fig. (7.11), were attempted. the displacement of the midsurface of the shell in the *y*-direction was plotted against the angle of curvature. together with the corresponding analytical solution, as shown in Fig. (7.12). It is clear that the results based upon the two fine meshes are closer to the analytical solution. hence the 32-element mesh was selected for further analysis as demonstrated in section 7.5.

7.3 DYNAMIC VALIDATION

It is essential to validate the developed package and to assess its potential to deal with the objectives it was designed for, therefore the aim of this section is to validate the package for the natural frequency analysis of plates and shells made of isotropic and multi-layered composite materials. The validation cases considered here are compared with published analytical results, experimental data, or alternative finite element solutions.

7.3.1 Isotropic square plate case

This case has published analytical results carried out by Narita and Leissa (1992), and it is advantageous to compare between their results and the results obtained by means of finite elements developed in this work. The case represents a square plate. as shown in Fig. (7.13), made of isotropic material with the following properties:-

$a = b =$	7.62×10^{-2}	m
$E =$	1.28×10^{11}	Pa
$h =$	1.04×10^{-3}	m
$\nu =$	0.333	
$\rho =$	1.5×10^{3}	kg/m^3

The plate is fixed at one edge, whilst the other three edges remain free. Several finite element meshes were attempted, and the convergence of results was reached with 4×4 mesh and finer, and the results obtained from the 4×4 mesh are represented here. The finite element analysis was carried out with the conforming, and non-conforming 4-node quadrilateral elements, and the non-conforming 3-node triangular element with its selected mesh as shown in Fig. (7.14). The results were compared with the

analytical solution given by Narita and Leissa (1992), as demonstrated in Table (7.1), where non-dimensional frequency parameters were displayed. The non-dimensional frequency parameter Φ is defined as follows:-

$$\Phi = \omega a^2 \sqrt{\frac{\rho h}{D}}$$

where $D = \dfrac{E h^3}{12(1 - \nu^2)}$ which represents the flexural rigidity of the plate, and ω is the frequency in rad/sec. It is clear from Table (7.1) that natural frequency parameters, for different modes of vibration, as obtained by means of different finite elements, agree very well with corresponding analytical solutions.

7.3.2 Composite layered square plate case

This case has overall dimensions similar to the previous case shown in Fig. (7.13), but it has 8 layers of a fibrous composite material. Each layer has a thickness of 0.13 *mm*, and made of a Hercules type AS/3501-6 Graphite/Epoxy composite material with material axes (x', y', z') as shown in Fig. (7.15), and properties as listed below:-

$$E_{x'} = 1.28\times10^{11} \quad Pa$$

$$E_{y'} = 0.11\times10^{11} \quad Pa$$

$$\mu_{x'y'} = 4.48\times10^{9} \quad Pa$$

$$\mu_{y'z'} = 1.53\times10^{9} \quad Pa$$

$$\mu_{z'x'} = 1.53\times10^{9} \quad Pa$$

$$\rho = 1.5\times10^{3} \quad kg/m^3$$

$$\nu_{y'x'} = 0.25$$

The fibre angles θ, in the 8 layers are 45°, -45°, -45°, 45°, 45°, -45°, -45°, 45°. The non-dimensional frequency parameter for the composite-layered case, is defined as follows:-

$$\Phi = \omega a^2 \sqrt{\frac{\rho h}{D_o}}$$

where $$D_{\circ} = \frac{E_x h^3}{12\left(1 - \nu_{xy}\,\nu_{yx}\right)}$$

and h represents the total thickness of the plate. Meshes similar to those shown in Figures (7.13) and (7.14) were used, and the non-dimensional frequency parameters obtained by means of the 4-node conforming quadrilateral element, 4-node non-conforming quadrilateral element, and 3-node non-conforming triangular element, developed in this work, were compared with the analytical solution published by Narita and Leissa (1992), and also compared with an experimental work published by Crawley (1979), and his finite element results which were based on a moderately thick quadrilateral shallow shell element developed by Lee and Pian (1978), as shown in Table (7.2). The package results have generally proved to be closer to the analytical solution than those based on Lee and Pian's element. However, some deviation (≈ 8%) between all theoretical results and corresponding experimental results was observed. Crawley (1979) mentioned that the experimental results represented an average of the measured natural frequencies of nominally identical samples. Since there was a slight variation in the finished thickness from plate to plate, the measured frequencies were linearly corrected to a reference thickness before averaging. No other correction such as for fibre volume fraction, has been applied.

It was also observed that when the analysis was carried out with double the thickness, the package results, *i.e.* the non-dimensional frequency parameters were very close to corresponding experimental results.

7.3.3 Composite layered rectangular plate case

This case represents a rectangular plate with aspect ratio a/b = 2:1, where a is the length in the x-direction and b is the width in the y-direction. The plate has 8 layers of composite material and thickness similar to the previous case described in section 7.3.2, but with the following dimensions:-

$a = 16.24\times10^{-2}$ m

$b = 7.62\times10^{-2}$ m

Two finite element meshes were employed in the dynamic analysis of this case, the first has 8×4 four-node quadrilateral elements as shown in Fig. (7.16), and the second has 64 three-node trianglular elements as shown in Fig. (7.17). The results obtained were compared with the published experimental and finite element results of Crawley (1979), as shown in Table (7.3). All finite element results of the package were very close to each other, but with a consistent deviation of about 8% from the experimental results.

7.3.4 Composite layered cylindrical shell cases

It is important to validate the dynamic analysis of the package for a curved shell, and a cylindrical shell with published results has been chosen to achieve that. The geometry of the cylindrical curved shell is shown in Fig. (7.18a), the boundary conditions are also illustrated in that figure, and the material properties are the same as in the previous two cases. Two different shells were attempted: the first has the fibres lie in angles 0, 0, 30°, -30°, -30°, 30°, 0, 0 and the angles of fibres in the second shell are 0, 45°, -45°, 90°, 90°, -45°, 45°, 0. The meshes employed for the finite element analysis are as shown Figures (7.18b) and (7.18c). The results were compared with published experimental results of Crawley (1979) and his finite element results based on the element of Lee and Pian (1978) as shown in Tables (7.4) and (7.5). Observations similar to those seen with the previous case are found, emphasizing the accuracy of the developed elements for the dynamic analysis of composite layered shells.

7.4 DYNAMIC ANALYSIS OF CANTILEVER PLATE CASE

In this case the cantilever plate described in section 7.2.1, and shown in Fig. (7.1) was employed for further dynamic studies, to investigate the performance of the devolved elements in a range of thickness and rotational speed, and to check forced vibration and resonant frequency analysis. Boundary conditions, material, mesh, and the geometry of the plate are as explained in section 7.2.1.

Although the non-conforming 3-node triangular element has shown results, at zero rotational speed, very close to those obtained by means of quadrilateral elements, it has displayed poor performance with the presence of a rotational speed, *i.e.* when there is a centrifugal loading. This has been attributed to the non-symmetry of the in-plane stresses generated by centrifugal loading, and because they are based upon Lagrangian shape functions, the values of those stresses are constant over each triangular element. Therefore, the 3-node non-conforming triangular element is not recommended for the analysis of rotating blades, unless a very fine mesh is selected.

7.4.1 Thickness effect for non-rotating plate

The non-dimensional frequencies of the first three bending modes of vibration have been obtained using the 4-node conforming and non-conforming quadrilateral elements for a wide range of thickness, and these results are plotted in Figs. (7.19) - (7.21). It is clear from these figures that the non-conforming and conforming elements give very close results, and the performance of these elements is stable in the full range of thickness, *i.e.* there is no shear locking phenomenon as experienced with Mindlin-type elements. It can also be ascertained from the above-mentioned figures that the transverse shear deformation, considered with the new elements, has an effect on the non-dimensional natural frequencies, since the first two bending modes of vibration are reduced with the increase of thickness.

7.4.2 Effect of centrifugal stiffening

Two cases of thickness, a thin plate case with $h = 0.01\ m$, and the other is a thick plate with $h = 0.1\ m$, were analysed with a wide range of rotational speed, where the plates were assumed to be rotating, with a uniform rotational speed, about an axis of rotation parallel to the y-axis, as shown in Fig. (7.22). The first three non-dimensional bending frequencies were plotted against the rotational speed, and shown in Figs. (7.23) - (7.25) for the thin case, and in Figs. (7.26) - (7.28) for the thick case.

The first comment on those figures is that the conforming and non-conforming quadrilateral elements have shown very close results, for the thin and thick cases. It

is clear that centrifugal stiffening, which results from an inertial force acting in the x-direction and resisting bending normal to that direction, will increase the bending frequencies, with the greatest effect on the lowest frequency. The second remark is that at a rotational speed of 1000 R.P.M. the first bending frequency of the thin case is increased by about 100%, the second increased by 21%, and the third by 8%. The thicker the plate the lower is the centrifugal stiffening effect at the same speed, and it can also be seen that at the 1000 R.P.M. the increase of the first three bending frequencies of the thick case were approximately 2%, 0.3%, and 0.1% respectively.

7.4.3 Forced vibration analysis

The plate chosen here has the same dimension, material, boundary conditions, and mesh as the one described in section (7.2.1), and it was subjected to an excitation force parallel to the z-axis, which is normal to the plate at the free edge, *i.e.* the excitation force will cause forced bending vibration to the plate. Several studies have been carried out as summarized next.

(a) Thickness effect

For non-rotating plate with excitation frequency of 100 *rad/sec*, the thickness of the plate was changed from very thin to thick, and the maximum displacement amplitude at the free edge, was plotted against thickness as shown in Fig. (7.29). The two quadrilateral elements developed in this work show close results. and a stable performance in the range of thickness . It was noticed that resonance at that excitation frequency occurred at $h = 0.0098\ m$.

(b) Speed effect

Several values were assumed for the speed of rotation of the plate, with the given excitation frequency, and the maximum displacement amplitude was plotted against the rotational speed for a thin plate ($h = 0.01\ m$) as shown in Fig. (7.30), and for a thick plate ($h = 0.1\ m$) in Fig. (7.31) . It is clear from the first figure that the critical rotational speed (at which the plate resonance will occur) can be easily detected, whilst there was no critical speed noticed, within the range of speed tested, for the thick plate case.

(c) *Resonant frequencies*

By changing the excitation frequency, and plotting the maximum displacement amplitude against the excitation frequency, one can detect the resonant frequencies. Fig. (7.32) demonstrates an example, using the 4-node conforming element, where the maximum displacement amplitude is plotted against excitation frequency for a non-rotating and a rotating plate at rotational speed of 600 R.P.M. From the figure it is clear that the resonant frequencies can easily be detected, and it is also noticeable that the Coriolis force has a damping effect on the displacement amplitude.

7.5 DYNAMIC ANALYSIS OF CIRCULAR SHELL

In this case different types of dynamic analysis investigations similar to those discussed in the previous section, are carried out on a circular shell. The shell case is similar in geometry and material properties to that shown in Fig. (7.7). The results which have been investigated in this section are summarized as follows:-

(a) *Thickness effect for a stationary case*

The non-dimensional frequency, for the first three modes of natural vibration, are plotted against the ratio of the shell thickness to the radius of curvature of its midsurface, as shown in Figs. (7.33)-(7.35).

(b) *Effect of centrifugal stiffening*

The circular shell was considered rotating about an axis of rotation, as shown in Fig. (7.36). The first three natural frequencies are plotted against rotational speed for a thin case of $h = 0.001\ m$ as shown in Figs. (7.37) - (7.39), and for a thick case of $h = 0.01\ m$ in Figs. (7.40) - (7.42). The centrifugal loading generated in this case does not oppose structure bending, and it leads, therefore, to a reduction in natural frequencies.

(c) *Forced vibration analysis*

The circular shell was subjected to an excitation force parallel to the y-axis at the free end. The maximum displacement amplitude, in the y-direction, was

plotted against thickness for a non-rotating case as shown in Fig. (7.43), and plotted against rotational speed for the thin and thick cases in Figs. (7.44) and (7.45). The maximum displacement amplitude is plotted against the excitation frequency for non-rotating and rotating shells in Fig. (7.46).

General comments on the displayed results can be summarized as follows:-

(i) There is a very close agreement between corresponding results obtained from the two different quadrilateral elements.

(ii) The elements have demonstrated a stable performance in a wide range of thickness.

(iii) The transverse shear effects reduce the non-dimensional natural frequency, as was observed for the flat plate case.

(v) The forced vibration analysis can be employed for the detection of the resonant frequencies.

(vi) It is clear from Fig. (7.46) that the centrifugal loading effect has reduced the resonant frequency, as expected for that case, and the Coriolis force effect has caused damping which results in reduction of the displacement amplitude.

7.6 CASE WITH VARIATION OF FIBRE ANGLES

This case represents a rectangular plate with the length along the x-direction being $a = 15.24\times10^{-2}\ m$ and the length in the y-direction $b = 7.62\times10^{-2}\ m$. Two plates were considered one with five layers, and the thickness of each layer is $0.13\times10^{-3}\ m$, where the angles of fibres are arranged as θ, $-\theta$, θ, $-\theta$, θ, and the second is a single layered plate with a thickness equal to the total thickness of the five-layer plate, and the fibres at an angle θ, as defined in Fig. (7.15). The meshes employed for the finite element analysis are similar to those displayed in Figs. (7.16) and (7.17). To

demonstrate the effect of the fibre angle, the natural frequency analysis has been carried out on plates with different values of θ, *i.e.* θ = 0, 15°, 30°, 45°, 60°, 75°, 90°.

7.6.1 Natural frequency analysis of non-rotating plates

The first five non-dimensional frequencies as obtained by finite element analysis with the conforming 4-node quadrilateral, non-conforming 4-node quadrilateral, and non-conforming 3-node triangular elements, together with the corresponding analytical solution of Narita and Leissa (1992), were plotted against fibre angles, for the 5-layer as well as the single-layer plates, as shown in Figs. (7.47) - (7.51). The results for the 5-layer and the single-layer plates are also displayed in Tables (7.6) and (7.7), respectively.

The following points can be deduced from the given results:-

(i) Results obtained using different finite elements for the single-layer plate at different fibre angles are in a very close agreement to those obtained by the analytical solution of Narita and Leissa (1992) for that case. Similarly, the finite element results for the 5-layer plate are in excellent agreement to the corresponding analytical solution given by the same authors.

(ii) Increasing the fibre angle θ, changes the natural frequency, both for the single layer and the 5-layer plates, at the five natural modes displayed.

(iii) The change in the fibre angle θ have a greater effect on the results of the 5-layer plate than on those of the single layer plate. This may indicate the advantage of using more layers if the fibre angle effect is to be fully exploited.

7.6.2 Thickness effect

The main objective of this case is to study the thickness effect on the natural frequencies of a multilayered plates, therefore the five-layer plate was employed for this analysis, with two values of plate thicknesses being considered, the first is the same as in section (7.6.1), but the second thickness was ten times greater than the first. The first five non-dimensional natural frequencies for the thin and thick plates

were plotted against fibre angles θ, as shown in Figs. (7.52) - (7.56). It is clear from those figures. that the transverse shear effect tends to reduce the non-dimensional frequency, as observed in previous cases, but this reduction is greater at higher θ. This means that the effect of the fibre angle on the natural frequency may be reduced by increasing the plate thickness.

7.6.2 Speed effect

The two plates of the previous case were analysed again but with a rotational speed to study its effect on the natural frequencies, and for this analysis the rotational speed was 150 R.P.M. The first five non-dimensional frequencies, obtained by means of conforming element meshes, have been plotted against fibre angle, for non-rotating and rotating cases as shown in Figs. (7.57) - (7.61). The effect of centrifugal stiffening in increasing the natural frequencies can be observed in all those figures, and it is also observed that the effects of the fibre angle θ and the transverse shear are similar to what observed in previous figures.

7.7 FLUTTER ANALYSIS

7.7.1 Isotropic rectangular panel

This case represents an application to two-dimensional panel flutter with a Mach number greater than 1.6. A finite element analysis, based upon considering the panel as a wide beam was introduced by Olson (1967), and exact analytical solutions were given by Houbolt (1958). The panel has a length a in the x-direction, and no length was specified in the y-direction. The effect of the flow speed was presented by means of the non-dimensional flutter parameter A, defined as follows:-

$$A = \frac{\rho_\infty V_\infty^2}{\sqrt{M_\infty^2 - 1}} \left(\frac{a^3}{D} \right)$$

and the non-dimensional eigenvalue is defined as $K = \lambda \left(\frac{a^4}{D} \right)$

where D is the flexural rigidity of the panel. The panel was assumed to be made of

an aluminium alloy with the following properties:-

$E = 7.5\times10^{10}$ Pa

$\rho = 3000$ Kg / m^3

$\nu = 0.33$.

Two cases of boundary conditions were considered, the first is a clamped panel with the two opposite sides at ($x = 0$) and ($x = a$) being clamped and the other sides are free, and the second is a simply-supported panel with only the sides at ($x = 0$) and ($x = a$) restrained from deformation in the z-direction. The length a was assumed 0.8 m, and since no length in y-direction was specified with the published results, it was considered that $b = 0.2$ m (an aspect ratio $a:b = 4:1$). Several meshes, with the two different types of boundary conditions were tried, and the results were converging with a consistent deviation from published results. In a try to improve that deviation the panel width b was increased to 0.4 m (an aspect ratio $a:b = 2:1$), and in return the results became closer to the published ones. The package results displayed here, are for a mesh with 8×2 square elements for the case with aspect ratio 4:1, and a mesh with 4×2 square elements for the case with aspect ratio 2:1.

(a) Simply-supported panel

The value of the non-dimensional flutter parameter A was increased gradually, and the first two eigenvalues λ_1 and λ_2 were monitored, until their coalescence was achieved. Detecting coalescence, or complex eigenvalues is not possible with the simple iteration algorithm and the subspace iteration solver, described in this thesis, and an automatic search scheme was, therefore, adopted when approaching the point of coalescence, as explained in chapter 5. Thus the detection of the critical flutter conditions within any given acceptable error limits becomes possible. The corresponding non-dimensional eigenvalues K_1 and K_2 were plotted against the non-dimensional flutter parameter A, using 4-node conforming and non-conforming quadrilateral elements, for rectangular plates with aspect ratios 4:1 and 2:1, together with the exact analytical solution of Houbolt (1958), which was extracted from Olson's report (Olson 1967), as shown in Fig. (7.62). The non-dimensional

eigenvalues at $A = 0$, and at flutter boundary. including the best results of Olson (1967) are displayed in Table (7.8). It is clear that the results of the case with aspect ratio 2:1, as obtained by the developed elements, are very close to the analytical solution.

(b) Clamped panel

An analysis similar to that performed with the previous case was carried out, and the non-dimensional eigenvalues K_1 and K_2 were plotted against the non-dimensional flutter parameter A as shown in Fig. (7.63). The values of K_1 and K_2 at $A = 0$, and the critical values of A and K at flutter boundary are also tabulated in Table (7.9). It is also clear that the results obtained by the developed elements, for the case with aspect ratio 2:1, are very close to the analytical solution.

It may be worth mentioning that, for the case where the analytical solution is based on a wide beam model, the non-conforming element yielded results closer to the analytical solution than the conforming element, for the simply-supported and clamped panels.

7.7.2 Isotropic square panel

This case represents a square panel, the length of each side was taken as $a = 0.8\ m$, and it was made of an isotropic material similar to that used in the previous case described in section 7.7.1. Considering the symmetry along the x-axis, the finite element meshes of half the panel were employed with 8×4 square conforming and non-conforming 4-node elements.

7.7.2.1 Simply-supported square panel

In this case the panel was assumed simply-supported at its 4 edges, and different values of non-dimensional flutter parameter A were considered until the critical flutter boundary is reached. Olson (1970) had published results based on thin plate-bending conforming and non-conforming finite elements, together with the exact solution of Houbolt (1958). Results based upon the conforming and non-conforming

elements developed in this work are displayed together with the above mentioned published results, at $A = 0$ and at flutter boundary, in Table (7.10). The coalescence of eigenvalues obtained by the package developed in this work was plotted together with a curve published by Sander *et al.* (1973) for a similar case based upon a thin conforming plate-bending element, as shown in Fig. (7.64). It is clear from those results that conforming elements lead to more accurate flutter results than non-conforming elements, as predicted by Olson (1970). However, there is no significant difference between the results obtained by means of the package conforming and non-conforming elements, as compared with those of Olson, specially the K_1 values.

7.7.2.2 Clamped square panel

In this case the four edges of the panel were clamped. The results published by Olson (1970) contains only those with the conforming thin plate-bending element. At $A = 0$, he compared K_1 and K_2 values with the upper and lower bounds of De Vito *et al.* (1966) and the flutter boundary was compared with the approximation of Houbolt (1958). Those results presented, taking Olson best results, together with finite element results of this work, which are based upon the conforming and non-conforming elements are displayed in Table (7.11). The conforming element results are very close to Olson's, with similar deviation from Houbolt's approximate solution. However at $A = 0$ the package results are closer to De Vito *et al.* results. Fig. (7.65) shows the coalescence of eigenvalues based upon conforming and non-conforming elements developed in this work. According to previous results, it can be concluded that the flutter results based upon conforming elements are more accurate than those obtained by means of non-conforming elements.

7.7.3 Composite rectangular panel

This case is a rectangular panel made of 8-layer fibrous composite material, with the following properties:-

$$E_{x'} = 112.0\times10^{9}\ Pa, \qquad E_{y'} = 9.2\times10^{9}\ Pa$$

$$\mu_{x'y'} = \mu_{y'z'} = \mu_{z'x'} = 5.0\times10^{9}\ Pa$$

$$\nu_{y\,x'} = 0.35, \qquad \nu_{y\,x} = 0.02875$$

where x'-axis is the fibre axis, which has an angle θ with the x-axis, as shown in Fig. (7.15). The fibre angles in the eight layers are as 0, 90°, 0, 90°, 90°, 0, 90°, 0.

To facilitate comparison with published results, non-dimensional parameters are defined for the composite case studies as follows:-

Non-dimensional flutter parameter $A = \dfrac{\rho_\infty V_\infty^2}{\sqrt{M_\infty^2 - 1}} \left(\dfrac{a^3}{E_y h^3} \right)$

Non-dimensional eigenvalue $K = \lambda \left(\dfrac{a^4}{E_y h^3} \right)$

Non-dimensional frequency $\Phi = \sqrt{K}$

Two different analytical solutions were presented for a clamped case, by Srinivasan and Babu (1987), the first (IE) is based upon an integral equation technique, the second (SER) is based on a double series consisting of beam characteristic functions. Finite element results, which are based upon the conforming and non-conforming elements developed in this work are displayed together with Srinivasan and Babu's results in Table (7.12), which proves that finite element results are very close to the analytical solutions of Srinivasan and Babu (1987). The coalescence of eigenvalues is plotted in Fig. (7.66), which shows a bigger deviation between conforming and non-conforming results than that observed for isotropic cases, mainly due to a big difference between K_2 values.

The same case was run again but with simply-supported edge conditions, and finite element results are demonstrated in Table (7.13), with the coalescence curves shown in Fig. (7.67). An observation similar to the clamped case can be concluded, regarding the deviation between conforming and non-conforming element results, though it is less than what observed in the clamped case.

7.7.4 Boron/Epoxy composite square panel

This case represents a composite square panel, constructed of 8 layers of a Boron/Epoxy composite material with the following properties:-

$$E_x = 31.0\times10^6\ psi \equiv 2.137\times10^{11}\ Pa$$

$$E_y = 2.7\times10^6\ psi \equiv 1.862\times10^{11}\ Pa$$

$$\mu_{xy} = \mu_{xz} = 0.75\times10^6\ psi \equiv 5.171\times10^{11}\ Pa$$

$$\nu_{yx} = 0.35, \qquad \nu_{yx} = 0.02875$$

The layer fibre angles are as the previous case, *i.e.* 0, 90°, 0, 90°, 90°, 0, 90°, 0. Analytical results for a clamped case was also given by Srinivasan and Babu (1987), and a finite element analysis based upon a shear deformable plate element was published by Lee and Cho (1991). Two different finite element meshes were attempted using half the plate with symmetry conditions with respect to the x-axis, the first is a coarse mesh modelled by means of 4×2 square elements, and the second is a fine mesh modelled in terms of 8×4 square elements. Conforming and non-conforming results are tabulated together with the published results in Table (7.14), and curves for the coalescence of eigenvalue, are shown in Fig. (7.68). It is clear that the results of the conforming elements are very close to the analytical solution, even with the coarse mesh. The fine mesh of the non-conforming element has more accurate answers than the coarse one.

The same case was run with simply-supported edge conditions, and convergence of coalescence results can be observed in Fig. (7.69), and frequencies at $A = 0$ and at the flutter boundary are tabulated in Table (7.15). It can also be noticed that the results based upon conforming and non-conforming elements when the fine meshes are employed came close to each other.

7.7.5 Graphite/Epoxy composite square panel

In this case the panel is square in shape and consists of an 8-layer composite made of a Graphite/Epoxy material with the following properties:-

$E_{x'} = 20.0\times10^6\ psi \equiv 1.379\times10^{11}\ Pa$

$E_{y'} = E_{z'}\ 1.4\times10^6\ psi \equiv 9.653\times10^9\ Pa$

$\mu_{x\,y'} = \mu_{x\,z'} = 0.8\times10^6\ psi \equiv 5.516\times10^9\ Pa$

$\mu_{x\,z} = 0.8\times10^6\ psi \equiv 5.516\times10^9\ Pa$

$\nu_{y\,x'} = 0.3, \qquad \nu_{y'x} = 0.021$

The fibre angles of the layers were θ, 45°, -45°, 0, 0, -45°, 45°, θ, where θ took the values: 0°, 15°, 30°, 45°, 60°, 75°, 90°, to study the effect of the fibre angle on flutter. This arrangement was dictated so as we can compare results with a similar case presented by Lee and Cho (1991). Two cases with different boundary conditions were considered, with the finite element meshes consisting of 4×2 square element, and the symmetry condition taken into consideration.

(a) Clamped square panel

This is the case with all edges being clamped, and the critical non-dimensional flutter parameter A_{cr} and the flutter frequency Φ_{cr}, as obtained from conforming and non-conforming elements, and published solution (Lee and Cho 1991) were plotted against fibre orientation angle θ, as shown in Figs. (7.70) and (7.71). It is clear from those figures that the package results are very close to the published ones, and that increasing fibre angle will reduce critical flutter conditions.

(b) Simply-supported square panel

The results of a simply-supported case were plotted in a way similar to the previous case, as shown in Figs. (7.72) and (7.73). It is also clear from those figures that the lower the fibre angle θ, the higher will be the critical flutter conditions. The deviation between conforming and non-conforming element results, are smaller than what observed with the case of clamped edge conditions.

7.8 GENERAL DISSCUSION

During the course of the analysis of the previous case studies, several interesting general points have been observed and they are summarized next:-

(a) *Conforming and non-conforming elements*

Conforming and non-conforming elements developed in this work have led to accurate and reliable static and dynamic results. The difference between their corresponding results was insignificant for static and dynamic analysis, with the conforming elements showing slightly more accurate answers. The major advantage of the conforming elements is the flexibility in use with curved shells and box structures. The conforming element requires boundary conditions to be in terms of slope angles with respect to global axes, whilst the non-conforming element requires them in terms of local axes, which are not easy for the user to know. The fact that the conforming element has stiffness and mass contributions corresponding to θ_x, θ_y, and θ_z will make them well conditioned.

(b) *Thickness effect*

The developed elements have shown stable performance in a wide range of thickness for plates and shells. Although they consider transverse shear effects, they did not suffer from shear locking as do Mindlin-type elements, and reduced integration techniques are not required for the elements developed in this work. Transverse shear effects, which are increased by increasing thickness, tend to reduce the non-dimensional frequencies, but one should remember that bending frequencies are proportional to thickness.

(c) *Centrifugal force effect*

The centrifugal force resulting from rotation does not always lead to a stiffening as some may believe. It stiffens and sometimes softens depending upon its direction with respect to the direction of deformation. If the

centrifugal force opposes deformation, it leads to a stiffening and higher natural frequencies, with the increase of rotational speed, as demonstrated by the flat plate cases. On the other hand, if it is in the direction of deformation it will lead to softening and lower natural frequencies with the increase of rotational speed, as observed in the circular shell cases. The centrifugal effect is negligible for some modes, like torsional ones, and is reduced for higher modes. The thicker the plate or shell, the lower will be the effect of centrifugal force on bending frequencies, compared at the same rotational speed.

(d) *Coriolis force effect*

The Coriolis force results in a damping term in the finite element dynamic equation of rotating structures. This may explain the reduction observed in the amplitude of a forced vibration with a frequency close to a resonant frequency. The Coriolis force does not have a significant effect on the values of resonant frequencies themselves.

(e) *Layers and fibre angles*

The fibre angle θ can have a significant effect on the stiffness matrix of composite layered plates and shells, and this will result in a corresponding effect on their natural frequencies. This effect can be increased by increasing the number of layers, while keeping the same thickness. However increasing the thickness may reduce the effect of θ. The θ effect may provide a tool for the designers to tune the natural frequencies away from resonance due to excitation frequency, by simply changing the fibre angles without having to modify the mechanical design.

(f) *Flutter*

Several additional comments, have been observed with flutter analysis. The conforming elements lead to more accurate results, with the same finite element mesh, than those obtained by means of non-conforming elements.

The critical flutter frequency is reduced when the first two-bending frequencies, are approaching each other, on increasing the flow speed. The fibre angle can have an effect on flutter parameters. and it can also be employed by designers, to tune the flutter frequency so as to be at higher flow speed than those panels will be subjected to in practice.

Table 7.1 Natural frequency parameters for isotropic square plate

Mode	1	2	3	4	5
Conf-Q	3.461	8.361	21.10	27.04	30.52
Nonconf-Q	3.456	8.362	21.34	26.81	30.47
Nonconf-T	3.453	8.393	21.34	26.82	30.67
Analytical	3.459	8.358	21.09	27.07	30.56

Table 7.2 Natural frequency parameters for 8-layer composite square plate

θ of layers (45°, -45°, -45°, 45°, 45°, -45°, -45°, 45°)					
Mode	1	2	3	4	5
Conf-Q	1.812	6.521	10.44	17.11	21.23
Nonconf-Q	1.807	6.512	10.70	17.00	21.31
Nonconf-T	1.820	6.506	10.90	16.98	21.40
Analytical	1.813	6.553	10.48	17.29	21.49
Published F.E.M	1.792	6.443	10.38	17.11	21.26
Experimental	1.692	6.089	10.20	15.07	19.17

Table 7.3 Natural frequencies for 8-layer composite rectangular plate.

θ of layers (45°, -45°, -45°, 45°, 45°, -45°, -45 , 45)					
Mode	Experimental	Published F.E.M	Conf-Q	Non-conf-Q	Non-conf-T
1	31.3	31.9	31.85	31.86	29.50
2	185.8	191.3	191.16	192.96	180.85
3	214.0	228.2	227.36	227.20	224.81
4	533.0	565.3	562.22	571.35	540.12
5	653.0	708.3	703.78	703.84	696.66

Table 7.4 Natural frequencies for 8-layer composite cylindrical first shell section.

θ of layers (0°,0°, 30°,-30°, -30°, 30°, 0°, 0°)					
Mode	Experimental	Published F.E.M	Conf-Q	Nonconf-Q	Nonconf-T
1	161.0	165.7	168.72	126.34	141.27
2	245.1	289.6	295.09	141.74	195.37
3	555.6	597.1	606.06	452.03	539.76
4	670.0	718.5	713.01	793.62	982.72
5	794.0	833.3	816.94	964.10	1156.19

Table 7.5 Natural frequencies for 8-layer composite cylindrical second shell section.

θ of layers (0°, 45°, -45°, 90°, 90°, 45°, -45°, 0°)					
Mode	Experimental	Published F.E.M	Conf-Q	Nonconf-Q	Nonconf-T
1	177.0	192.4	196.53	190.24	210.59
2	201.8	236.1	246.74	244.77	315.18
3	645.0	705.8	720.91	674.14	773.32
4	754.0	808.2	813.96	1091.27	1196.09
5	884.8	980.6	985.06	1376.14	1441.25

Table 7.6 Non-dimensional natural frequencies for 5-layer rectangular plate at different fibre angle θ.

Fibres angle (Degrees)		θ =0	θ = 15	θ = 30	θ = 45	θ = 60	θ = 75	θ = 90
Mode 1	Conf-Q	3.511	3.152	2.445	1.703	1.176	0.942	0.894
	Nonconf-Q	3.499	3.137	2.423	1.690	1.172	0.942	0.894
	Nonconf-T	3.501	3.145	2.443	1.701	1.177	0.945	0.896
	Analytical	3.513	3.153	2.442	1.700	1.176	0.946	0.897
Mode 2	Conf-Q	7.057	8.452	10.260	10.070	7.263	5.889	5.388
	Nonconf-Q	7.061	8.433	10.230	10.120	7.345	5.905	5.389
	Nonconf-T	7.056	8.455	10.260	10.060	7.367	5.971	5.432
	Analytical	7.068	8.474	10.310	10.080	7.259	5.888	5.390
Mode 3	Conf-Q	21.910	19.830	15.200	11.130	9.431	6.921	5.601
	Nonconf-Q	21.270	20.040	15.840	11.430	9.485	6.938	5.606
	Nonconf-T	21.590	19.680	15.270	11.270	9.485	6.990	5.701
	Analytical	21.970	19.910	15.260	11.190	9.476	6.931	5.602
Mode 4	Conf-Q	25.230	27.110	31.410	28.980	20.6	16.5	15.7
	Nonconf-Q	25.150	26.570	30.920	29.290	21.05	16.6	15.70
	Nonconf-T	26.260	27.480	31.220	28.960	21.2	17.1	16.3
	Analytical	25.840	27.490	31.470	28.980	20.62	16.5	15.7
Mode 5	Conf-Q	27.760	30.850	36.520	33.870	29.010	21.450	16.930
	Nonconf-Q	26.030	30.010	36.190	34.610	29.260	21.540	16.940
	Nonconf-T	27.360	31.27	36.850	34.020	29.190	21.790	17.300
	Analytical	27.840	31.340	37.120	33.950	29.090	21.490	16.950

Table 7.7 Non-dimensional natural frequencies for single layer rectangular plate at different fibre angle θ.

Fibres angle (Degrees)		θ = 0	θ = 15	θ = 30	θ = 45	θ = 60	θ = 75	θ = 90
Mode 1	Conf-Q	3.500	2.822	1.913	1.356	1.062	0.926	0.891
	Nonconf-Q	3.488	2.824	1.915	1.357	1.061	0.926	0.891
	Nonconf-T	3.491	2.821	1.925	1.365	1.066	0.929	0.893
	Analytical	3.513	2.832	1.922	1.365	1.066	0.930	0.897
Mode 2	Conf-Q	7.036	7.477	7.603	6.920	6.042	5.491	5.371
	Nonconf-Q	7.040	7.418	7.442	6.743	5.934	5.452	5.373
	Nonconf-T	7.034	7.504	7.593	6.848	5.980	5.485	5.416
	Analytical	7.068	7.538	7.653	6.932	6.056	5.514	5.390
Mode 3	Conf-Q	21.850	18.440	12.930	9.180	7.053	5.961	5.584
	Nonconf-Q	21.210	18.910	14.000	9.894	7.361	6.046	5.589
	Nonconf-T	21.530	18.560	13.380	9.457	7.254	6.114	5.682
	Analytical	21.970	18.770	13.410	9.448	7.154	5.991	5.602
Mode 4	Conf-Q	25.150	23.590	21.380	19.180	17.12	15.860	15.630
	Nonconf-Q	25.080	22.970	20.770	18.570	16.69	15.680	15.650
	Nonconf-T	26.180	23.710	21.260	18.950	16.97	15.980	16.200
	Analytical	25.840	23.840	21.490	19.250	17.17	15.920	15.690
Mode 5	Conf-Q	27.680	29.970	32.770	26.900	21.33	18.070	16.880
	Nonconf-Q	25.960	28.800	31.770	28.830	22.75	18.510	16.890
	Nonconf-T	27.280	30.630	32.990	27.470	22.08	18.780	17.240
	Analytical	27.840	30.760	33.490	27.640	21.67	18.200	16.950

Table 7.8 Flutter results of simply-supported isotropic rectangular panel.

	A= 0		Flutter boundary	
	K_1	K_2	A_{cr}	K_{cr}
Conf 4:1	89.207	1447.440	317.582	970.980
Non-conf 4:1	89.207	1447.420	324.174	980.840
Conf 2:1	96.778	1538.060	336.042	1033.430
Non-conf 2:1	97.390	1570.520	344.050	1050.820
Olson (1967)	97.460	1570.870	342.343	1043.460
Exact value	97.410	1558.550	343.356	1051.797

Table 7.9 Flutter results of clamped isotropic rectangular panel.

	A= 0		Flutter Boundary	
	K_1	K_2	A_{cr}	K_{cr}
Conf 4:1	479.640	3572.600	603.585	2611.000
Non-conf 4:1	483.77	3566.300	620.998	2666.477
Conf 2:1	498.810	3855.500	632.905	2707.100
Non-conf 2:1	501.920	3878.000	636.810	2723.450
Olson (1967)	501.113	3833.960	636.724	2733.990
Exact value	500.564	3803.540	636.569	2741.360

Table 7.10 Flutter results of simply-supported isotropic square panel.

	A= 0		Flutter boundary	
	K_1	K_2	A_{cr}	K_{cr}
Conf	389.30	2430.90	511.630	1845.10
Non-conf	383.30	2374.80	498.820	1801.80
Olson conf	389.66	2437.80	511.786	1843.29
Olson non-conf	378.71	2335.5	488.703	1766.24
Exact value	389.636	2435.23	512.651	1848.21

Table 7.11 Flutter results of clamped isotropic square panel.

	A= 0		Flutter boundary	
	K_1	K_2	A_{cr}	K_{cr}
Conf	1295.30	5393.30	850.94	4287.60
Non-conf	1257.00	5189.60	748.11	3619.80
Olson conf	1296.11	5406.70	850.42	4282.03
Upper and lower bounds (De Vito, *et al.*)	1294.96	5386.70		
	1294.93	5386.40		
Approximate			876.80	4077.00

Table 7.12 Flutter results of clamped composite square panel.

		A = 0		Flutter boundary	
		Φ_1	Φ_2	A_{cr}	Φ_{cr}
Conforming		59.510	79.000	569.720	74.451
Non-conforming		58.420	75.877	459.300	70.189
Srinivasan	IE	59.420	79.720	561.580	74.250
	SER	59.600	79.760	563.820	74.350

Table 7.13 Flutter results of simply-supported composite square panel.

	A = 0		Flutter boundary	
	Φ_1	Φ_2	A_{cr}	Φ_{cr}
Conforming	27.443	45.798	329.800	41.036
Non-conforming	27.038	43.974	293.330	39.456

Table 7.14 Flutter results of Boron/Epoxy clamped square panel.

		A= 0		Flutter boundary	
		Φ_1	Φ_2	A_{cr}	Φ_{cr}
Conf (coarse)		23.388	54.135	453.06	46.115
Non-conf (coarse)		22.259	51.281	405.44	43.629
Conf (fine)		23.358	53.679	453.3	46.256
Non-conf (fine)		23.009	52.773	436.66	45.434
Srinivasan	IE	23.33	53.77	446.36	46.09
	SER	23.63	53.76	474.6	47.19
Lee & Cho (1991)		23.34	53.62	471.16	46.89

Table 7.15 Flutter results of Boron/Epoxy simply-supported square panel.

	A = 0		Flutter boundary	
	Φ_1	Φ_2	A_{cr}	Φ_{cr}
Conf (coarse)	10.66	33.1	233.22	27.93
Non-conf (coarse)	10.28	32.67	226.95	27.28
Conf (fine)	10.75	34.04	246.9	28.37
Non-conf (fine)	10.63	33.67	241.11	28.01

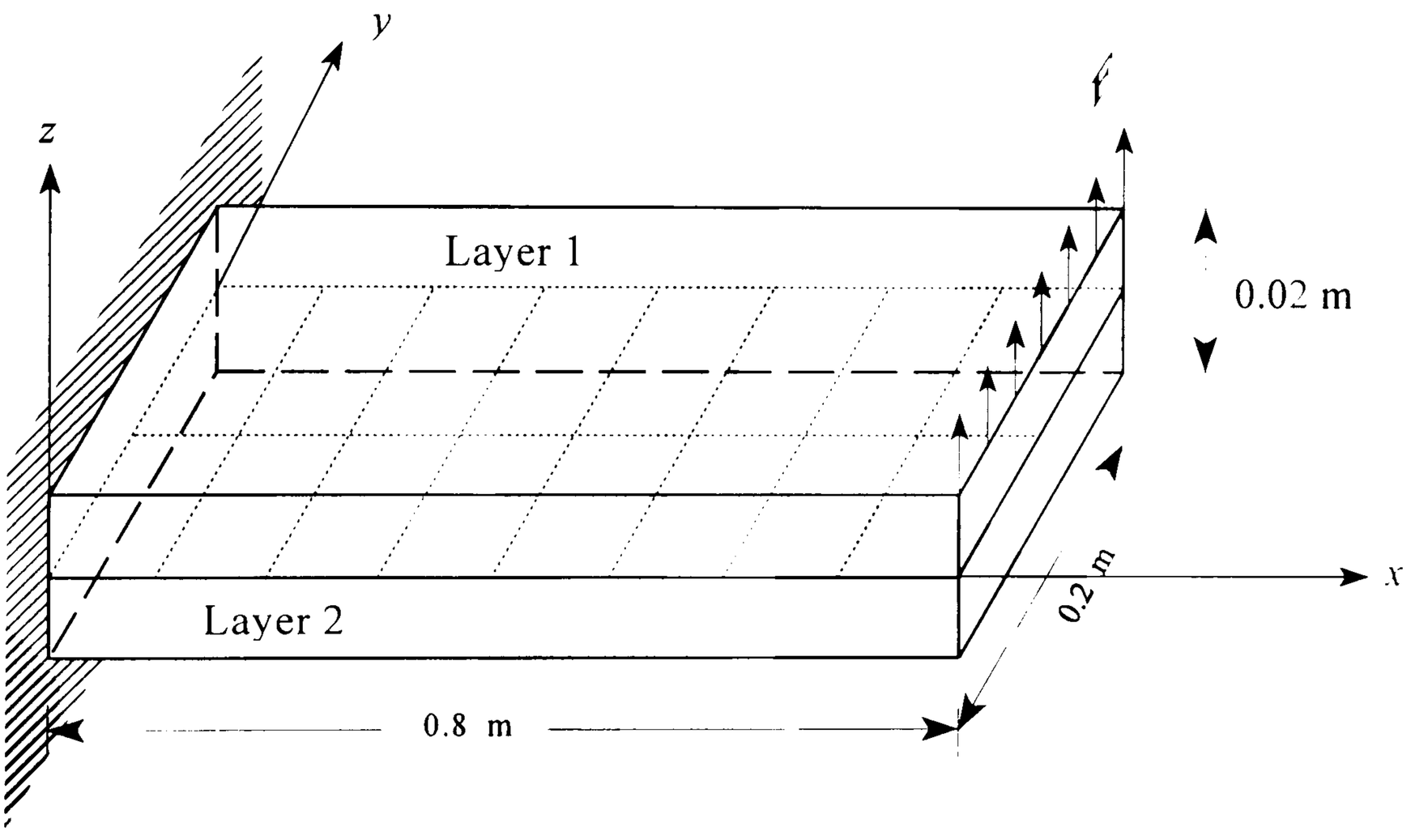

Figure 7.1 Rectangular cantilever plate.

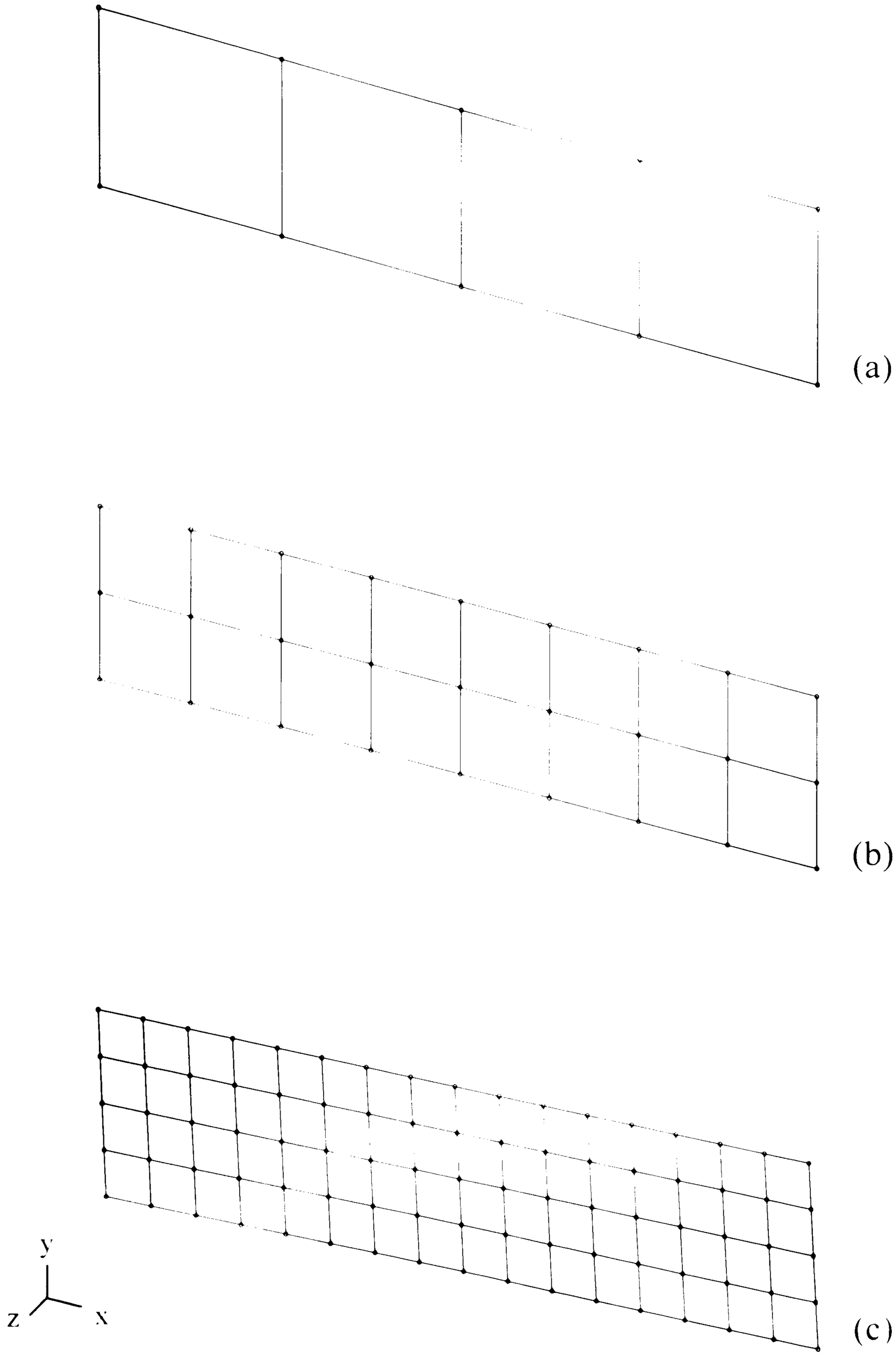

Figure 7.2 Quadrilateral element meshes used for validation of plate case.

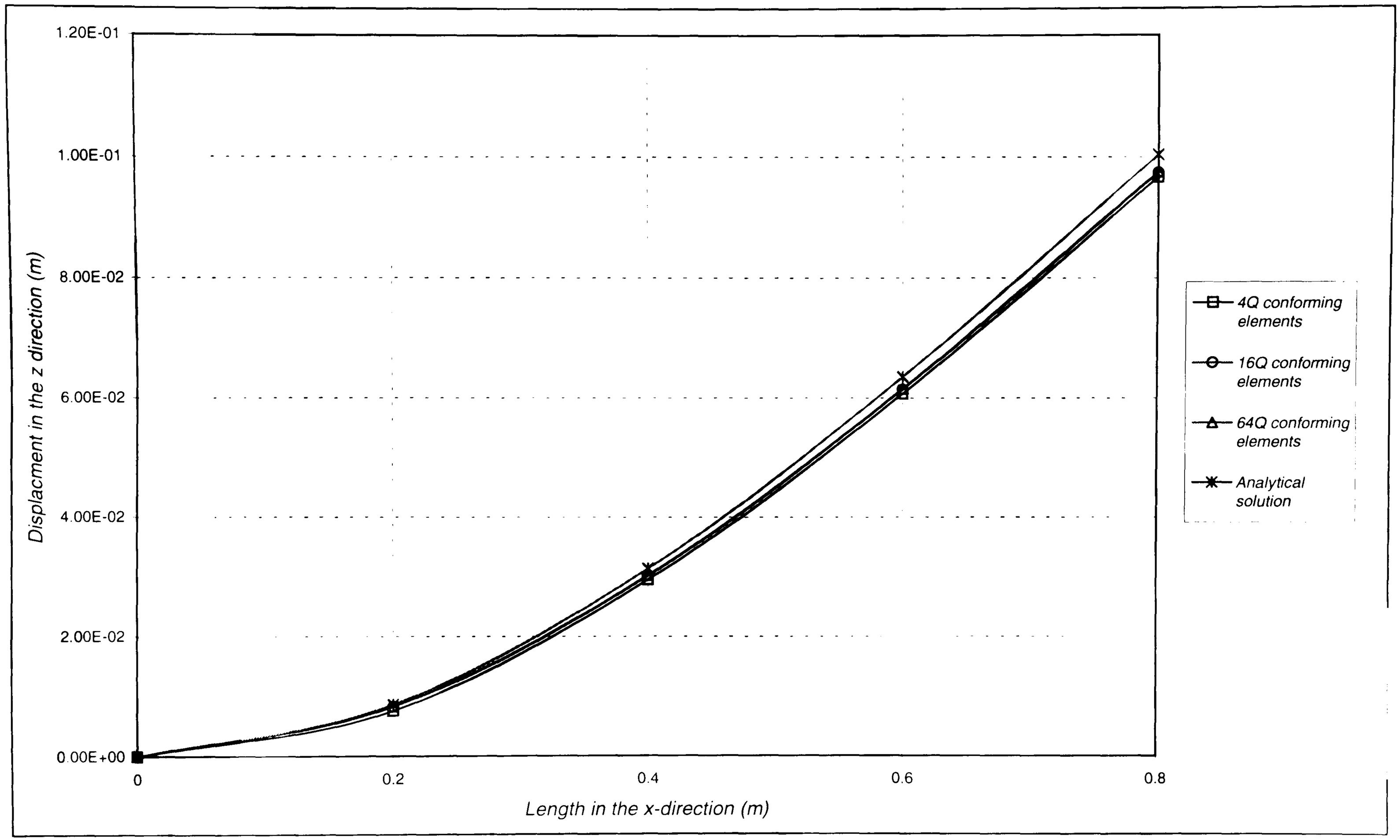

Figure 7.3 Cantilever plate displacement distribution using 4-node conforming element.

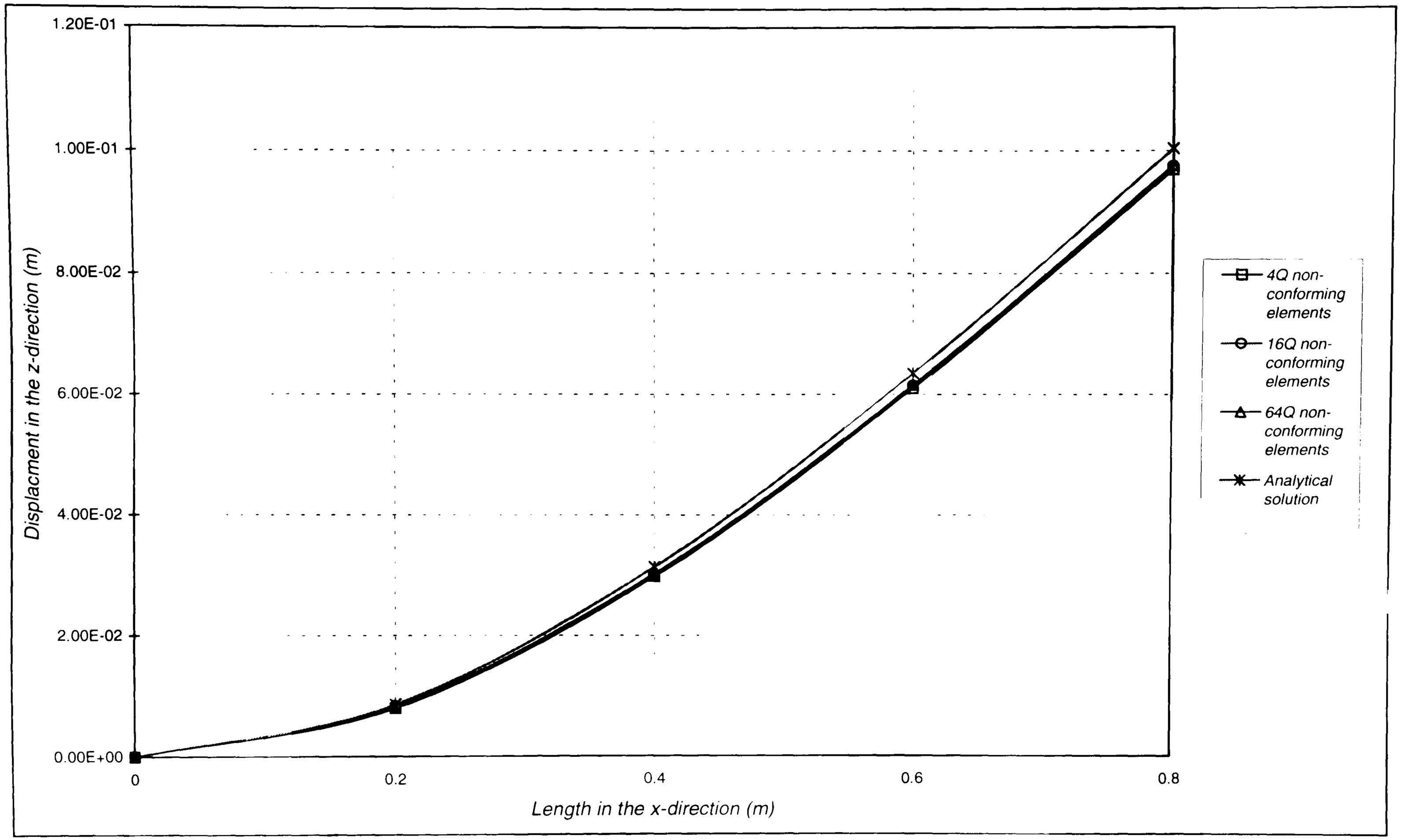

Figure 7.4 Displacment distribution for cantilever plate using 4-node non-conforming elelments

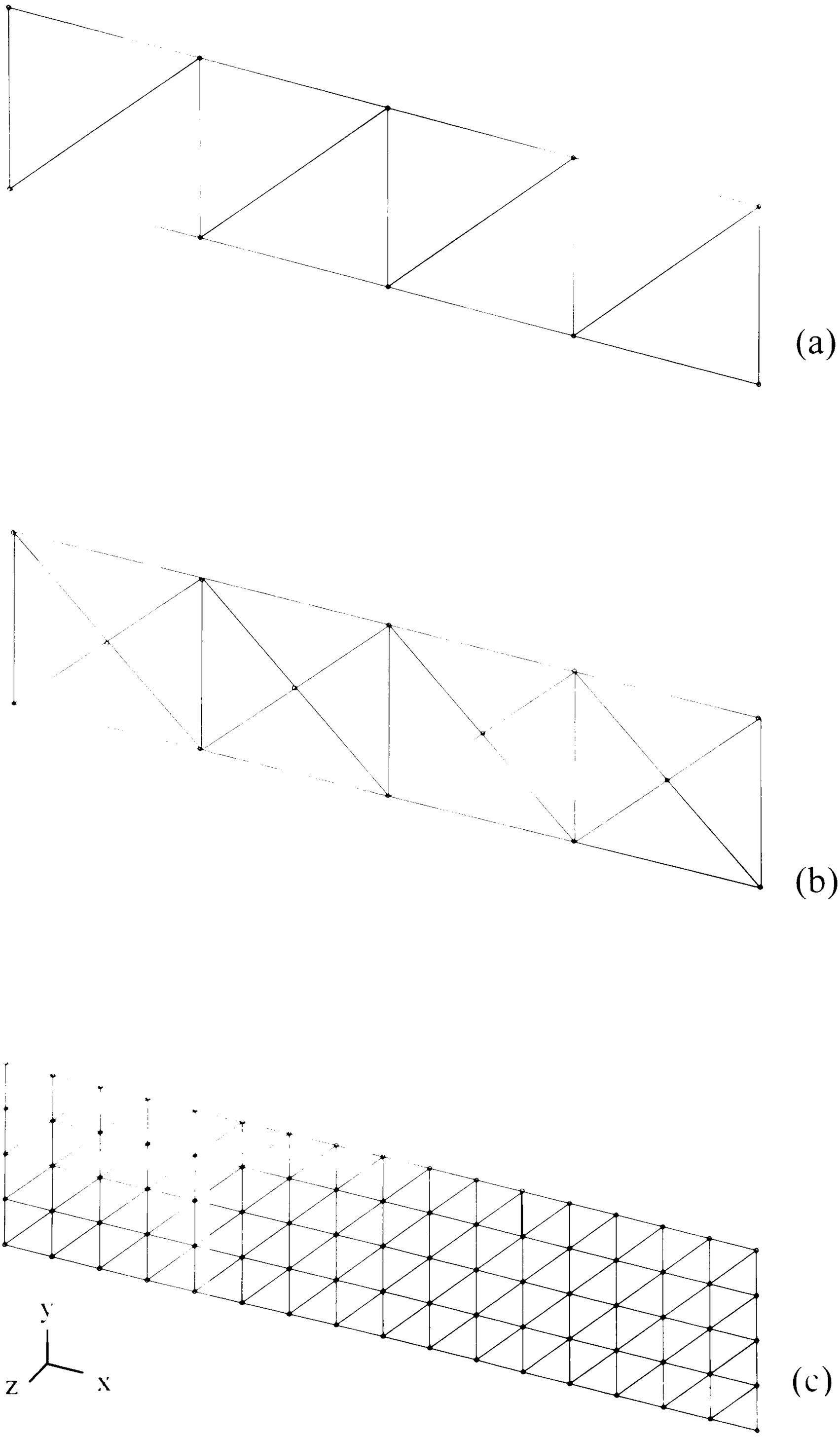

(a)

(b)

(c)

Figure 7.5 Three-node triangular element meshes used for validation of plate case.

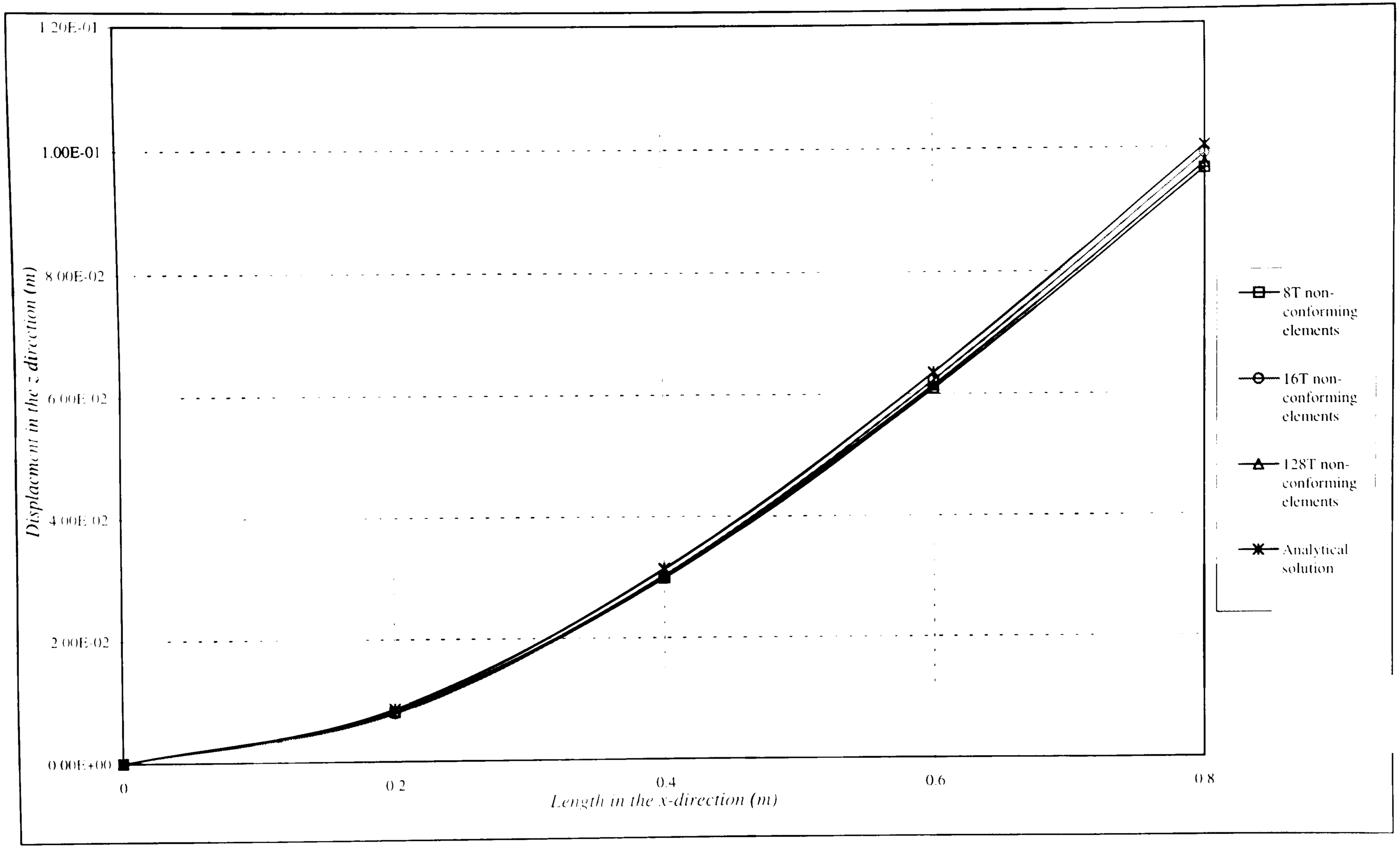

Figure 7.6 Displacement distribution for cantiliver plate using 3-node non-conforming element

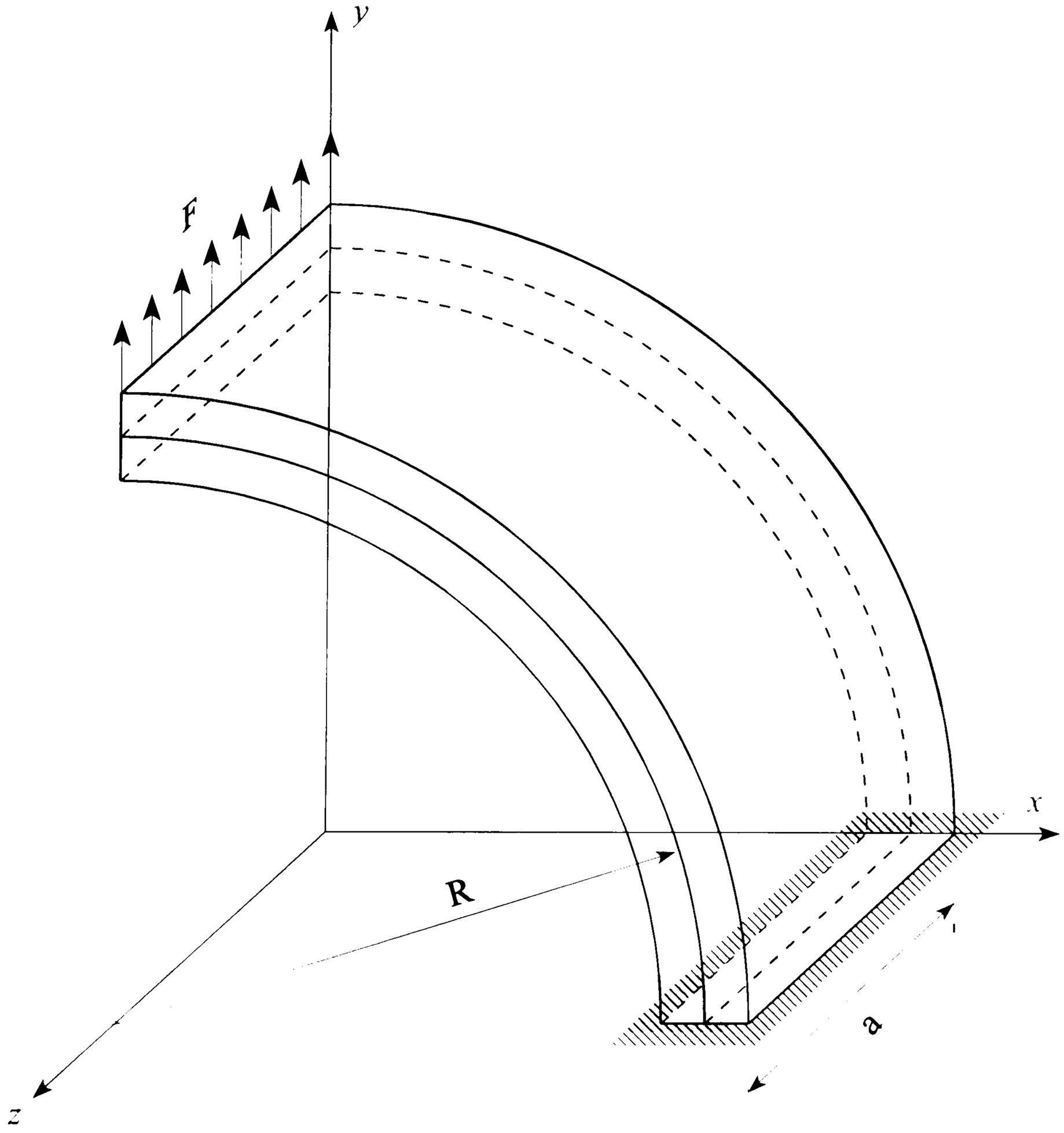

Figure 7.7 Circular cantilever shell

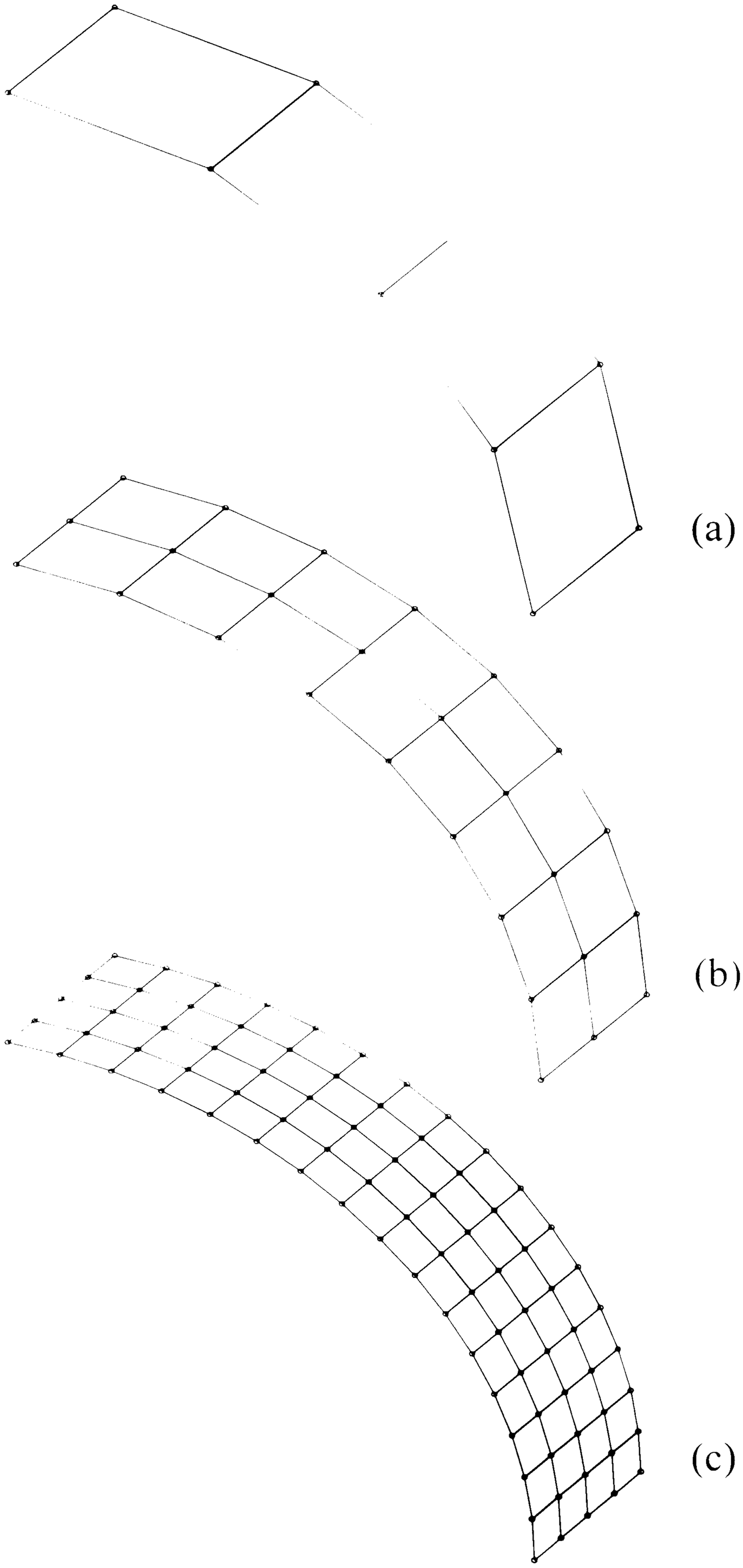

Figure 7.8 Four-node element meshes used for validation of shell case.

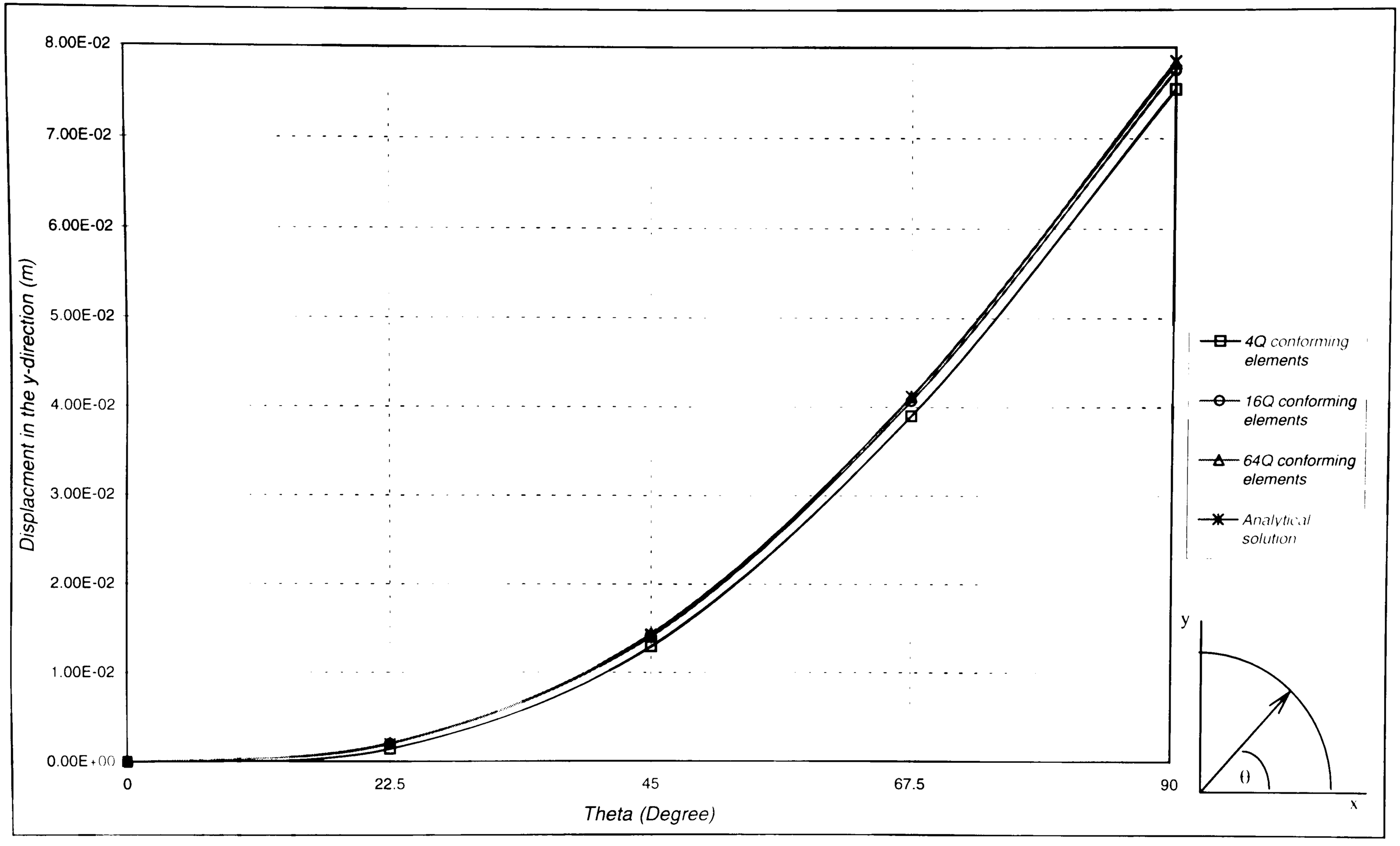

Figure 7.9 Cantilever shell displacment distribution using 4-node conforming element.

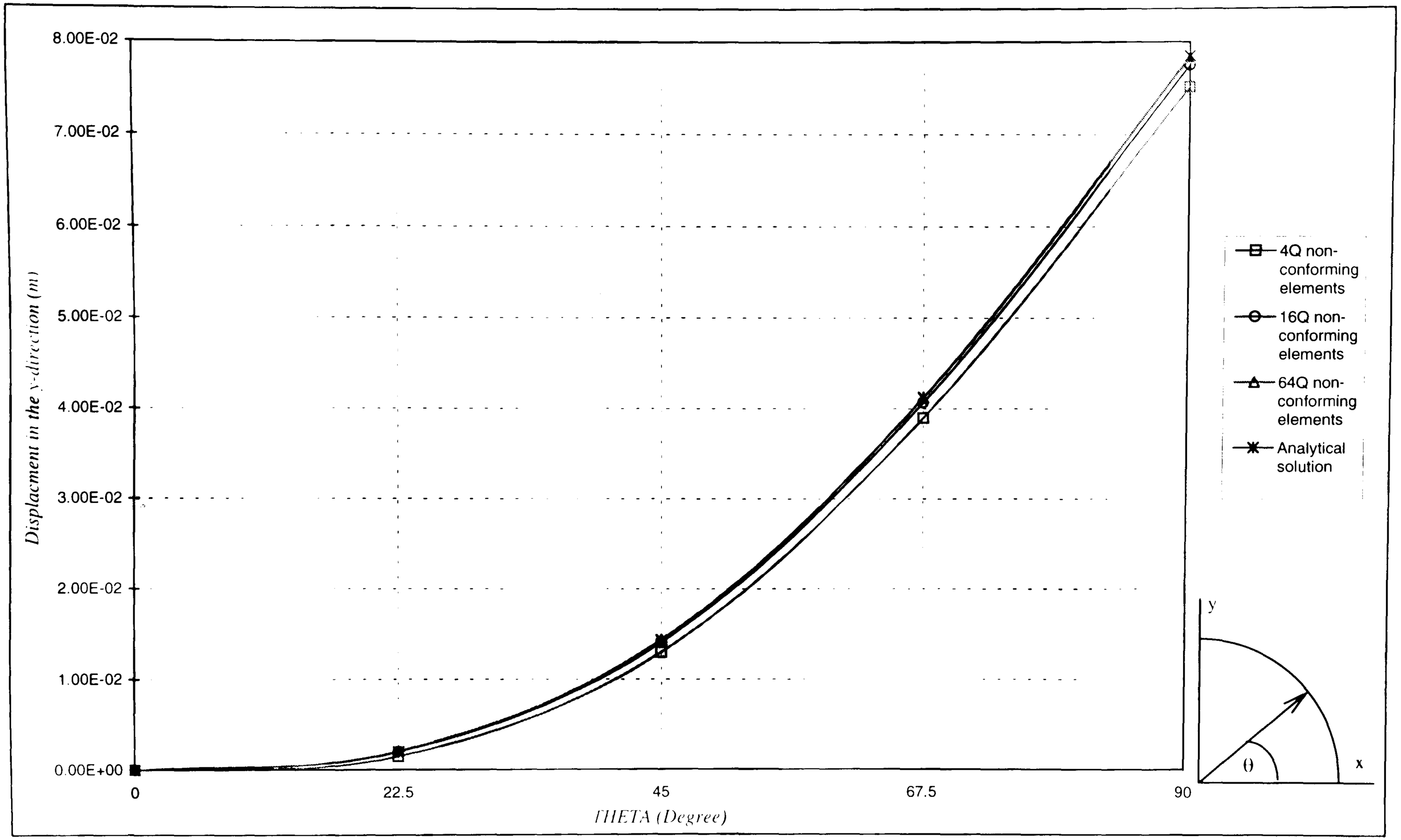

Figure 7.10 Cantilever shell displacment distribution using 4-node non-conforming element.

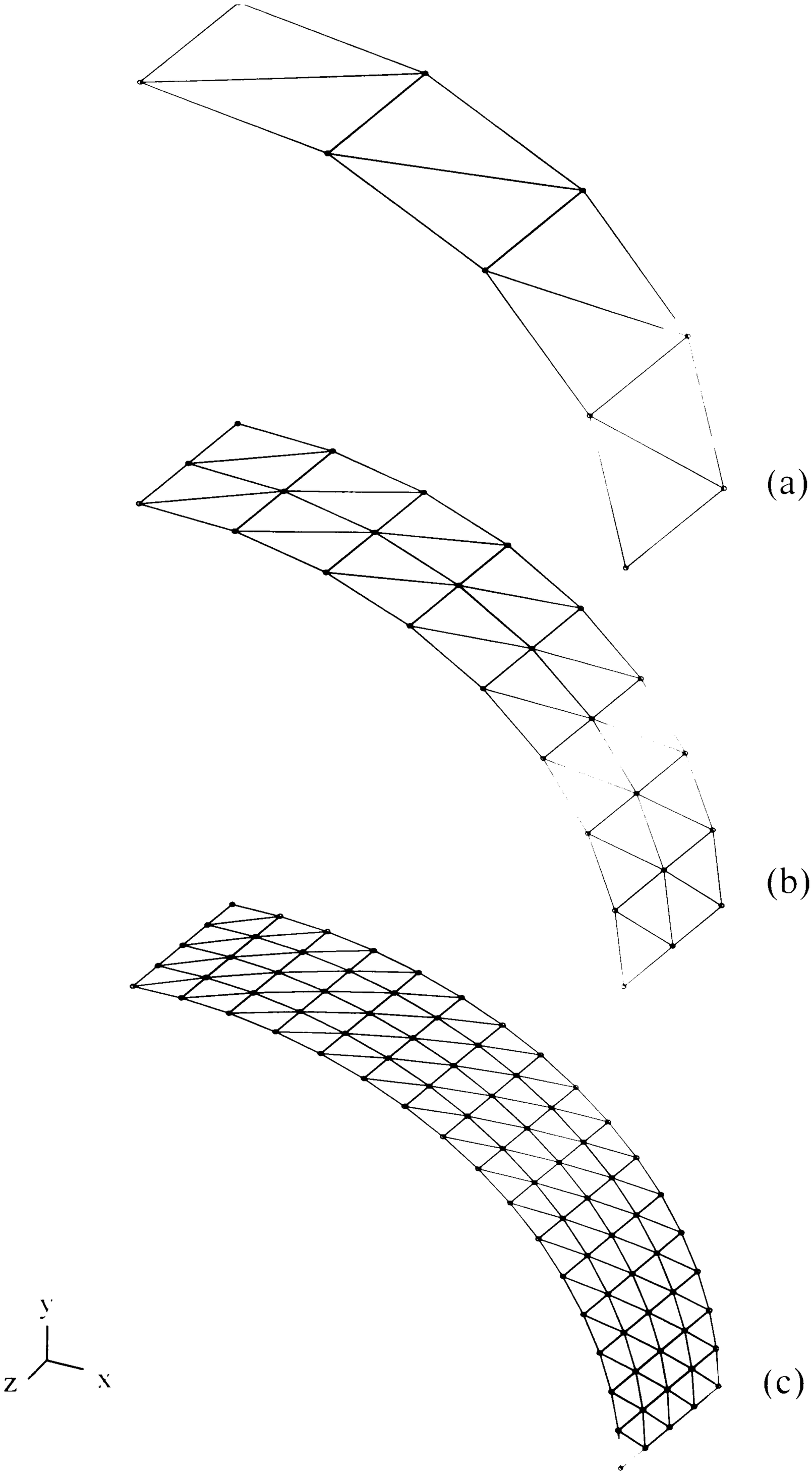

Figure 7.11 Three-node triangular element meshes used for validation of shell case.

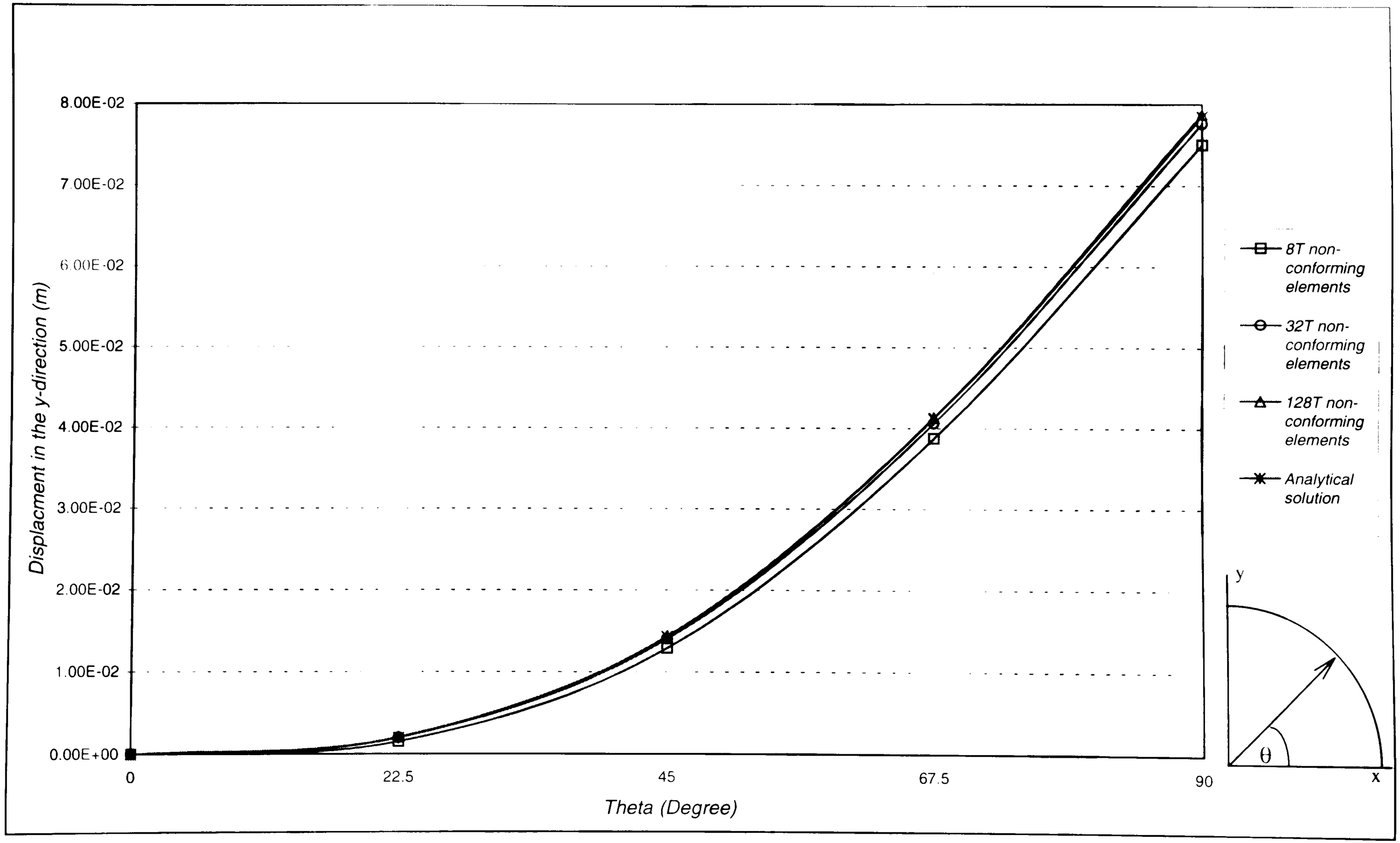

Figure 7.12 Cantilever shell displacment distribution using 3-nod non-conforming element.

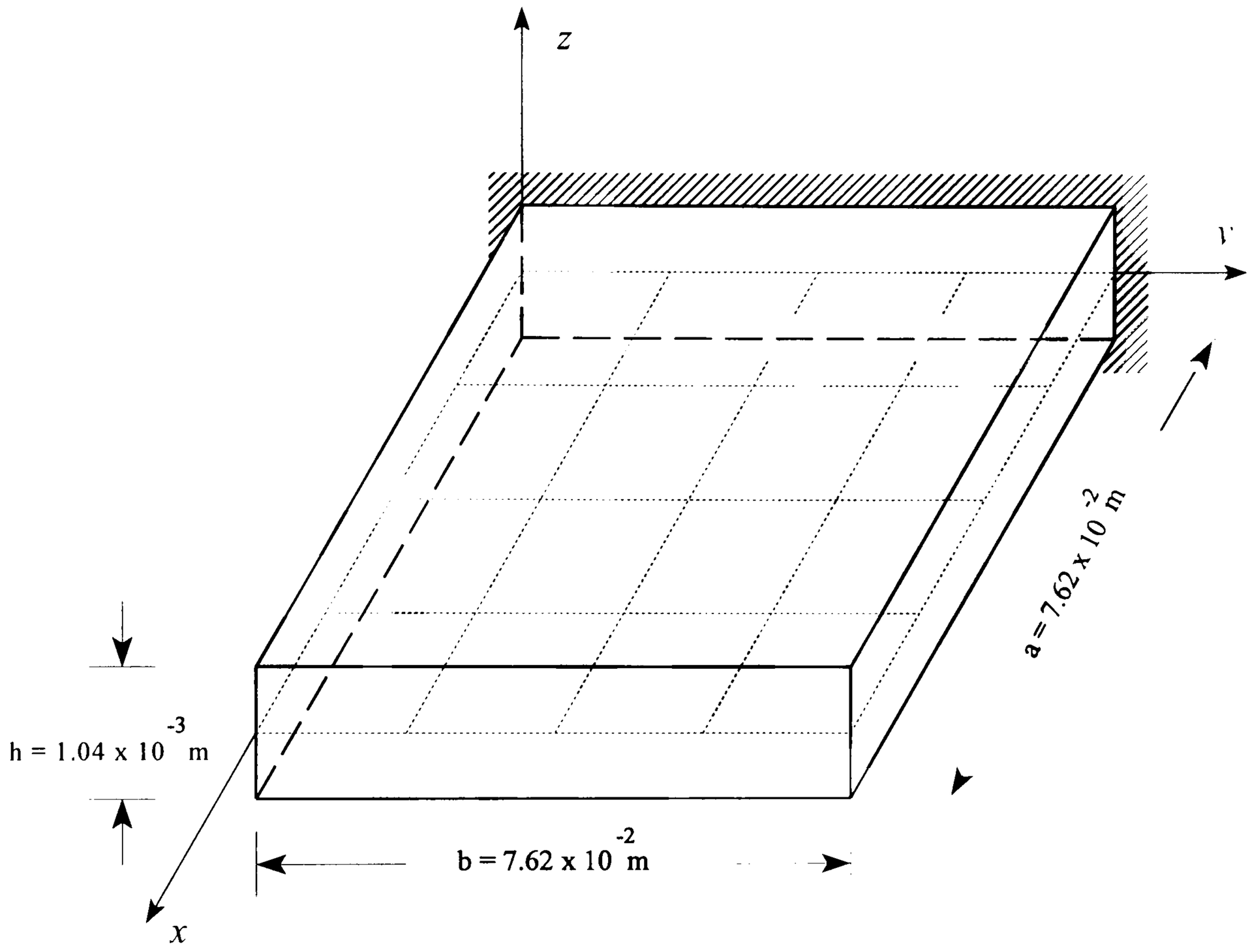

Figure 7.13 Isotropic square plate with 16 four-node quadrilateral elements.

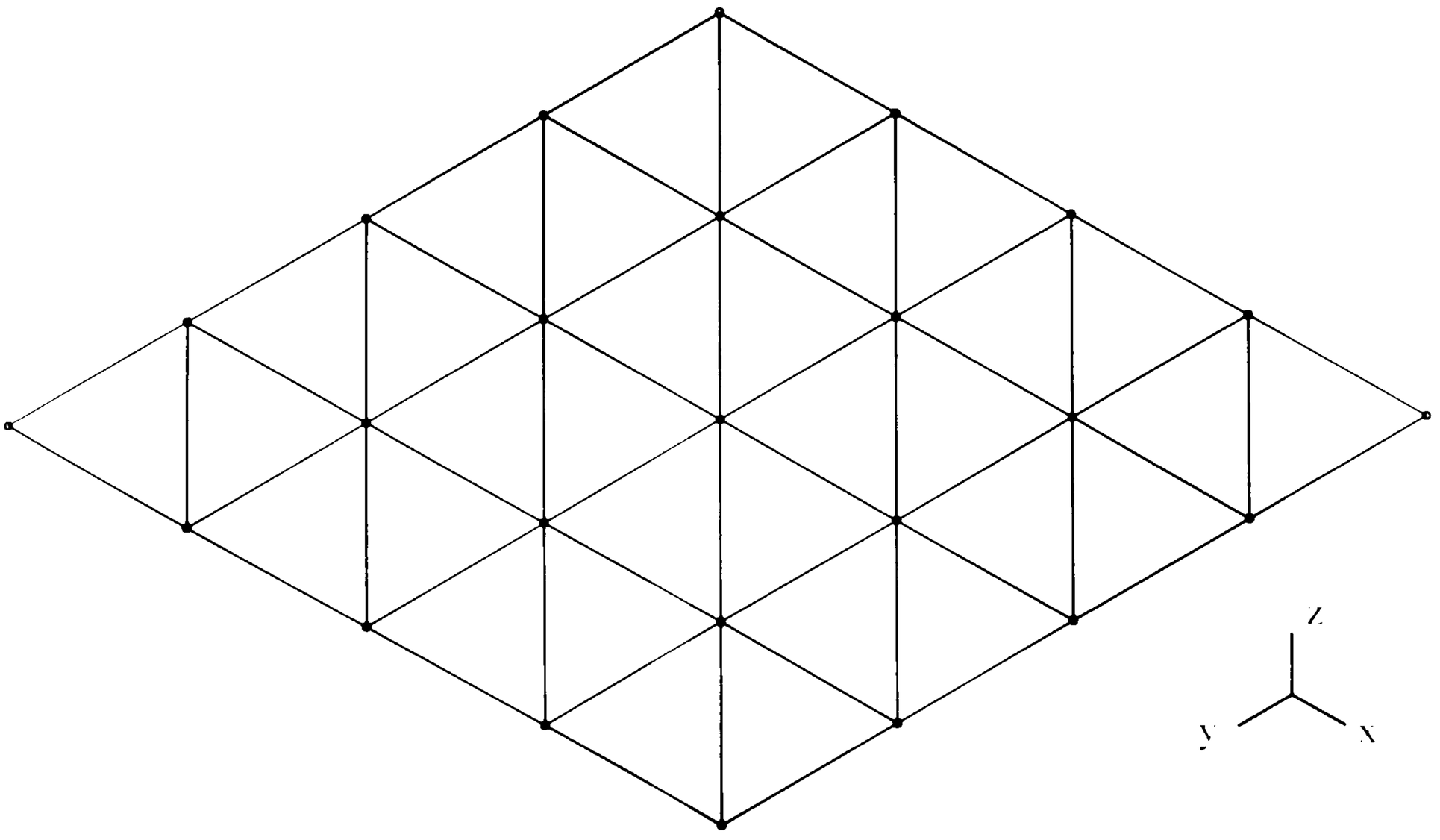

Figure 7.14 Finite element mesh for isotropic square plate case using 32 three-node triangular elements.

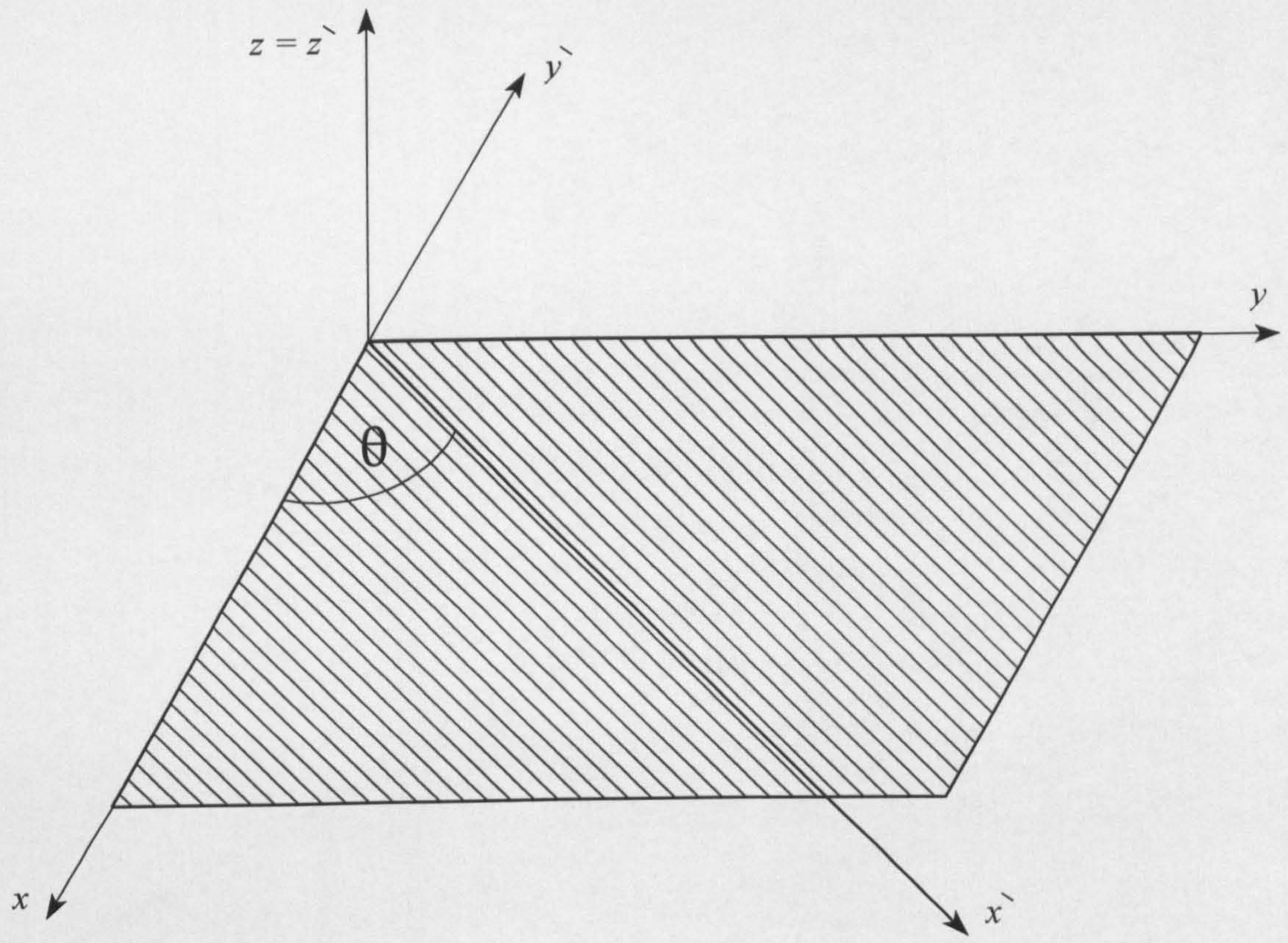

Figure 7.15 Layer material axes.

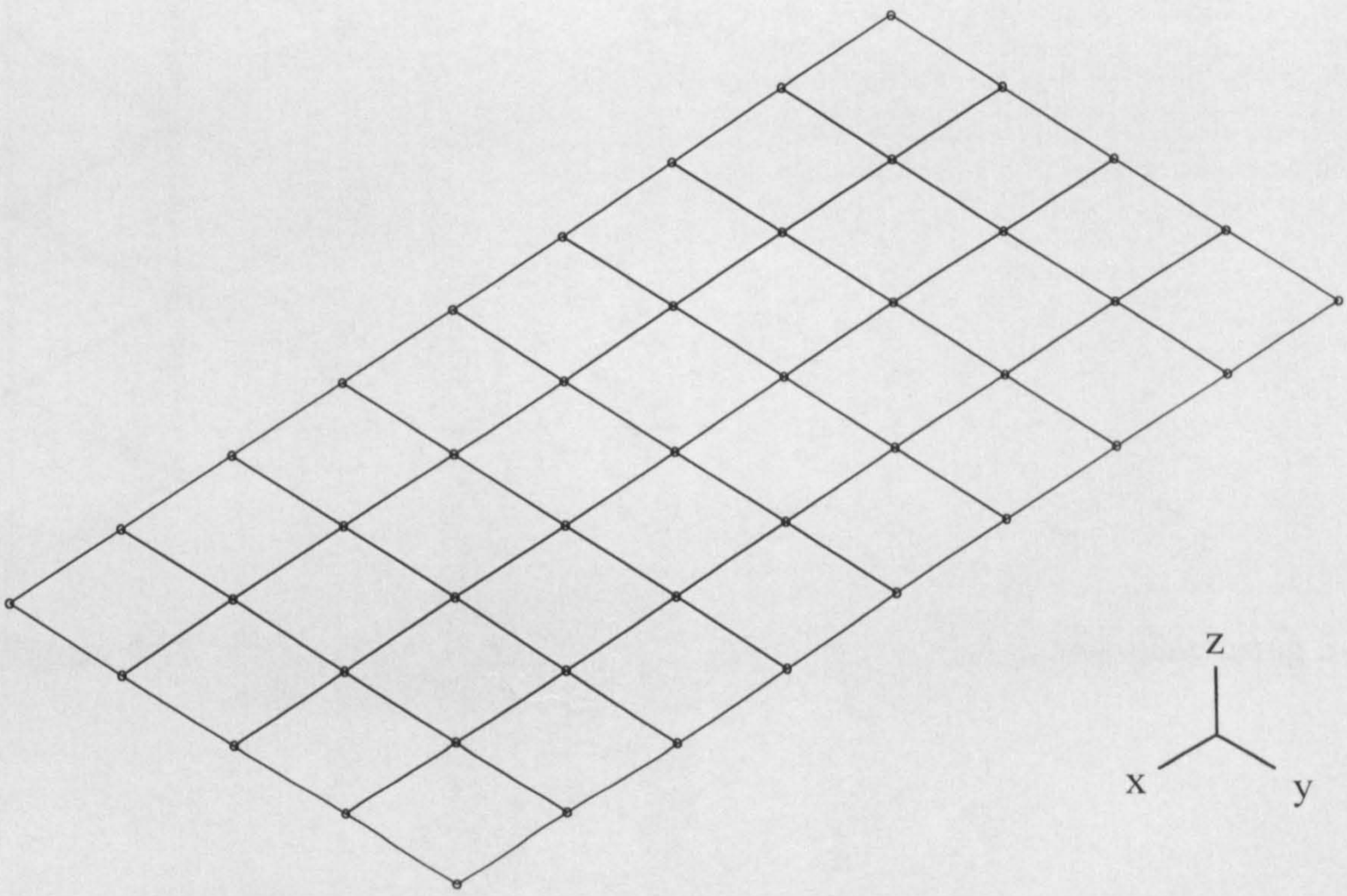

Figure 7.16 Finite element mesh for composite layered rectangular plate case using 4-node quadrilateral element.

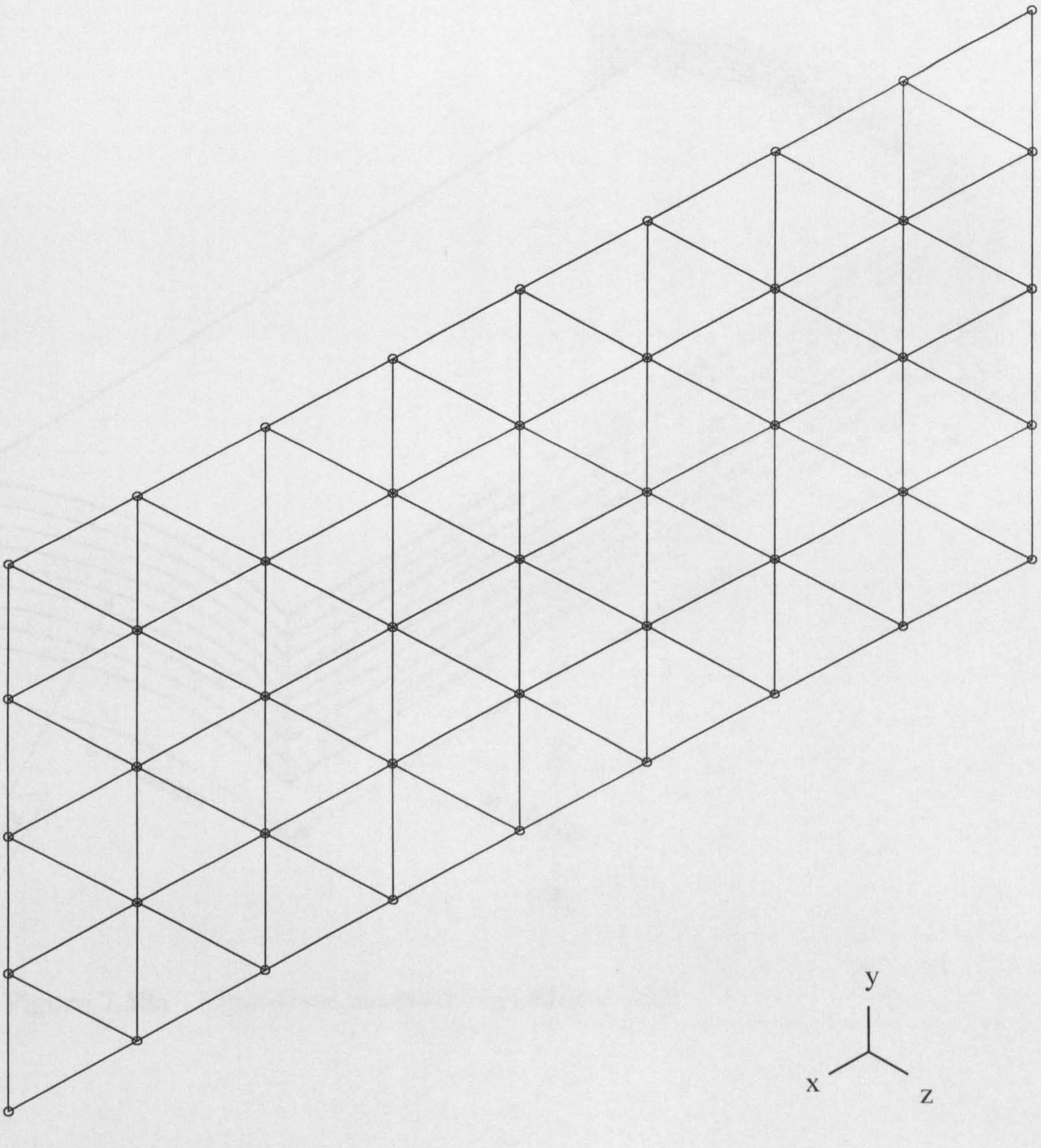

Figure 7.17 Finite element mesh for composite layered rectangular plate using 3-node triangular element.

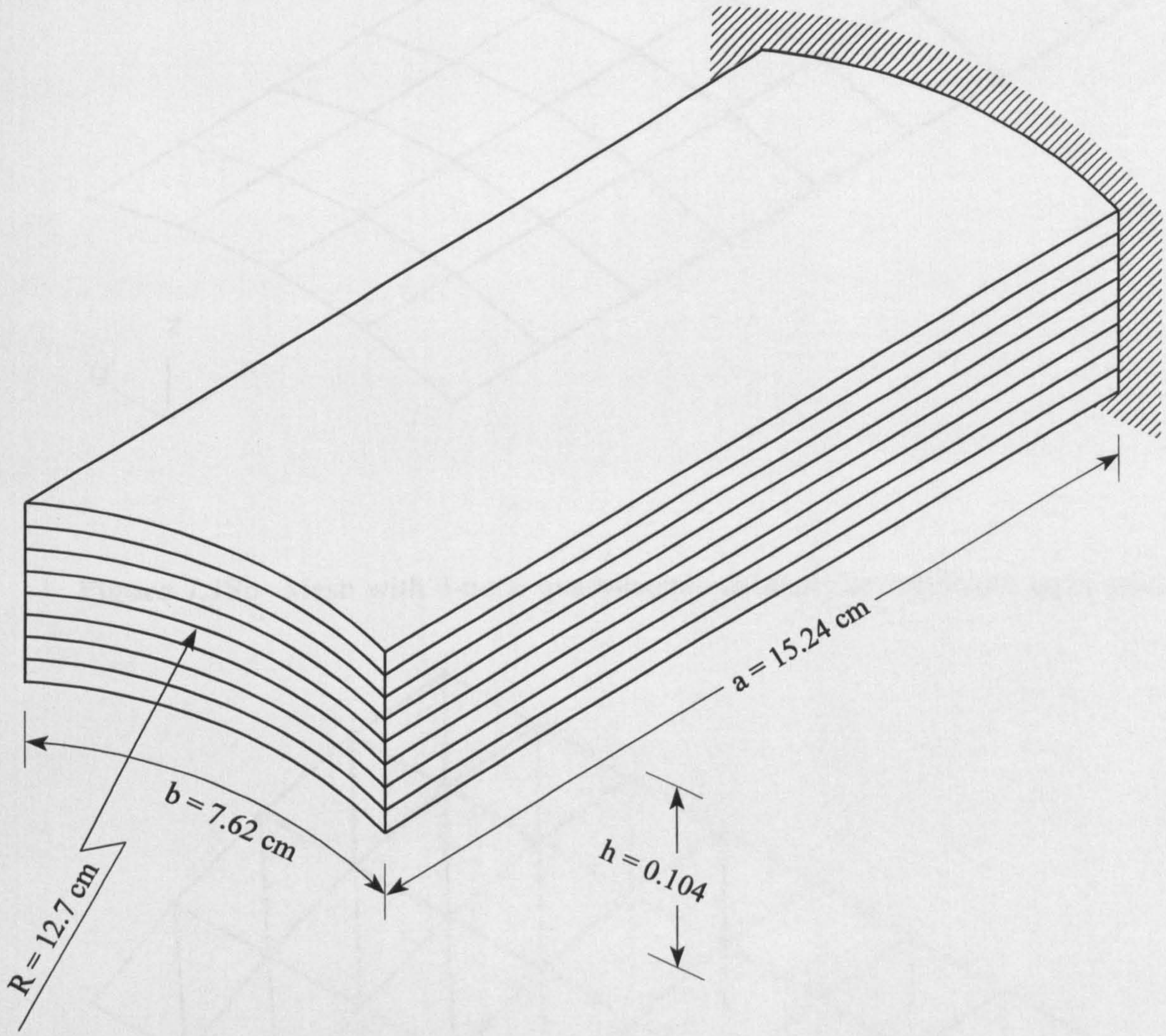

Figure 7.18a Eight-layer composite cylindrical shell

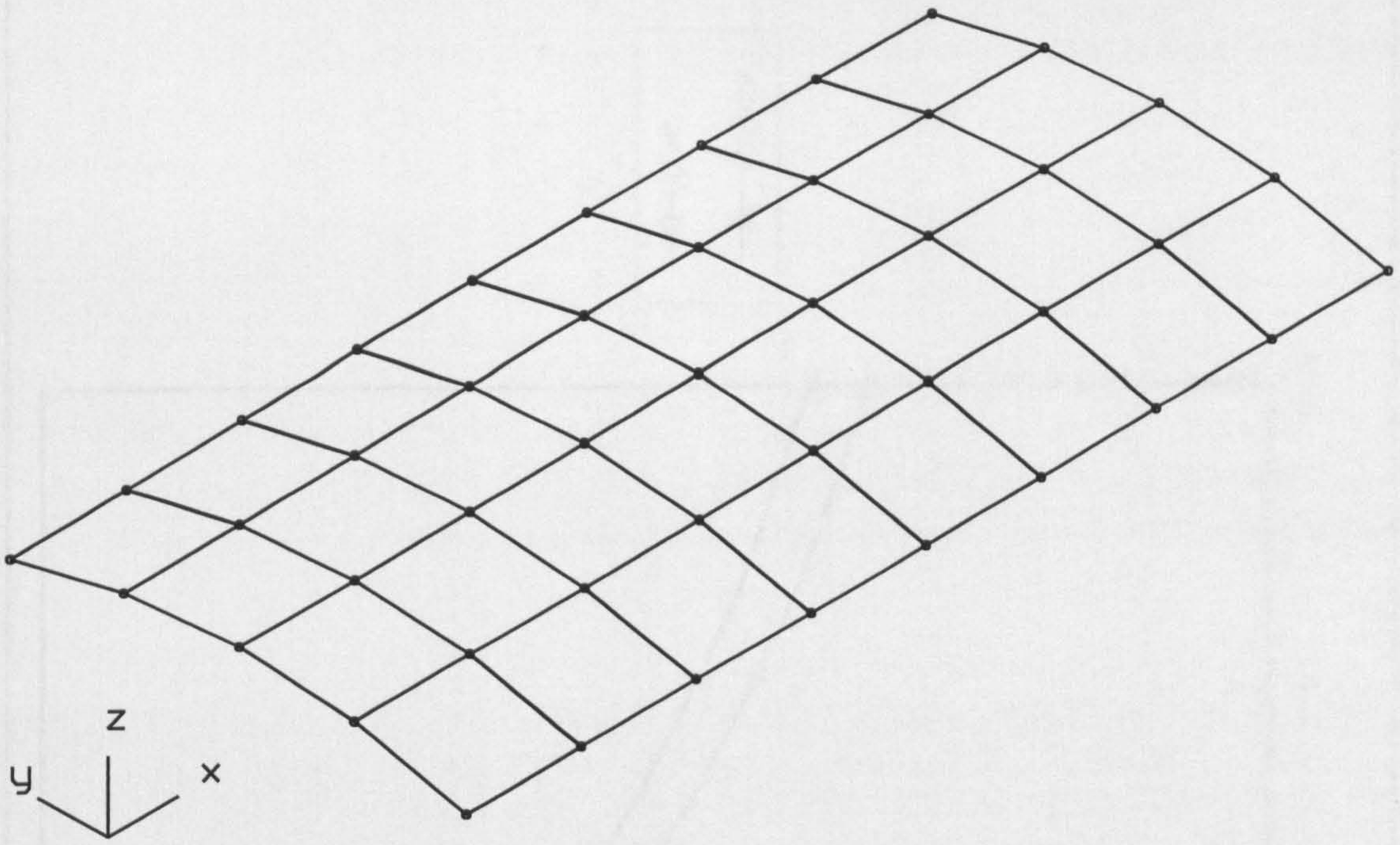

Figure 7.18b Mesh with 4-node quadrilateral element for composite layer shell.

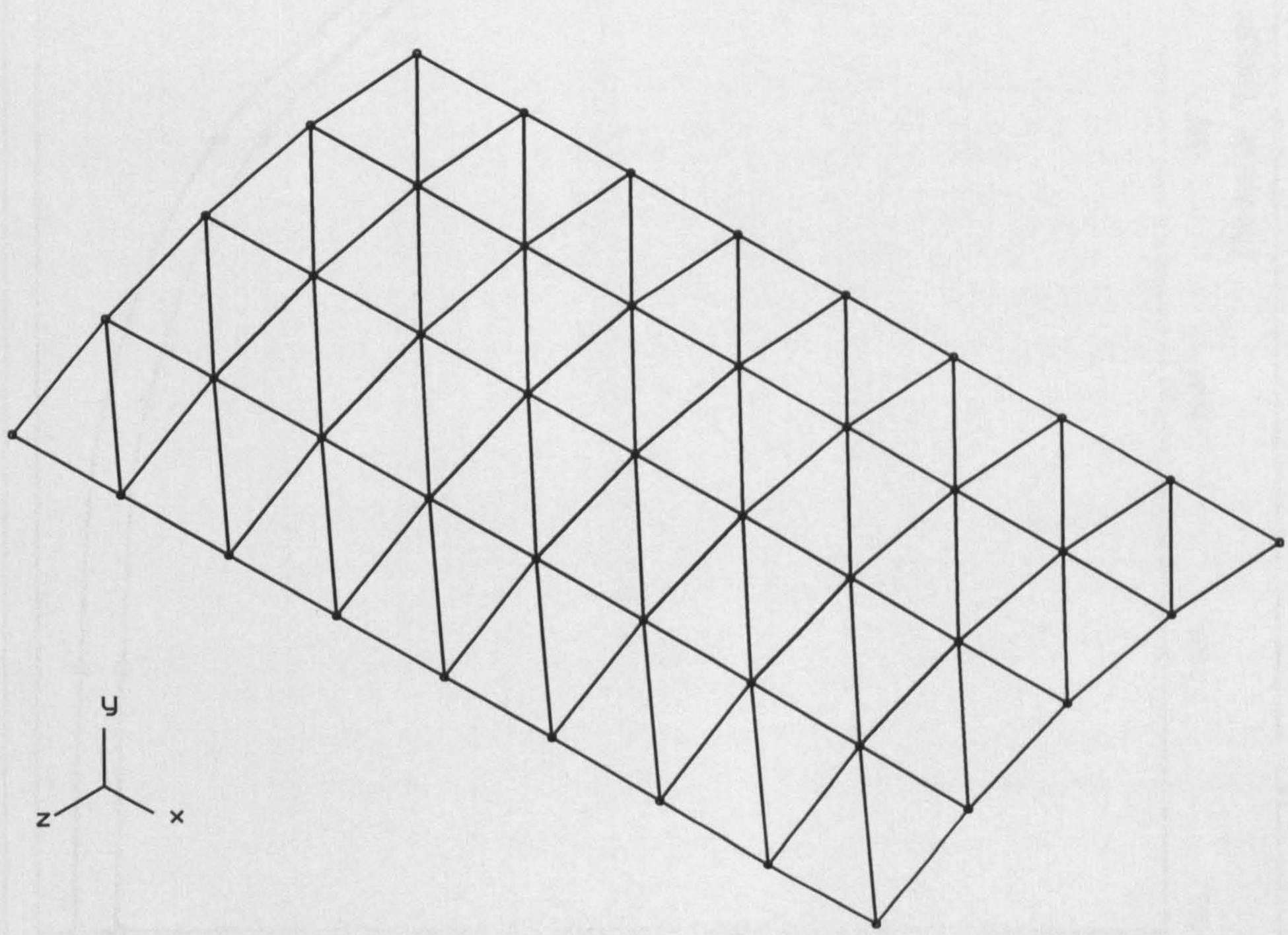

Figure 7.18c Mesh with 3-node triangle element for composite layer shell.

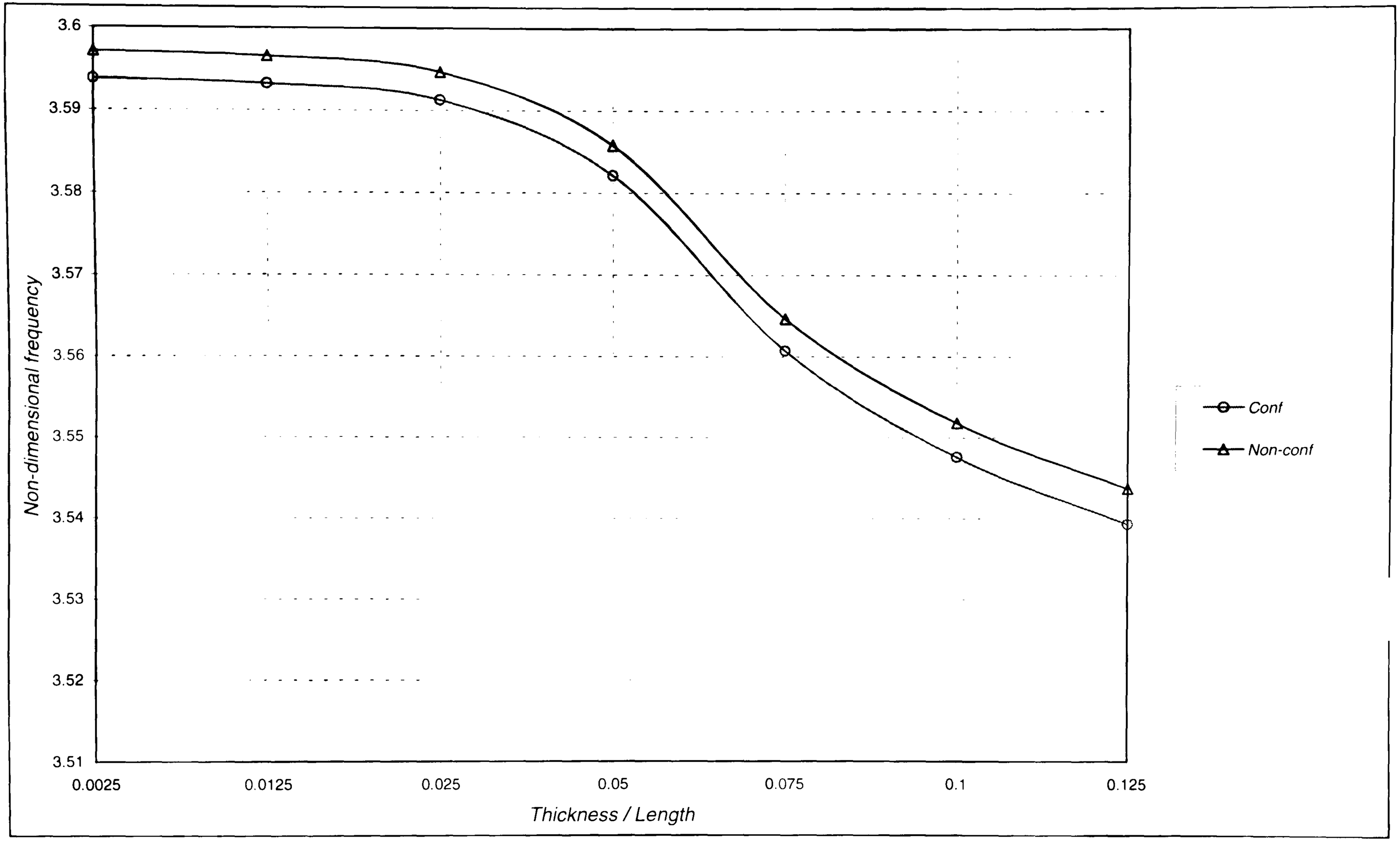

Figure 7.19 First non-dimensional natural frequency for a non-rotating flat plate.

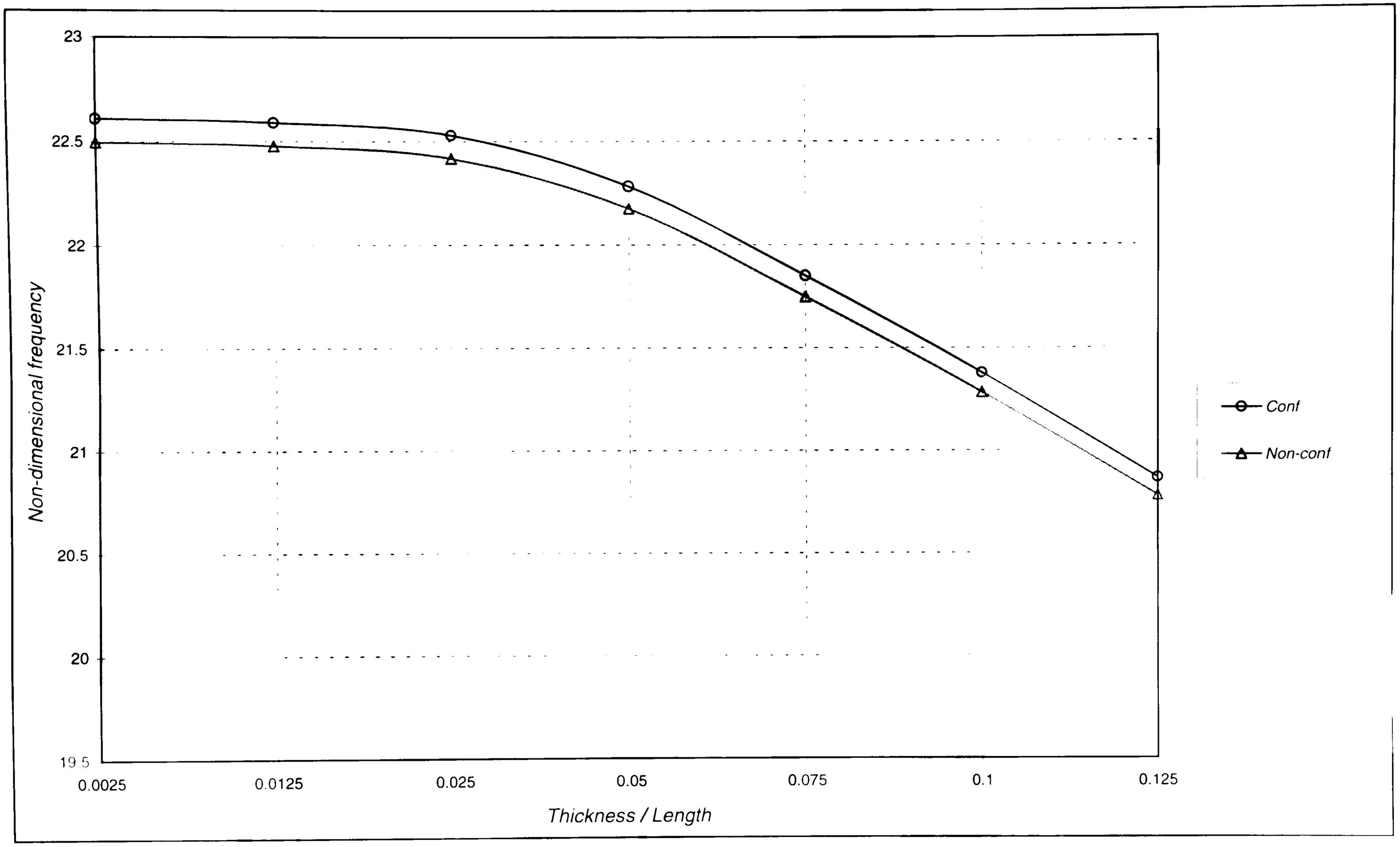

Fig 7.20 Second non-dimensional natural frequency for a non-rotating flat plate.

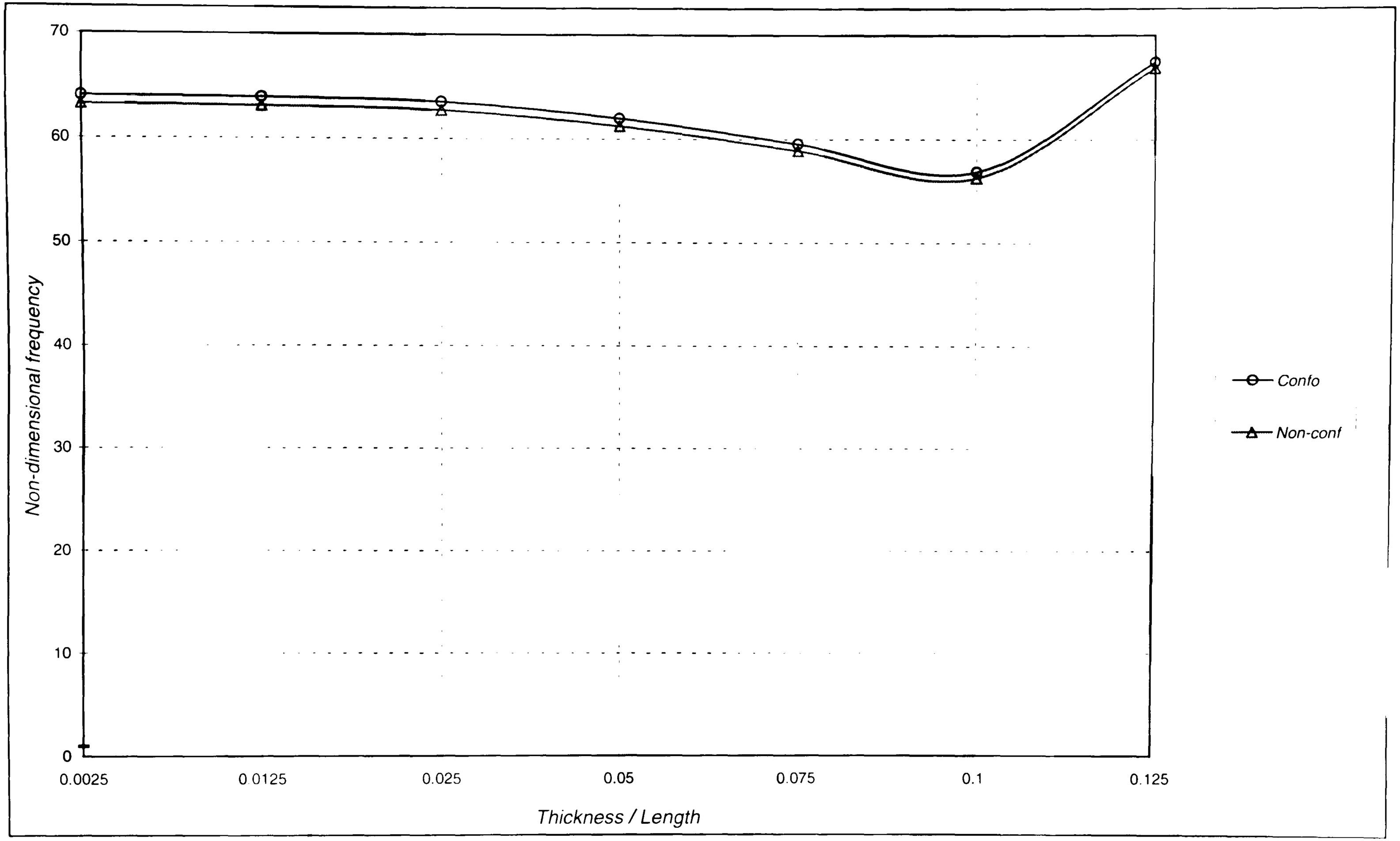

Figure 7.21 Third non-dimensional natural frequency for a non-rotating flat plate.

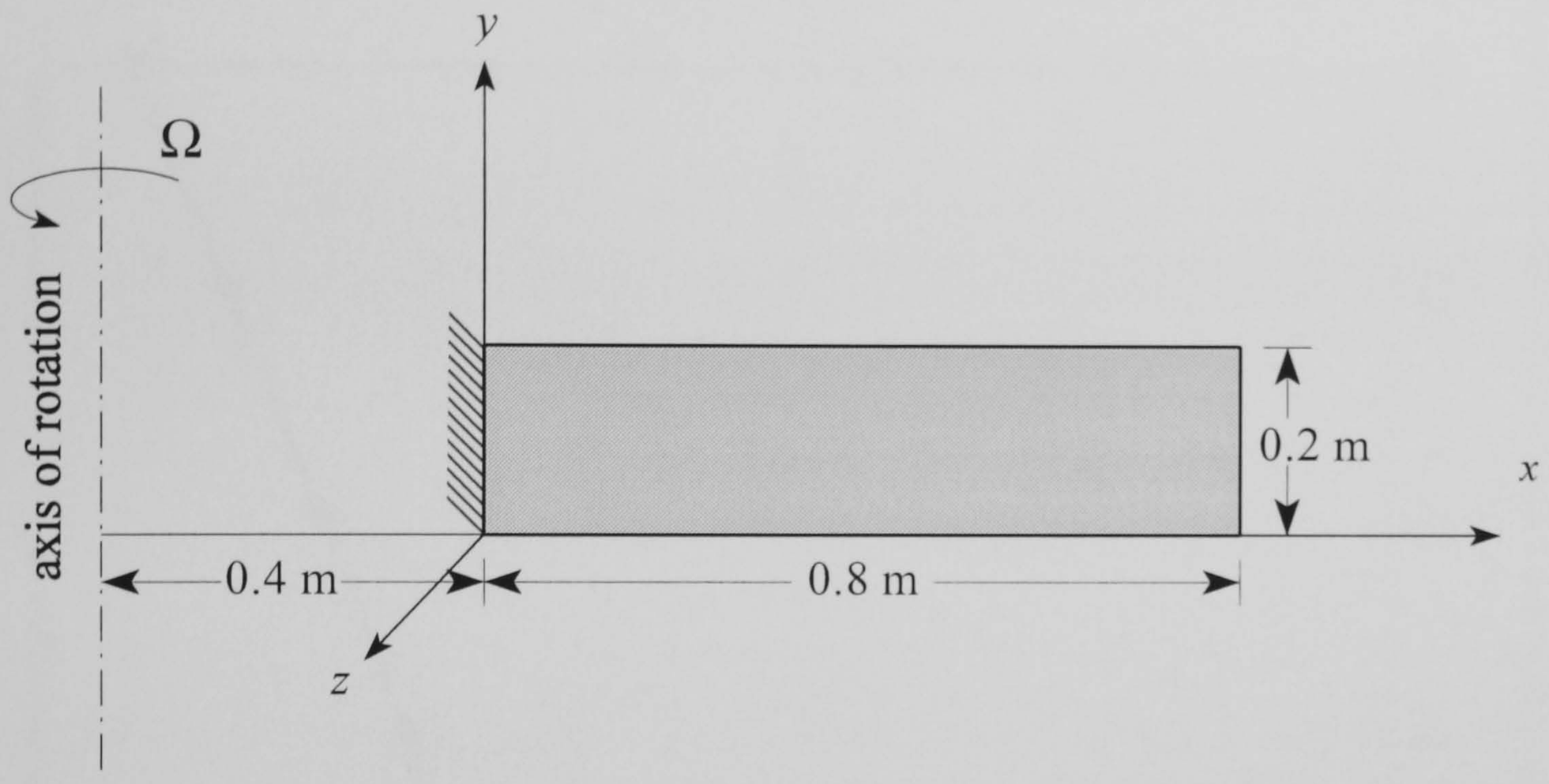

Figure 7.22 Axis of rotation for plate.

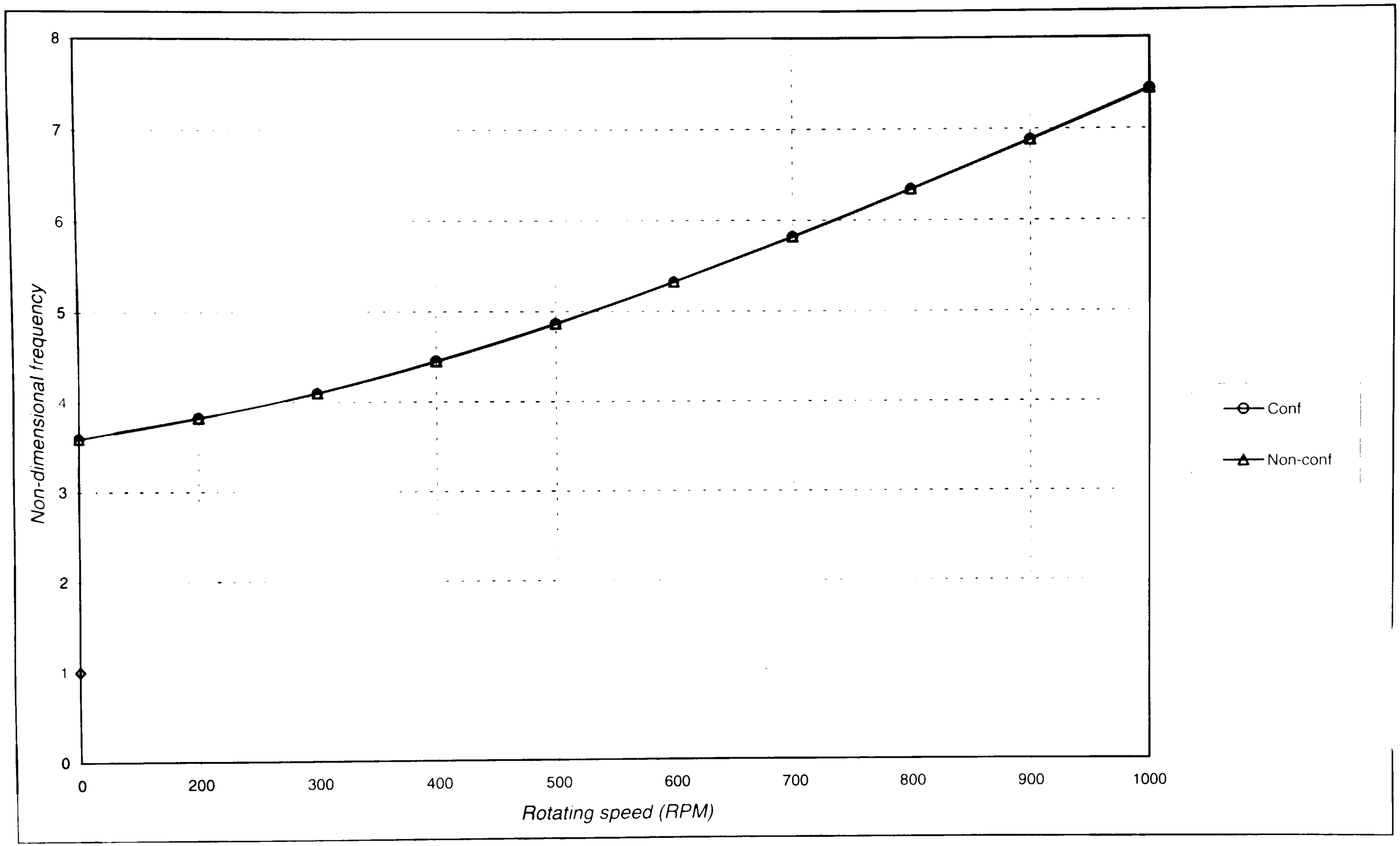

Figure 7.23 First non-dimensional natural frequency for rotating thin flat plate.

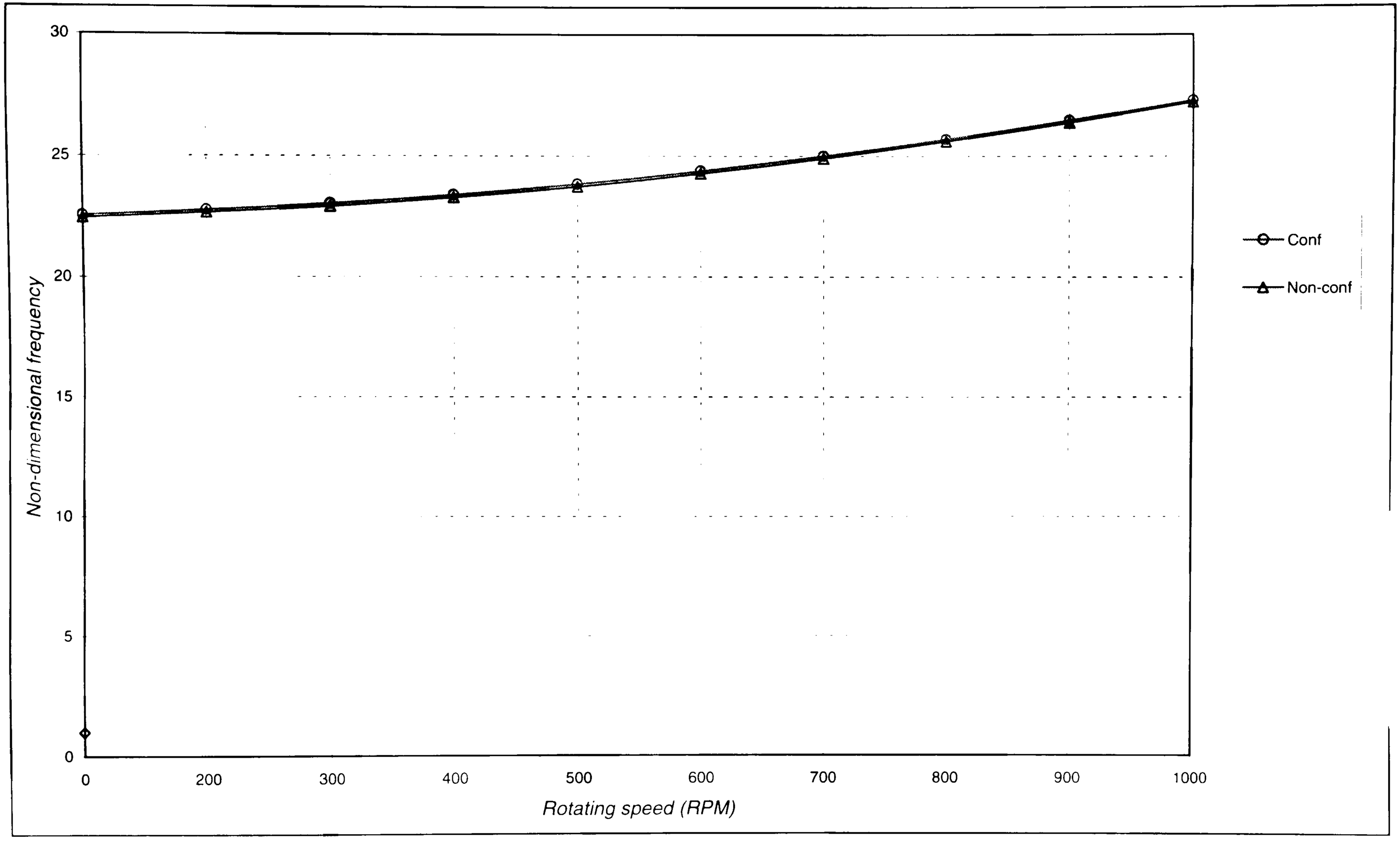

Figure 7.24 Second non-dimensional natural frequency for rotating thin flat plate.

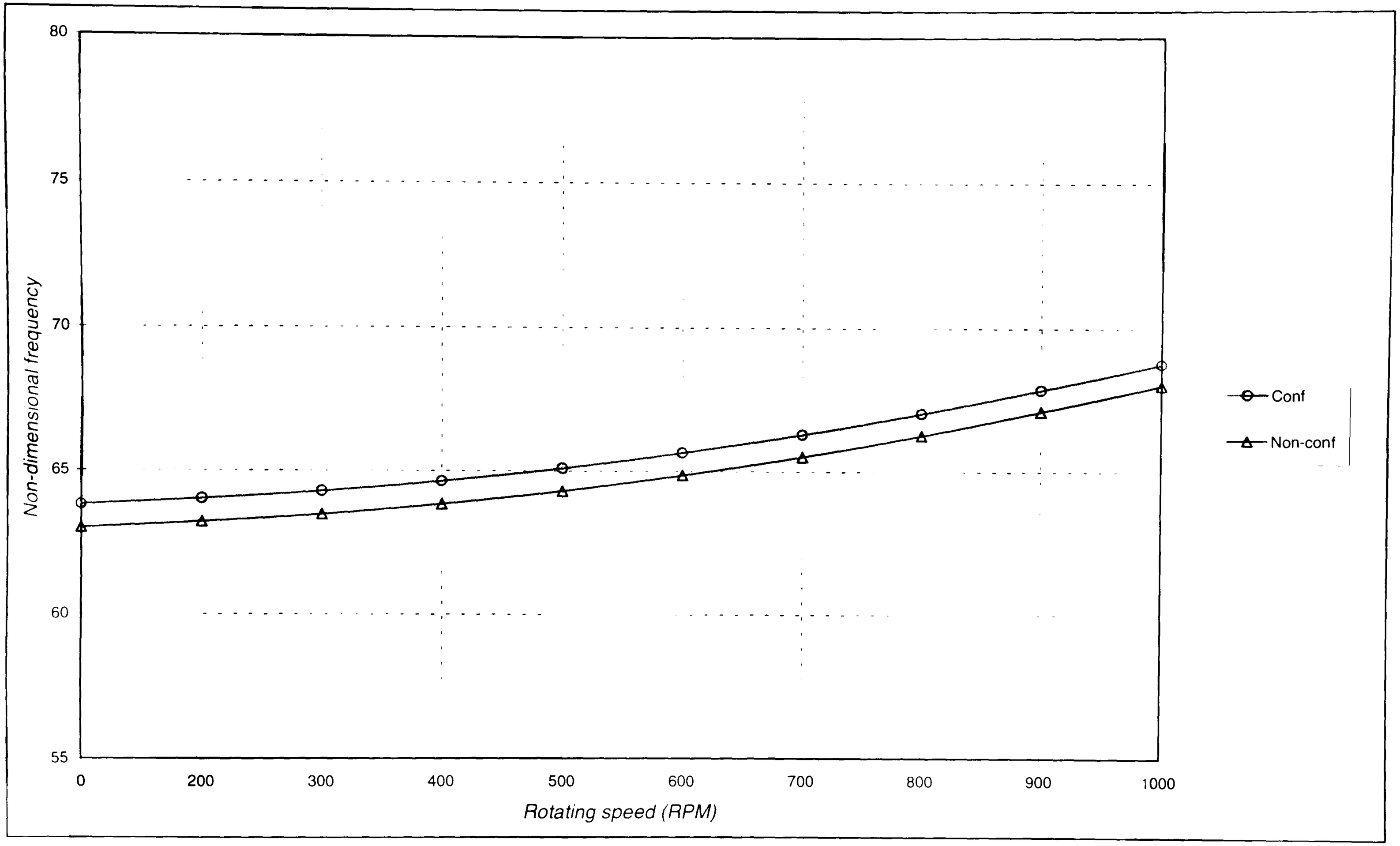

Figure 7.25 Third non-dimensional natural frequency for rotating thin flat plate.

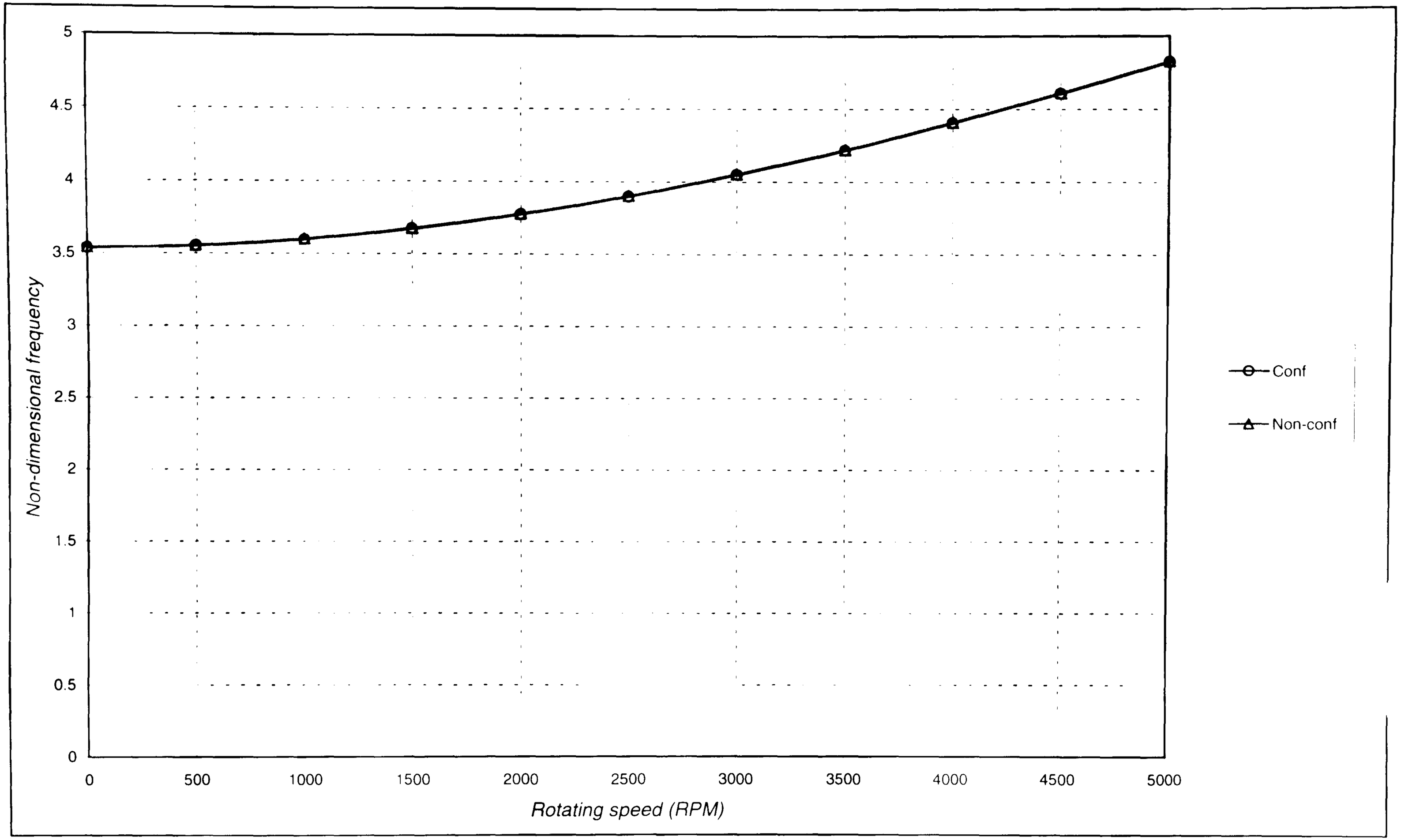

Figure 7.26 First non-dimensional natural frequency for rotating thick flat plate.

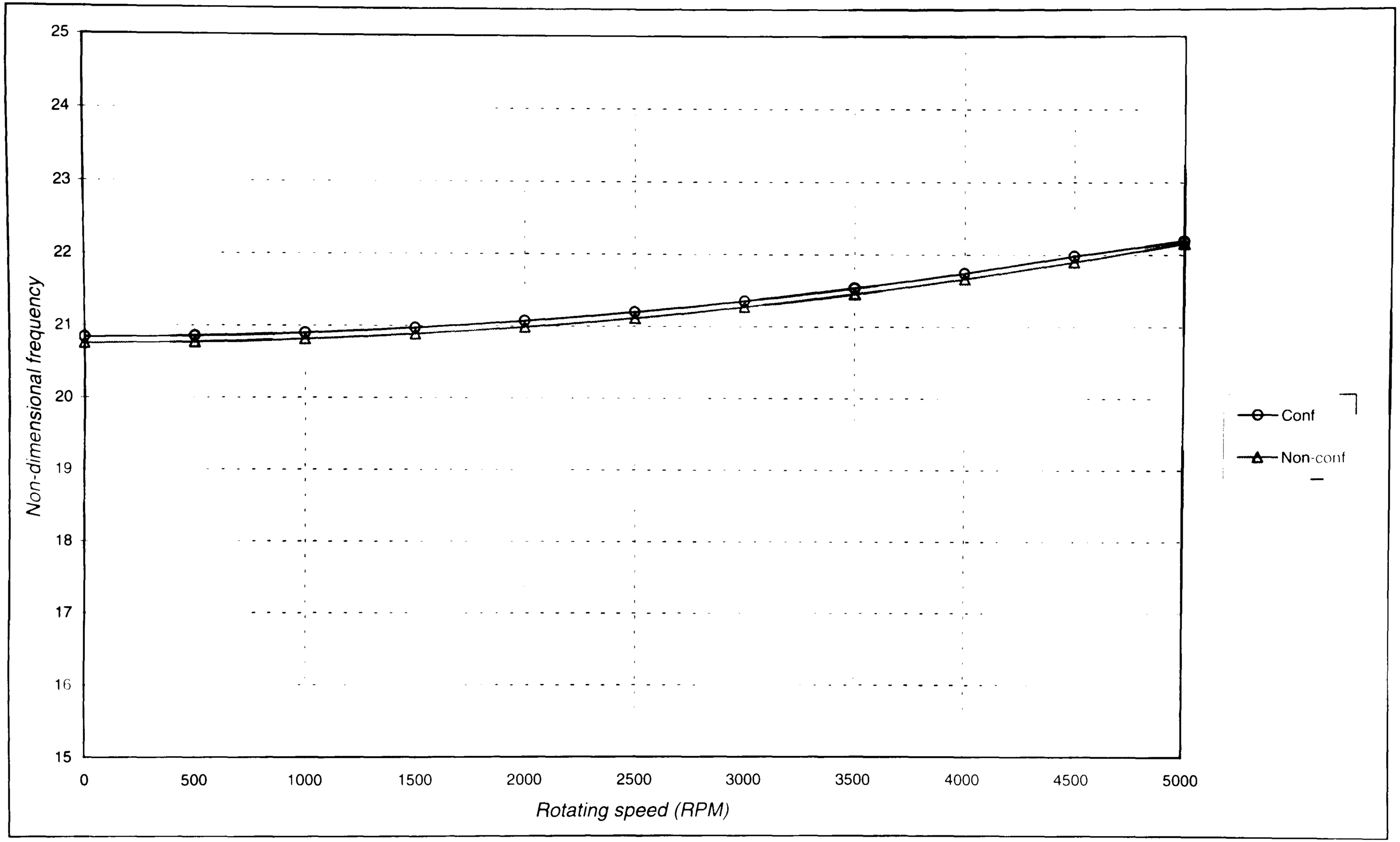

Figure 7.27 Second non-dimensional natural frequency for rotating thick flat plate.

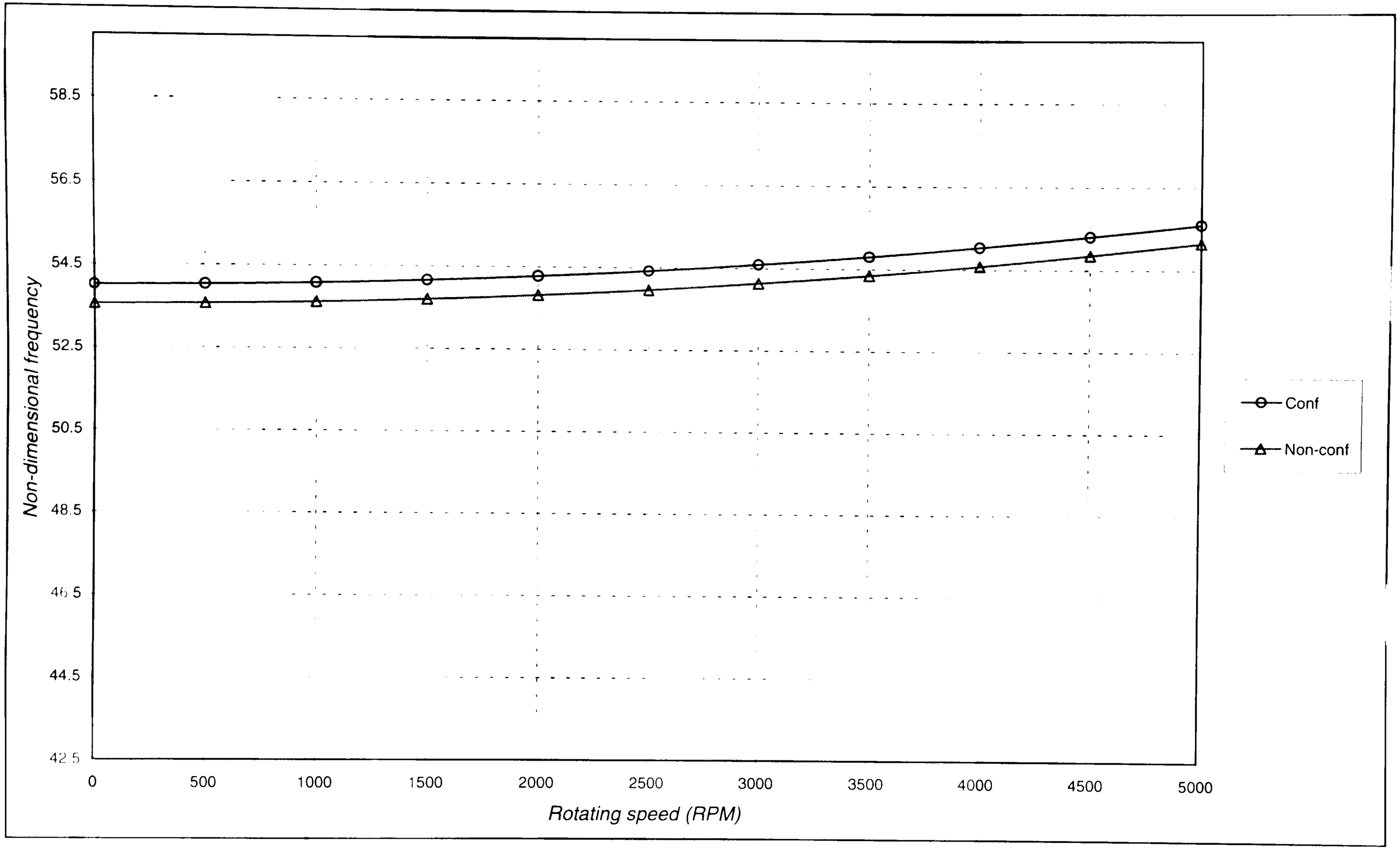

Figure 7.28 Third non-dimensional natural frequency for rotating thick flat plate.

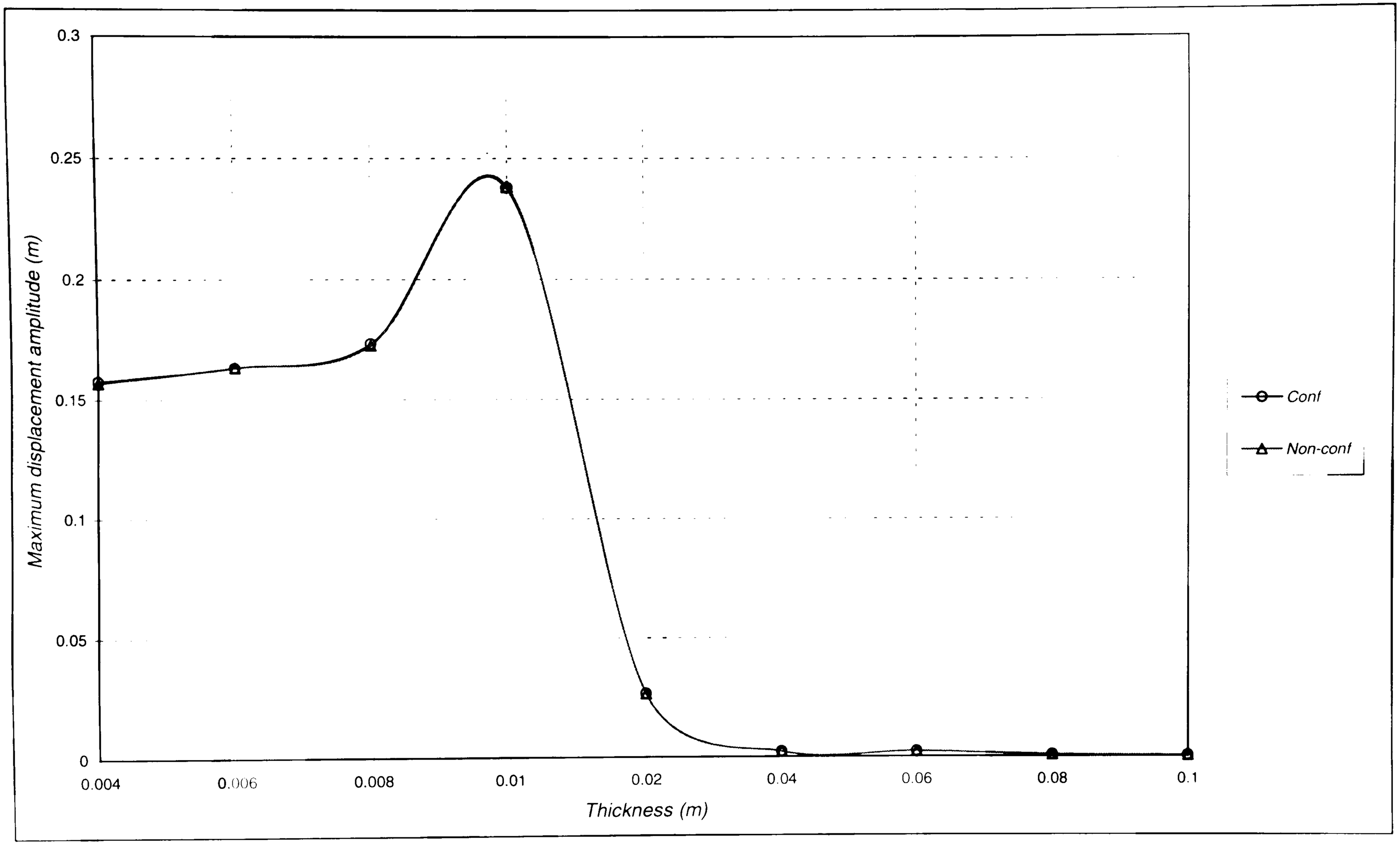

Figure 7.29 Maximum displacement amplitude versus thickness for non-rotating flat plate under exciting force.

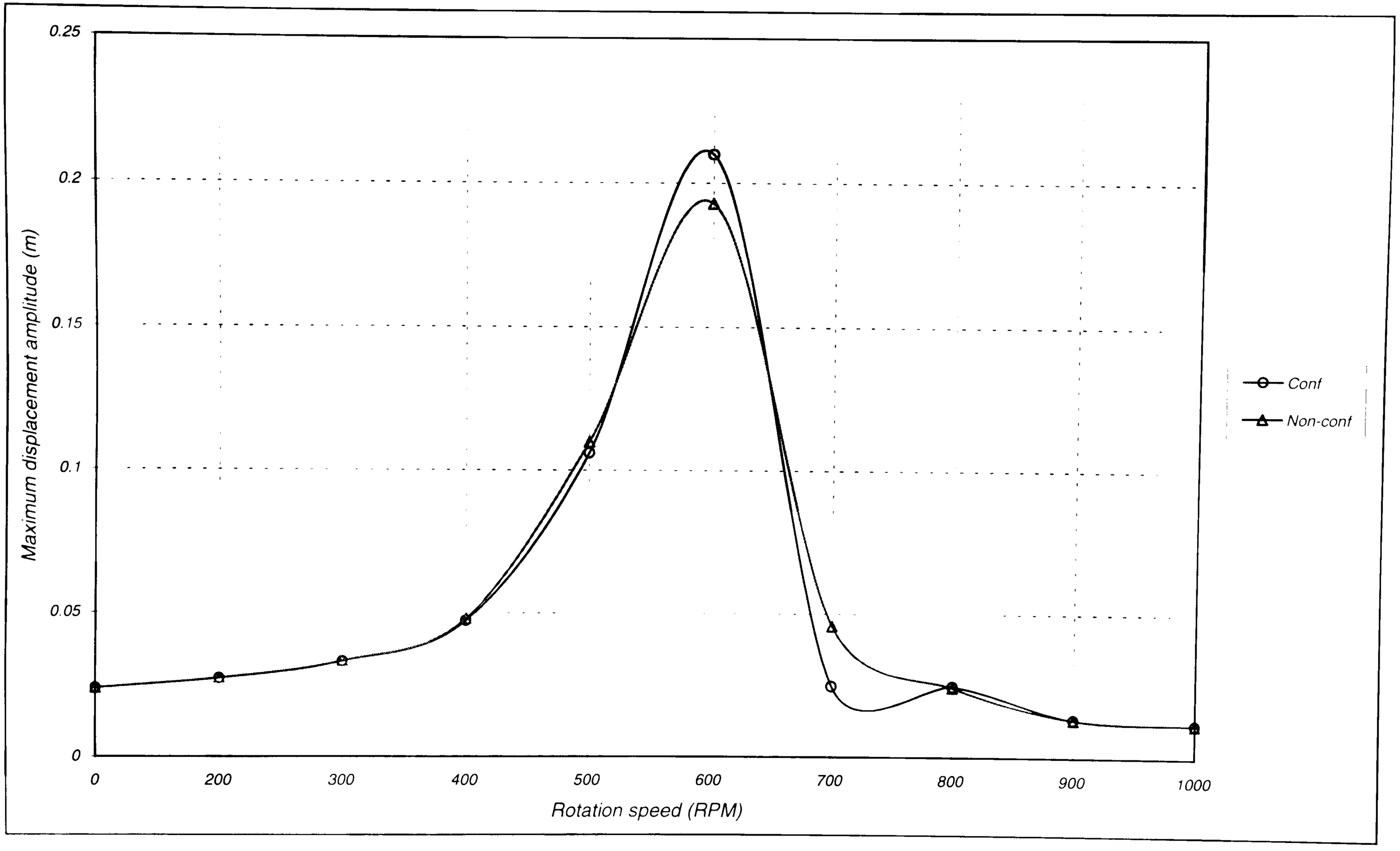

Figure 7.30 Maximum displacement amplitude versus rotation speed for rotating thin flat plate under exciting force.

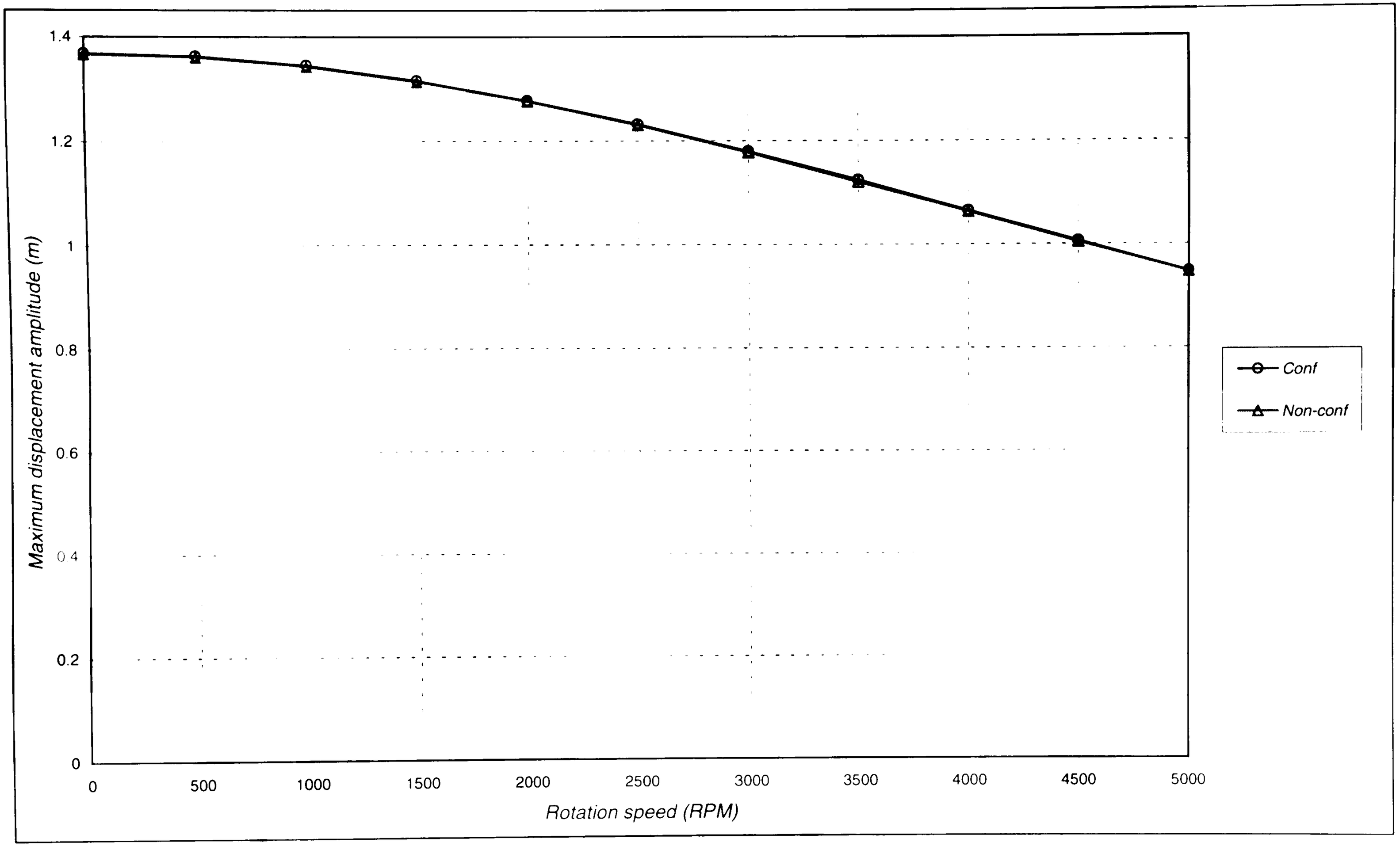

Figure 7.31 Maximum displacement amplitude versus rotation speed for rotating thick flat plate under exciting force.

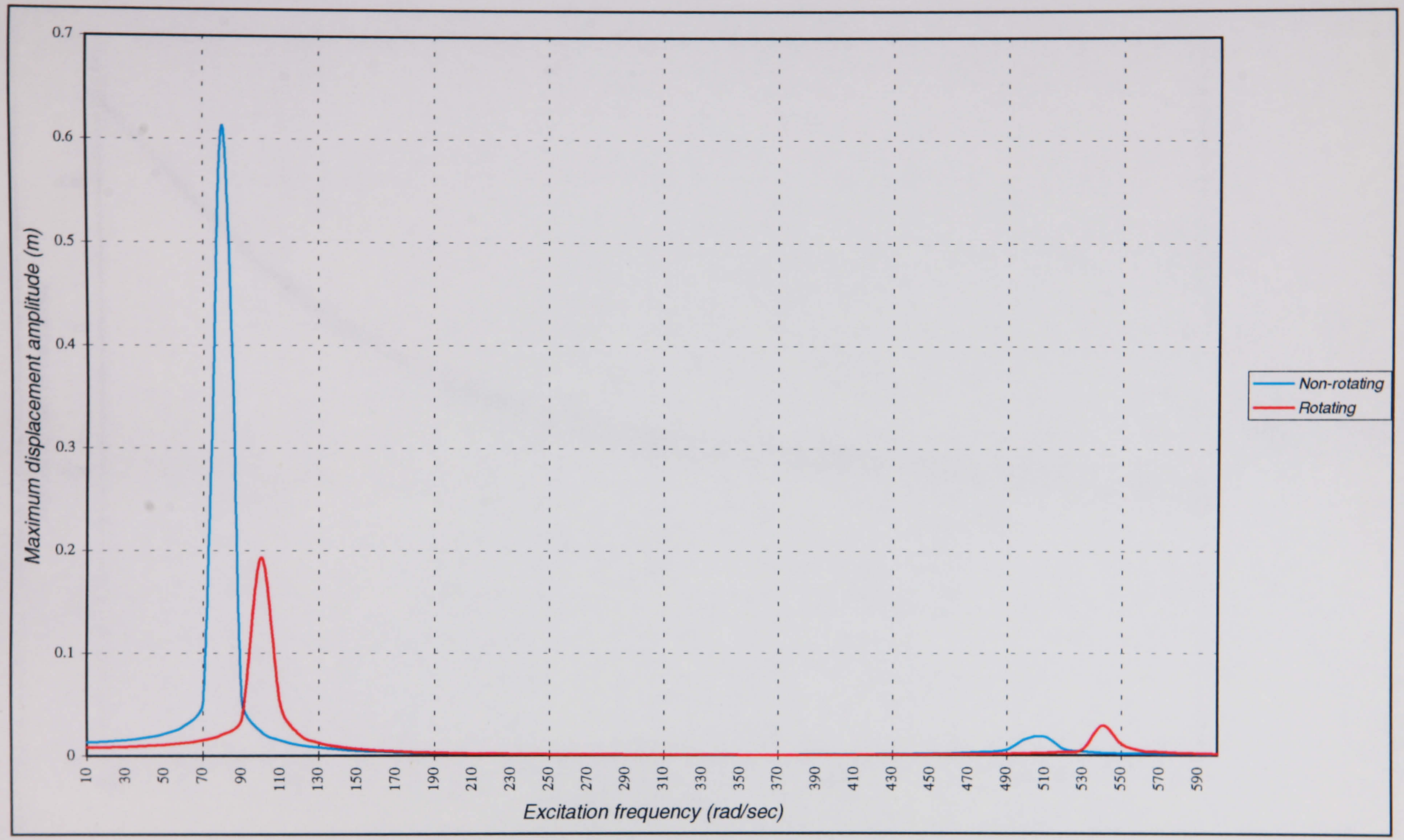

Figure 7.32 Maximum displacement amplitude versus excitation frequency for rotating plate under exciting force.

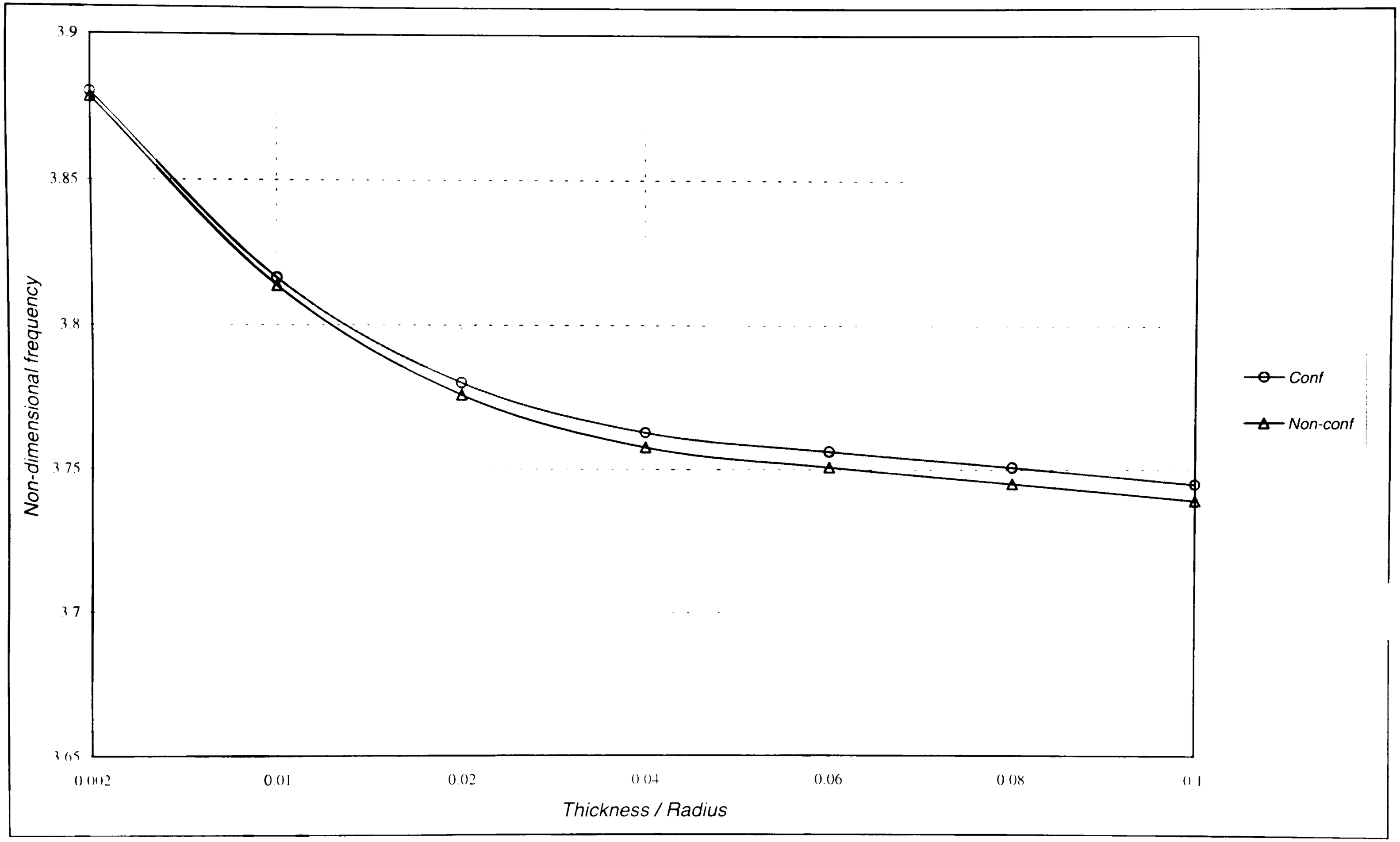

Figure 7.33 First non-dimensional natural frequency for a non-rotating curved shell.

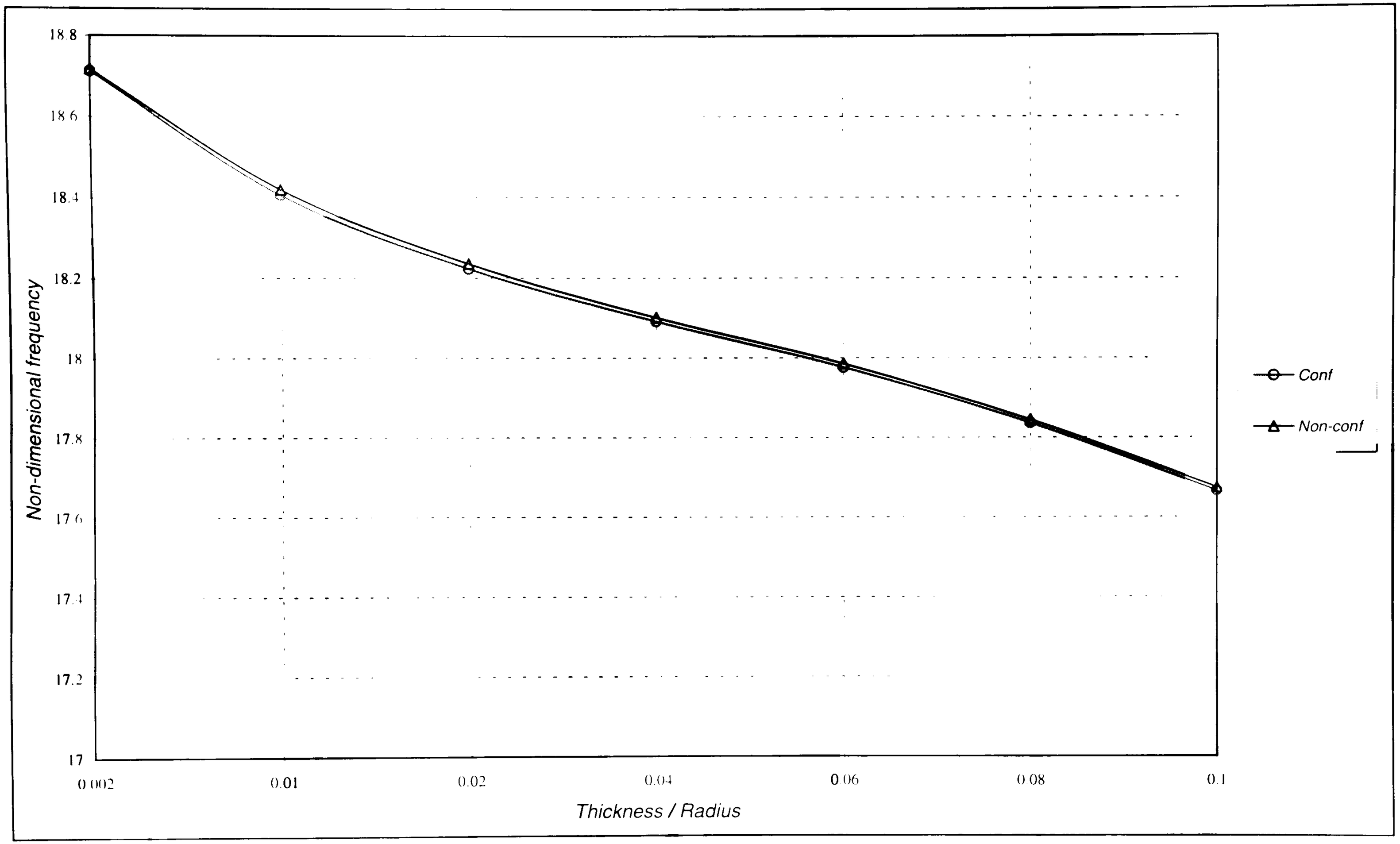

Figure 7.34 Second non-dimensional natural frequency for a non-rotating curved shell.

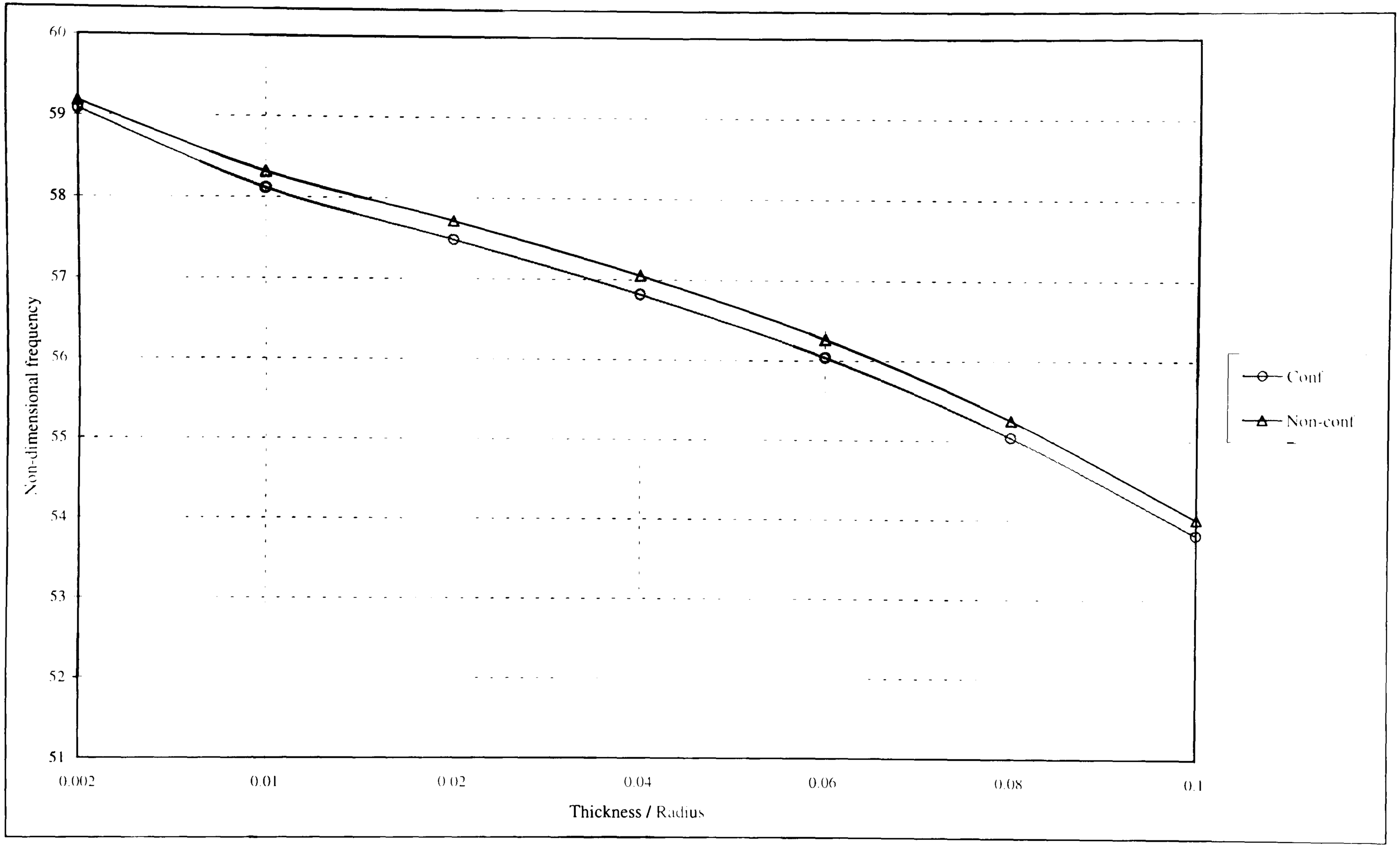

Figure 7.35 Third non-dimensional natural frequency for a non-rotating curved shell.

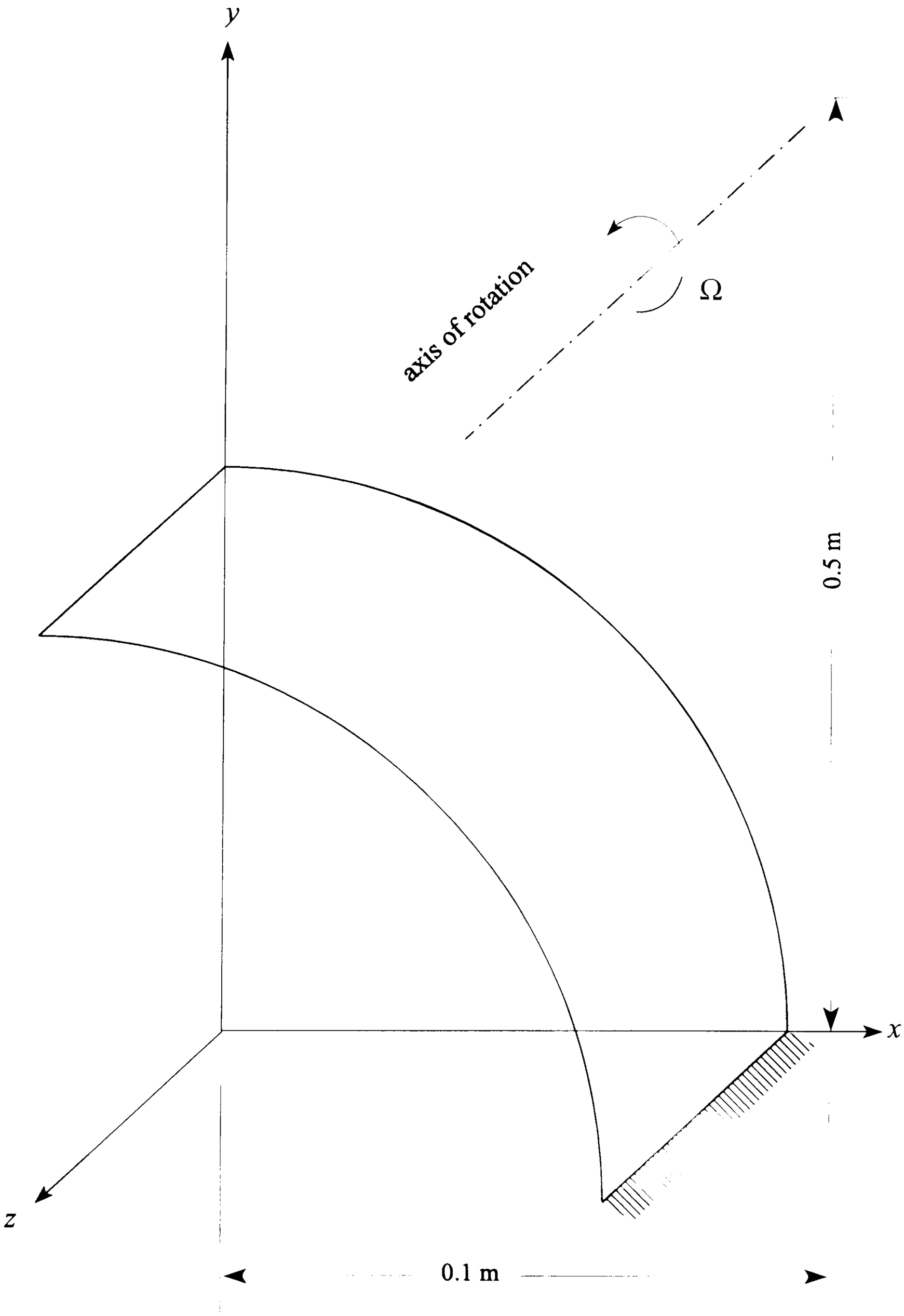

Figure 7.36 Axis of rotation for circular shell.

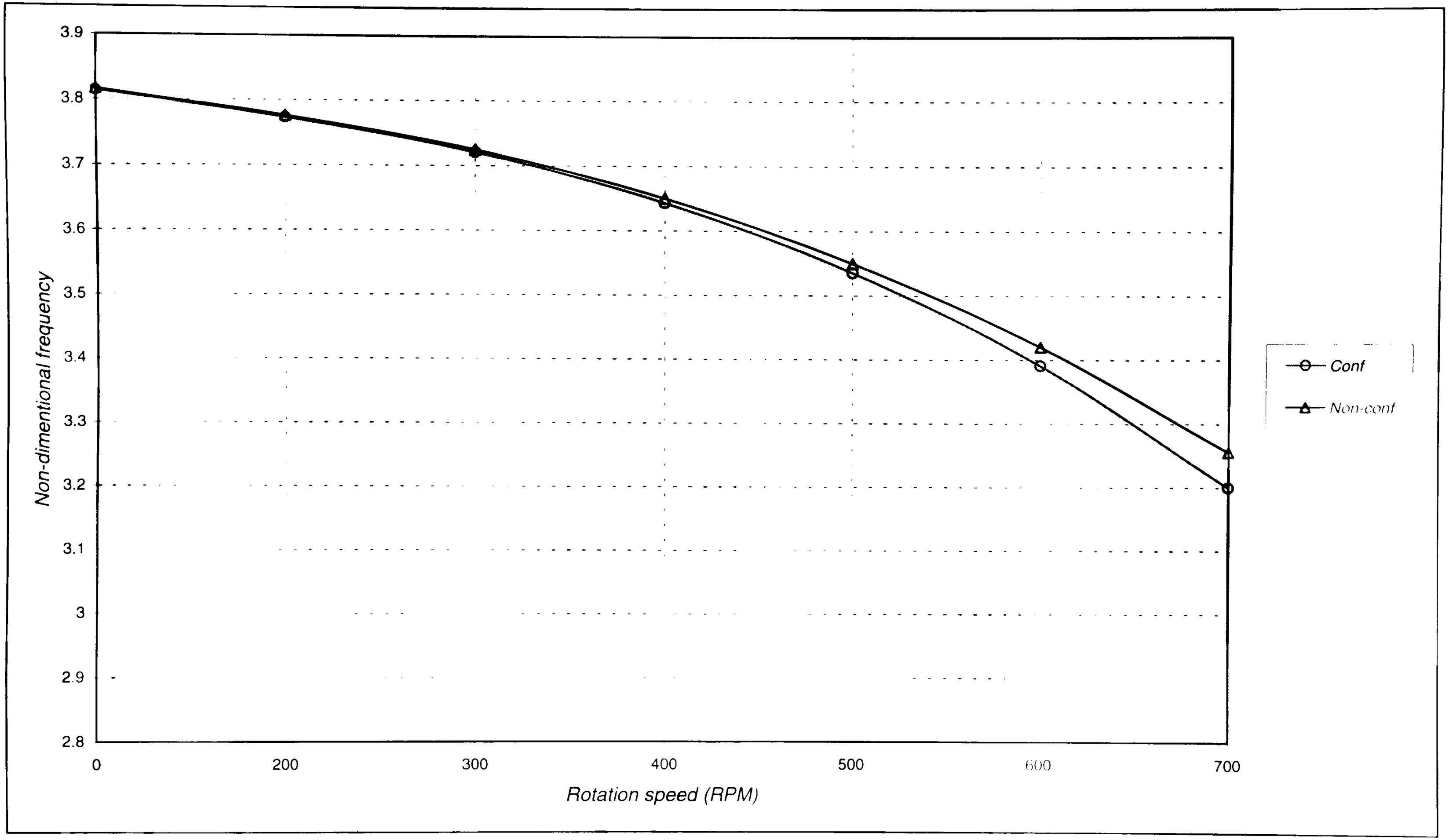

Figure 7.37 First non-dimensional natural frequency for rotating thin curved shell.

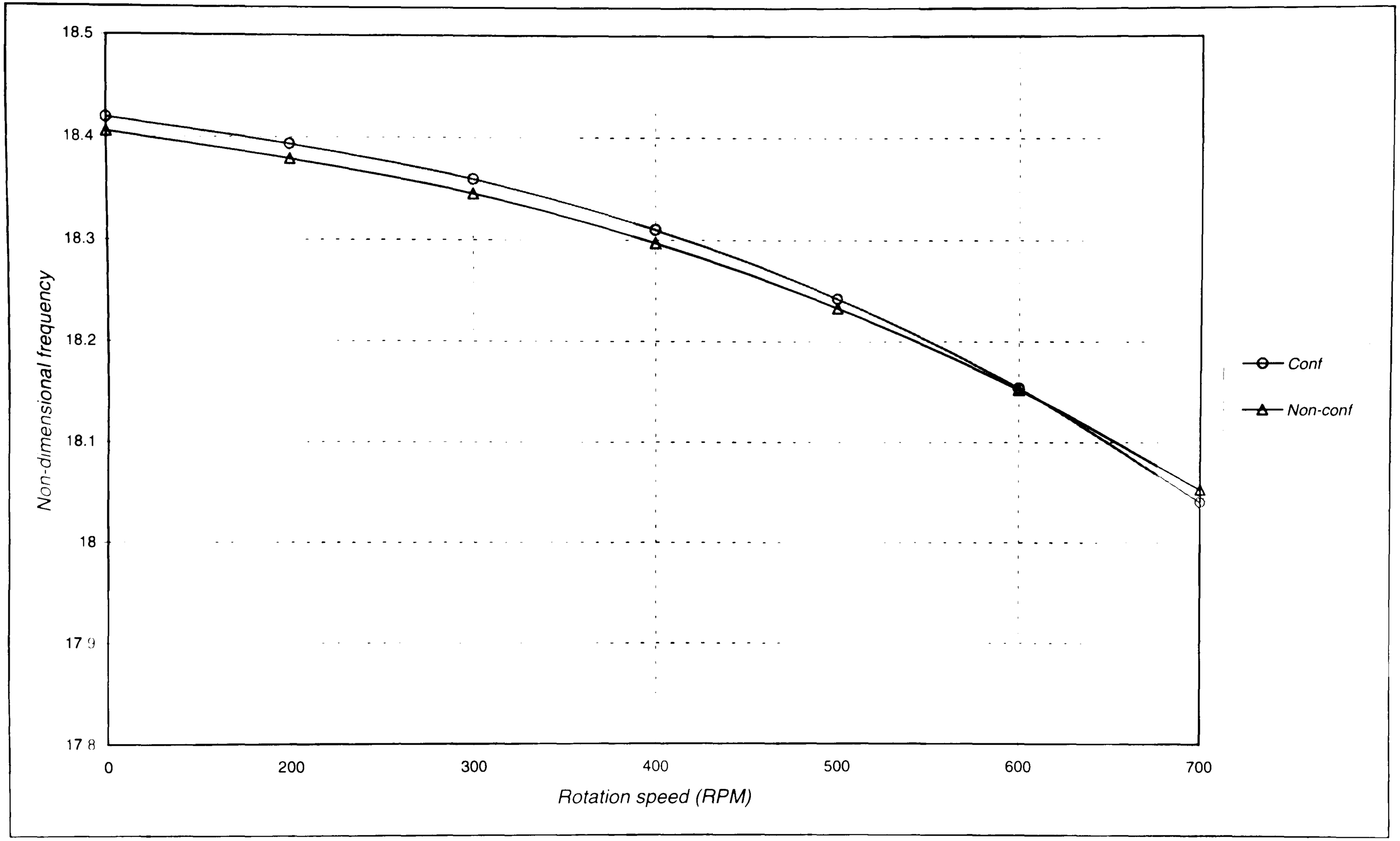

Figure 7.38 Second non-dimensional natural frequency for rotating thin curved shell.

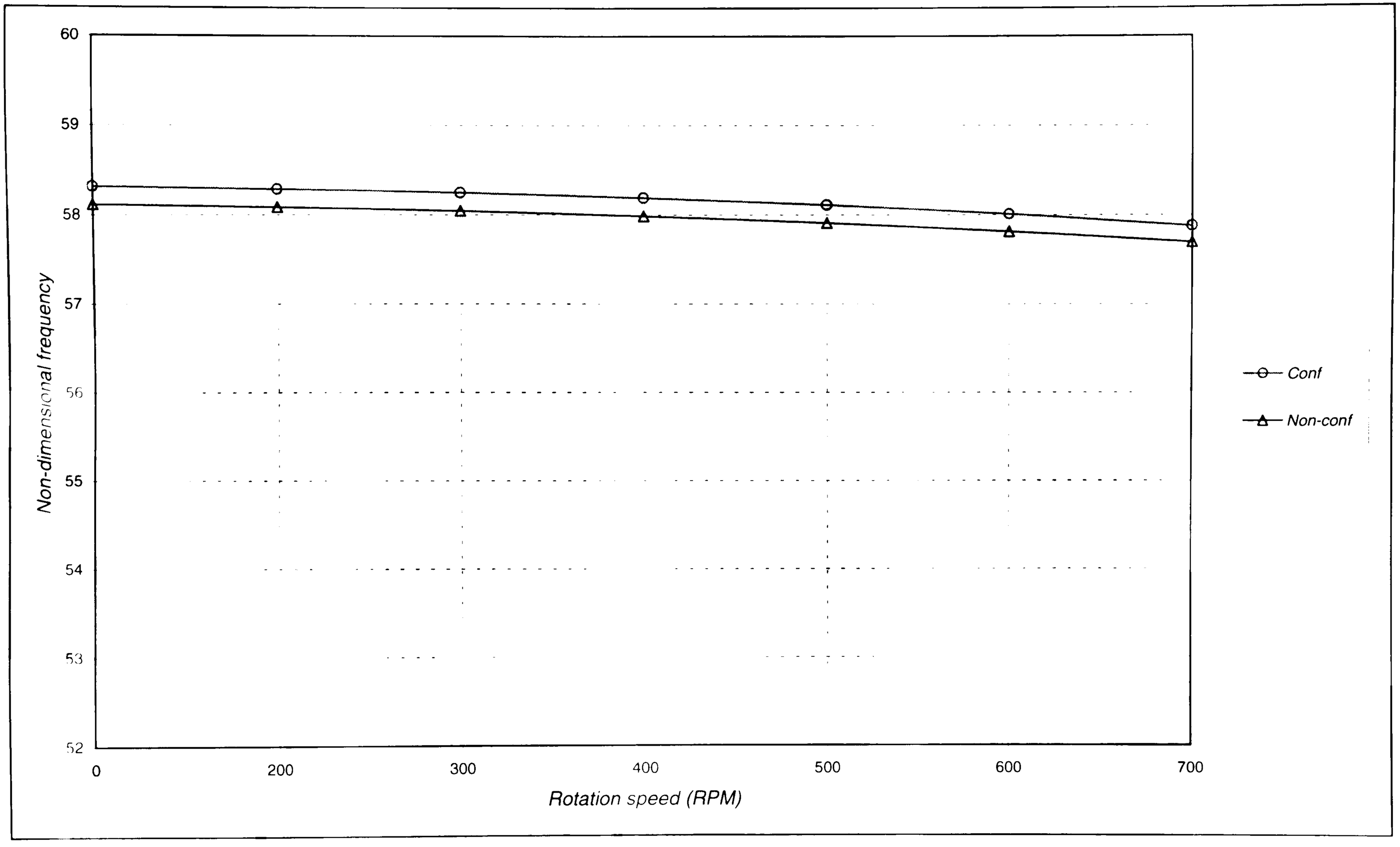

Figure 7.39 Third non-dimensional natural frequency for rotating thin curved shell.

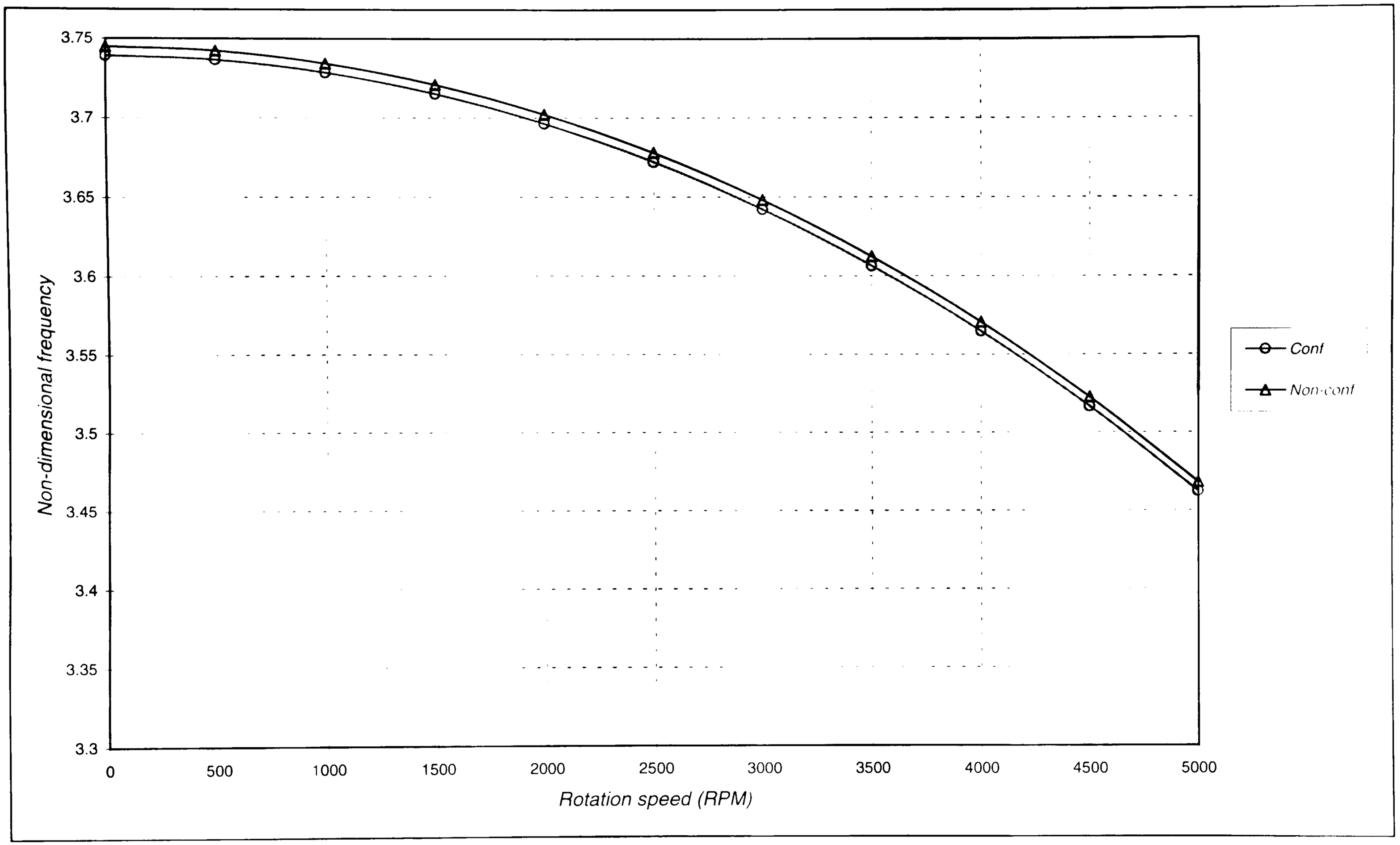

Figure 7.40 First non-dimensional natural frequency for rotating thick curved shell.

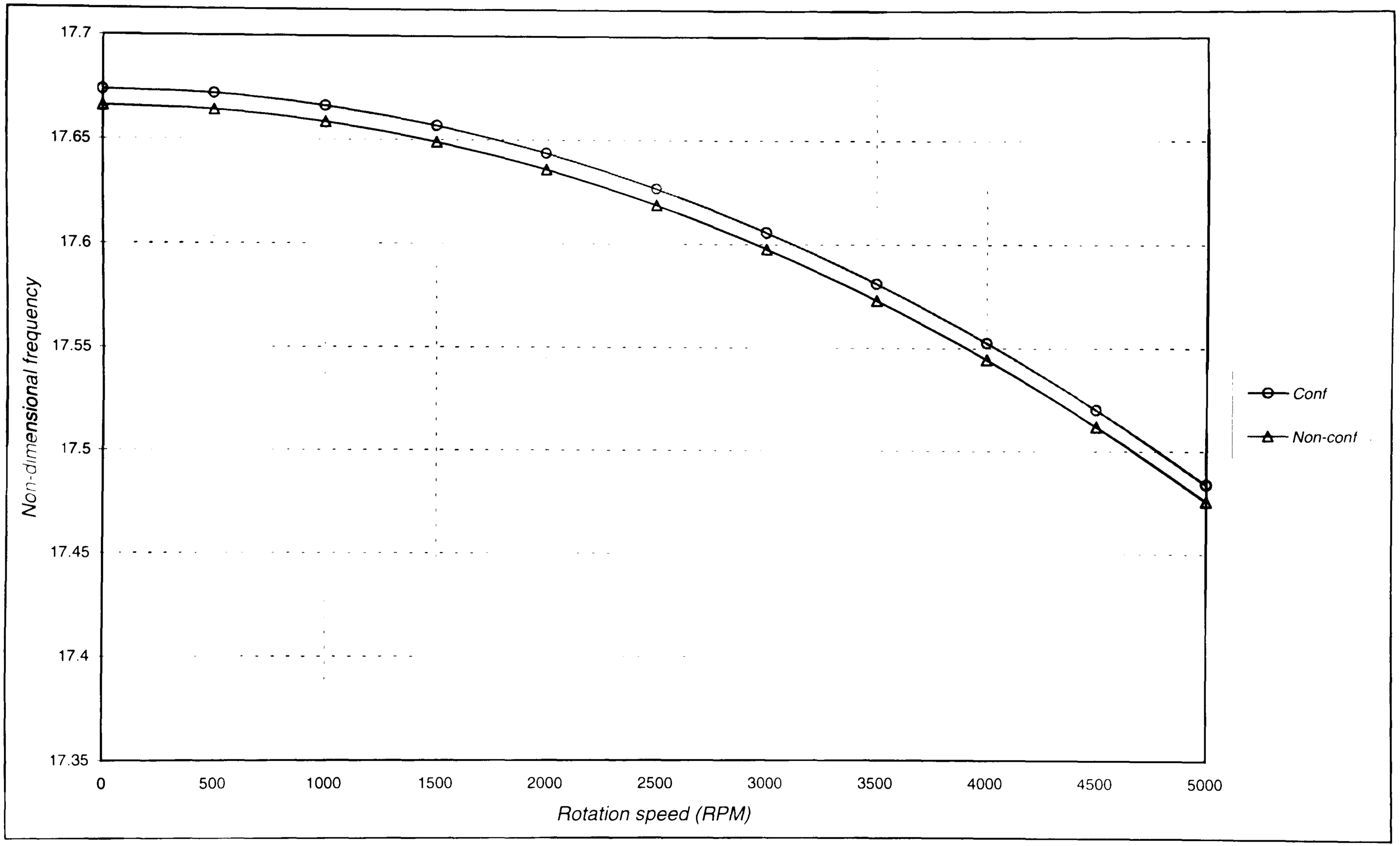

Figure 7.41 Second non-dimensional natural frequency for rotating thick curved shell.

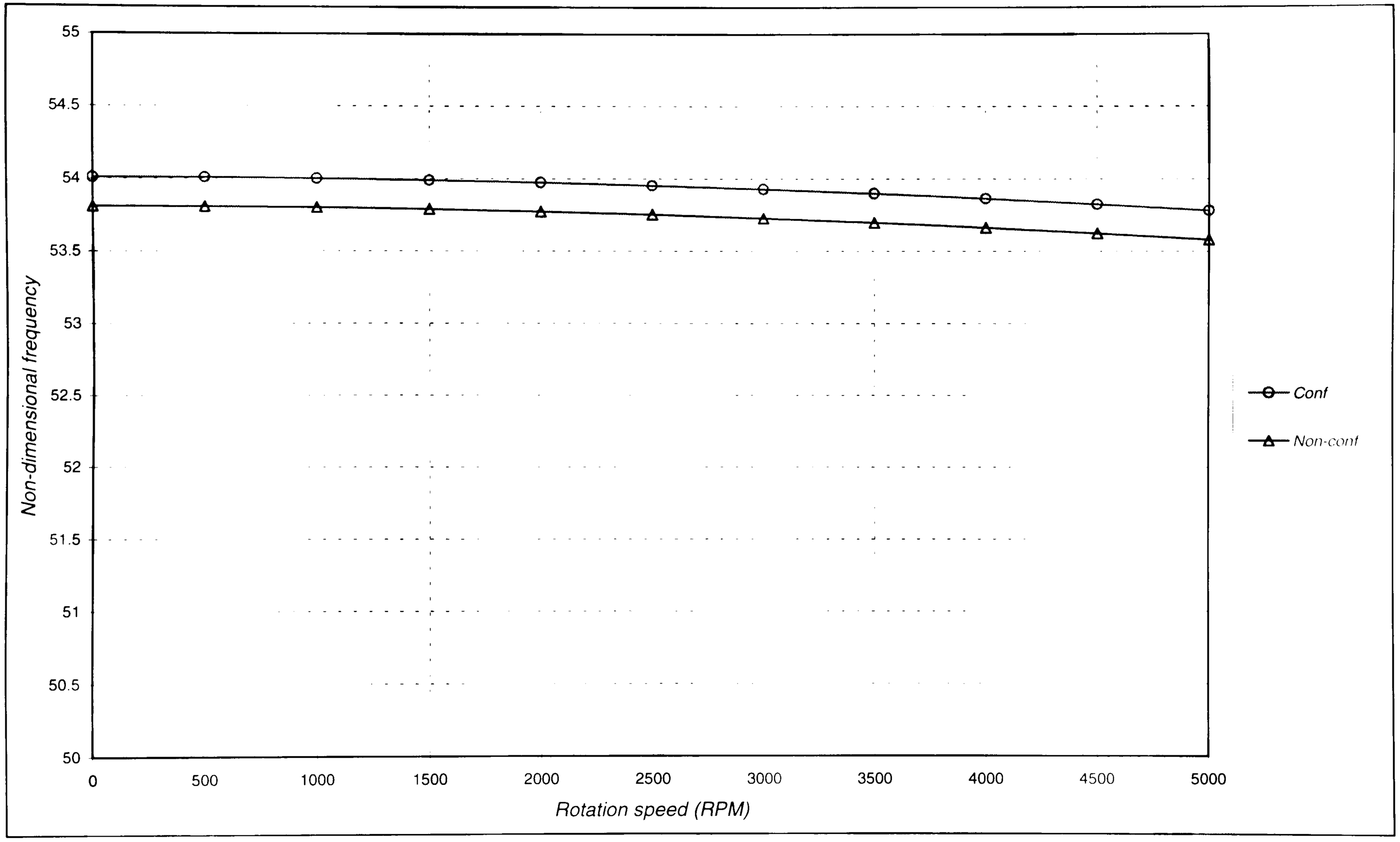

Figure 7.42 Third Non-dimensional natural frequency for rotating thick curved shell.

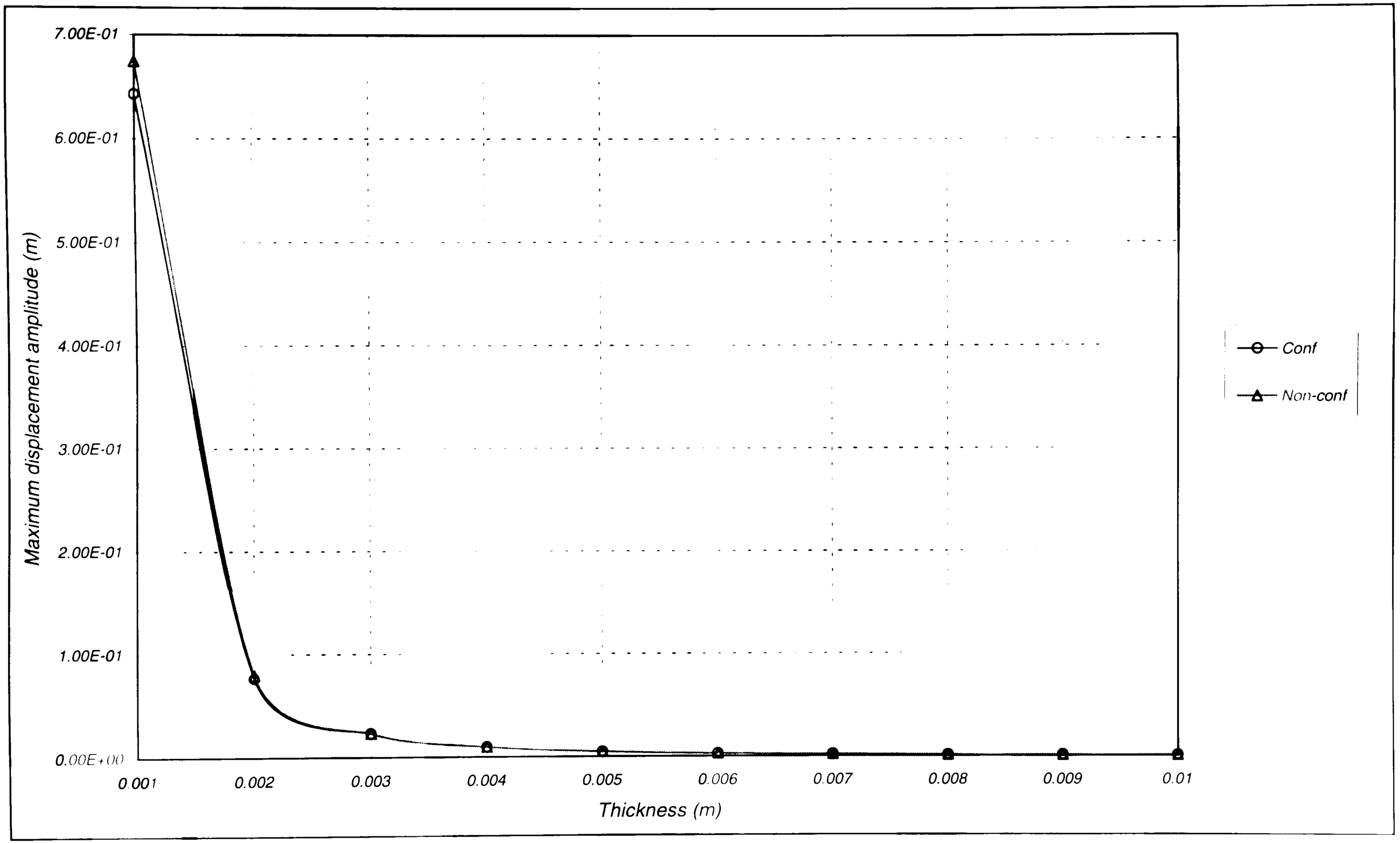

Figure 7.43 Maximum displacement amplitude versus thickness for non-rotating cuved shell under exciting force.

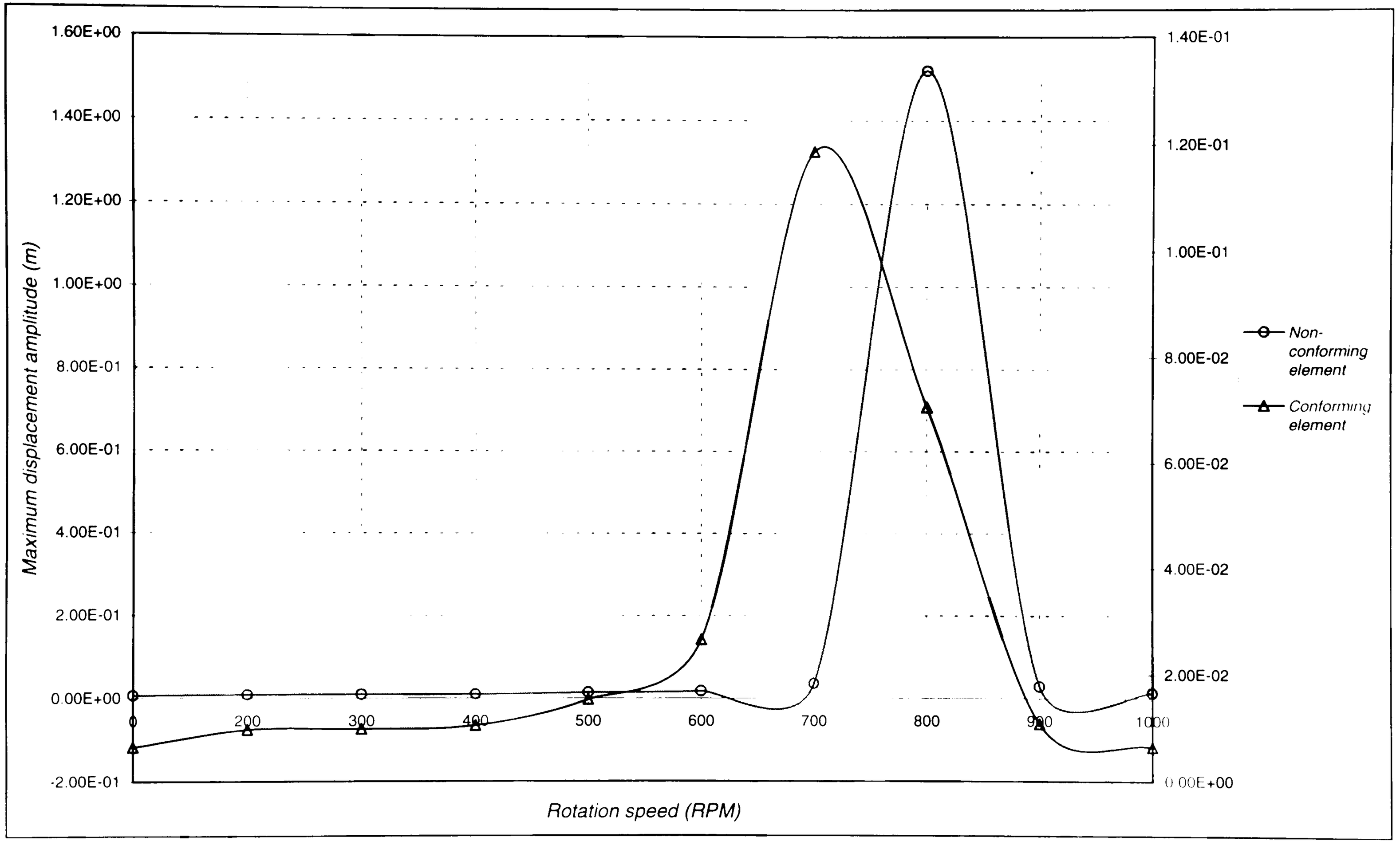

Figure 7.44 Maximum displacement amplitude versus rotation speed for rotating thin curved shell under exciting force.

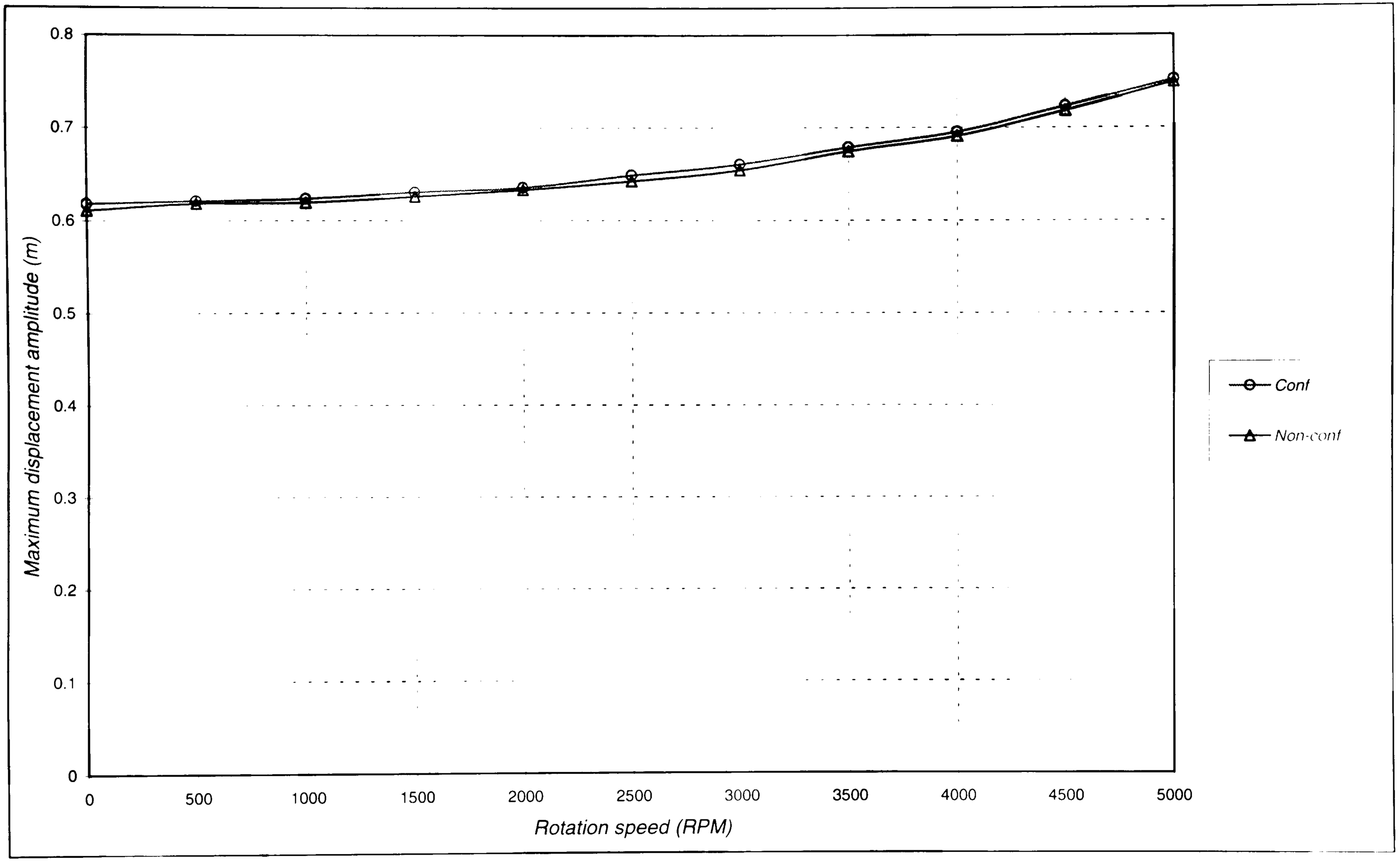

Figure 7.45 Maximum displacement amplitude versus rotation speed for rotating thick curved shell under exciting force.

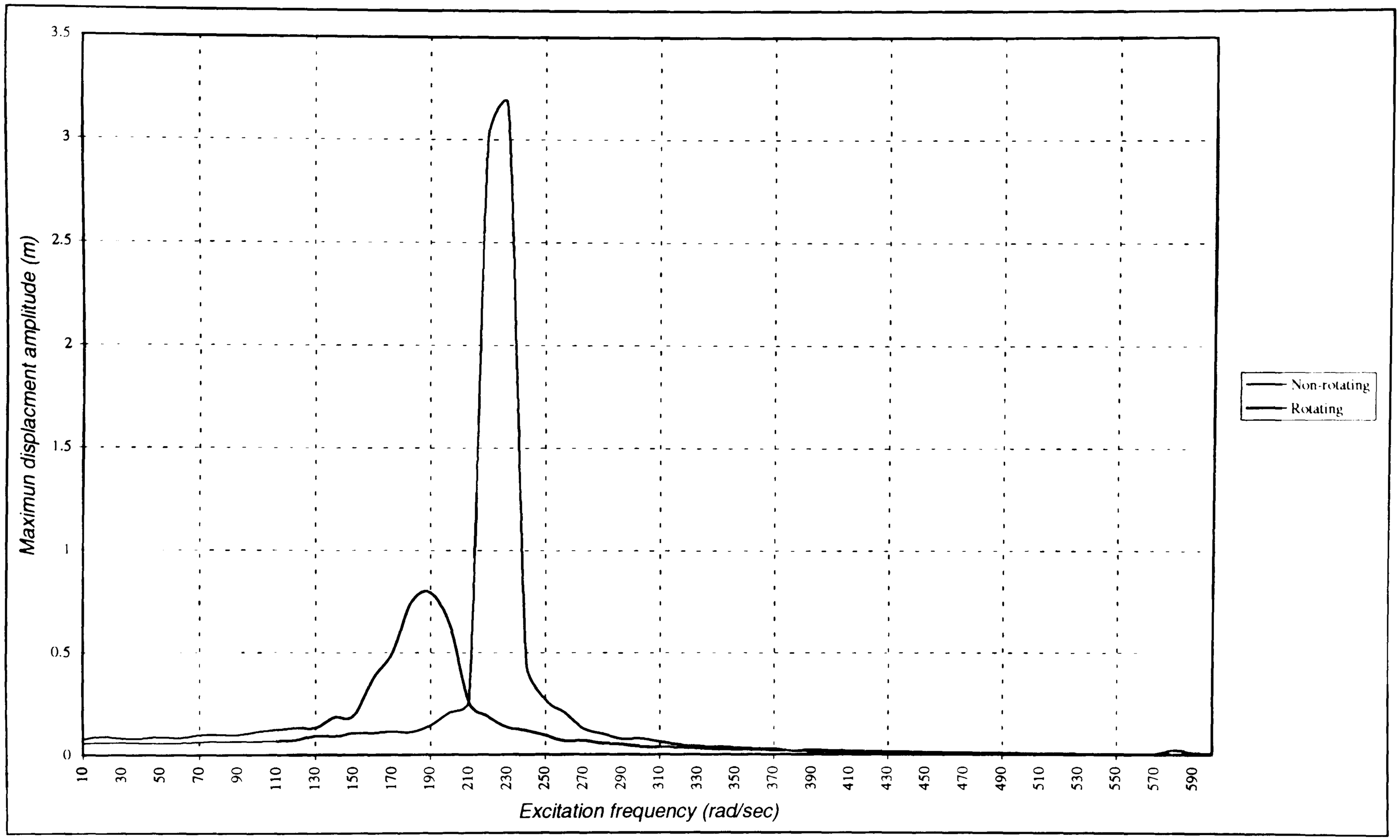

Figure 7.46 Maximum displacement amplitude versus excitation frequency for curved shell under exciting force.

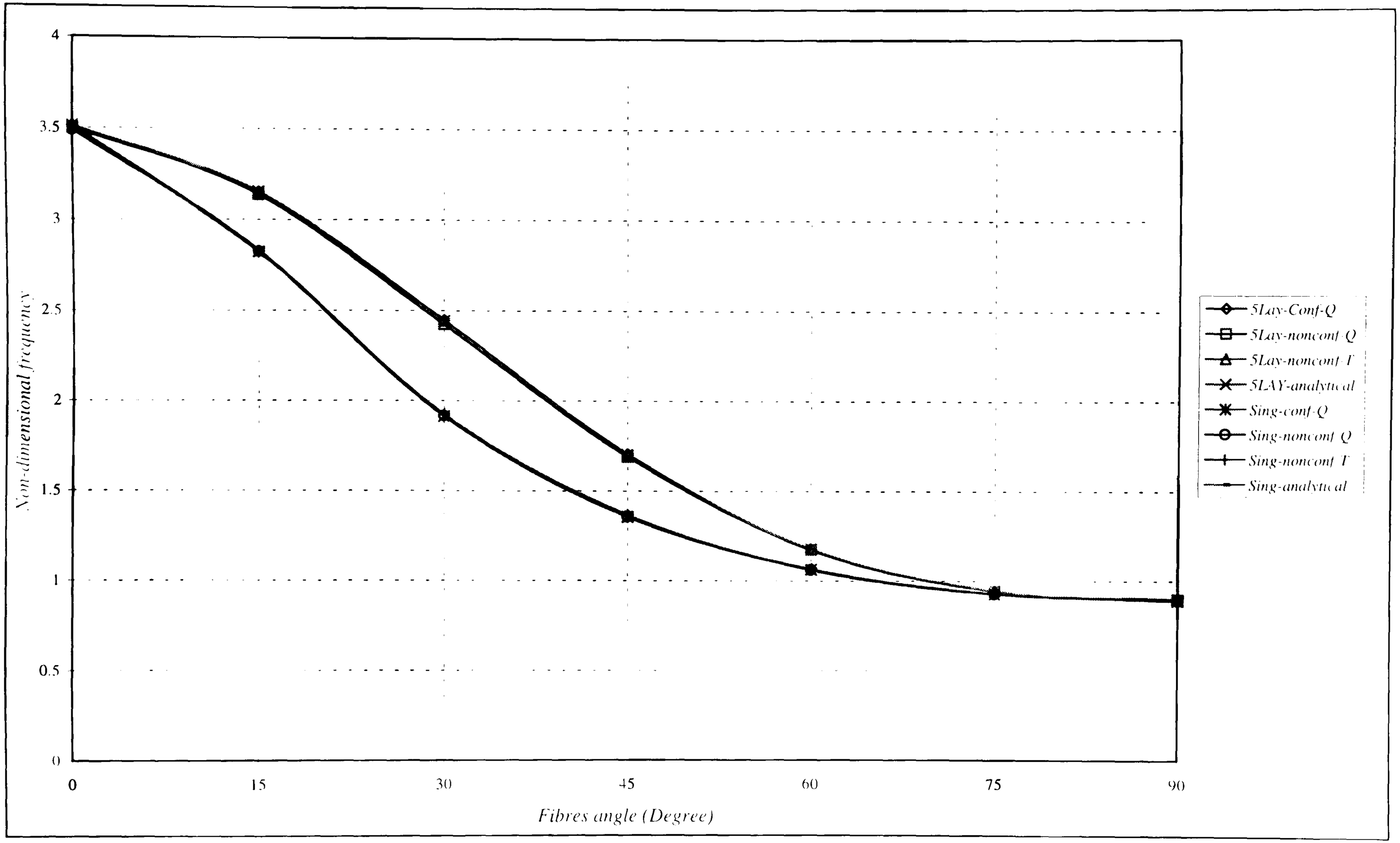

Figure 7.47 Effect of fibre angle on the first natural frequency for single-layer and 5-layer composite plates.

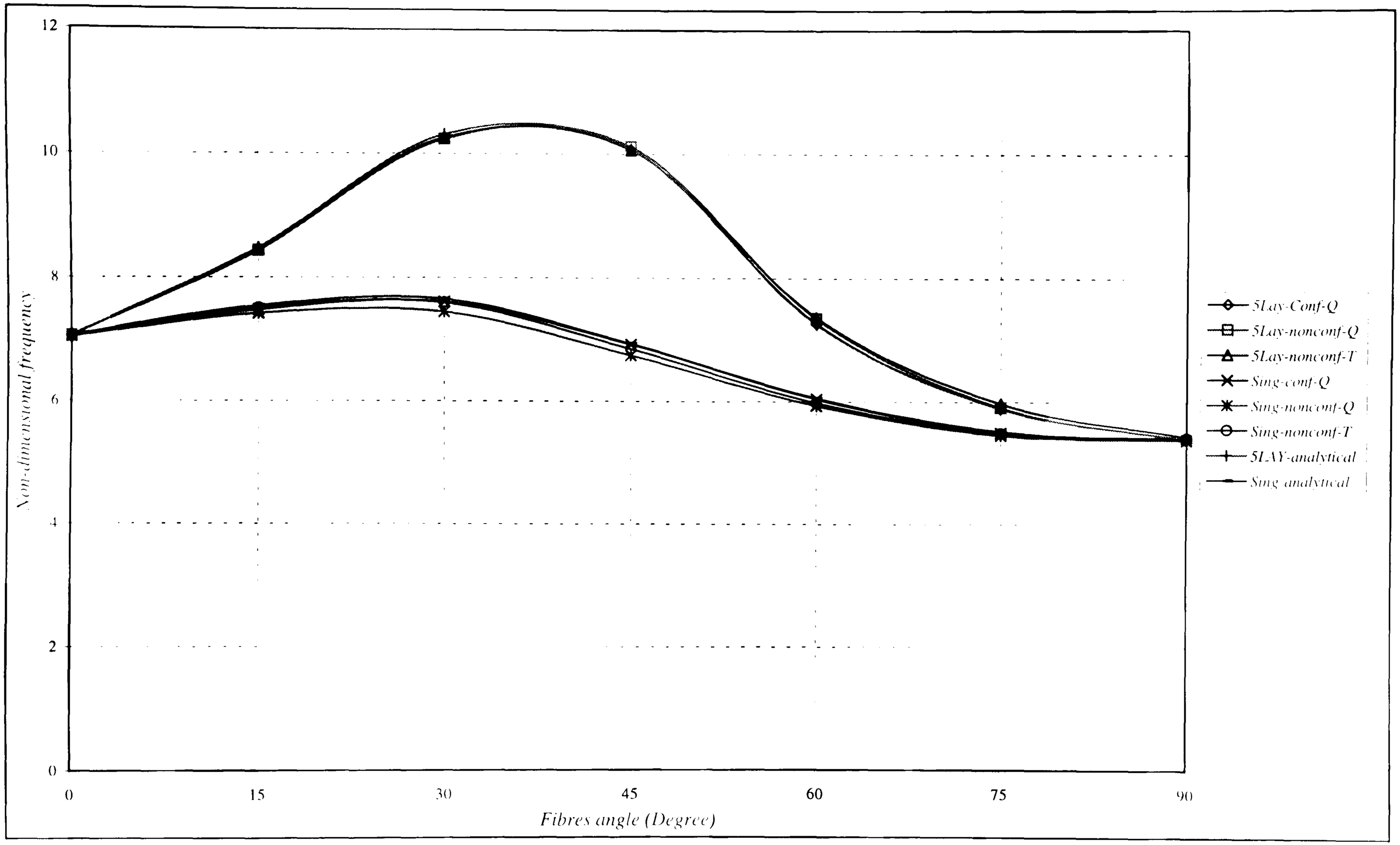

Figure 7.48 Effect of fibre angle on the second natural frequency for single-layer and 5-layer composite plates.

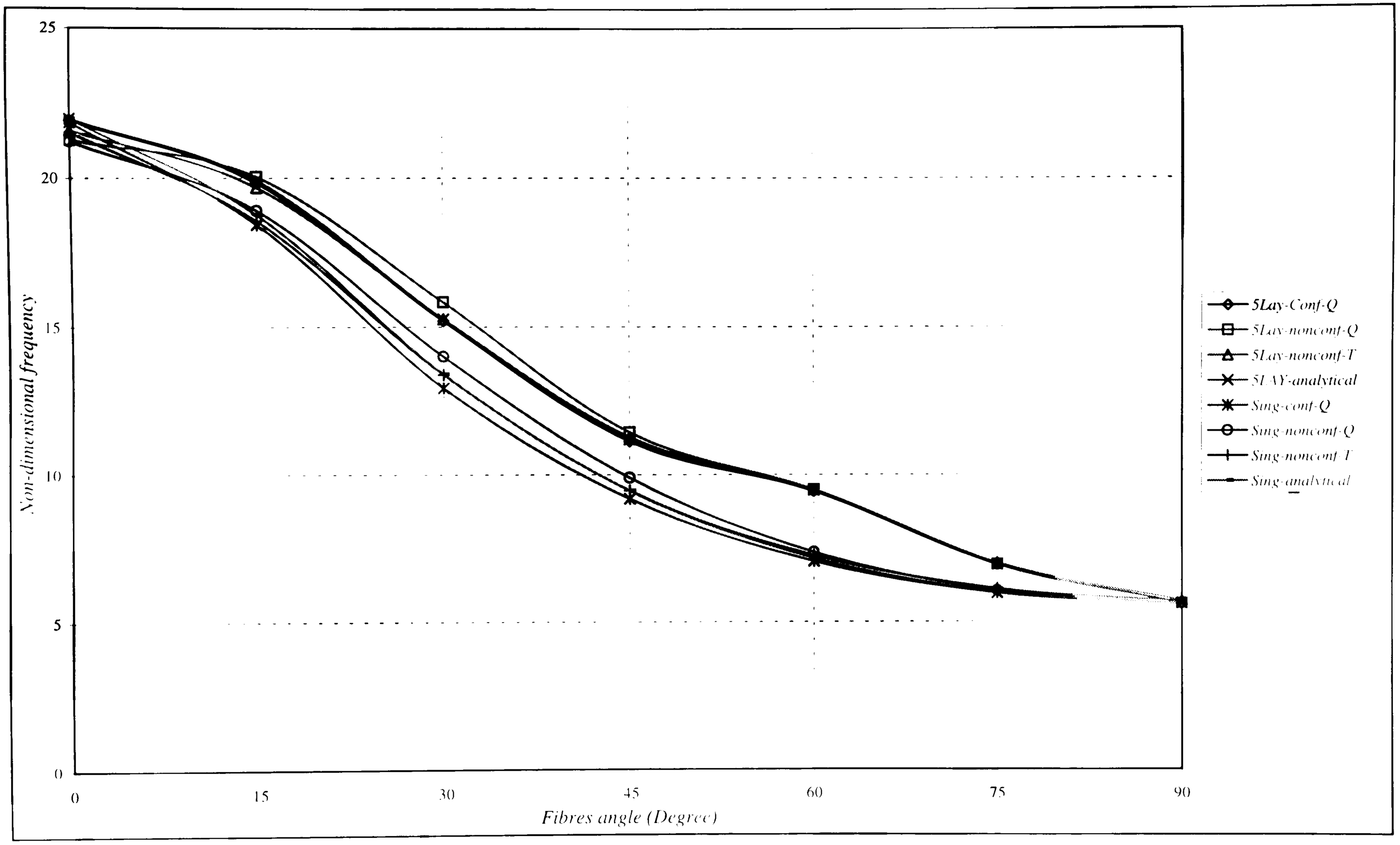

Figure 7.49 Effect of fibre angle on the third natural frequency for single-layer and 5-layer composite plates.

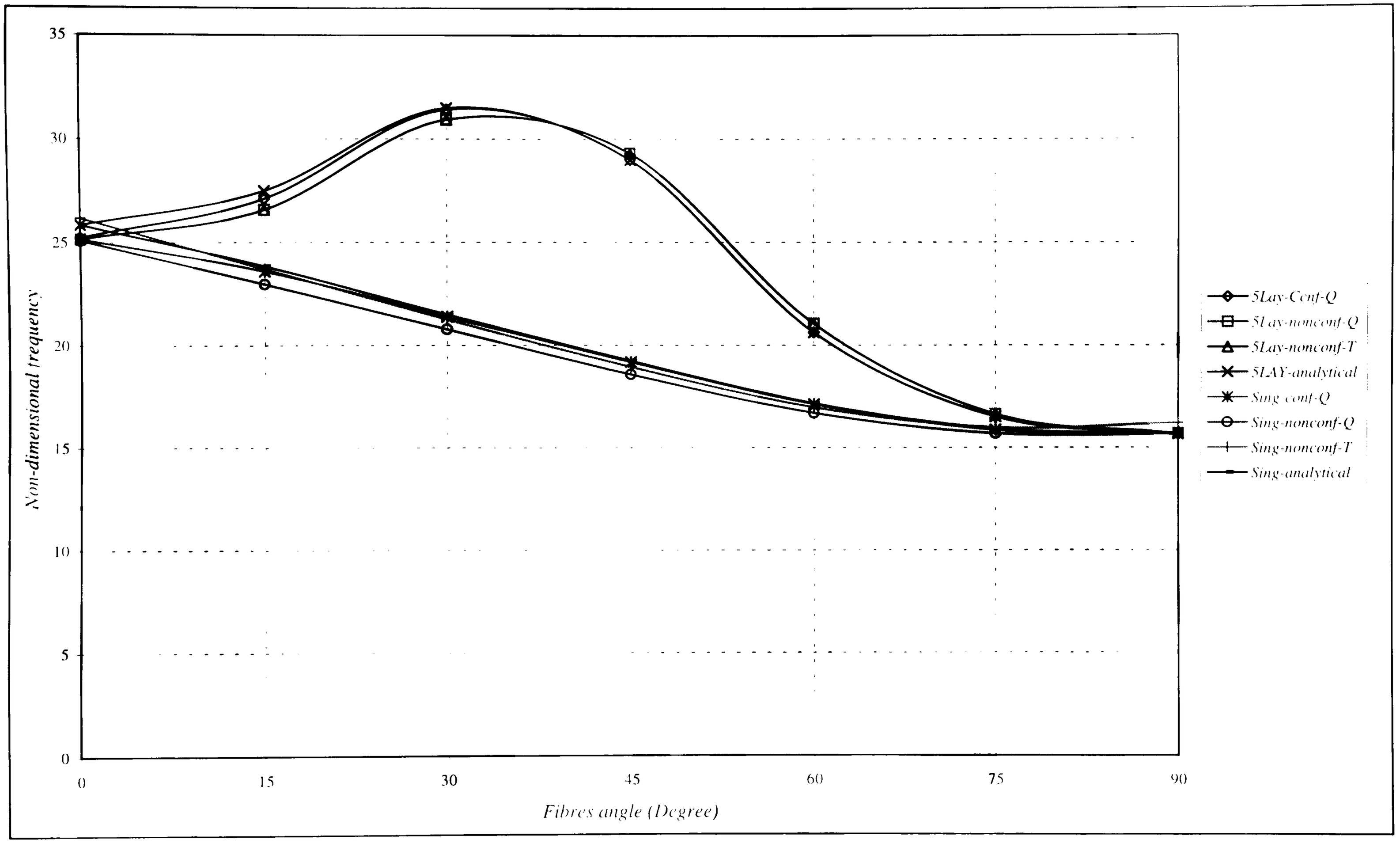

Figure 7.50 Effect of fibre angle on the fourth natural frequency for single-layer and 5-layer composite plates.

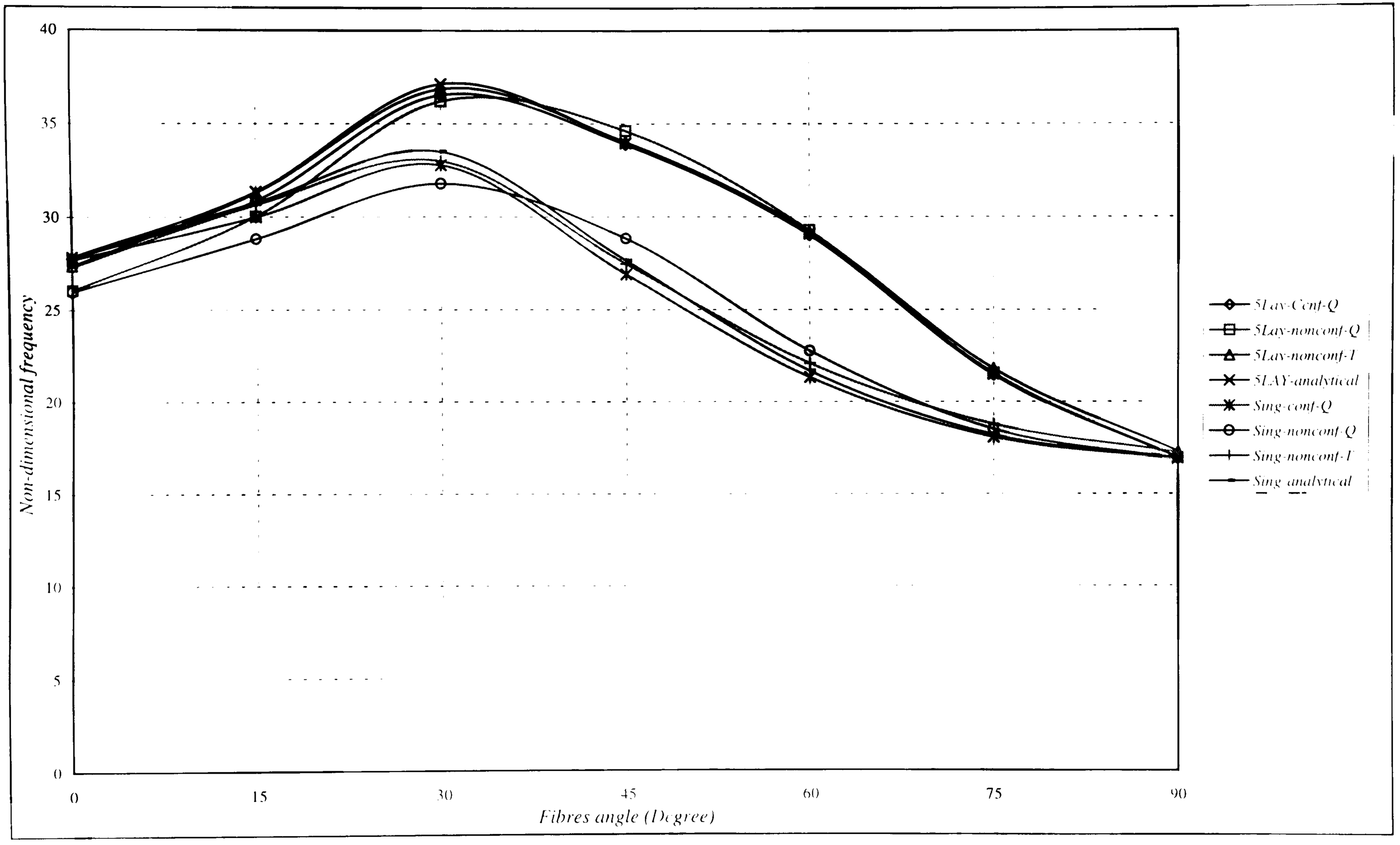

Figure 7.51 Effect of fibre angle on the fifth natural frequency for single-layer and 5-layer composite plates.

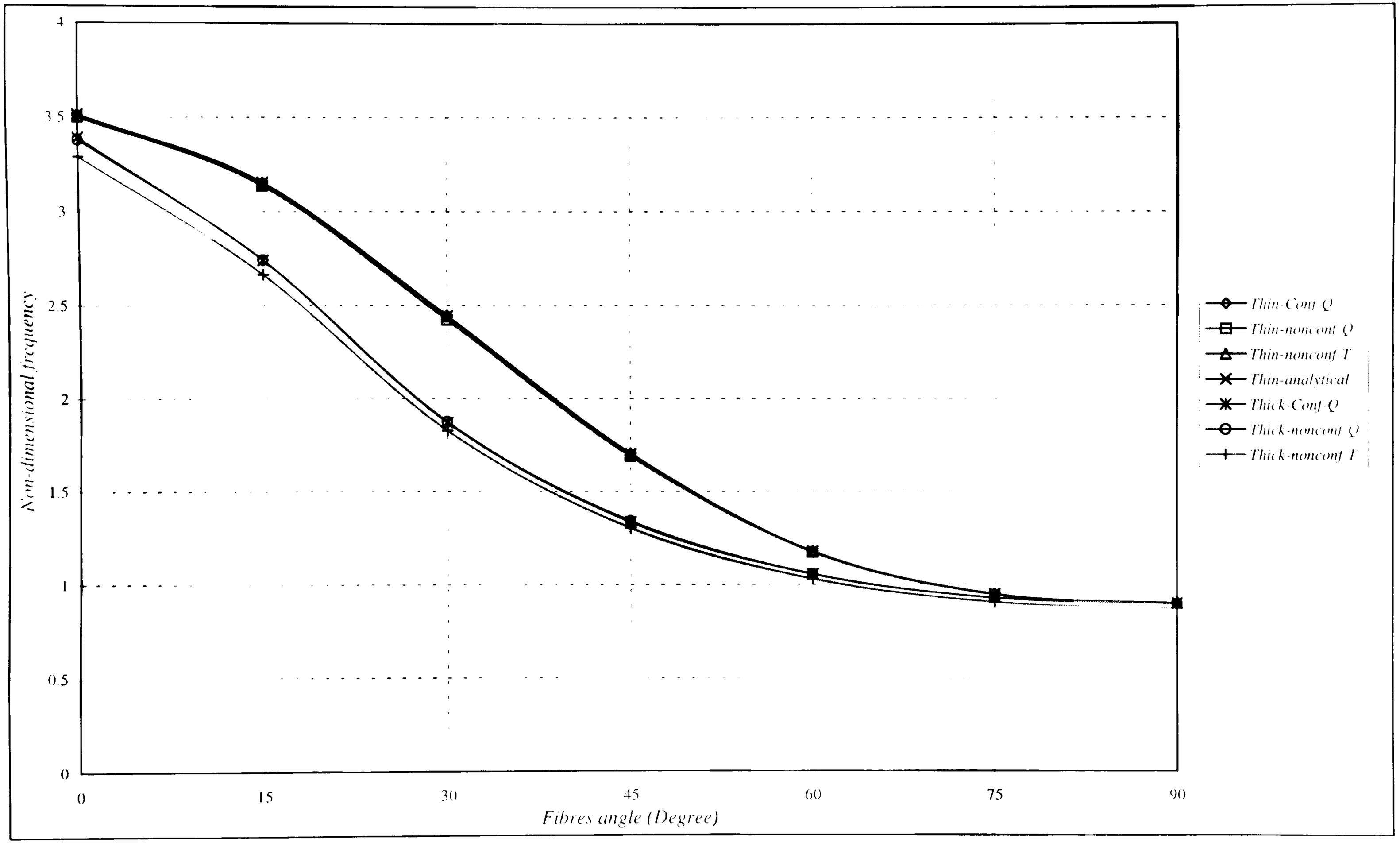

Figure 7.52 Thickness effect on the first natural frequency for 5-layer composite plate.

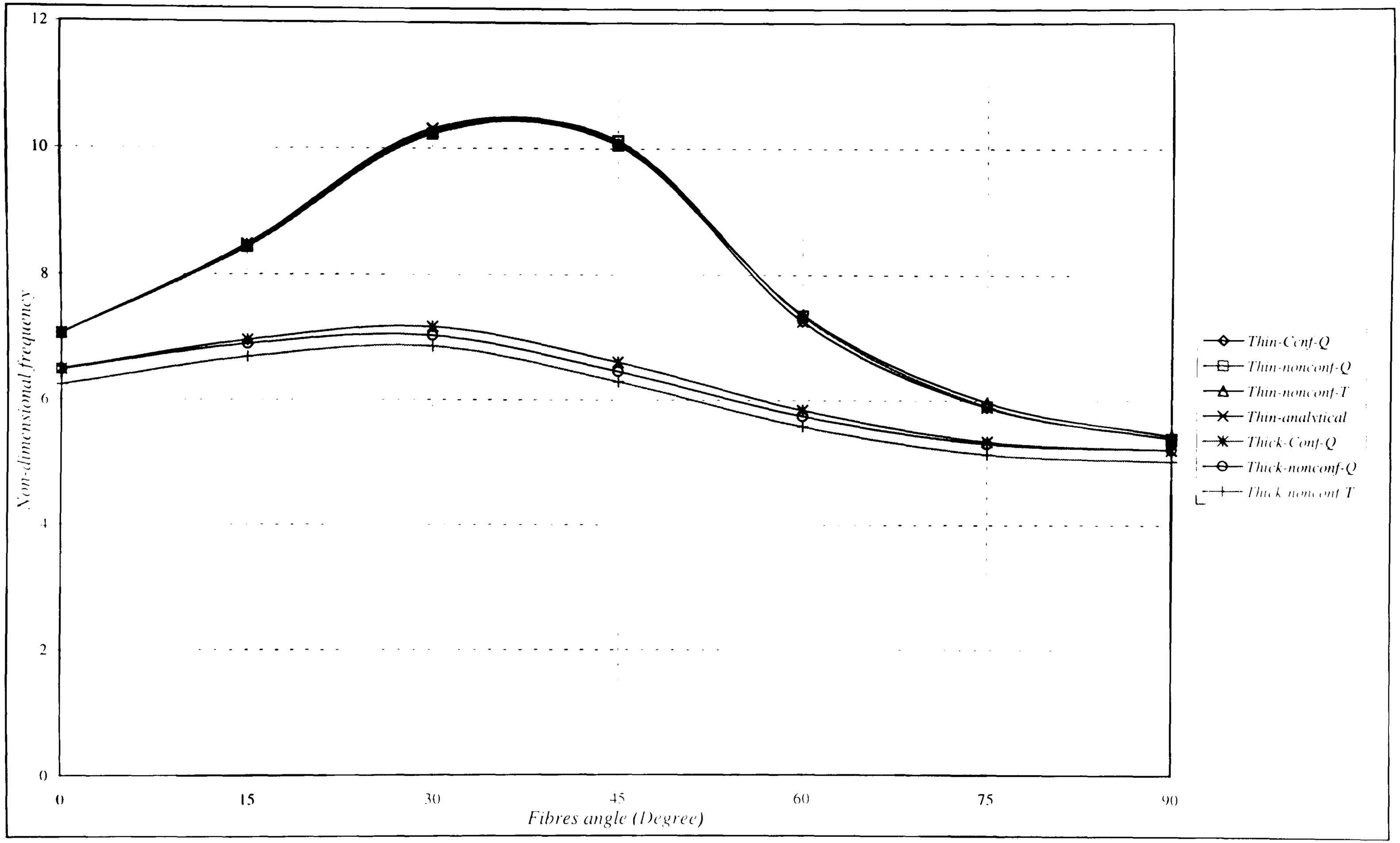

Figure 7.53 Thickness effect on the second natural frequency for 5-layer composite plate.

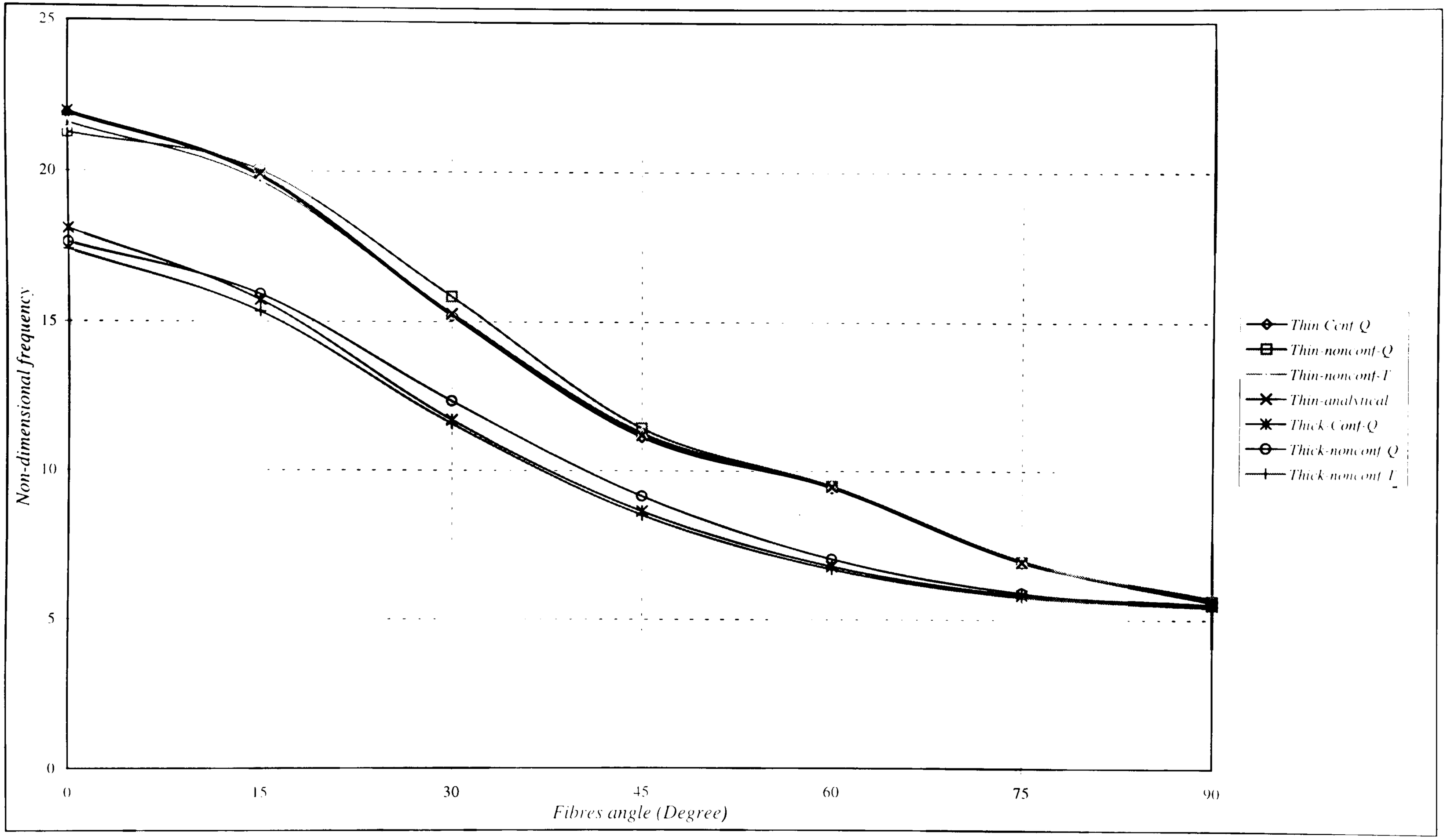

Figure 7.54 Thickness effect on the third natural frequency for 5-layer composite plate.

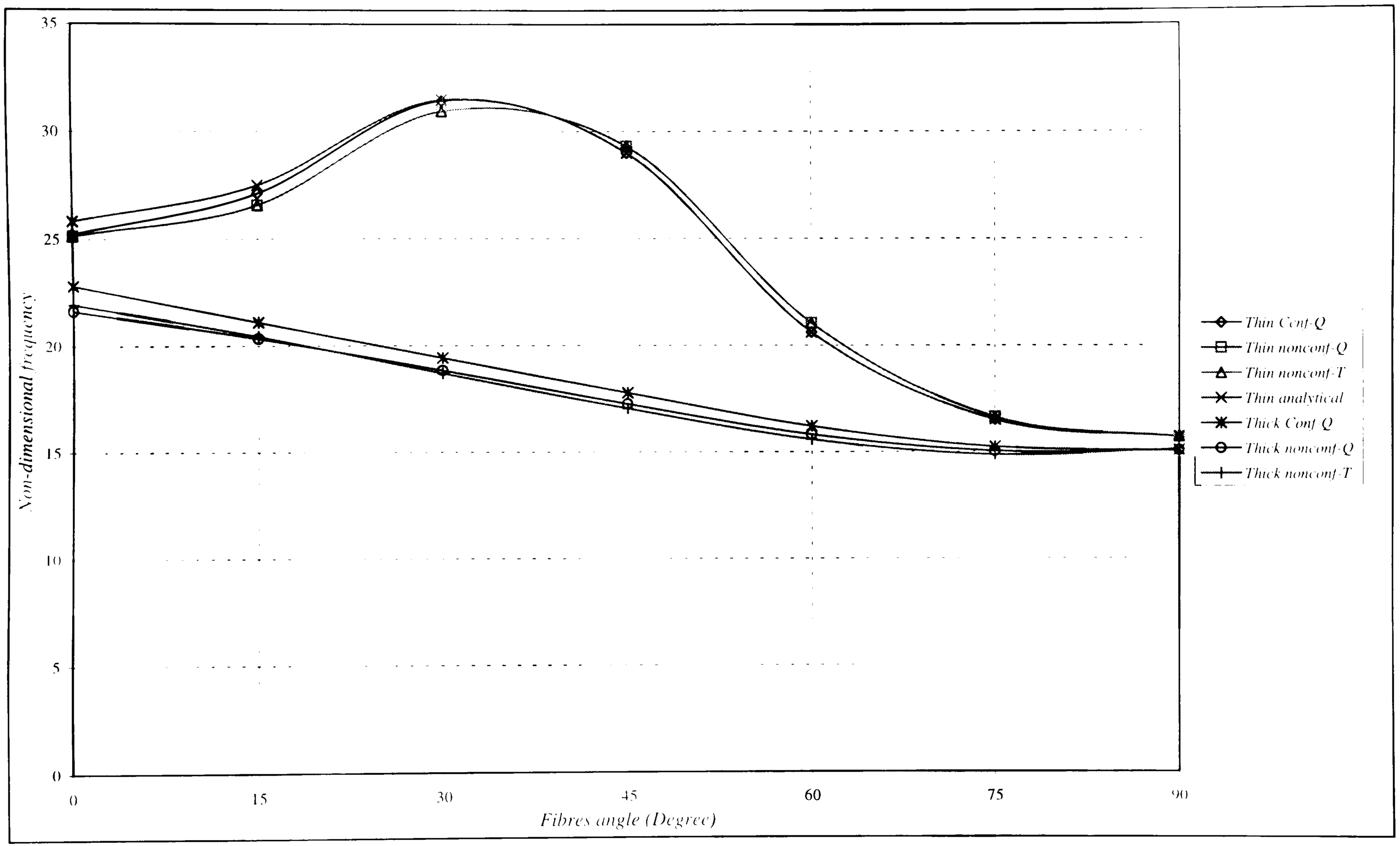

Figure 7.55 Thickness effect on the fourth natural frequency for 5-layer composite plate.

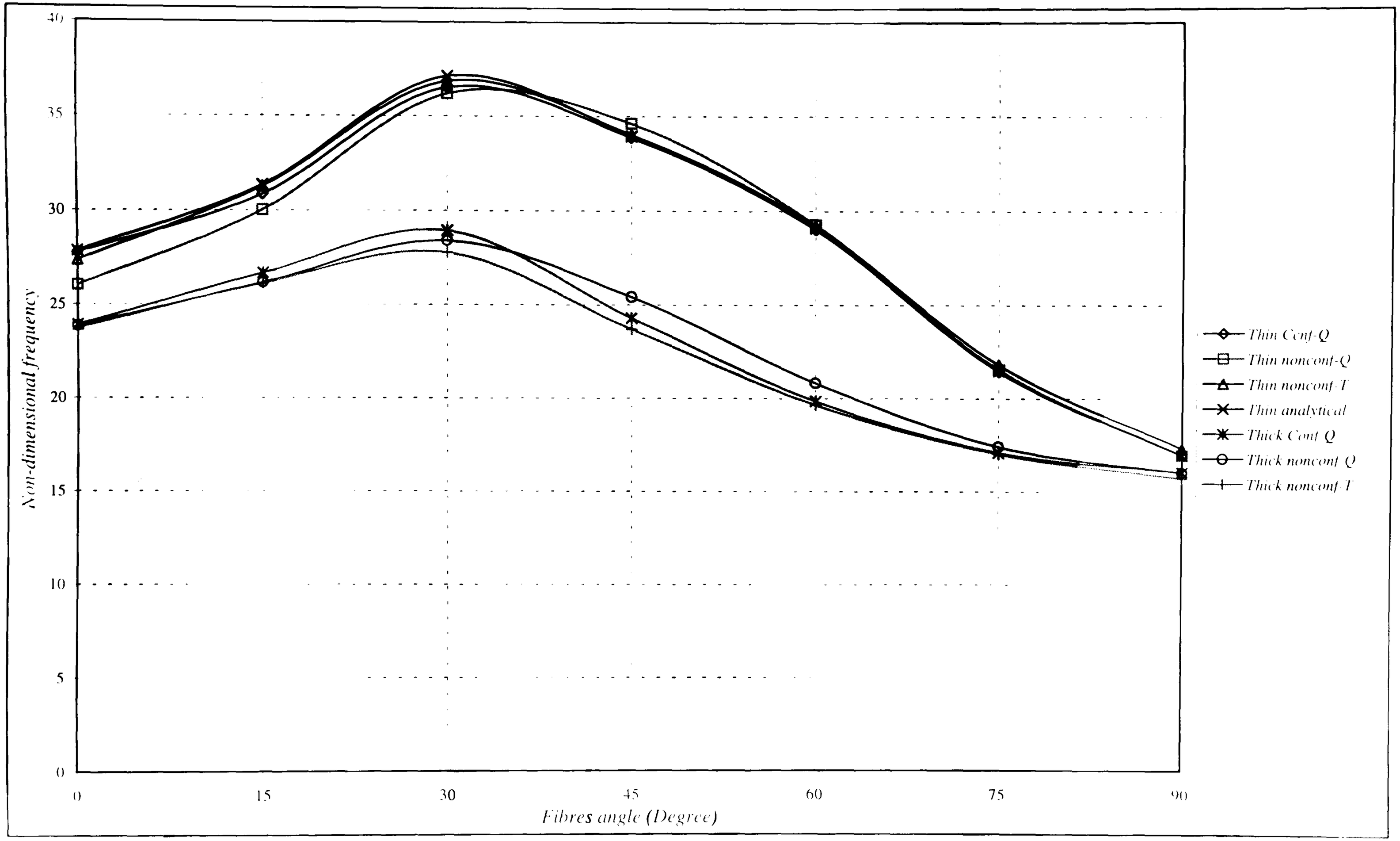

Figure 7.56 Thickness effect on the fifth natural frequency for 5-layer composite plate.

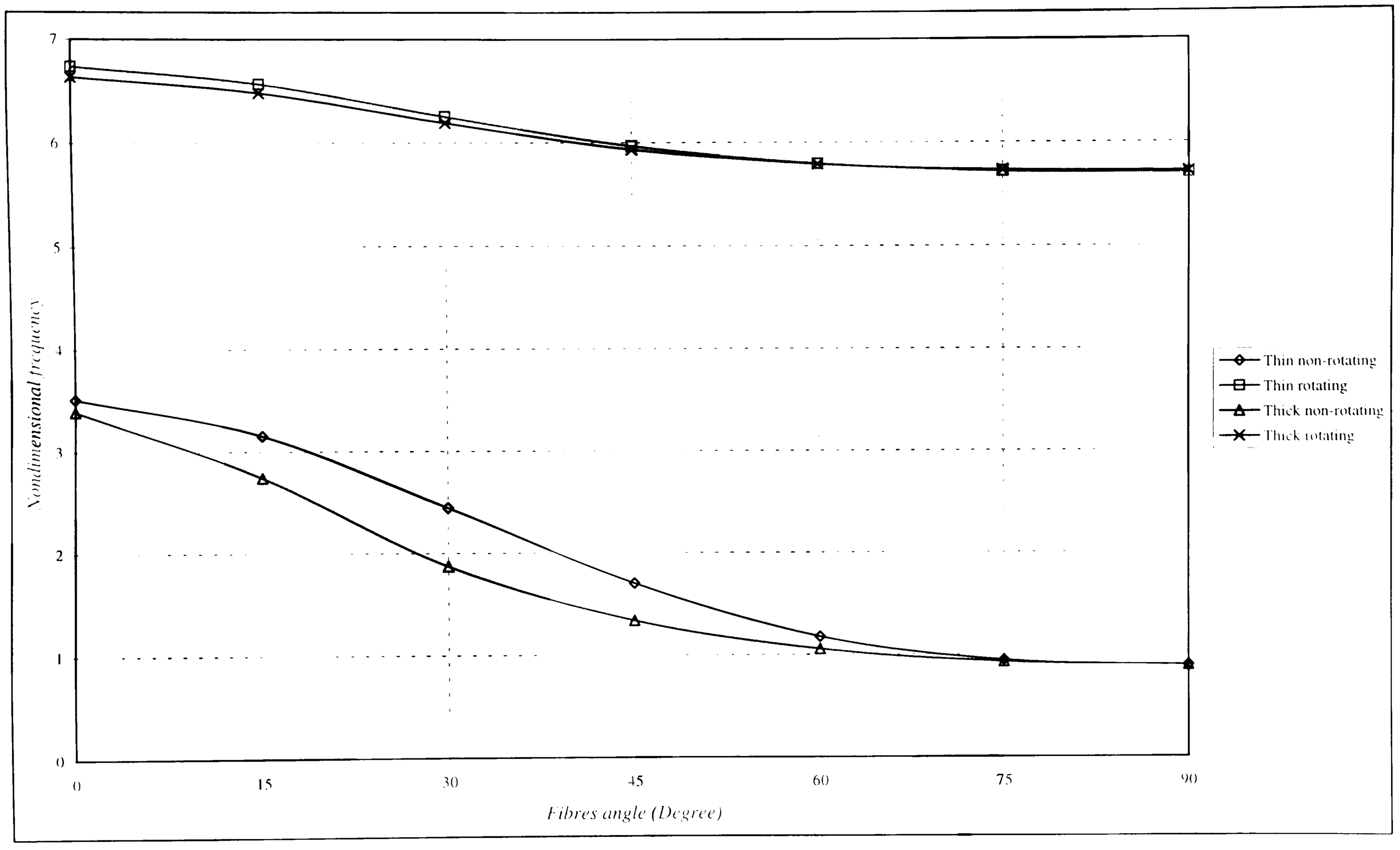

Figure 7.57 Rotational speed effect on the first natural frequency for thin and thick 5-layer composite plate.

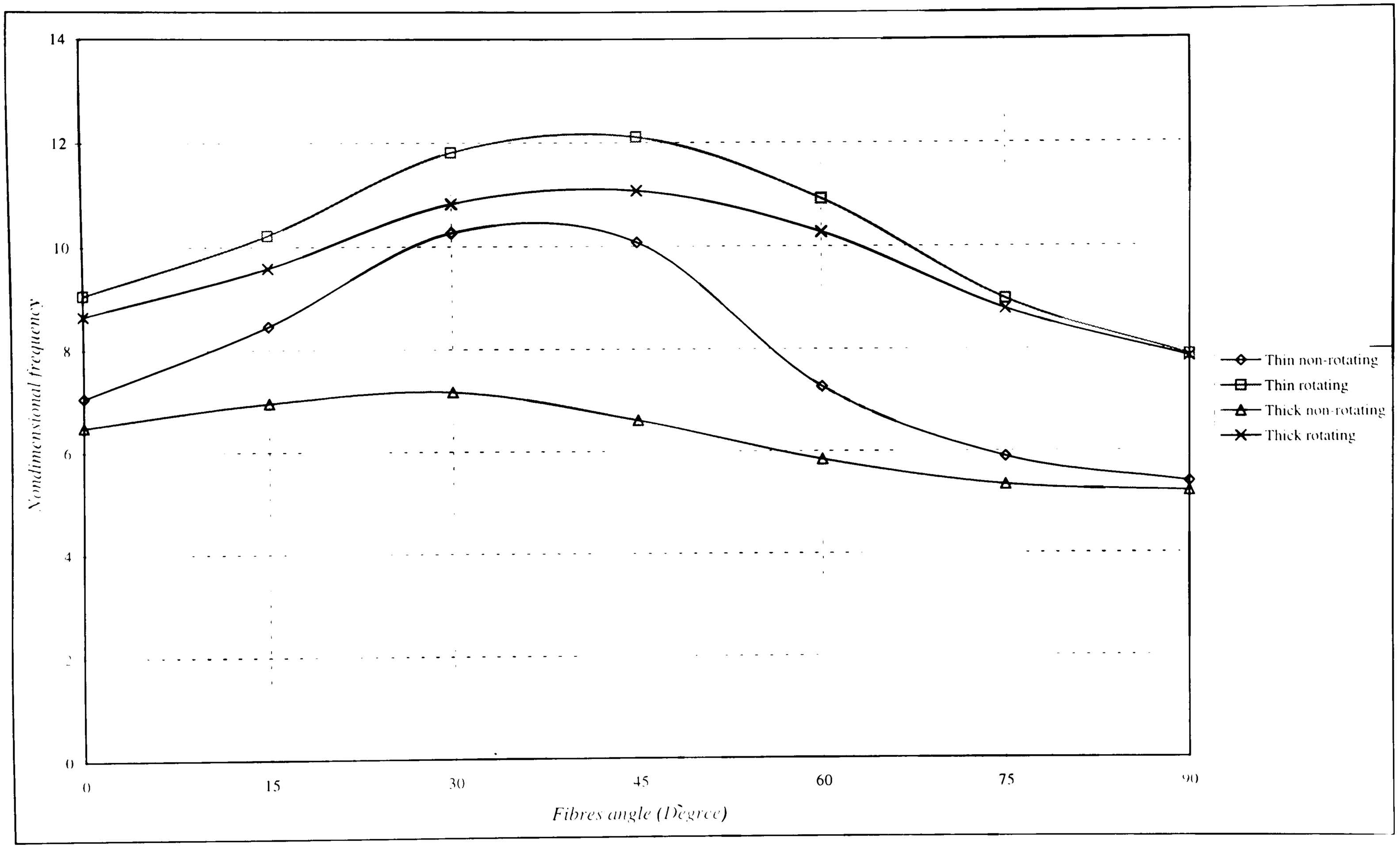

Figure 7.58 Rotational speed effect on the second natural frequency for thin and thick 5-layer composite plate.

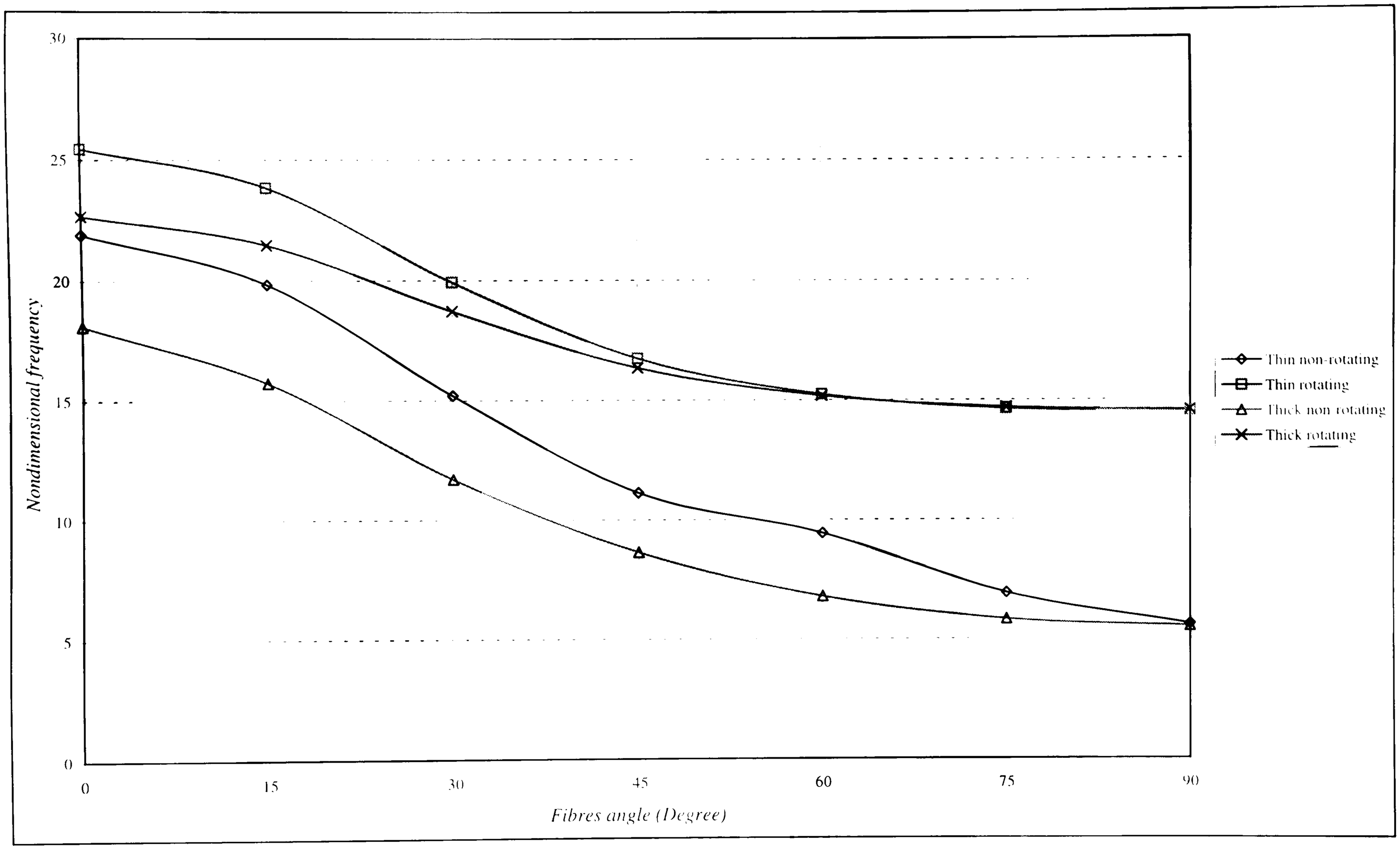

Figure 7.59 Rotational speed effect on the third natural frequency for thin and thick 5-layer composite plate.

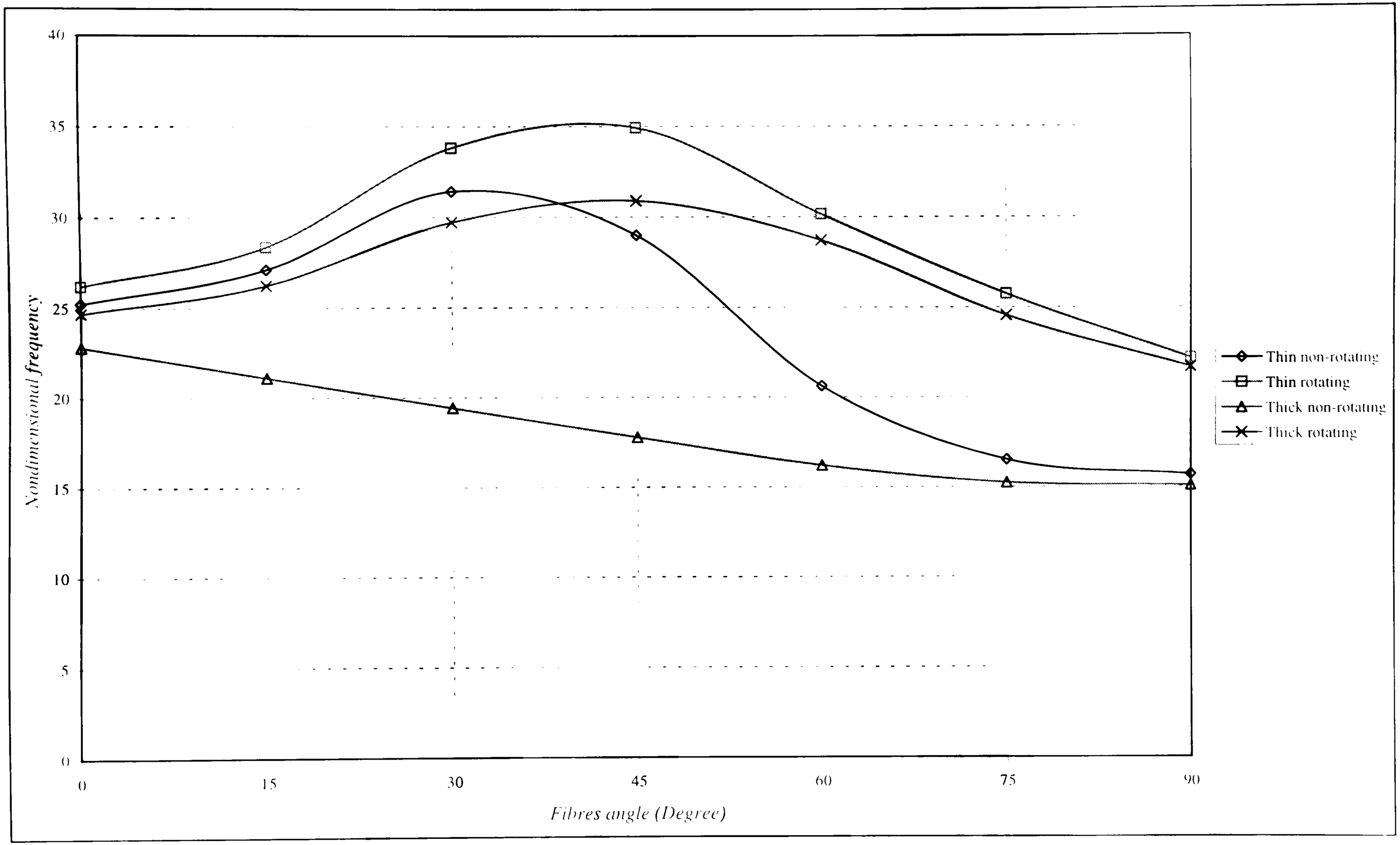

Figure 7.60 Rotational speed effect on the fourth natural frequency for thin and thick 5-layer composite plate.

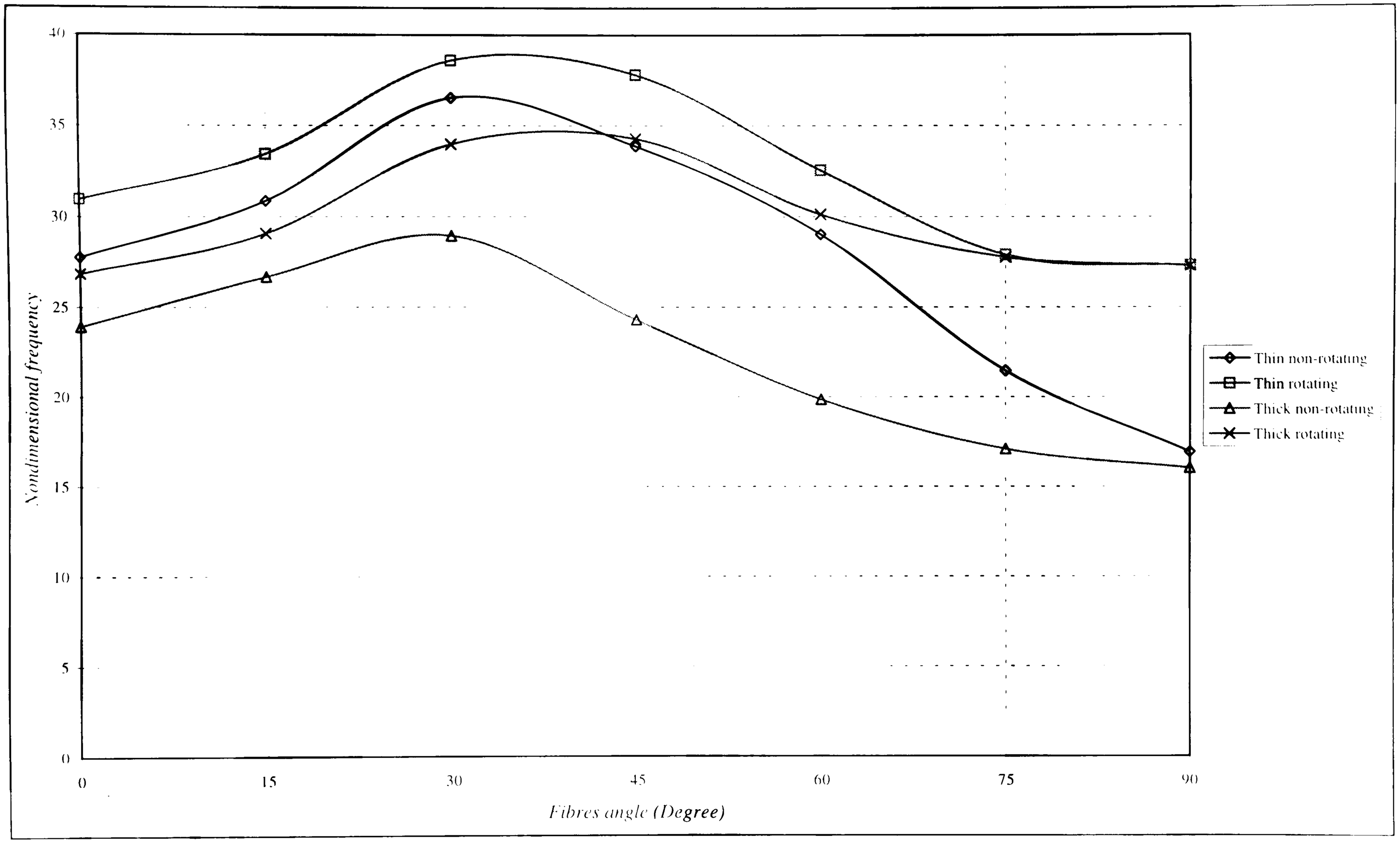

Figure 7.61 Rotational speed effect on the fifth natural frequency for thin and thick 5-layer composite plate.

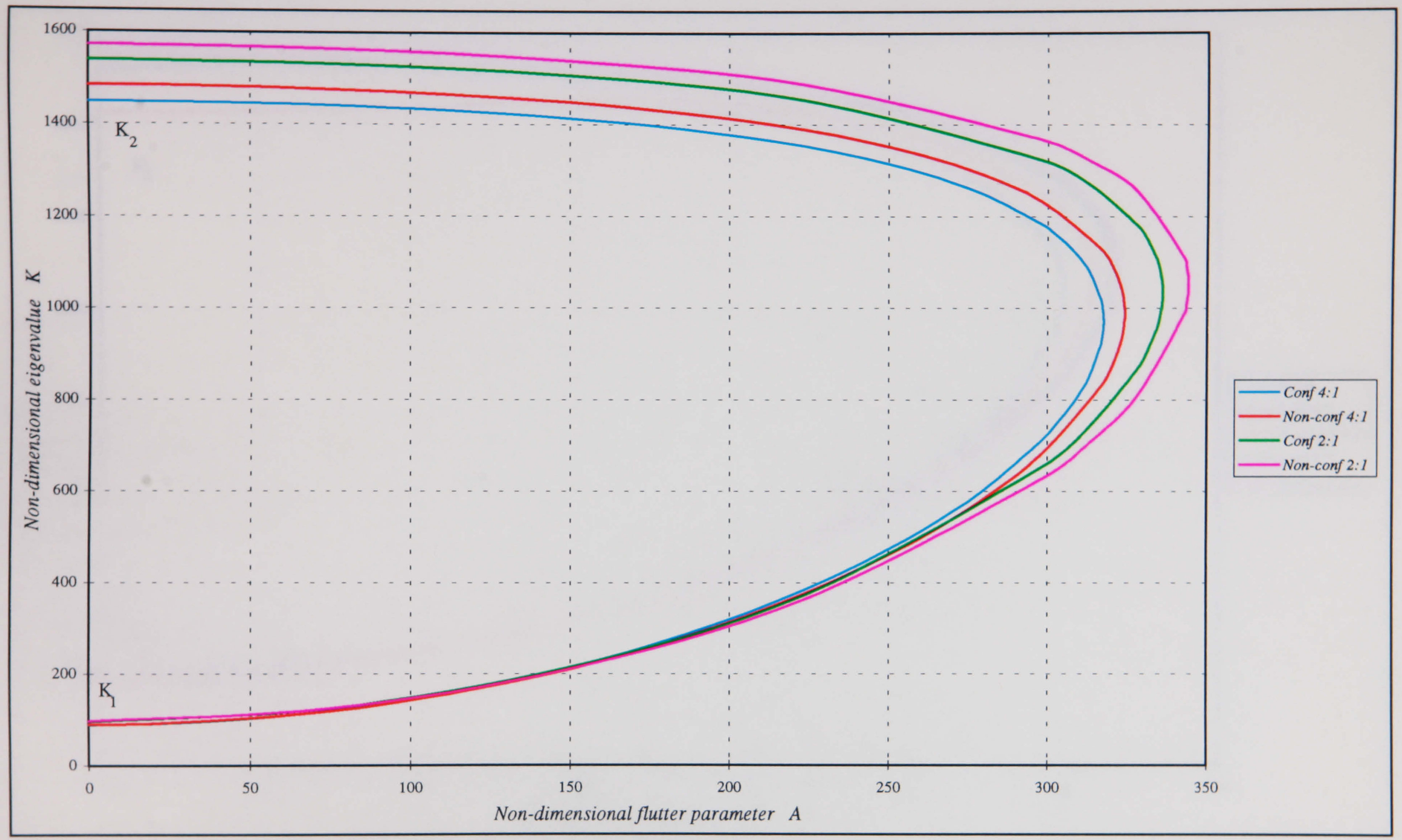

Figure 7.62 Coalescence of eigenvalues for isotropic simply supported rectangular panel.

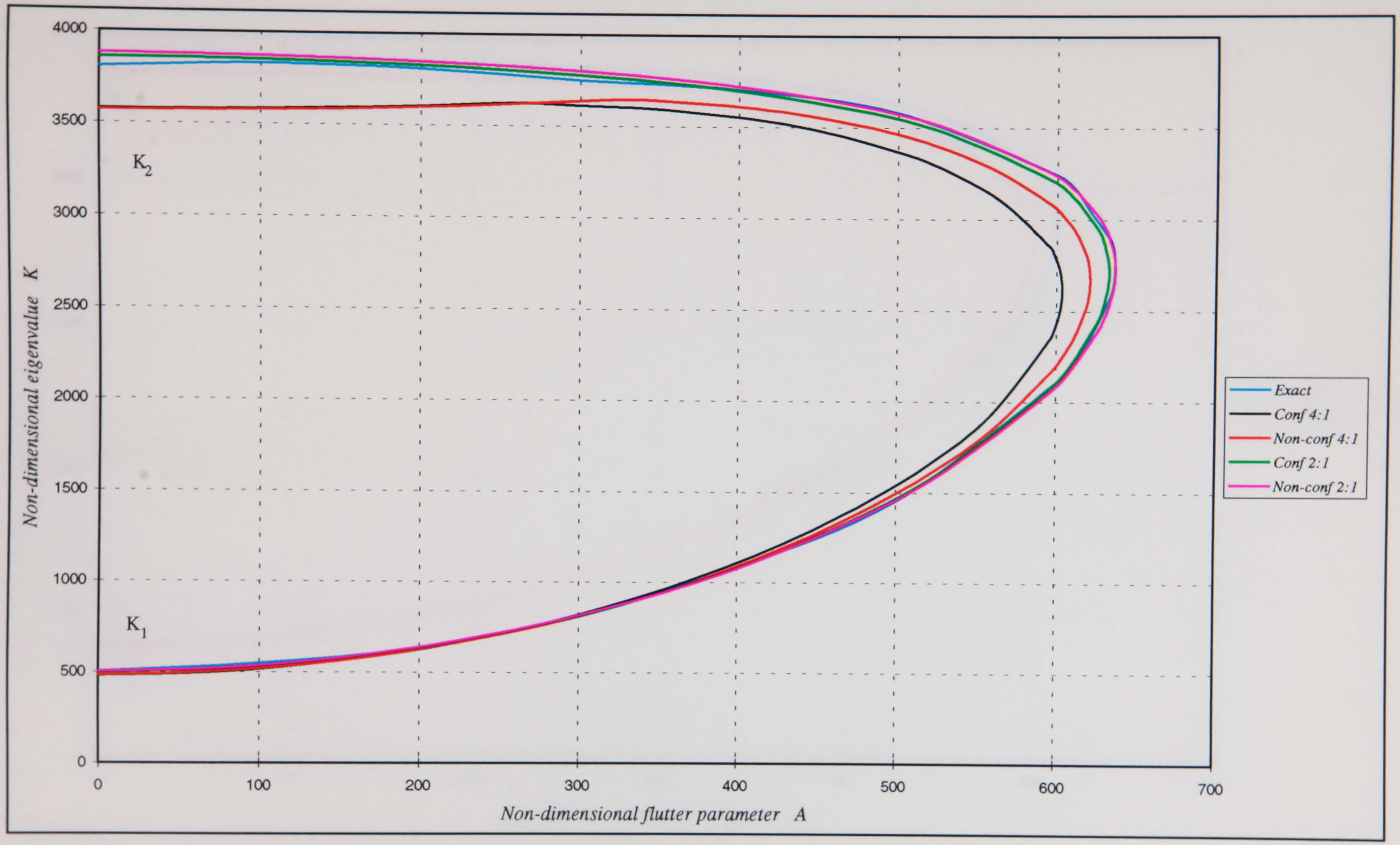

Figure 7.63 Coalescence of eigenvalues for isotropic clamped rectangular panel.

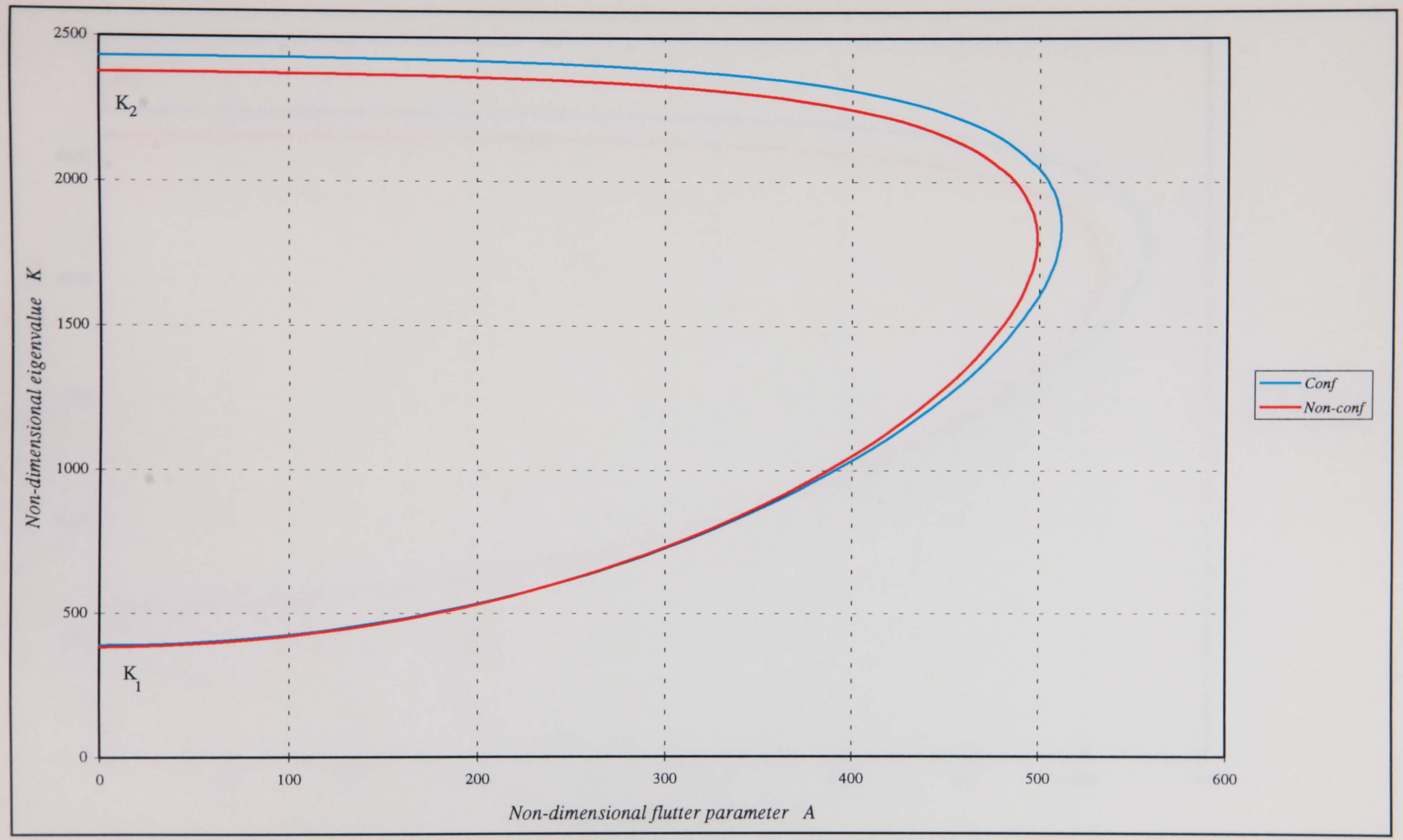

Figure 7.64 Coalescence of eigenvalues for isotropic simply-supported square panel.

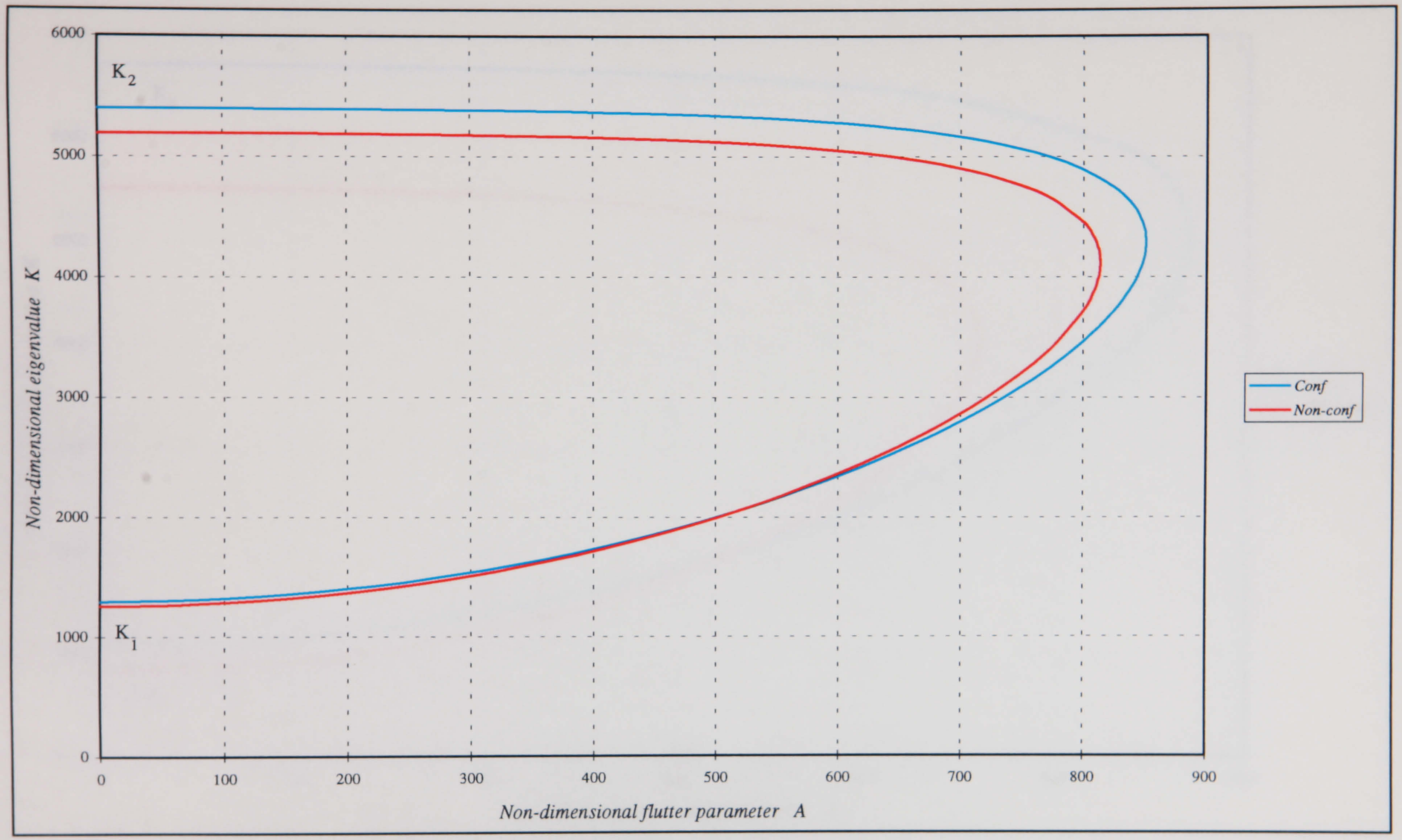

Figure 7.65 Coalescence of eigenvalues for isotropic clamped square panel.

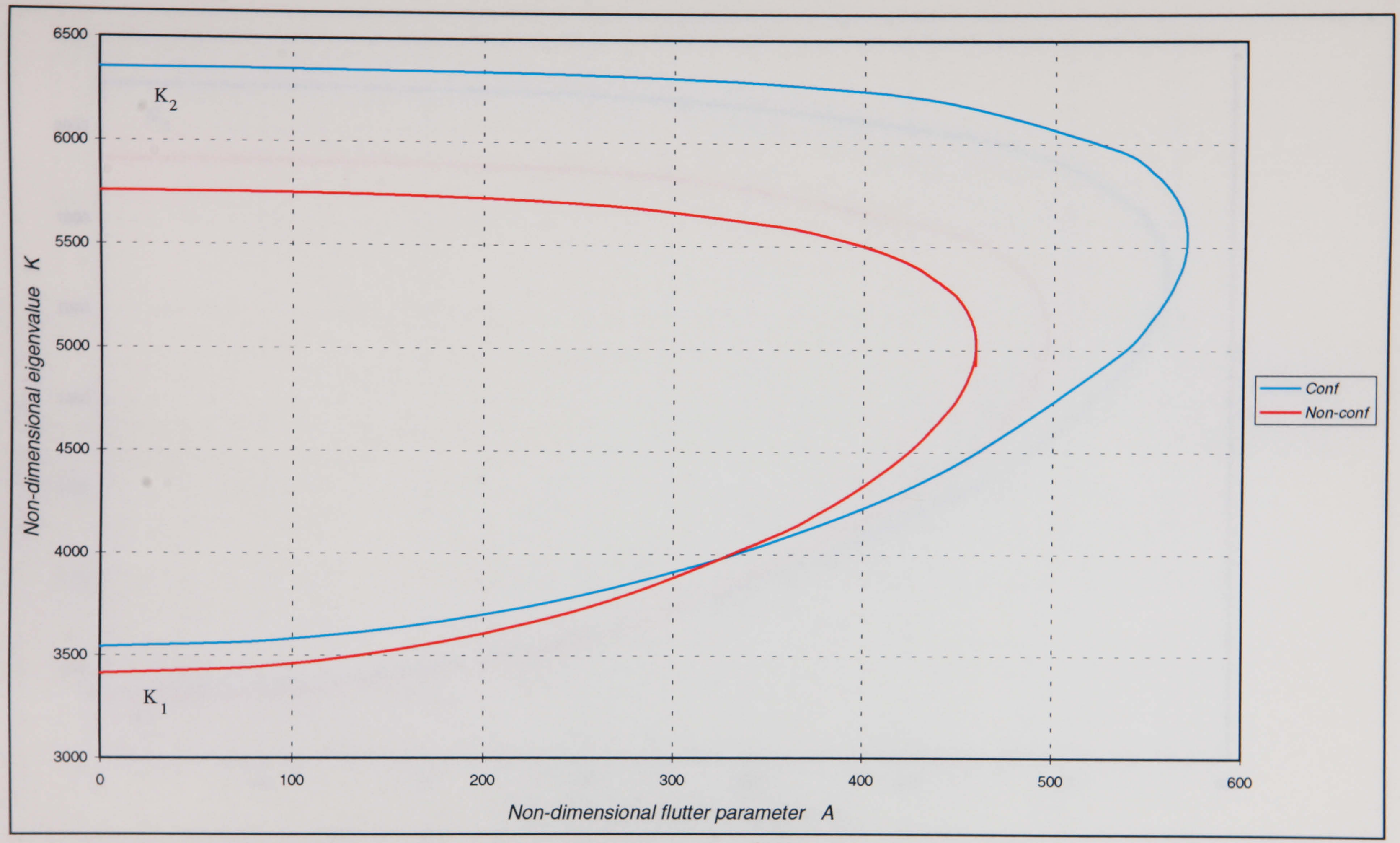

Figure 7.66 Coalescence of eigenvalues for composite clamped rectangular panel.

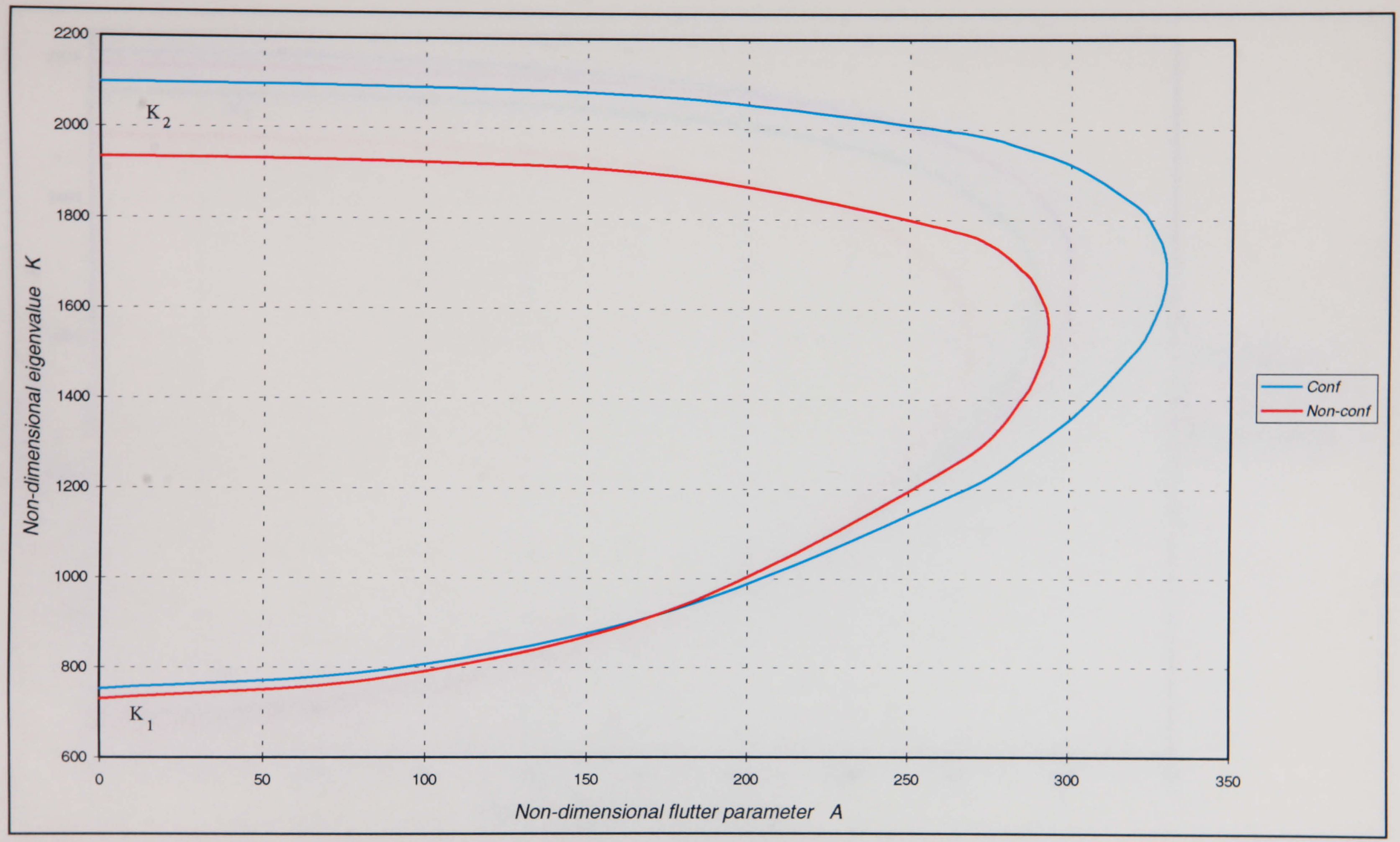

Figure 7.67 Coalescence of eigenvalues for composite simply-supported rectangular panel.

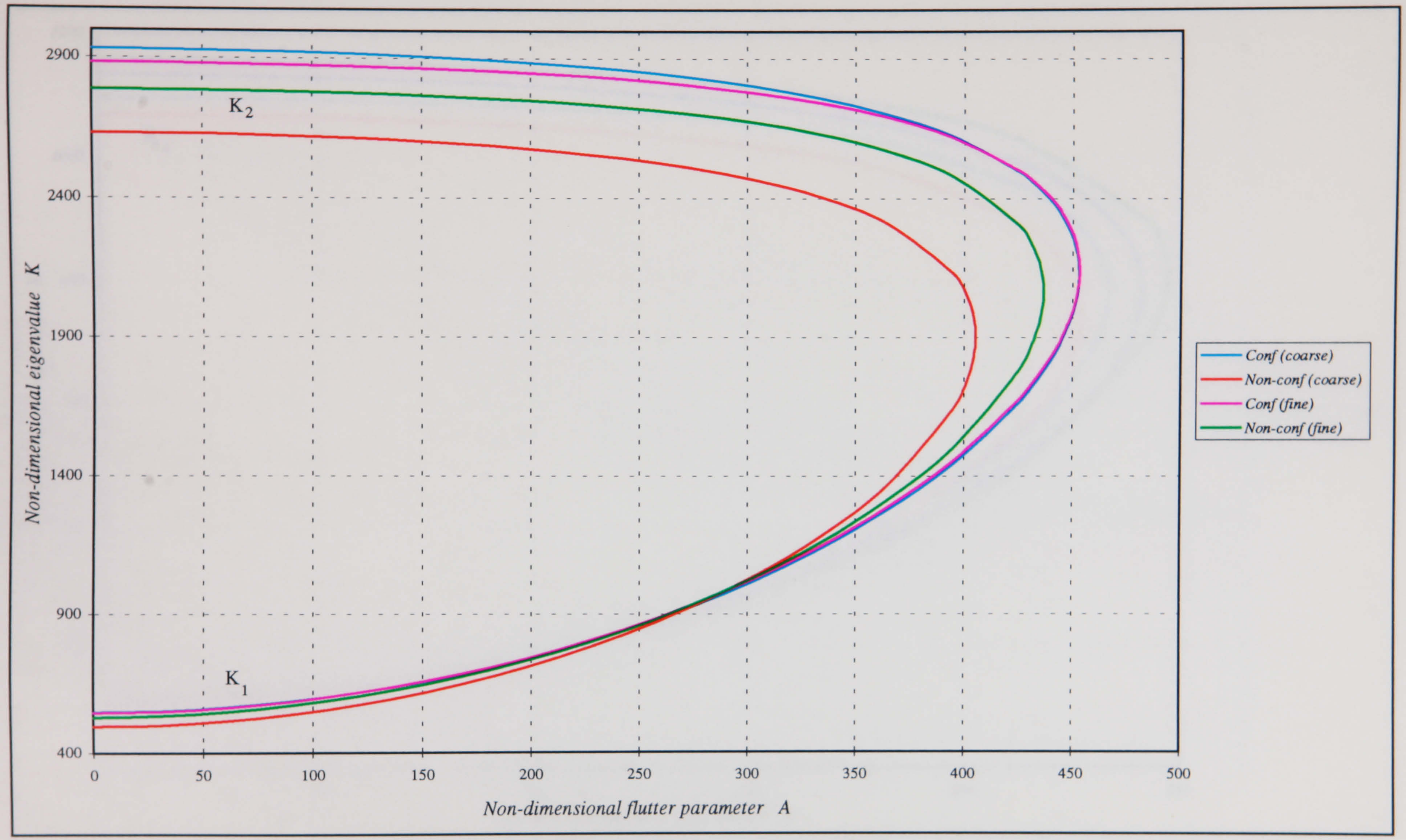

Figure 7.68 Coalescence of eigenvalues for Boron/Epoxy clamped square panel.

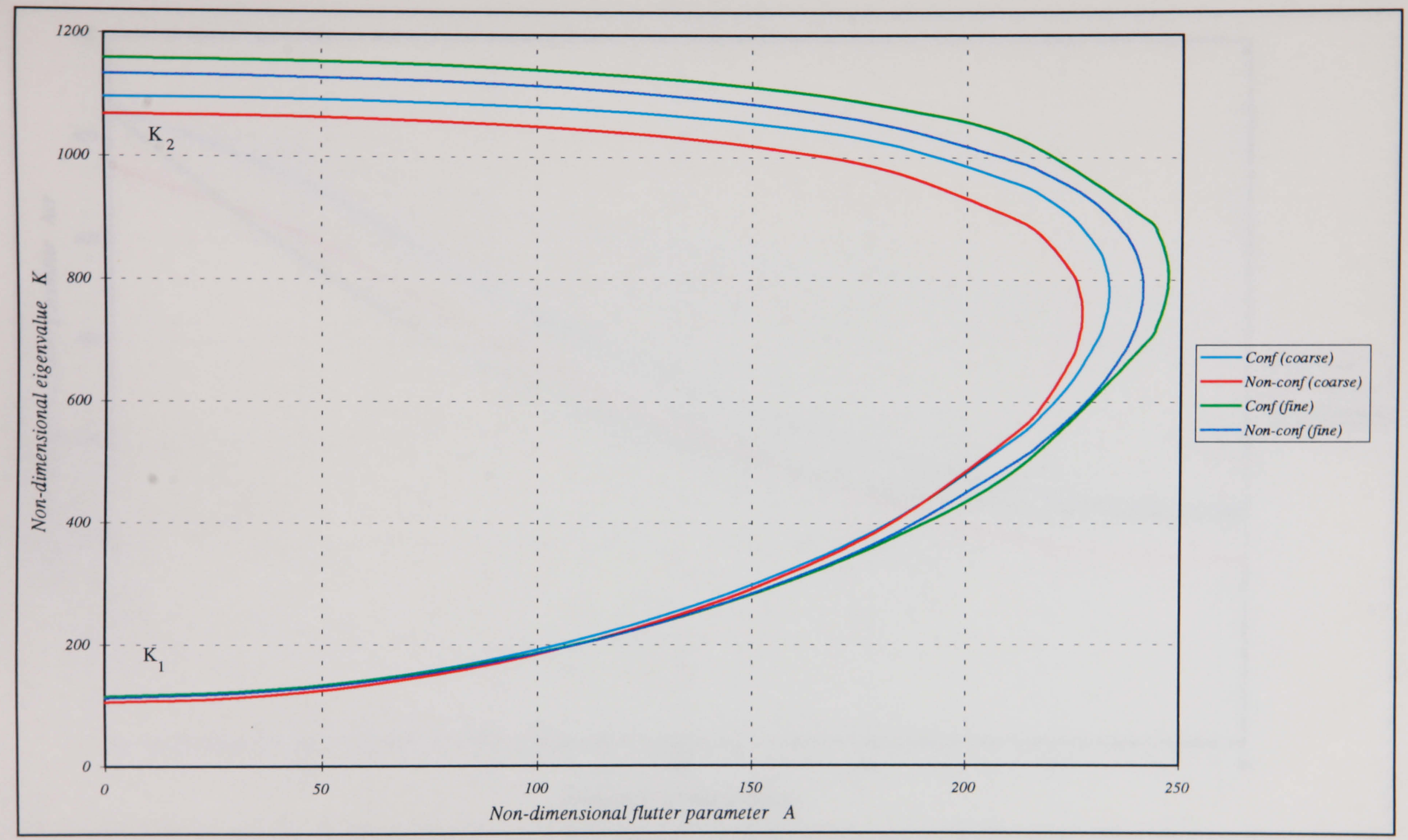

Figure 7.69 Coalescence of eigen values for Boron/Epoxy simply-supported square panel.

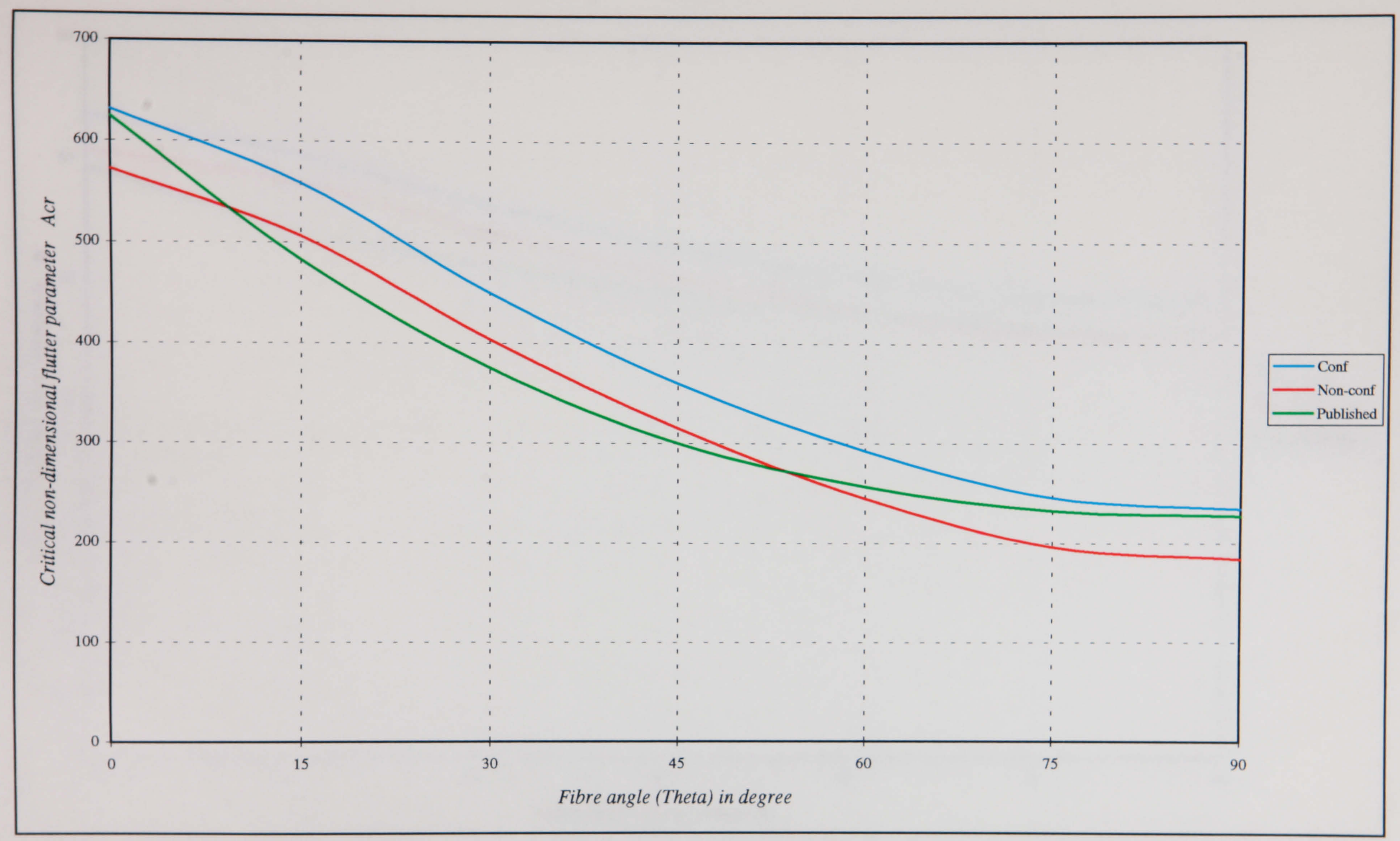

Figure 7.70 Effect of fibre orientation on critical flutter parameter for Graphite/Epoxy clamped square panel.

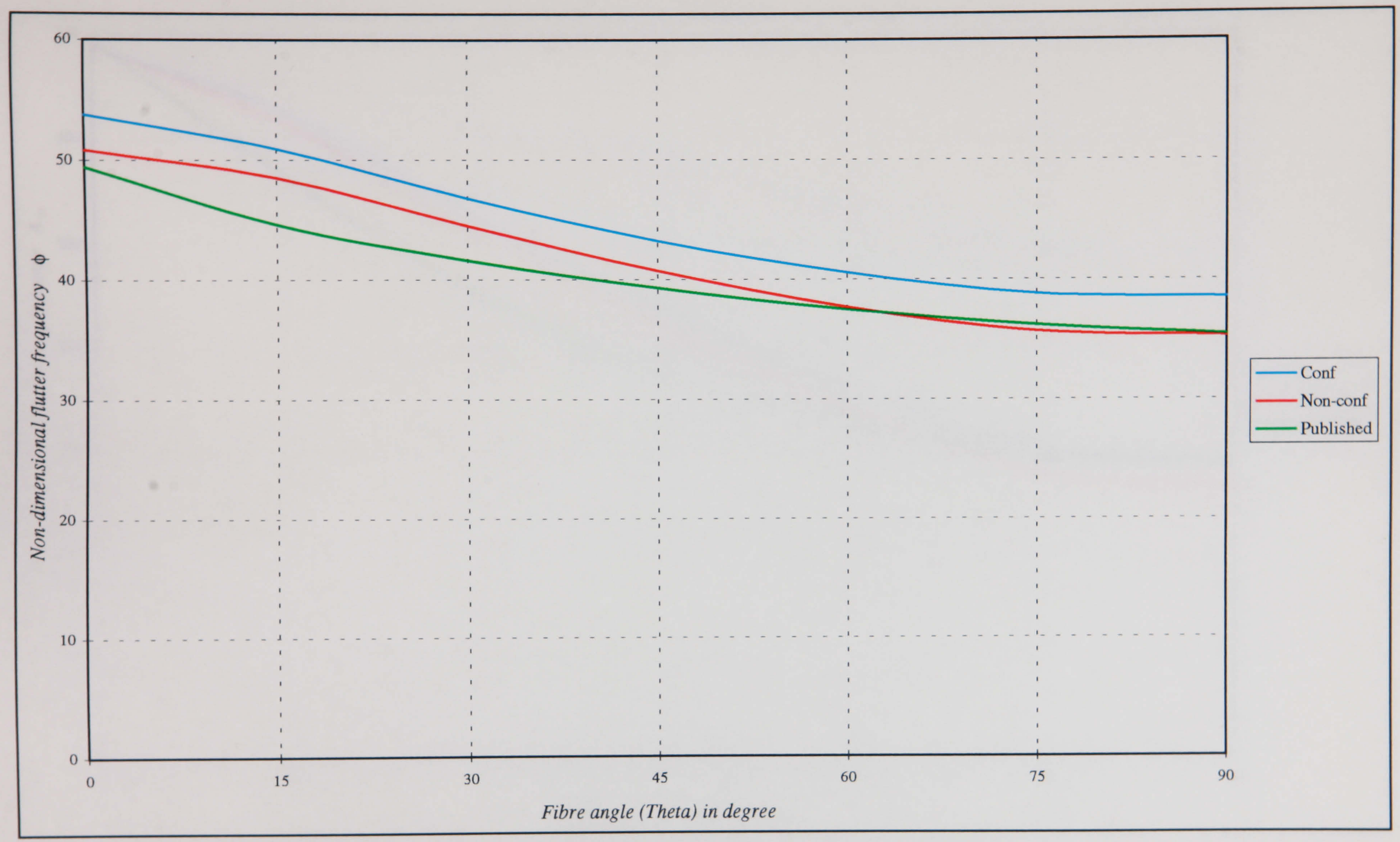

Figure 7.71 Effect of fibre orientation on flutter frequency for Graphite/Epoxy clamped square panel.

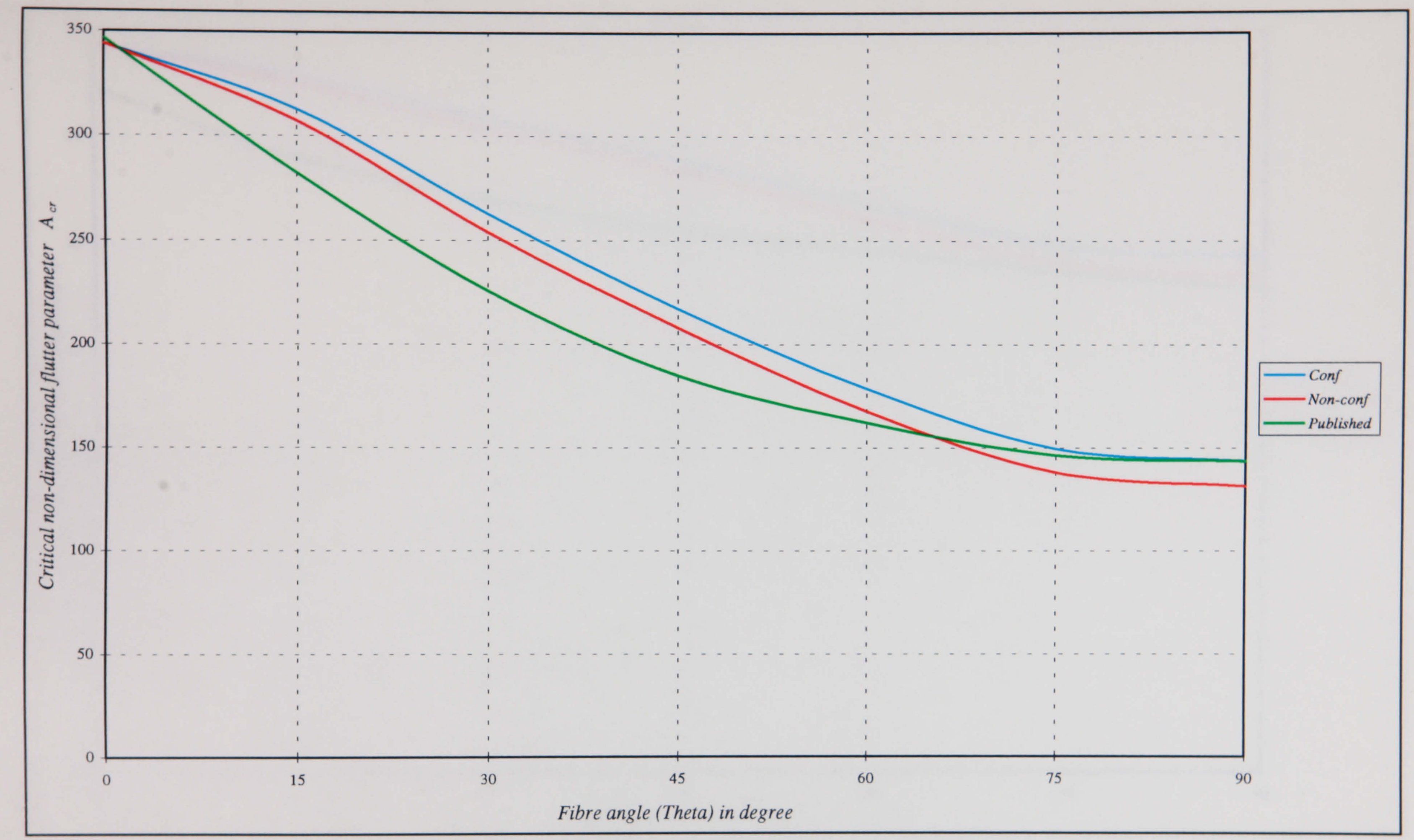

Figure 7.72 Effect of fibre orientation on critical flutter parameter for Graphite/Epoxy simply supported-square panel.

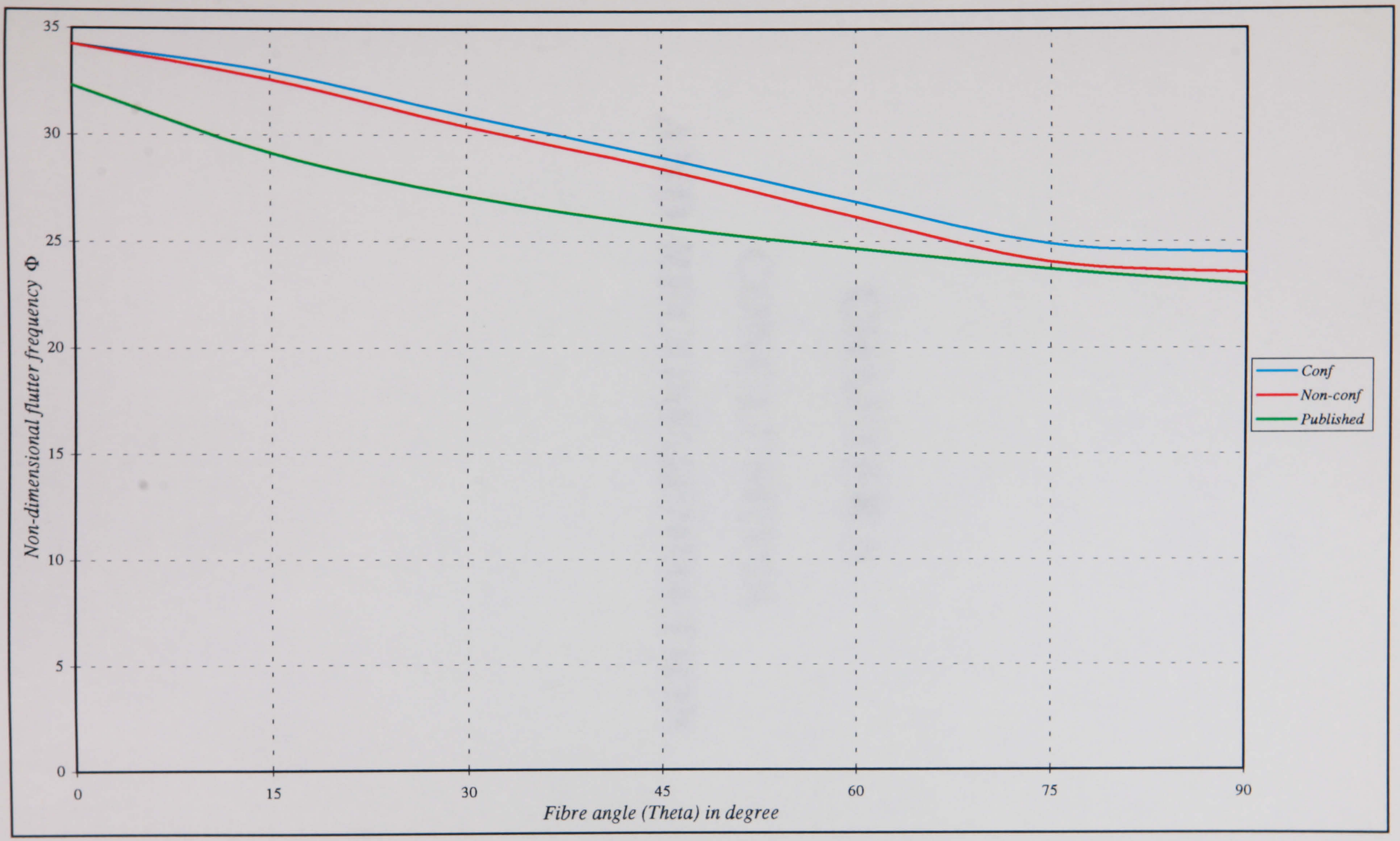

Figure 7.73 Effect of fibre orientation on flutter frequency for Graphite/Epoxy simlpy-supported square panel.

CHAPTER 8

CONCLUSIONS AND RECOMMENDATION

8.1 CONCLUSIONS

It is clear from previous chapters that the author has managed successfully to achieve the basic research objectives. New conforming and non-conforming elements have been developed for the analysis of rotating and non-rotating plate and shell structures made of isotropic or composite layered materials.

A modular user-friendly computer finite element package based upon the developed elements has been created, and properly validated against published theoretical and experimental work. This package is capable of static stress analysis, natural frequency analysis, forced vibration analysis, resonant frequencies prediction for rotating blades, and flutter analysis of panels in supersonic flow.

Several case studies have been analysed with the developed package, and some useful comments have been concluded in the course of their analysis, which are summarized as follows:-

(i) Conforming and non-conforming elements have led to accurate static and dynamic results in general. Nevertheless, it was observed that conforming elements are more accurate to be adopted for flutter analysis of rectangular panels.

(ii) The results obtained by means of developed elements proved to be accurate for a wide range of plate or shell thickness.

(iii) Centrifugal stiffening increases the values of natural frequencies if the generated centrifugal loading opposes the deformation. However, the centrifugal effects decrease with the increase of structure thickness.

(iv) It has been proved through the forced vibration analysis of plates and shells by means of the developed package that, the Coriolis force effects lead to a reduction in forced vibration amplitudes.

(v) One of the debatable findings is that the non-conforming three-node triangular element has shown poor performance, when used for the analysis of rotating plate or shell structures.

(vi) The package came to be a very useful tool for the design optimization of composite layered plates and shells, by means of using different fibre angles as it was demonstrated through a number of case studies.

The original work produced in this thesis is summarized as follows:-

(i) A newly developed theory for higher order conforming and non-conforming elements for composite layered plates and shells, with the use of extra degrees of freedom to accurately represent the transverse shear distributions over the thickness. The new elements were based on a combination of Lagrangian and Hermitian shape functions, and they are valid for a wide range of structural thickness.

(ii) The derivations of the contributions of centrifugal stiffening, Coriolis and centripetal acceleration, and equivalent nodal force, are considered in the new elements, for the analysis of rotating composite layered plates and shell structures.

(iii) Derivation of aeroelastic effects in the newly developed elements, and the derivation of the corresponding element matrices.

(iv) The design of a modular, user-friendly, computer programming package based upon the developed elements. The package is capable of carrying out different types of analysis for isotropic and composite layered plate and shell structures.

8.2 RECOMMENDATIONS FOR FUTURE WORK

This work has been achieved within the time and resources available without sparing any effort, nevertheless, it is the author's view that the work can be improved if the following points are considered:-

(i) Derivation of 6-node higher order triangular elements in order to improve the accuracy of the analysis of rotating plate and shell structures with triangular elements.

(ii) In order to generalize the flutter analysis, the developed package should be coupled with an appropriate CFD package to carry out aeroelastic and flutter analysis for more practical applications such as turbomachine blades.

REFERENCES

Appa, K. and Somashekar, B. R. (1969) Application of matrix displacment methods in the study of panel flutter. *AIAA Journal* **3,** 50-53.

Appa, K., Somashekar, B. R., and Shah, C.G. (1970) Discrete element approach to flutter of skew panels with in-plane forces underyawed supersonic flow. *AIAA Journal* **8,** 2017-2022.

Archer, J. S. (1963) Consistent mass matrix for disturbed mass systems. *Proc. Am. Soc. Civil Engrs.* **89,** 161-178.

Archer, J. S. (1965) Consistent matrix formulation for structural analysis using finite element techniques. *AIAA Journal* **3,** 1910-1918.

Argyris, J. H. (1965) *Continua and discontinua.* Air force flight dynamic lab. AFFDL-TR-66-80.

Ashley, H. and Zartarian, G. (1956) Piston theory- a new aeordynamic tool for the aeroelastician. *J. aeronaut. Soc.* **23,** 1109-1118.

Barbero, E. J. Reddy, J. N., and Teply, J. (1990) An accurate determination of stresses in thick laminates using a generalized plate theory. *Int. J. Numer. Meth. Engng.* **29,** 1-14.

Basar, Y. and Ding, Y. (1990) Finite-rotation elements for the nonlinear analysis of thin shell structures. *Int. J. Solids Structures* **26,** 83-97.

Bathe, K. J. and Wilson, E. L. (1973) Solution methods for eigenvalue problems in structural dynamics. *Int. J. Numer. Methods Engng.* **6,** 213-226.

Bisplinghoff, R. I., Ashley, H., and Holfman, R. L. (1955) *Aeroelasticity.* Addison-Wesley Publishing Company. Mass.

Bisplinghoff, R. I. and Ashley, H. (1962) *Principles of Aeroelasticity.* John Wiley & Son.

Bismarck-Nasr, M. (1993) Supersonic panel flutter analysis of shallow shells. *AIAA Journal* **31,** 1349-1351.

Blocki, J. (1992) A highter-order linear theory for isotropic plates - I theoretical considerations. *Int. J. Solids Structures* **29,** 825-836.

Bogner, F. K., Fox, R. L., and Schmit, L. A. (1965) The generation of interelement compatible stiffness and mass matrices by the use of interpolation formulae. *Proc. Conf. Matrix methods in Struct. Mech.* Air force Inst. of Tech. Wright Patterson A. F. Base, Ohio.

Chang, B., Chen, D.C., and Shabana, A. A. (1990) Effect of the coupling between stretching and bending in the large displacment analysis of plates. *Int. J. Numer. Meth. Engng.* **30,** 1233-1262.

Cho, M. and Parmerter, R. (1994) Finite element for composite plate bending based on efficient higher order theory. *AIAA Journal* **11,** 2241-2248.

Clough, R. W. (1960) The finite element method in plane stress analysis. *J. Structures Div.* ASCE, Proc. 2nd Conf. Elect. Computation, 345-378.

Cofer, W. F. and Will, K. M. (1991) A three-dimensional, shell-solid transition element for general nonlinear analysis. *Computers & Structures* **38,** 449-462.

Cook, R. D. (1981) *Concepts and applications of finite element analysis.* 2nd Ed. John Wiely & Son.

Crawley, E. F. (1979) The natural modes of Graphite/Epoxy cantilever plates and shells. *J. Composite Materials* **13,** 195-205.

Dawe, D. F. (1965) A finite element approach to plate vibration problems. *J. Mech. Eng. Sci.* **7,** 28-32.

De Vito, L. *et al.* (1966) Sul calcolo degli autovalori della piastra quadrata ineastrata lungo il bordo. *Rendiconti dell Accademina Nazionale dei Lincei.* **8,** 725-733.

Dowell, E. H. (1970) A review of the aeroelastic stability of plates and shells. *AIAA Journal* **8**, 385-399.

Dowell, E. H. (1975) *Aeroelasticity of plates and shells.* Noordhoff International Publishers.

Dowell, E. H., Cutiss, H. C., Scanlan, R. H.. and Sisto, F. (1978) *A modern course in aeroelasticity.* Sijthoff & Noordhoff International Publishers.

Dowell, E. H. and Ilgamov, M. (1988) *Studies in nonlinear aeroelasticity.* Spring-Verlag New York Inc.

Dungundji, J. (1986) Theoretical consideration of panel flutter at high supersonic Mach numbers. *AIAA Journal* **4,** 1257-1266.

El-Zafrany, A. M. (1994) *Finite element techniques for engineering analysis.* Ellis Horwood.

El-Zafrany, A. M. (1995) *Plasticity.* Lecture notes, Cranfield University, Cranfield, Bedford, U.K.

El-Zafrany, A. M. and Cookson, R. A. (1985) An explicit formula for the generalized Hermitian interpolation problem. *Communication in Applied Numerical Methods.* **1,** 85 - 91.

El-Zafrany, A. M. and Cookson, R. A. (1986a) Derivation of Lagrangian and Hermitian shape functions for triangular elements. *Int. J. Numer. Meth. Engng.* **23,** 275-285.

El-Zafrany, A. M. and Cookson, R. A. (1986b) Derivation of Lagrangian and Hermitian shape functions for quadrilateral elements. *Int. J. Numer. Meth. Engng.* **23,** 1939-1958.

Epstein, M. and Huttelmaier, H. P. (1983) A finite element formulation for multilayered and thick plates.*Computers & Structures* **16,** 645-650.

Fung, Y. C. (1955) *An introduction to the theory of aeroelasticity.* John Wiley & Son, Inc.

Gebhardt, H. and Schweizerhof, K. (1993) Interpolation of curved shell geometries by low order finite element errors and modifications. *Int. J. Numer. Meth. Engng.* **36**, 287-302.

Gray, C. E., Mei, C., and Shore, C. P. (1991) Finite element method for large amplitude two-dimensional panel flutter at hypersonic speeds. *AIAA Journal* **29,** 290-298.

Guyan, R. J. (1965) Distributed mass matrix for plate vibration problems. *AIAA Journal* **3,** 567-568.

Has, T. M. and Wang, J. T. S. (1970) A theory of laminated cylinderical shells consisting of orthotropic laminae. *AIAA Journal* **8,** 2141-2146.

Hinton, E., Razzaque, A., Zienkiewicz, O. C., and Davies, J. D. (1975) A simple finite element solution for plates of homogeneous, sandwich and cellular construction. *Proc. Instn Civ. Engrs.* **2,** 43-65.

Hinton, E. and Owen, D. R. J. (1984) *Finite element software for plates and shells.* Pineridge Press limited.

Houbolt, J. C. (1958) *A study of several aerothermoelastic problems of aircraft structure in high-speed flight.* Doctoral Thesis, Swiss Fedral Institute Technology, Zurich.

Irons, B. (1970) A frontal solution program for finite element analysis. *Int. J. Numer. Meth. Engng.* **2**, 5-32.

Irons, B. and Ahmed, S. (1980) *Techniques of finite elements.* Ellis Horwood Ltd., Publishers.

Jacquet-Richardet, G. and Henry, R. (1994) A modal aeroelastic finite element analysis method for advanced turbomachinery stages. *Int. J. Numer. Meth. Engng.* **37,** 4205-4217.

Kabir, H. R. H. (1992) A double fourier series approach to the solution of a moderately thick simply supported plate with antisymmetric angle-ply laminations. *Computers & Structures* **43,** 769-774.

Karakostas, C., and Talaslidis, D. (1993) Triangular C^0 bending elements based on the Hu-Washizu principle and orthogonality conditions. *Int. J. Numer. Meth. Engng.* **36,** 181-200.

Leckie, F. A. and Lindberg, G. M. (1963) The effect of lumped parameters on beam frequencies. *Aeronaut. Quart.* **XIV,** 224-240.

Lee, I. and Cho, M. H. (1991) Finite element analysis of composite panel flutter. *Computers & Structures* **39,** 165-172.

Lee, S. W. and Pian, T. H. (1978) Improvements of plate and shell finite elements by mixed formulations. *AIAA Journal* **16**

Lindberg, G. M. (1963) *Lumped parameter methods applied to elastic vibrations.* PhD. Thesis Univ. of Cambridge, England.

Love, A. E. H. (1944) *A treatise on the mathematical theory of elasticity.* 4th Ed. Dover, New York.

McGee, O. G., Leissa, W. A., and Huang, C. S. (1992) Vibration of cantilevered skewed plates with corner stress singularities. *Int. J. Numer. Meth. Engng.* **35,** 409-424.

Melosh, R. J. (1963) Basis for derivation of matrices for direct stiffness method. *AIAA Journal* **1,** 1631-1637.

Mindlin, R. D. (1951) Influence of rotatory inertia and shear on flexural motion of isotropic elastic plates. *J. Appl. Mech.* **18,** 31-38.

Namini, A. H. (1991) Analytical modling of flutter derivatives as finite elements. *Computers & Structures* **41,** 1055-1064.

Narita, Y. and Leissa, A. W. (1992) Frequencies and mode shapes of cantilevered laminated composite plates. *J. of Sound and Vibration* **154,** 161-172.

Nelson, R. B. and Lorch, D. R. (1974) A refined theory for laminated orthotropic plates. *J. Appl. Mech* 177-183.

Olson, M. D. (1967) Finite element applied to panel flutter. *AIAA Journal* **5**, 2267-2270.

Olson, M. D. (1970) Some flutter solutions using finite elment. *AIAA Journal* **8**, 747-752.

Onate, E., Zienkiewicz, O. C., Suarez, B., and Taylor. R. L. (1992) A general methodology for deriving shear constrained Reissner Mindlin plate elements. *Int. J. Numer. Meth. Engng.* **33,** 345-367.

Pillasch, D. W., Majerus, J. N., and Zak, A. R. (1983) Dynamic finite element model for laminated structures. *Computers & Structures* **16,** 449-455.

Ramm. E. and Buechter, N. (1992) Shell theory versus degeneration - a comparison in large rotation finite element analysis. *Int. J. Numer. Meth. Engng.* **34,** 39-59.

Rao, S. K. and Rao, V. G. (1980) Large amplitude supersonic flutter of panels with end elastically restrained againest rotation. *Computers & Structures* **11,** 197-201.

Reddy, J. N. (1984a) A refined nonlinear theory of plates with transverse shear deformation. *Int. J. Solids Structures* **20,** 881-896.

Reddy, J. N. (1984b) A refined nonlinear theory of plates with transverse shear deformation. *Int. J. Solids Structures* **20,** 881-896.

Reddy, J. N. (1985) A simple higher order theory for laminated composite plates. *J. Appl. Mech.* **51,** 745-752.

Reissner, E. (1945) On the theory of bending of elastic plates. *J. Math. Phys.* **23,** 184-191.

Sacco, E. (1992) A consistent model for first order moderate rotation plate theory. *Int. J. Numer. Meth. Engng.* **35,** 2049-2066.

Sander, G., Bon, C., and Geradin, M. (1973) Finite element analysis of supersonic panel flutter. *Int. J. Numer. Meth. Engng.* 7, 379-394.

Sarma, B. S. and Varadan, T. K. (1988) Nonlinear panel flutter by finite element method. *AIAA Journal* **26,** 566-574.

Shi, G. and Voyiadjis, G. Z. (1991) Geometerically nonlinear analysis of plates by assumed strain element with explicit tangent stiffness matrix. *Computers & Structures* **41,** 757-763.

Shiau, L. C. and Chang, J. T. (1991) Finite element analysis of supersonic flutter of multibay composite panels. *Computers & Structures* **39,** 269-276.

Srinivasan, R. S. and Babu, B. J. C. (1987) Free vibration and flutter of laminated quadrilateral plates. *Computers & Structures* **27,** 297-304.

Tessler, A. (1993) An improved plate theory of {1,2}-order for thick composite laminates. *Int. J. Solids Structures* **30**, 981-1000.

Timoshenko, S. and Kreiger, S. (1959) *Theory of plates and shells*. 2nd Ed. McGraw-Hill.

Todhunter, I. and Pearson, K. (1986) *A history of the theory of elasticity*. Cambridge University Press.

Turner, M. J., Clough, R.J., Martin. H. C., and Topp, L. J. (1956) Stiffness and deflection analysis of complex structures. *J. Aero. Sci.* **23,** 805-623.

Wang, F. Y. (1990) Two dimensional theories deduced from three-dimension theory for a transversely isotropic body--I. plate problems. *Int. J. Solids Structures* **26,** 445-470.

Widera, G. E. O and Moumene, M. (1984) Cutout in laminated plates and shells. *Adv. Macro-Mech. Composite Material Vessls Components*, **146,** 155-158.

Wilkinson, J. H. (1965) *The algebraic eigenvalue problem.* Oxford Clarendon Press, U. K.

Witt, M. and Sobczyk, K. (1980) Dynamic response of laminated plates to random loading. *Int. J. Solids Structures* **16**, 231-3238.

Wung, P. M. and Reddy, J. N. (1991) A transverse deformation theory of laminated composite plates. *Computers & Structures* **41**, 821-833.

Xue, D. Y., and Mei, C. (1993) Finite element nonlinear panel flutter with arbitary temperatures temperatures in supersonic flow. *AIAA Journal* **31**, 154-162.

Yang, T. Y., and Sung, S. H. (1977) Finite-element panel flutter in three-dimensional supersonic unsteady potential flow. *AIAA Journal* **15**, 1677-1683.

Yang, H. T. Y., Saigal, S., and Liaw. D. G. (1990) Advances of thin shell finite elements and some applications-version I. *Computers & Structures*. **35**, 505-522.

Yuqin, L. and Fei, X. (1992) A universal method for including shear deformation in thin plate elements. *Int. J. Numer. Meth. Engng*. **34**, 171-177.

Zhongnian, X. (1992) A thick-thin traiagular plate element. *Int. J. Numer. Meth. Engng*. **33**, 963-973.

Zienkiewicz, O. C. and Cheung, Y. K. (1964) The finite element method for analysis of elastic isotropic and orthotropic slabs. *Proc. Inst. Civil Engrs*. **28**, 471-488.

Zienkiewicz, O. C. (1977) *The finite element Method*. 3rd Ed. McGraw-Hill.

Zienkiewicz, O. C., Taylor, R. L., Papadopoulos, P., and Onate, E. (1990) Plate bending elements with discrete constraints: new triangular elements. *Computers & Structures* **35**, 505-522.

APPENDIX A

LAGRANGIAN SHAPE FUNCTIONS

A1 4-NODE QUADRILATERAL ELEMENT

(i) Shape functions

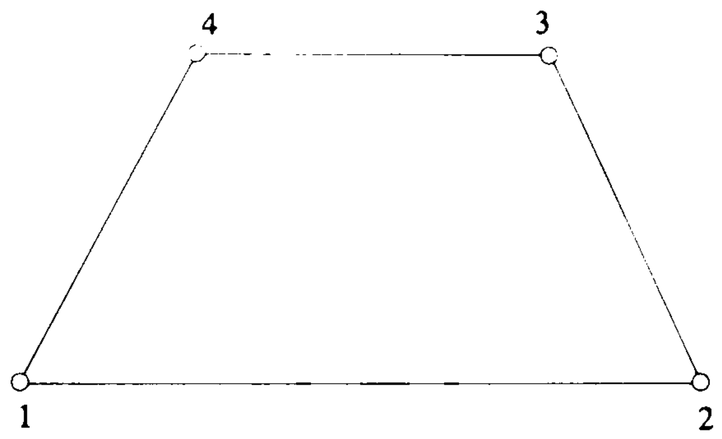

$$N_1 = (1-\xi)\ (1-\eta) \tag{A.1}$$

$$N_2 = \xi\ (1-\eta) \tag{A.2}$$

$$N_3 = \xi\ \eta \tag{A.3}$$

$$N_4 = (1-\xi)\ \eta \tag{A.4}$$

(ii) First order derivatives

$$\frac{\partial N_1}{\partial \xi} = -1+\eta \tag{A.5}$$

$$\frac{\partial N_2}{\partial \xi} = 1-\eta \tag{A.6}$$

$$\frac{\partial N_3}{\partial \xi} = \eta \tag{A.7}$$

$$\frac{\partial N_4}{\partial \xi} = -\eta \tag{A.8}$$

$$\frac{\partial N_1}{\partial \eta} = -1+\xi \tag{A.9}$$

$$\frac{\partial N_2}{\partial \eta} = -\xi \tag{A.10}$$

$$\frac{\partial N_3}{\partial \eta} = \xi \tag{A.11}$$

$$\frac{\partial N_4}{\partial \eta} = 1-\xi \tag{A.12}$$

A2 3-NODE TRIANGULAR ELEMENT SHAPE FUNCTIONS

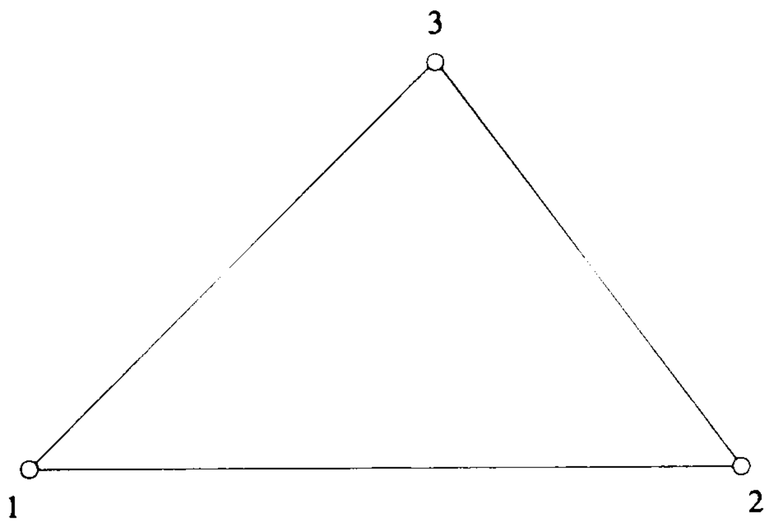

$$N_1 = 1 - \xi - \eta \tag{A.13}$$

$$N_2 = \xi \tag{A.14}$$

$$N_3 = \eta \tag{A.15}$$

APPENDIX B

NON-CONFORMING HERMITIAN SHAPE FUNCTIONS

B1 FOUR-NODE RECTANGULAR ELEMENT

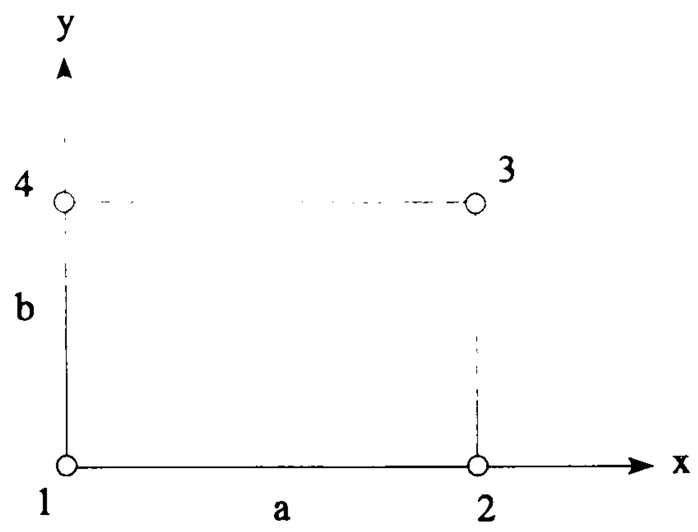

$$f_1 = (1-\eta)H_1^{1,0}(\xi) + (1-\xi)H_1^{1,0}(\eta) - (1-\xi)(1-\eta) \tag{B.1}$$

$$g_1 = a(1-\eta)H_1^{1,1}(\xi) \tag{B.2}$$

$$h_1 = b(1-\xi)H_1^{1,1}(\eta) \tag{B.3}$$

$$f_2 = (1-\eta)H_2^{1,0}(\xi) + \xi H_1^{1,0}(\eta) - \xi(1-\eta) \tag{B.4}$$

$$g_2 = a(1-\eta)H_2^{1,1}(\xi) \tag{B.5}$$

$$h_2 = b\,\xi H_1^{1,1}(\eta) \tag{B.6}$$

$$f_3 = \eta H_2^{1,0}(\xi) + \xi H_2^{1,0}(\eta) - \xi\eta \tag{B.7}$$

$$g_3 = a\,\eta H_2^{1,1}(\xi) \tag{B.8}$$

$$h_3 = b\,\xi H_2^{1,1}(\eta) \tag{B.9}$$

$$f_4 = \eta H_1^{1,0}(\xi) + (1-\xi)H_2^{1,0}(\eta) - \eta(1-\xi) \tag{B.10}$$

$$g_4 = a\,\eta H_1^{1,1}(\xi) \tag{B.11}$$

$$h_4 = b(1-\xi)H_2^{1,1}(\eta) \tag{B.12}$$

where

$$H_1^{1,0}(\eta) = 1 - 3\eta^2 + 2\eta^3$$

$$H_1^{1,1}(\eta) = \eta - 2\eta^2 + \eta^3$$

$$H_2^{1,0}(\eta) = 3\eta^2 - 2\eta^3$$

$$H_2^{1,1}(\eta) = -\eta^2 + \eta^3$$

B2 THREE-NODE TRIANGULAR ELEMENT

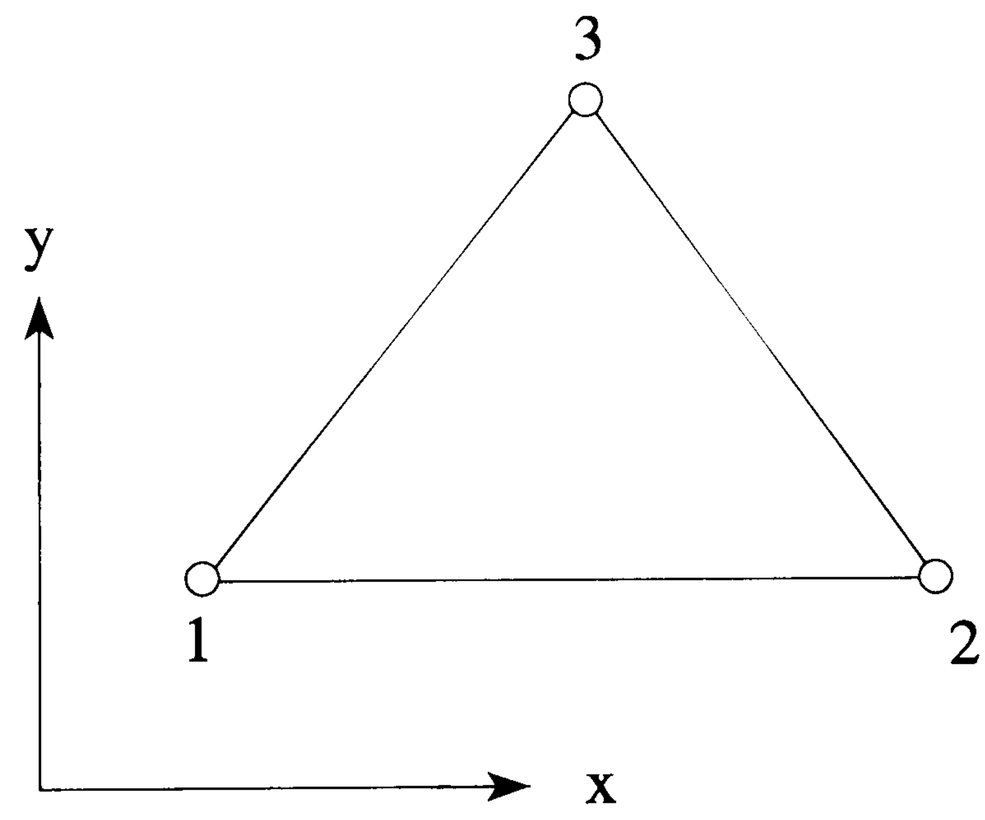

$$f_1 = (1-\xi-\eta)^2[3-2(1-\xi-\eta)] + 2\xi\eta(1-\xi-\eta) \qquad \text{(B.13)}$$

$$g_1 = (x_2-x_1)\left[(1-\xi-\eta)^2\xi + \tfrac{1}{2}\xi\eta(1-\xi-\eta)\right]$$
$$+ (x_3-x_1)\left[(1-\xi-\eta)^2\eta + \tfrac{1}{2}\xi\eta(1-\xi-\eta)\right] \qquad \text{(B.14)}$$

$$h_1 = (y_2-y_1)\left[(1-\xi-\eta)^2\xi + \tfrac{1}{2}\xi\eta(1-\xi-\eta)\right]$$
$$+ (y_3-y_1)\left[(1-\xi-\eta)^2\eta + \tfrac{1}{2}\xi\eta(1-\xi-\eta)\right] \qquad \text{(B.15)}$$

$$f_2 = \xi^2(3-2\xi) + 2\xi\eta(1-\xi-\eta) \qquad \text{(B.16)}$$

$$g_2 = (x_1 - x_2)\left[\xi^2(1-\xi-\eta) + \frac{1}{2}\xi\eta(1-\xi-\eta)\right]$$

$$+ (x_3 - x_2)\left[\xi^2\eta + \frac{1}{2}\xi\eta(1-\xi-\eta)\right] \qquad \text{(B.17)}$$

$$h_2 = (y_1 - y_2)\left[\xi^2(1-\xi-\eta) + \frac{1}{2}\xi\eta(1-\xi-\eta)\right]$$

$$+ (y_3 - y_2)\left[\xi^2\eta + \frac{1}{2}\xi\eta(1-\xi-\eta)\right] \qquad \text{(B.18)}$$

$$f_3 = \eta^2(3-2\eta) + 2\xi\eta(1-\xi-\eta) \qquad \text{(B.19)}$$

$$g_3 = (x_1 - x_3)\left[\eta^2(1-\xi-\eta) + \frac{1}{2}\xi\eta(1-\xi-\eta)\right]$$

$$+ (x_2 - x_3)\left[\eta^2\xi + \frac{1}{2}\xi\eta(1-\xi-\eta)\right] \qquad \text{(B.19)}$$

$$h_3 = (y_1 - y_3)\left[\eta^2(1-\xi-\eta) + \frac{1}{2}\xi\eta(1-\xi-\eta)\right]$$

$$+ (y_2 - y_3)\left[\eta^2\xi + \frac{1}{2}\xi\eta(1-\xi-\eta)\right] \qquad \text{(B.20)}$$

APPENDIX C

CONFORMING HERMITIAN SHAPE FUNCTIONS

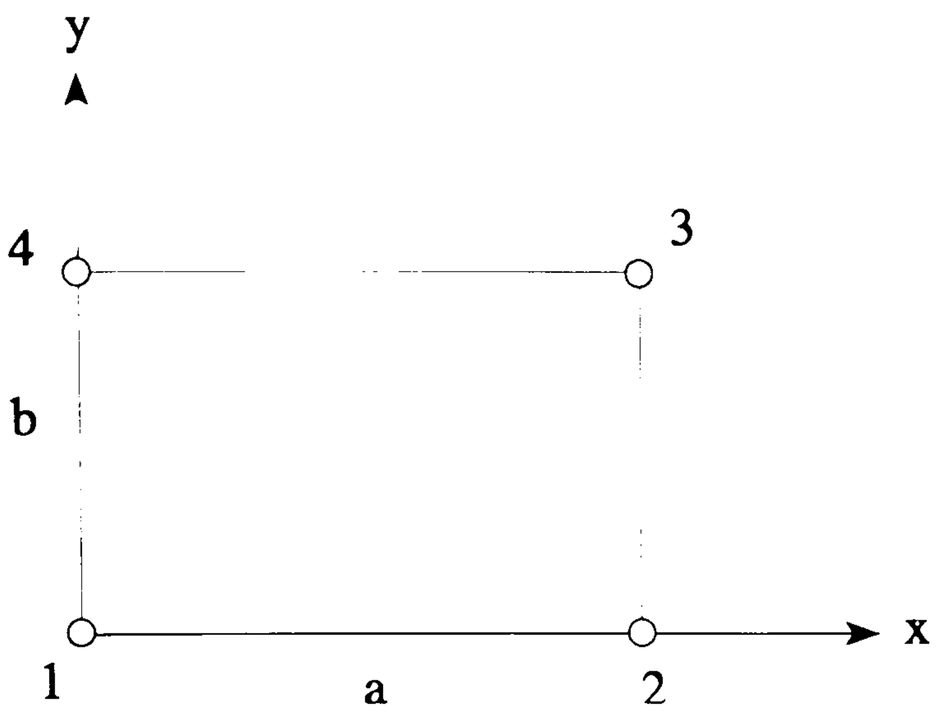

$$F_1 = H_1^{1,0}(\xi)\,H_1^{1,0}(\eta) \tag{C.1}$$

$$G_1 = a\,H_1^{1,1}(\xi)\,H_1^{1,0}(\eta) \tag{C.2}$$

$$H_1 = b\,H_1^{1,0}(\xi)\,H_1^{1,1}(\eta) \tag{C.3}$$

$$Q_1 = ab\,H_1^{1,1}(\xi)\,H_1^{1,1}(\eta) \tag{C.4}$$

$$F_2 = H_2^{1,0}(\xi)\,H_1^{1,0}(\eta) \tag{C.5}$$

$$G_2 = a\,H_2^{1,1}(\xi)\,H_1^{1,0}(\eta) \tag{C.6}$$

$$H_2 = b\,H_2^{1,0}(\xi)\,H_1^{1,1}(\eta) \tag{C.7}$$

$$Q_2 = ab\,H_2^{1,1}(\xi)\,H_1^{1,1}(\eta) \tag{C.8}$$

$$F_3 = H_2^{1,0}(\xi)\,H_2^{1,0}(\eta) \tag{C.9}$$

$$G_3 = a\,H_2^{1,1}(\xi)\,H_2^{1,0}(\eta) \tag{C.10}$$

$$H_3 = b\,H_2^{1,0}(\xi)\,H_2^{1,1}(\eta) \tag{C.11}$$

$$Q_3 = ab\,H_2^{1,1}(\xi)\,H_2^{1,1}(\eta) \tag{C.12}$$

$$F_4 = H_1^{1,0}(\xi)\,H_2^{1,0}(\eta) \tag{C.13}$$

$$G_4 = a H_1^{1,1}(\xi) H_2^{1,0}(\eta) \tag{C.14}$$

$$H_4 = b H_1^{1,0}(\xi) H_2^{1,1}(\eta) \tag{C.15}$$

$$Q_4 = ab H_1^{1,1}(\xi) H_2^{1,1}(\eta) \tag{C.16}$$

APPENDIX D

ADDITIONAL MATHEMATICAL ASPECTS OF ELEMENTS

D1 GEOMETRICAL REPRESENTATION

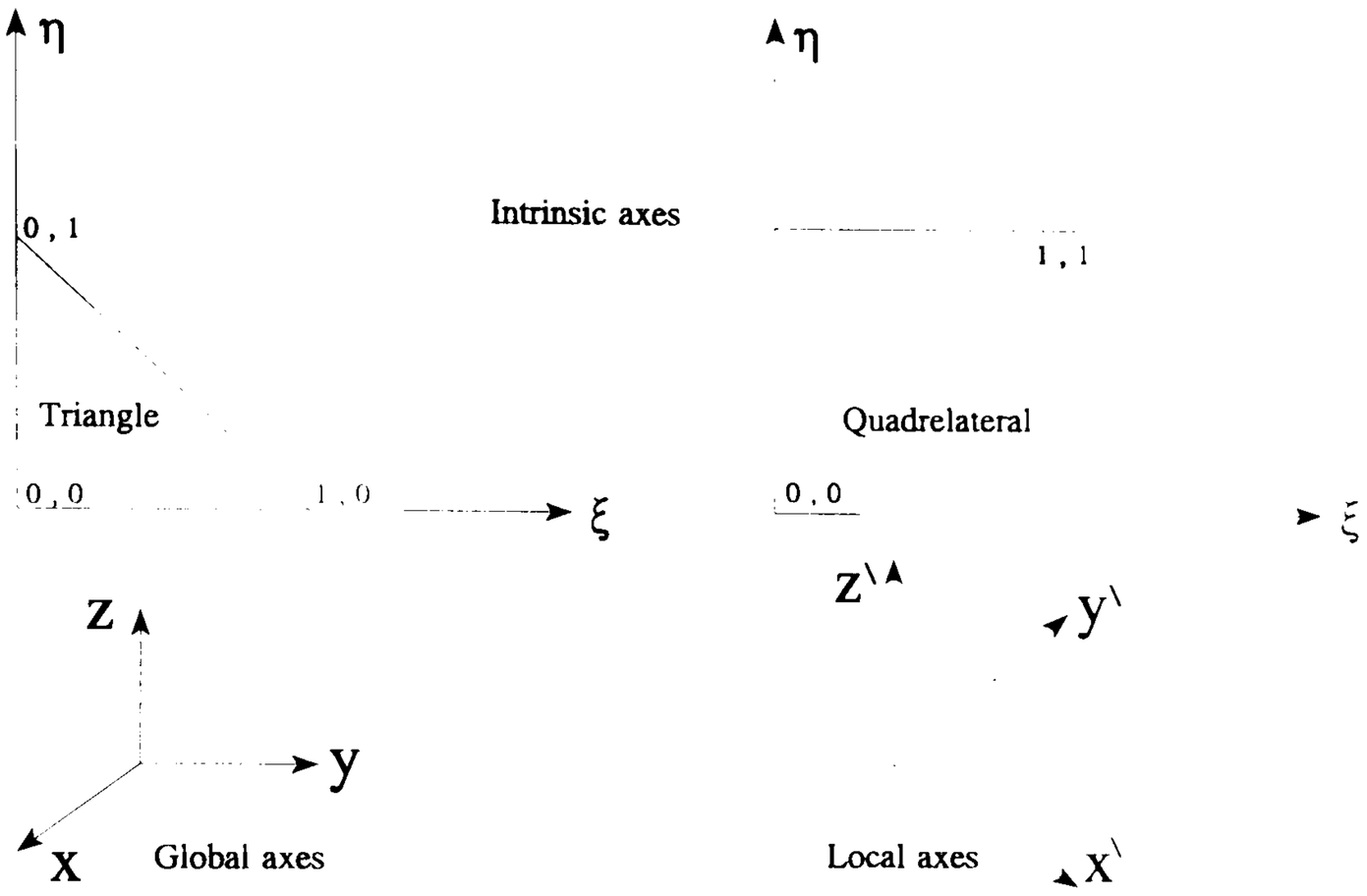

The element is represented with respect to a global system of axes (x, y, z) in terms of the following parameters:-

(a) the global coordinates of midplane nodes, and

(b) the thickness distribution by means of specifying layers thickness at every node.

For an n-node element, the following parameters are specified :-

$$(x_i, y_i, z_i), \qquad i = 1, 2, \ldots, n$$

$$h_i^{(l)}, \quad l = 1, 2, \ldots, N_l, \quad i = 1, 2, \ldots, n$$

where x_i, y_i, z_i are the global coordinates of the node i on the element midplane,

$h_i^{(l)}$ is the l^{th} layer thickness at node i measured in the normal direction to the element midplane.

The material axes are defined with respect to element local axes, as described in section (3.1). For plate problem the local axes are same as global axes, *i.e.*

$$x_i^{\backprime} = x_i, \qquad y_i^{\backprime} = y_i, \qquad z_i^{\backprime} = z_i = 0$$

and the coordinate z_i is also a redundant parameter. For curved shells the local

axes $x^{\backprime}, y^{\backprime}, z^{\backprime}$ are obtained as described in section (3.1), and with direction cosines (l_1, m_1, n_1), (l_2, m_2, n_2) and (l_3, m_3, n_3). Hence the local coordinates are defined as follows :-

$$\left.\begin{aligned} x_i^{\backprime} &= l_1 (x_i - x_1) + m_1 (y_i - y_1) + n_1 (z_i - z_1) \\ y_i^{\backprime} &= l_2 (x_i - x_1) + m_2 (y_i - y_1) + n_2 (y_i - y_1) \\ z_i^{\backprime} &= 0 \end{aligned}\right\} \qquad \text{(D.1)}$$

where $i=1, 2, \ldots, n$

The total thickness at node i will be :

$$H_i \equiv H(x_i^{\backprime}, y_i^{\backprime}) = \sum_{i=1}^{N_l} h_i^{(l)} \qquad \text{(D.2)}$$

and the z coordinates at the lower and upper surfaces of the l^{th} layer, along the line which passes through node i and is parallel to the $z^{\backprime}$ axis, is :-

$$Z_L^{(l)}(x_i^{\backprime}, y_i^{\backprime}) = -\frac{H_i}{2} + \sum_{k=1}^{l-1} h_i^{(k)} \qquad \text{(D.3)}$$

$$Z_U^{(l)}(x_i^{\backprime}, y_i^{\backprime}) = Z_L^{(l)}(x_i^{\backprime}, y_i^{\backprime}) + h_i^{(l)} \qquad \text{(D.4)}$$

The element is represented in the ξ-η plane as shown in the previous figure, by the following isoparametric transformation :-

$$x^{\backprime}(\xi, \eta) = \sum_{i=1}^{n} x_i^{\backprime} N_i(\xi, \eta) \qquad \text{(D.5)}$$

$$y^{\backprime}(\xi, \eta) = \sum_{i=1}^{n} y_i^{\backprime} N_i(\xi, \eta) \qquad \text{(D.6)}$$

where N_i (ξ , η) represents Lagrangian shape functions.

The definitions of modified $\boldsymbol{D}$ matrices and ρ parameters imply integrations over the $z^{\backprime}$ axis, at a given ($x^{\backprime}$, $y^{\backprime}$) or (ξ , η). The thickness will also be interpolated by means of the same Lagrangian shape functions, *i.e.*

$$h^{(l)}(\xi,\eta) = \sum_{i=1}^{n} h_i^{(l)} N_i(\xi,\eta) \tag{D.7}$$

Hence, Equations similar to (D.3) and (D.4) can be employed, *i.e.*

$$Z_L^{(l)}(\xi,\eta) = -\frac{H_i(\xi,\eta)}{2} + \sum_{k=1}^{l-1} h_i^{(k)}(\xi,\eta) \tag{D.8}$$

$$Z_U^{(l)}(\xi,\eta) = Z_L^{(l)}(\xi,\eta) + h_i^{(l)}(\xi,\eta) \tag{D.9}$$

$$H(\xi,\eta) = \sum_{i=1}^{N_l} h_i^{(l)}(\xi,\eta) \tag{D.10}$$

D2 NUMERICAL EVALUATION OF ELEMENT MATRICES

Consider any element matrix, which is as described in previous sections, for example $\boldsymbol{K}_{bb}$ defined by Equation (4.72). Using intrinsic coordinates, it can be shown that :-

$$\boldsymbol{K}_{bb} = \int_0^1 \int_0^{f(\eta)} \boldsymbol{B}_b^t \boldsymbol{D}_{bb} \boldsymbol{B}_b \left| \boldsymbol{J}\left(\frac{x,y}{\xi,\eta}\right) \right| d\xi\, d\eta \tag{D.11}$$

where $f(\eta) = 1$ for quadrilateral elements,
$= 1 - \eta$ for triangle elements, and

$$\boldsymbol{J}\left(\frac{x,y}{\xi,\eta}\right) = \begin{bmatrix} \dfrac{\partial x}{\partial \xi} & \dfrac{\partial y}{\partial \xi} \\ \dfrac{\partial x}{\partial \eta} & \dfrac{\partial y}{\partial \eta} \end{bmatrix} \equiv \begin{bmatrix} J_{11} & J_{12} \\ J_{21} & J_{22} \end{bmatrix} \tag{D.11}$$

which is the Jacobian matrix.

Using the modified Gaussian quadrature (El-Zafrany,1994), it can be shown that :-

$$\boldsymbol{K}_{bb} = \sum_{s=1}^{N_Q} \sum_{r=1}^{N_Q} f(\eta_s)\, w_r\, w_s \left(\boldsymbol{B}_b^t \boldsymbol{D}_{bb} \boldsymbol{B}_b \,|\boldsymbol{J}| \right)_{\text{at } \xi_{rs},\, \eta_s} \tag{D.12}$$

where $\xi_{rs} = \eta_r f(\eta_s)$, and η_s , w_s are the abscissa and weight of the modified

quadrature scheme with N_Q points. Notice also that $\boldsymbol{D}_{bb}$ should be calculated at (ξ_{rs}, η_s), from Equation (4.63), *i.e.*

$$\boldsymbol{D}_{bb}(\xi,\eta) = \sum_{l=1}^{N_l} \left[\frac{(Z_U^{(l)})^3(\xi,\eta) - (Z_L^{(l)})^3(\xi,\eta)}{3} \right] \boldsymbol{D}_{xy}^{(l)} \qquad \text{(D.13)}$$

A similar procedure can be employed for every other element matrix.

D3 SHAPE FUNCTION DERIVATIVES

The $\boldsymbol{B}$ matrices and some other matrices, are in terms of first or second order cartesian derivatives of intrinsic shape functions. Using the chain rule of partial differentiation twice, it can be proved that for a function $f(\xi,\eta)$:-

$$\begin{bmatrix} \frac{\partial f}{\partial x} \\ \frac{\partial f}{\partial y} \\ \frac{\partial^2 f}{\partial x^2} \\ \frac{\partial^2 f}{\partial y^2} \\ \frac{\partial^2 f}{\partial x \partial y} \end{bmatrix} = \boldsymbol{J}_{(2)}^{-1}\left(\frac{x,y}{\xi,\eta}\right) \begin{bmatrix} \frac{\partial f}{\partial \xi} \\ \frac{\partial f}{\partial \eta} \\ \frac{\partial^2 f}{\partial \xi^2} \\ \frac{\partial^2 f}{\partial \eta^2} \\ \frac{\partial^2 f}{\partial \xi \partial \eta} \end{bmatrix} \qquad \text{(D.14)}$$

where (x, y) represents here for simplicity, the local coordinates, and $\boldsymbol{J}_{(2)}\left(\frac{x,y}{\xi,\eta}\right)$ is the second order Jacobian matrix defined as follows :-

$$\boldsymbol{J}_{(2)}\left(\frac{x,y}{\xi,\eta}\right) = \begin{bmatrix} J_{11} & J_{12} & 0 & 0 & 0 \\ J_{21} & J_{22} & 0 & 0 & 0 \\ \dfrac{\partial^2 x}{\partial \xi^2} & \dfrac{\partial^2 y}{\partial \xi^2} & J_{11}^2 & J_{12}^2 & 2J_{11}J_{12} \\ \dfrac{\partial^2 y}{\partial \eta^2} & \dfrac{\partial^2 y}{\partial \eta^2} & J_{21}^2 & J_{22}^2 & 2J_{21}J_{22} \\ \dfrac{\partial^2 x}{\partial \xi\, \partial \eta} & \dfrac{\partial^2 y}{\partial \xi\, \partial \eta} & J_{11}J_{21} & J_{12}J_{22} & J_{11}J_{22} + J_{12}J_{21} \end{bmatrix} \qquad \text{(D.15)}$$

and $J_{11}, J_{12}, J_{21}, J_{22}$ are the terms of the first order Jacobian matrix, as defined by Equation (D.11).

For the special case of simple elements, which can be defined geometrically in terms of three nodes, and quadrilateral elements with parallel opposite sides (parellelgram) it can be shown that (El-Zafrany,1994) the isoparametric Equations (D.5) and (D.6) are reduced to :-

$$\left.\begin{aligned} x(\xi,\eta) &= a_1 + b_1\xi + c_1\eta \\ y(\xi,\eta) &= a_2 + b_2\xi + c_2\eta \end{aligned}\right\} \qquad \text{(D.16)}$$

i.e.

$$\frac{\partial^2 x}{\partial \xi^2} = \frac{\partial^2 x}{\partial \eta^2} = \frac{\partial^2 x}{\partial \xi\, \partial \eta} = 0$$

$$\frac{\partial^2 y}{\partial \xi^2} = \frac{\partial^2 y}{\partial \eta^2} = \frac{\partial^2 y}{\partial \xi\, \partial \eta} = 0$$

and the derivative equations can be decoupled as follows :-

$$\begin{bmatrix} \dfrac{\partial f}{\partial x} \\ \dfrac{\partial f}{\partial y} \end{bmatrix} = \boldsymbol{J}^{-1}\left(\frac{x,y}{\xi,\eta}\right) \begin{bmatrix} \dfrac{\partial f}{\partial \xi} \\ \dfrac{\partial f}{\partial \eta} \end{bmatrix} \qquad \text{(D.17)}$$

$$\begin{bmatrix} \dfrac{\partial^2 f}{\partial x^2} \\ \dfrac{\partial^2 f}{\partial y^2} \end{bmatrix} = \boldsymbol{J}^{-1}_{\substack{(2) \\ reduced}} \left(\frac{x, y}{\xi, \eta} \right) \begin{bmatrix} \dfrac{\partial^2 f}{\partial \xi^2} \\ \dfrac{\partial^2 f}{\partial \eta^2} \end{bmatrix} \tag{D.18}$$

where

$$\boldsymbol{J}_{\substack{(2) \\ reduced}} \left(\frac{x, y}{\xi, \eta} \right) = \begin{bmatrix} J_{11}^2 & J_{12}^2 & 2 J_{11} J_{12} \\ J_{21}^2 & J_{22}^2 & 2 J_{21} J_{22} \\ J_{11} J_{21} & J_{12} J_{22} & J_{11} J_{22} + J_{12} J_{21} \end{bmatrix} \tag{D.19}$$

APPENDIX E

ANALYTICAL SOLUTIONS

E1 Euler-Bernoulli beam solution

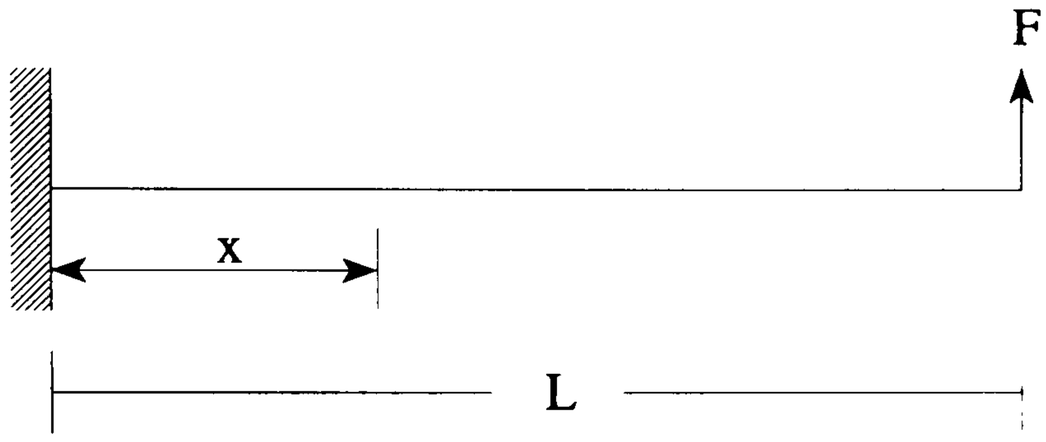

$$\delta\ (x)\ =\ \frac{F x^2\ (3L\ -\ x)}{6EI}$$

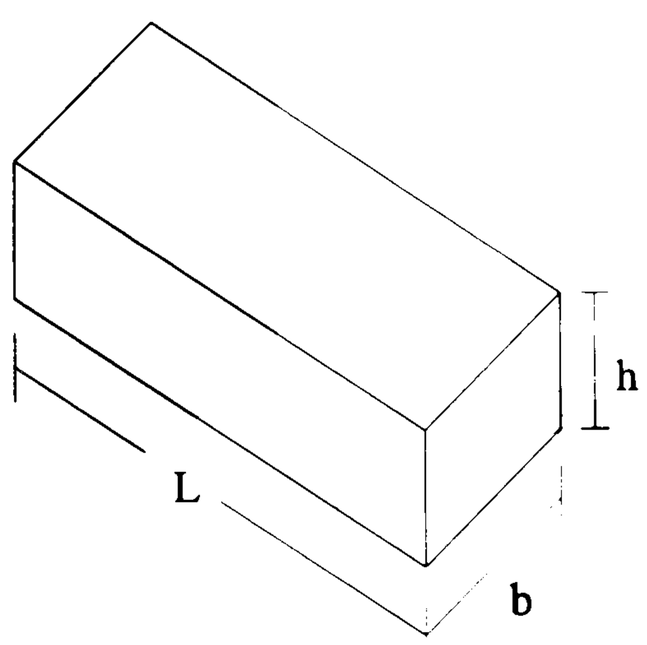

where $$I\ =\ \frac{1}{12}\ bh^3$$